New Jersey Institute of Technology
Digital Commons @ NJIT

Dissertations | Electronic Theses and Dissertations

Spring 5-31-2014

Field methods for rapidly characterizing contaminant mobility in paint waste during bridge rehabilitation

Zhan Shu
New Jersey Institute of Technology

Follow this and additional works at: https://digitalcommons.njit.edu/dissertations

 Part of the Environmental Engineering Commons

Recommended Citation

Shu, Zhan, "Field methods for rapidly characterizing contaminant mobility in paint waste during bridge rehabilitation" (2014). *Dissertations*. 166.
https://digitalcommons.njit.edu/dissertations/166

This Dissertation is brought to you for free and open access by the Electronic Theses and Dissertations at Digital Commons @ NJIT. It has been accepted for inclusion in Dissertations by an authorized administrator of Digital Commons @ NJIT. For more information, please contact digitalcommons@njit.edu.

Copyright Warning & Restrictions

The copyright law of the United States (Title 17, United States Code) governs the making of photocopies or other reproductions of copyrighted material.

Under certain conditions specified in the law, libraries and archives are authorized to furnish a photocopy or other reproduction. One of these specified conditions is that the photocopy or reproduction is not to be "used for any purpose other than private study, scholarship, or research." If a, user makes a request for, or later uses, a photocopy or reproduction for purposes in excess of "fair use" that user may be liable for copyright infringement,

This institution reserves the right to refuse to accept a copying order if, in its judgment, fulfillment of the order would involve violation of copyright law.

Please Note: The author retains the copyright while the New Jersey Institute of Technology reserves the right to distribute this thesis or dissertation

Printing note: If you do not wish to print this page, then select "Pages from: first page # to: last page #" on the print dialog screen

NJIT New Jersey's Science & Technology University

The Van Houten library has removed some of the personal information and all signatures from the approval page and biographical sketches of theses and dissertations in order to protect the identity of NJIT graduates and faculty.

ABSTRACT

FIELD METHODS FOR RAPIDLY CHARACTERIZING CONTAMINANT MOBILITY IN PAINT WASTE DURING BRIDGE REHABILITATION

by
Zhan Shu

Currently, the New York State Department of Transportation (NYSDOT) uses a conservative approach of classifying all paint waste as hazardous from bridges undergoing rehabilitation which were constructed before 1989. This practice stems from the fact that there is no approved reliable, fast, and efficient method for classifying paint waste in-situ as non-hazardous. The main objective of this study was to develop a model that can predict the leachability of trace metals in paint waste generated during bridge rehabilitation. A statistically significant number of bridge sites were sampled based on hypothesis testing. Samples were then evaluated for total concentration of Resource Conservation and Recovery Act (RCRA) metals (i.e., Ag, As, Ba, Cd, Cr, Hg, Pb, and Se), iron as well as zinc. Leaching studies included the U.S. Environmental Protection Agency (U.S. EPA) toxicity characteristic leaching procedure (TCLP) and the multiple extraction procedure (MEP). Interestingly, although elevated Pb (5 to 168,090 mg kg^{-1}) and other metal concentrations were observed in the paint samples, leaching results revealed only up to 22.6 mg L^{-1} for Pb and 9.52 mg L^{-1} for Cr. The relatively low concentrations observed are attributed to the use of iron-based abrasives (steel grit) in the paint removal process. In New York State, steel grit is typically applied as an abrasive material to remove paint during bridge rehabilitation. Although magnetic separation is applied to collect and reuse the steel grit, the fraction remaining in the paint waste ranges from 5 to 80% by weight. Using the suite of analyses, ferrihyidrite was observed to be an

important mineral surface on the steel grit; spherical particle aggregates ranged from 20 to 200 nm in diameter. In addition, sequential extraction revealed trace metal sorption to the iron oxide surface may be the dominant mechanism responsible for the reduced leaching observed. The sorption process was further modeled using the diffuse layer model. Based on an understanding of mechanistic processes along with a demonstrated analysis of variables through principal component analysis (PCA), statistically-based models for leaching from paint waste were developed. Results of this work assist in better understanding and predicting the mobility of trace metals as well as in addressing disposal and management of paint waste during bridge rehabilitation.

FIELD METHODS FOR RAPIDLY CHARACTERIZING CONTAMINANT MOBILITY IN PAINT WASTE DURING BRIDGE REHABILITATION

By
Zhan Shu

A Dissertation
Submitted to the Faculty of
New Jersey Institute of Technology
in Partial Fulfillment of the Requirements for the Degree of
Doctor of Philosophy in Environmental Engineering

Department of Civil and Environmental Engineering

May 2014

Copyright © 2014 by Zhan Shu

ALL RIGHTS RESERVED
.

APPROVAL PAGE

FIELD METHODS FOR RAPIDLY CHARACTERIZING CONTAMINANT MOBILITY IN PAINT WASTE DURING BRIDGE REHABILITATION

Zhan Shu

Dr. Lisa Axe, Dissertation Advisor — Date
Professor, Department of Civil and Environmental Engineering, NJIT

Dr. Priscilla P. Nelson, Committee Member — Date
Chair and Professor, Department of Mining Engineering, Colorado School of Mines

---

Dr. Robert Dresnack, Committee Member — Date
Professor, Department of Civil and Environmental Engineering, NJIT

Dr. Andrew Pole, Committee Member — Date
Director, MS Program in Mathematical and Computational Finance, NJIT

Dr. Juyoung Ha, Committee Member — Date
Assistant Professor, School of Environmental and Life Sciences, Kean University

BIOGRAPHICAL SKETCH

Author: Zhan Shu

Degree: Doctor of Philosophy

Date: May 2014

Undergraduate and Graduate Education:

- Doctor of Philosophy in Environmental Engineering,
  New Jersey Institute of Technology, Newark, NJ, 2014

- Master of Engineering in Environmental Engineering,
  National Hua Chiao University, Quanzhou, Fujian, P. R. China, 2009

- Bachelor of Engineering in Environmental Engineering,
  National Hua Chiao University, Quanzhou, Fujian, P. R. China, 2006

Major: Environmental Engineering

Presentations and Publications:

Shu, Z., Axe, L. Jahan, K. Ramanujachary, K. V., Field Methods for Rapidly Characterizing Paint Waste during Bridge Rehabilitation (submitted to Chemosphere).

Shu, Z., Axe, L. Jahan, K. Ramanujachary, K. V., Metal Leaching from the Bridge Paint Waste in the Presence of Steel Grit (submitted to Chemosphere).

Shu, Z., Axe, L. Jahan, K. Ramanujachary, K. V., Metal Concentrations and Distribution in Paint Waste Generated during Bridge Rehabilitation in New York State (submitted to Environmental Engineering Science).

Shu, Z., Axe, L. Jahan, K. Ramanujachary, K. V., Rapid On-site Waste Characterization Tool for Managing Paint Waste from Bridge Rehabilitation, New Jersey Department of Transportation (NJDOT) 15th Annual Research Showcase, West Windsor, New Jersey, October 23, 2013.

Shu, Z., Axe, L. Jahan, K. Ramanujachary, K. V., Trace Metal Leaching from Bridge Paint Waste in the Presence of Iron Oxide Surfaces, Division of Colloid and

Surface Chemistry, 246th American Chemical Society (ACS) National Meeting, Indianapolis, Indiana, September 8-12, 2013.

Shu, Z., Axe, L. Jahan, K. Ramanujachary, K. V., Leaching Behavior of Lead and Chromium from Bridge Paint Waste in the Presence of Steel Grit, Session of Steel Bridges Committee, Transportation Research Board 92nd Annual Meeting, Washington, D.C., January 13-17, 2013.

Shu, Z., Axe, L. Jahan, K. Ramanujachary, K. V., Leaching Behavior of Lead and Chromium from Bridge Paint Waste in the Presence of Steel Grit. Session 748 of Steel Bridge Coating Systems, Part 2: Existing Structures, Transportation Research Board 92nd Annual Meeting, Washington, D.C., January 13-17, 2013.

Shu, Z., Axe, L. Jahan, K. Ramanujachary, K. V., Leaching Behavior of Lead and Other Metals in the Presence of Steel Grit, Session of Environmental Chemistry for Fe-Oxides and Fe-Hydroxides, 244th American Chemical Society (ACS) National Meeting, Philadelphia, Pennsylvania, August 19-23, 2012 .

Shu, Z., Axe, L. Jahan, K. Ramanujachary, K. V., Field Methods for Rapidly Characterizing Paint Waste during Bridge Rehabilitation, Session of Environmental Chemistry for a Sustainable World, 243rd American Chemical Society (ACS) National Meeting, San Diego, California, March 25-29, 2012.

To my parents, Fuxia Yin and Yong Shu,
for their patience, understanding, support, and love.

ACKNOWLEDGMENT

I would like to express my deepest appreciation to Dr. Lisa Axe, who not only served as my research supervisor, providing valuable and countless resources, insight, and intuition, but also constantly gave me support, encouragement, and reassurance. Special thanks are given to Dr. Priscilla P. Nelson, Dr. Robert Dresnack, Dr. Andrew Pole, and Dr. Juyoung Ha, for actively participating in my committee and providing valuable input from their own areas of expertise.

My appreciation goes out to the NYSDOT Grant No. C-08-19 for providing financial support for this research.

I would like to thank all my professors, laboratory staff, and the secretaries in the Department of Civil and Environmental Engineering for their constant guidance and help. I would also like to thank Project manager Mr. Carl Kochersberger for his support and input, and Civil Engineer Mr. John Connor for his assistance in sampling bridge paint over the years.

All my fellow graduate students are deserving of recognition for their support. I've cherished their friendship for five years, and this will go on and be an asset in my life forever.

TABLE OF CONTENTS

TABLE OF CONTENTS
(Continued)

Chapter **Page**

TABLE OF CONTENTS
(Continued)

TABLE OF CONTENTS
(Continued)

Chapter **Page**

LIST OF TABLES

LIST OF TABLES
(Continued)

LIST OF FIGURES

LIST OF FIGURES
(Continued)

LIST OF FIGURES
(Continued)

Figure **Page**

LIST OF FIGURES
(Continued)

Figure **Page**

CHAPTER 1

INTRODUCTION

The general practice for protecting steel bridges from corrosion involves applying paint coatings (Boxall and Von Fraunhofer, 1980; Gooch, 1993; Strivens and Lambourne, 1999). Between 1950 and 1980, these paint coatings used a number of metals including lead and chromium for corrosion protection. However, concerns stemming from human health impacts of lead-based paint (LBP) prompted its ban in 1978 from most applications in the United States (Davis et al., 1993; Hall, 1972; Jacobs et al., 2002). Lead release from LBP has been associated with health effects including damage to the brain and central nervous system in children, reproductive problems, and high blood pressure (Gidlow, 2004; Landrigan, 1989; Todd et al., 1996). In response to these concerns, the Department of Housing and Urban Development (HUD) and Consumer Product Safety Commission (CPSC) have prohibited residential use of LBP since 1978 (CPSC, 1977; National Institute for Occupational Safety and Health (NIOSH), 1992). In New York State, LBP has been prohibited from commercial use since 1989 (NYSDOT, 1988).

However, although rehabilitation and subsequent repainting were conducted more than once since 1989, LBP may not be entirely removed. The degree to which paint remains on the bridge is based on surface preparation methods applied in the paint removal procedure (NYSDOT, 2008). One of the more effective approaches for removing paint and rust from steel bridges is through abrasive blasting (Appleman, 1992), where abrasive particles are propelled against the surface using a concentrated stream of

compressed air. Dust, abrasive, and paint debris are vacuumed simultaneously in the blasting operation. Debris is separated for disposal and the abrasive particles are returned for reuse. Paint waste remains a pervasive problem in U.S. cities (Axe et al., 2009; Caravanos et al., 2006; Mielke and Gonzales, 2008; Mielke et al., 2001; Townsend et al., 2004a), and an increasing problem in the developing world where it is still manufactured and used (Adebamowo et al., 2007; Clark et al., 2006; Nduka et al., 2008). Furthermore, during maintenance, reconstruction, and demolition of bridges and other steel structures, solid waste (Townsend et al., 2004a) and paint wash-water (Davis and Burns, 1999; Hopwood et al., 2003) are generated on-site.

At this time, a number of transportation agencies (i.e., NYSDOT, 2008) apply a conservative approach by assuming all the paint waste generated from bridges as hazardous material (Axe et al., 2009). This practice stems from the fact that there is no approved reliable, fast, and efficient method for classifying paint waste in-situ as non-hazardous. This conservative practice eliminates the need for extensive testing, but also results in greater expense and increased regulatory burdens than are likely required. With the advent of more accurate and sophisticated analytical equipment for in-situ field measurements, state DOTs will benefit from research focused on the reliability of such field equipment for waste characterization. Therefore, the purpose of this study is to understand the mechanism responsible for metal leaching and to develop a model that can predict the metal leachability in paint waste generated during bridge rehabilitation.

Between October 2010 and November 2011, 117 samples of paint waste were obtained from 24 bridges under rehabilitation in New York State. Studies were conducted to evaluate Resource Conservation and Recovery Act (RCRA) metals (i.e., Ag, As, Ba,

Cd, Cr, Hg, Pb, Se), zinc as well as iron concentrations in the paint waste. Leachable and extracted metal concentrations were obtained from the toxicity characteristic leaching procedure (TCLP), multiple extraction procedure (MEP), and sequential extraction (SE). In addition, to understand the mechanism responsible for metal leaching, a suite of analyses was conducted on the paint waste samples. Mechanistic modeling (surface complexation along with precipitation/dissolution modeling) was applied to support principal component analysis (PCA) of data obtained with field portable x-ray fluorescence (FP-XRF). As a result, statistically-based models for leaching from paint waste were developed. Results of this work assist in better understanding and predicting the mobility of trace metals as well as in addressing disposal and management of paint waste during bridge rehabilitation.

The following chapters include Chapter 2, a literature review of metal distribution in paints, paint removal methods, techniques applied for analyzing paint waste and bridge wash water on site, leaching studies and waste classification, and modeling applied for depicting metal mobility; Chapter 3, the objectives and hypotheses for this research; Chapter 4, Sampling Approach; Chapter 5, Experimental Methods; Chapter 6, Metal Concentrations and Distribution in Paint Waste Generated During Bridge Rehabilitation in New York State; Chapter 7, Metal Leaching from the Paint Waste in the Presence of Steel Grit; Chapter 8, Trace Metal Leaching Mechanisms from Bridge Paint Waste in the Presence of Steel Grit; Chapter 9, Statistical Model Development to Predict Metal Leaching from the Paint Waste; and, Chapter 10, Conclusions and Future Work.

CHAPTER 2

LITERATURE REVIEW

In this chapter, studies on metal distribution in paints are first introduced, and then a review of literature is presented in terms of paint removal methods and contaminant release into the environment during bridge rehabilitation, and techniques applied for analyzing paint waste and wash water generated on site. The chapter continues with leaching studies and waste classification. Modeling applied for metal leaching follows. The chapter concludes with a summary of key points and questions raised based on the literature.

2.1 Metal Distribution in Paints

Prior to the 1960's (National Paint & Coatings Association [NPCA], 1992), paints generally contained pigments using lead and/or chromium compounds as corrosion inhibitors. LBP functioned well and was used in practically all painting applications, from bridges to sign trusses, from light poles to fire hydrants. The primary lead compound used in paints was lead carbonate (white lead $2PbCO_3 \cdot Pb(OH)_2$) with concentrations as great as 40% dry paint. Lead chromate (chrome yellow) was used in (colored) paint at 5 to 7%, while lead tetraoxide (red lead Pb_3O_4, Pb_2O_4, $PbO_2 \cdot 2PbO$) was also a component of paints (Gooch, 1993) (Table 2.1). Because lead is poisonous and a carcinogen, in the early 1970's it became apparent there were worker health and safety problems associated with LBP. In 1977, the Consumer Product Safety Commission (CPSC) banned residential use of paint containing greater than 0.06% lead (U.S. CPSC, 1977). At the same time (1978), the Department of

Table 2.1 Lead Compound Used in Paints[a,b]

Pigment	Color	Chemical Formula	Dates Used[c,d]
Lead acetate	White	$Pb(CH_3COO)_2$	1900's – 1960's
Dry white lead, basic carbonate	White	$2PbCO_3 \cdot Pb(OH)_2$	1900's – 1970's
Dry white lead, basic sulfate	White	$PbSO_4 \cdot PbO$	Widely used as a primer and in building finishes. First introduced between 1855 and 1866, leaded zinc oxide form introduced in 1896.
Litharge (lead oxides)	Yellow	PbO – yellow	1940's – 1970's
	Black	Pb_2O (sub-oxide)	
	Red	Pb_2O_4 – red	
Lead tetraoxide (red lead)	Orange	Pb_3O_4 ($PbO_2 \cdot 2PbO$)	Primer coating
Lead chromate/oxide	Orange	$PbCrO_4 \cdot PbO$	1935 – 1970's
Basic lead chromate	Red	$Pb_2(OH)_2CrO_4$	Discovered 1809
Lead chromate	Yellow	$PbCrO_4$	1910's – 1970's

Source: [a] Weast, 1978
[b]Gooch, 1993
[c]Crown,1968
[d]Alphen, M., 1998

Housing and Urban Development (HUD) banned the use of paint with greater than 5,000 ppm or 1.0 mg/cm^2 lead concentrations (HUD, 1978). As a result, LBP has been phased-out of residential use (Gooch, 1993). In New York state, lead-based paint has been prohibited for commercial use since 1989 (NYSDOT, 1988).

As the application of lead paint declined, substantial quantities of zinc based paint were used in bridge paint. Mixtures of zinc oxide and lead sulfate based paint grew in the market between 1920's and 1970's. Beginning about the same time, lithophone (a mixture of 30% zinc sulfide and 70% barium sulfate) exceeded the use of lead in interior paint as the primary pigment. However, lithophone lacked durability and therefore its use declined. During the time between the mid and late 1970's, zinc chromate was used in primers along with a vinyl topcoat; in the late 1980's (International Agency for Research on Cancer [IARC], (Tomatis, 1987) this compound was found to be toxic and was phased out. Beginning in the late 1970's zinc silicate was applied as a primer for shop and field paint; experience suggests resulting wastes are not hazardous. Other metal based compounds were used as well including rutile, a titanium dioxide, which was more effective and less costly than other pigments (NPCA, 1992; Ferlauto, 1994). Titanium dioxide continues to be used today for bridge paint.

In addition to the metals discussed above, other compounds of arsenic, barium, cadmium, chromium, mercury, selenium, and silver, were used in paint as pigments and preservatives as well (Table 2.2). Since the 1950's, arsenic was applied as a pigment; however, because of the risk of poisoning, the actual use of the associated compounds was for the most part restricted to that of insecticides (Alphen, 1998). Barium was also included as a pigment and a corrosion inhibitor (NPCA, 1992) from the 1950's, as was.

Table 2.2 Typical Pigments and Associated Compounds in Paints[a]

White		**Protective**	
Titanium dioxide [TiO_2]	15-20%	Basic lead silichromate [$4(PbCrO_4 \cdot PbO) + 12(SiO_2 \cdot PbO)$]	25-35%
Zinc oxide [ZnO]	15-20%	Basic lead sulfate [$PbO \cdot PbSO_4$]	15-20%
Antimony oxide [Sb_2O_3]	15-20%	Calcium plumbate [Ca_2PbO_4]	30-40%
White lead [$2PbCO_3 \cdot Pb(OH)_2$]	15-20%	Red lead [Pb_3O_4]	30-35%
		Zinc phosphate [$Zn_3(PO_4)_2$]	25-30%
		Zinc tetroxychromate [$ZnCrO_4 \cdot 4Zn(OH)_2$]	20-25%
		Zinc chromate [$ZnCrO_4$]	30-40%

Green		**Blue**	
Chromium oxide [Cr_2O_3]	10-15%	Prussian blue[b] [$MFeFe(CN)_6 \cdot H_2O$]	5-10%
Lead chrome green [$PbCrO_4$]	10-15%	Ultramarine blue [$Na_{6.9}Al_{5.6}Si_{6.4}O_{24}S_{4.2}$]	10-15%

Black		**Metallic**	
Black iron oxide [$Fe_2O_3 + MnO_2$]	10-15%	Zinc	60-70%
Carbon black	1-5%	Lead	40-50%

Yellow	
Lead chromates [$Pb(Cr,S)O_4$]	10-15%
Zinc chromates [$ZnCrO_4$]	10-15%
Cadmium sulfide [CdS]	5-10%

Source: a: Boxall and von Frauhoffer (1980) , Alphen et al. (1998).
b: M could include K, Na or CH_3

cadmium (after 1920's) which is a pigment that produces bright colors in paint. Zinc chromate was used for a short period of time and because of its toxicity it was an effective barrier to microorganisms. Prior to 1992, the mercury compound phenylmercuric acetate (PMA) was added to some latex paints as a preservative to control bacteria, mildew, and other fungi (U.S. EPA, 1990; 2000). Selenium and silver were rarely used in paint (Alphen, 1998).

As a consequence of their application, RCRA metals along with Zn are now found in paints on older buildings and surface structures (Table 2.3) (Boxall and von Frauhoffer, 1980; Crown, 1968). With aging and weathering, paints tend to chalk, chip, flake, and otherwise deteriorate, resulting in an accumulation of pigment material on and within soils or surface water surrounding painted structures. Subsequently, the impact from exposure poses a threat when dust and fumes are inhaled and when contaminants are ingested via contaminated hands, food, water, cigarettes, and clothing (National Institute for Occupational Safety and Health [NIOSH], 1998). For example, once in the bloodstream, lead replaces other useful elements (e.g., calcium, iron) and adversely affects oxygen transport to a number of organs including the liver, kidneys, reproductive system, and the brain (Tong et al., 2000). Lead is also a carcinogen. The effects of lead are the same whether it enters the body through inhalation or ingestion, and can affect almost every organ and system in the body. Exposure to high lead levels can damage the nervous system especially in young children, cause disorders in the blood and brain systems, and ultimately result in death. Long-term exposure to lead or its salts (especially soluble salts or the strong oxidant PbO_2) can cause nephropathy, and colic-like abdominal pains. For other metals such as hexavalent chromium, inhalation can cause damage to the

Table 2.3 Metal Concentrations in Paint Used on Surface Structures

Sources	Concentration of Metals in paint by dry weight (mg/kg)									Reference
	Pb	Hg	As	Cd	Cr	Se	Ag	Ba	Zn	
Exterior house paint	464 – 317,151	0.8–214.0	–	–	–	–	–	–	–	Mielke and Gonzales (2008)
Interior house paint	24 – 63,313	0.03–39.2	–	–	–	–	–	–	–	
New Orleans houses	112 – 256,797	–	–	7 - 439	2 - 417	–	–	–	52 – 98,056	Mielke et al. (2001)
Exterior paint from a military barrack	35,700 – 96,600									Wadanambi et al. (2008)
Interior latex paint	–	930-955	–	–	–	–	–	–	–	U.S. EPA (1990)
Solvent-based paint	15,680 ± 11,780.00	–	100 ± 20.00	ND	ND	–	–	–	30,460 ±10,580.00	Huanga et al. (2010)
Water-based paint	57.46 ± 22.42	–	20.65 ± 6.11	ND	ND	–	–	–	1,660 ± 1,260	

ND not detected

– Not measured

nose, throat, and lungs (respiratory tract); it also can lead to lung cancer and death. Chronic exposure to mercury can cause disruption of the nervous system, damage to deoxyribonucleic acid (DNA) and the chromosomal system, as well as result in allergic reactions (Clarkson, 1988). Mercury is a carcinogen. Long-term exposure to mercury can lead to damage of the brain, kidney, and lungs. Damaged brain functions may result in learning disabilities, personality changes, tremors, vision changes, and deafness. Dermal exposure may also result in skin rashes, tiredness, and headaches (U.S. EPA, 2009). Mercury poisoning can result in several diseases, including acrodynia (pink disease), Hunter-Rusell syndrome, and Minamata disease.

In response to these health concerns, the federal government has promulgated a series of regulations to reduce exposure to these metals. In 1977, CPSC banned residential use of paint containing greater than 0.06% lead (U.S. CPSC, 1977) (Table 2.4). HUD (1978) set up the regulation that banned the use of paint with greater than 5,000 ppm or 1.0 mg/cm^2 lead concentrations. In 1993, Occupational Safety and Health Administration (OSHA) reduced permissible exposure limit (PEL) for workers to 50 µg/dL of blood (OSHA, 1993). In 1996, U.S. EPA and HUD together enacted requirements for disclosure of known LBP used in housing (CFR 61(45), 1996). In 2001, the U.S. EPA (CFR 66(4), 2001) announced the final rule for lead levels in dust on floors, windowsills, and play areas as potentials hazards. The U.S. EPA (CFR 66(4), 2001) has established 400 ppm of lead in bare soil as the maximum allowable level for children's play areas and an average of 1,200 ppm as the maximum concentration allowed in a residential yard. In 2009, regulated lead concentrations in paint for residential applications were lowered to 90 ppm (Consumer Product Safety Improvement Act

Table 2.4 Regulations Related to Metals in Paint

Date	Hazardous Materials Used in Paint	References
1972	The Lead Based Paint Poisoning Prevention Act established the level of 0.5% in house paints.	U.S. CPSC (1972)
1972	Mercury compounds were banned by the U.S. EPA from use in marine paint.	U.S. EPA (1972)
1977-1978	The final 1977 LBP Poisoning Prevention Act regulation set the maximum allowable level at 0.06% became effective by U.S. CPSC, and it is 1.0 mg/cm^2 or 5,000 ppm set by HUD (1978), as such greater concentrations were banned from consumer paints.	U.S. CPSC (1977) HUD (1978)
1990	Mercury in interior latex paint was banned by the U.S. EPA. Most buildings constructed before 1990 contain mercury in their paint.	U.S. EPA (1990)
1992	Mercury in interior paint was banned although its use had been reduced.	U.S. EPA (1992)
1993	A CPSC study of consumer paint samples found that lead in paints on the market meet the standard and are actually below the 0.06 % level.	U.S. CPSC (1993)
1996	Lead was not banned from gasoline used in transportation until December 1995. U.S. EPA and HUD together enacted requirements for disclosure of known LBP used in housing (CFR 61(45), 1996).	HUD, FR 61(45), (1996)
2001	The U.S. EPA has established 400 ppm of lead in bare soil as the maximum allowable level for children's play areas and an average of 1,200 ppm as the maximum concentration allowed in a residential yard.	U.S. EPA (2001)
2006	Work practice standards proposed to reduce lead exposure during residential renovation activities in 40 CFR Part 745	TSCA, 40 CFR Part 745, revised in April 22, 2009
2008	EPA finalized Toxic Substances Control Act (TSCA) regulations in 40 CFR Part 745. The rule addressed LBP hazards during residential renovation, repair, and painting activities.	
2009	The lead concentration in paint was lowered to 90 ppm, it applied to (i) paint and other similar surface coatings; (ii) toys and other articles intended for use by children; and (iii) certain furniture articles that are not otherwise exempt under our regulations.	CPSIA (2008), effective in August 14, 2009

[CPSIA], (Flaherty, 2009)). However, auto exhaust from leaded gasoline used as an octane-booster and anti-knock compound has been another source of lead in the environment. Between 1940 and 1989, twice as much lead in the form of lead oxide and tetraethyl lead was used in leaded gasoline as compared to that used in lead based paints (Weaver, 1989). Seventy-five percent of lead associated with auto exhaust mobilized into the environment and settled in soil and on structures (Ferlauto, 1994). Other metals also pose potential risk from release. For example, because of exposure concerns regarding mercury in interior paints, limits were placed on PMA additives in 1990 (U.S. EPA, 1990); subsequently these were banned in 1991 (Flaherty, 1999).

2.2 Paint Removal Method and Metal Release in the Environment

The majority of steel bridges in the interstate system were constructed between 1950 and 1980. As infrastructure ages, undergoes weathering, and paint coatings degrade, a large percentage of the existing steel bridges are reaching a critical level of deterioration, and release of metal contaminants into the environment becomes an issue. In this section, the paint removal process is presented, and metal release into surrounding soils and surface water along with infiltration into groundwater are discussed. Furthermore, during rehabilitation, particles can be dispersed as aerosols as well, and released into soils and surface water; this mode of transport is also reviewed in this section.

2.2.1 Paint Removal Method

Prior to paint removal, high pressure water (about 3000 psi) is applied to remove salt, bird droppings, and other associated debris from bridge structures (NYSDOT, 2008). The

most effective and productive method for removing paint and rust from steel has been abrasive blasting (Appleman, 1992). In this method, abrasive particles are propelled against the surface using a concentrated stream of compressed air. Dust, abrasive, and paint debris are vacuumed simultaneously with the blasting operation. Debris is separated for disposal and the abrasive is returned for reuse. Typically, hard metallic abrasives are used in these systems, where for example, magnetic particles can be easily separated (Appleman, 1992). This approach can effectively remove paint from crevices and other hard-to-reach areas. In New York State, a complete containment (which is negative pressure in a vacuum system) is constructed around the work area to control emissions of dust and debris (NYSDOT, 2008). Cast steel grit is used as abrasive blasting material on all the bridges in New York State because of the availability and the hardness. The abrasive agent is recycled during the separation procedure; however, the steel grit is not entirely removed. The percent remaining with the waste is reported to be the smallest size fraction. To qualify the degree to which steel grit remains with waste, this research will include a statistical analysis of the 117 samples collected.

Another commonly used method is power tool cleaning (Appleman, 1992), where electric and/or air operated impact grinding or brushing tools are applied and include power chippers, needle guns, descalers, power wire brushes, and grinding wheels. Power tool cleaning produces dust and can generate airborne debris. In contrast to using abrasive particles, power tool cleaning does not require a medium. As a result, essentially the only debris generated is the material being removed (paint, rust, mill scale, and other surface debris). Often the power tool is surrounded with its own shroud that is equipped with a vacuum. This method creates a miniature containment around the tool for collecting

waste as it is generated, transporting it from the work area through hoses. During the removal process, the potential for release to the environment exists along with releases from aging infrastructure.

2.2.2 Metals Found in the Soil and Surface Water

Because lead concentrations in paint far exceed that of other metals (Boxall and Fraunhofer, 1977; Boxall and Fraunhofer, 1980), the following discussion is focused on lead. The elevated concentrations of lead observed in the environment that originate from deteriorating exterior LBP (Davis and Burns, 1999; Binstock et al., 2009) results in leaching through soil around the foundation of a bridge or building and into groundwater (Binstock et al., 2009) as well as transport into surface waters (Davis and Burns, 1999).

Decades of peeling exterior paint along with remodeling and renovation activities, give rise to dust and debris that contribute to further dispersal of elevated lead concentrations in soil (U.S. EPA 1996; 1999). Once lead as well as other metals are released from painted structures, they can be attenuated via interactions with surrounding soil. Studies (Francek, 1992) indicate lead sorption and attenuation in soils can be significant, residing in systems potentially for several thousand years. For example, lead concentrations in soil surrounding buildings constructed after 1978 revealed background levels, whereas prior to 1978 concentrations greater than 1,000 ppm were found (Francek, 1992; Francek et al., 1994). Binstock et al. (2009) observed lead concentrations as great as 2,540 ppm during an evaluation of soil around housing with LBP applied to exterior surfaces. Caravanos et al. (2006) studied deposition of lead in ambient dust for the boroughs of New York City from 2003 - 2004 and observed concentrations ranging from

175 µg/ft^2 to 730 µg/ft^2. When compared to the HUD/EPA dust standard of 40 µg/ft^2 (U.S. EPA/HUD, 2003), they reported that in Manhattan and Queens areas, renovations at bridges and other construction/demolition activities are potential lead sources and may in part explain the lead deposited in this area.

In paved areas, dissolved lead and lead contaminated paint particulates are transported either directly or indirectly to surface water through storm drains. Specifically, metals may be mobilized through rainfall, and urban stormwater runoff is considered to be a major source of metals to surface waters. Lead contaminated paint particles will continue to dissolve as they are being transported, releasing lead into solution. The dissolution rate can be enhanced by complexing ligands commonly found in natural waters, such as humic acid and chloride (Davis and Barnes, 1999). The mobility of metals in the environment is a function of their speciation. While metals in general prefer to be bound to surfaces, cations desorb as the pH decreases and anions are released as the pH increases. Actually, a number of factors affect metal behavior including sorbents present in the subsurface, pH, ionic strength, complexing ligands, reduction oxidation potential, competing ions, and time.

In addition, as mentioned earlier, LBP removal projects may generate wastewater from cleaning painted surfaces, wet abrasive blasting, or decontamination of personnel or equipment. Although wastewater containing lead or paint solids must be collected, properly treated, and discharged to a permitted location to prevent water pollution, some may inadvertently flow into the surface water sources. Lead distribution in the rain water and wash water from paint has been investigated (Table 2.5). Many of these studies reveal concentrations greater than the U.S. EPA fresh water chronic and acute criteria of

Table 2.5 Lead Concentrations Observed in Wastewater and Rain Water

Sample type	Total lead (mg/L)	Reference
Wastewater obtained by high pressure wash	2.3 – 130 (without filtration) 2.0 – 220 (with filtration)	Hopwood et al. (2003)
Runoff obtained from synthetic rain water	Block 0 - 0.59 Wood 0 - 1.9 Brick 0 - 28	Davis and Burns (1999)
Storm water runoff	140	Granier et al. (1990)
Storm water runoff from residential areas	9 – 72 (composite) 0 – 62 (grab)	Maryland Department of Environmental Resources (1993)
Storm water runoff from commercial land use areas	14 ± 39 (composite) 54 ± 230 (grab)	

2.5 and 65 µg/L, respectively (U.S. EPA, 2009) (Table 2.6). Hopwood et al. (2003) attempted to apply geotextile fabric to filter wastewater from bridges undergoing maintenance prior to its release. Lead concentrations both dissolved and total generated by high pressure (3,000 to 10,000 psi) washing ranged from 0 – 5.5 mg/l and 2.3 – 130 mg/l, respectively; after filtration, concentrations were 0 – 4.1 mg/l and 2.0 – 220 mg/l, respectively. These results demonstrated that the filter was ineffective in removing suspended fines or dissolved metals ions. One possible explanation for the inefficiency may be attributed to the pore size of the filter. Hopwood et al. also analyzed the water pressure, nozzle type, as well as paint parameters (thickness, adhesion, and lead content). No significant correlations were observed between the lead concentration in wash water and the factors associated with the high pressure washing. Davis and Burns (1999) found that concentrations in the runoff were a function of the intensity (flow rate/spray area) of the synthetic rain water applied, the greater the ratio the greater the concentration. To assess the effect of acid rain on LBP structures, Davis and Burns (1999) used synthetic rain water with a pH range of 4.2 to 4.4 and composed of 23 mM NaCl, 18 mM HNO_3, and 18 mM H_2SO_4. Results revealed that the total lead concentrations (Table 2.5) in the runoff were a function of paint age (> 10 y) > (5-10 y) > (0-5 y); the older the structure the greater the concentration observed. Additionally, the authors found the structure type was important where concentrations followed the trend of wood > brick > block. Yet, 69 – 84% of lead was associated with particulates. Concentrations in the runoff were dependent on the intensity (flow rate/spray area) of the synthetic rain water applied, the greater the ratio the greater the concentration. The first flush of the painted structures revealed greater lead concentrations than the wash water generated during subsequent

Table 2.6 Water Quality Criteria for the Protection of Aquatic Life and Human Health in Surface Water

Contaminant	Freshwater		Saltwater		Human Health for the consumption of	
	CMC (acute) (µg/L)	CCC (chronic) (µg/L)	CMC (acute) (µg/L)	CCC (chronic) (µg/L)	Water + Organism (µg/L)	Organism Only (µg/L)
Arsenic	340	150	69	36	0.018	0.14
Barium	NA	NA	NA	NA	1,000	NA
Cadmium	2	0.25	40	8.8	A	NA
Chromium (III)	570	74	NA	NA		NA
Chromium (VI)	16	11	1,100	50	A	NA
Lead	65	2.5	210	8.1	NA	NA
Mercury	1.4	0.77	1.8	0.94	NA	0.3 mg/kg
Selenium	NA	5	290	71	170A	4,200
Silver	3.2	NA	1.9	NA	NA	NA
Zinc	120	120	90	81	7,400	26,000

Source: National Recommended Water Quality Criteria, United States Environmental Protection Agency, Office of Water Office of Science and Technology, (4304T) 2006.
NA: Not Applicable
A: A more stringent MCL has been issued by U.S. EPA. Refer to drinking water regulations (40 CFR 141) or Safe Drinking Water Hotline (1-800-426-4791) for values.
CMC: The Criteria Maximum Concentration (CMC) is an estimate of the highest concentration of a material in surface water to which an aquatic community can be exposed briefly without resulting in an unacceptable effect.
CCC: The Criterion Continuous Concentration (CCC) is an estimate of the highest concentration of a material in surface water to which an aquatic community can be exposed indefinitely without resulting in an unacceptable effect.

contact. As the lead concentration in the peeling paint chips increased, concentrations in the runoff increased as well. Similarly, air contamination may result from aerosolized paint particles during rehabilitation.

2.2.3 Metals Released into Air

Lead contaminated particles are aerosolized during abatement, and as a result pose a potential health hazard. NIOSH (1992) evaluated eight bridge construction sites where abrasive blasting occurred and showed airborne lead concentrations ranged from 2 to 29,400 $\mu g/m^3$. Furthermore, worker blood levels ranged from 51 to 160 µg/dL (NIOSH, 1992). OSHA (1993) promulgated an interim final rule for lead exposure in construction (29 CFR 1926.62); the standard reduced the permissible exposure limit (PEL) from 200 $\mu g/m^3$ of air as an eight-hour time weighted average (TWA) to 50 $\mu g/m^3$ of air (Table 2.7). This regulation also set air action levels for workers without respirators to 30 µg lead/m^3 of air (Table 2.7) (OSHA, 1993). Sullivan et al. (1996) studied whether concentrations of lead, cadmium, and chromium in air during abrasive blasting exceeded the OSHA standards. Airborne lead and cadmium concentrations measured at several locations inside the containment structure as well as near the workers' breathing zones did exceeded OSHA PEL (Table 2.8) by factors of 219 and 3.1, respectively. Because metal contaminants are present in subsurface paint layers during bridge rehabilitation, there is a dire need to identify rapid cost effective methods for lead detection in-situ.

Table 2.7 Lead Exposure Limits

Environment	Lead limits	Reference
Paint	600 ppm	U.S. CPSC (1977)
	1.0 mg/cm^2 or 5,000 ppm	HUD (1978)
Dust	40 µg /ft^2– clearance for floors	U.S. EPA / HUD (2003)
	250 µg /ft^2 –clearance for window sills	
	400 µg /ft^2 –clearance for window wells	
Dust lead hazard screens only	25 µg /ft^2 – floors	U.S. EPA / HUD (2003)
	125 µg /ft^2 –window sills	
Soil	500-1,000 ppm- superfund limit	U.S. EPA (2001)
	400 ppm– high contact play areas (communicate)	
	1,200 ppm – other residential yard areas (average)	
	5,000 ppm – require permanent abatement	
	Background or < 400ppm –replacement soil	
Air	1.5 µg /m^3 - EPA national air quality standard (quarterly)	OSHA (1993)
	30 µg /m^3 – OSHA action level[1]	
	50 µg /m^3 – OSHA permit exposure limit (PEL) (8 hour average)	
Blood	10 µg /dl (CDC) level of concern for children	OSHA (1993)
	40 µg /dl permissible blood lead level	
	50 µg /dl worker removal – lead level	

[1] Action level: means employee exposure, without regard to the use of respirators, to an airborne concentration of lead of 30 micrograms per cubic meter of air (30 µg /m3) averaged over an 8-hour period.

Table 2.8 Permissible Exposure Limits (PEL)

Metal	Permissible exposure limit (PEL) (µg/m^3)	Reference
As	10.0	CFR 29, 1910.1018
Ba		
Soluble compounds	0.5	CFR 29, 1910.1000 Table Z-1[1]
Barium sulfate		
Total dust	15.0	
Respirable fraction	5.0	
Cd	5.0	CFR 29, 1910.1027
Cr		
Chromic acid and chromates (as CrO_3)	2.0	
Chromium (II) compounds	0.5	CFR 29, 1910.1000 Table Z-1
Chromium (III) compounds	0.5	
Chromium metal and insoluble salts	5.0	CFR 29, 1910.1026
Chromium (VI) compounds	1.0	
Pb	50.0	CFR 29, 1910.1025
Hg		
Aryl and inorganic	2.0	CFR 29, 1910.1000 Table Z-1
Organo alkyl compounds	2.0	
Vapor	2.0	
Se		
Selenium compounds	0.2	CFR 29, 1910.1000 Table Z-1
Selenium hexafluoride	0.4	
Ag	0.01	CFR 29, 1910.1000 Table Z-1
Zn		
Zinc chloride fume	1.0	CFR 29, 1910.1000 Table Z-1
Zinc oxide fume	5.0	
Zinc oxide		
Total dust	15.0	
Respirable fraction	5.0	
Zinc stearate		
Total dust	15.0	
Respirable fraction	5.0	

[1] http://www.osha.gov/pls/oshaweb/owadisp.show_document?p_table=STANDARDS&p_id=9992

2.3 Techniques Applied for Analyzing Paint Waste and Wastewater Generated On Site

Solid waste and paint wash-water are generated on-site whenever LBP is disturbed during maintenance, reconstruction, and demolition of bridges and other steel structures. FP-XRF meters and portable spectrophotometers are field tools used in providing lead and metal concentrations present in bridge paint waste and wash water. While these measurements have been found to be reliable, their effectiveness in classifying a waste or wash water as hazardous or not requires investigation.

2.3.1 Field Portable X-Ray Fluorescence (FP-XRF)

Protocols for testing LBP with an XRF analyzer have been established by U.S. EPA (U.S. EPA, 2001) and HUD (HUD, 1995). Several methods such as the U.S. EPA Method 6200 (U.S. EPA, 1998) and NIOSH Method 7702 (NIOSH, 1998) involve the use of portable XRF technology. During the past several years, there has been a marked improvement in the technology of the FP-XRF, which has resulted in increased sensitivity and allowed for their use in such applications as air monitoring of particles (Morley et al., 1999; Zamurs et al., 1998), dust samples (Zamurs et al., 1998), soil samples (Clark et al., 1999), and paint (Daniels et al., 2001). FP-XRF instruments use either a sealed radioisotope source or an X-ray tube to provide the excitation energy. Radioisotope sources for irradiating samples include Fe^{55}, Co^{57}, Cd^{109}, Am^{241}, and Cm^{244} (Table 2.9); these sources undergo decay described with the half-life, which can be as short as 270 days (Co^{57}). As such, manufacturers of FP-XRF technology recommend source replacement at regular intervals based on the half-life and activity

Table 2.9 Commonly Used Radioisotope Source Characteristics for XRF

Source	Activity (mCi)	Half Life (years)	Excitation Energy (keV)	Elemental Analysis Range	
Fe^{55}	20 – 50	2.7	5.9	Sulfur to chromium	K Lines
				Molybdenum to bariur	L Lines
Co^{57}	40	0.75	121.9 and 136	Cobalt to cerium	K Lines
				Barium to lead	L Lines
Cd^{109}	5 – 30	1.3	22.1 and 87.9	Calcium to rhodium	K Lines
				Tantalum to lead	K Lines
				Barium to uranium	L Lines
Am^{241}	5 – 30	432	26.4 and 59.6	Copper to thalium	K Lines
				Tungsten to uranium	L Lines
Cm^{244}	60 – 100	17.8	14.2	Titanium to selenium	K Lines
				Lanthanum to lead	L Lines

Source: Kalnicky and Singhvi (2001).

(Kalnicky and Singhvi, 2001). Table 2.10 lists representative isotope and X-ray tube sources for FP-XRF instrumentation. Isotope sources give off radiation at specific energy levels and, therefore, efficiently excite elements within a specific atomic number range (L line or K line or both). As a result, no single radioisotope source is sufficient for exciting the entire range of elements of interest in environmental analysis. Some instruments provide dedicated element analysis (e.g., Pb in paint), while others provide a variety of elemental analyses depending on source and detector configuration. These units generally are readily adaptable to field operations, though they may be limited by the capacity of the battery. Units evaluated provide a minimum of 8 h of field use with rechargeable and replacement batteries.

Miniature X-ray tubes have become available since 2002 (Martin and Sackett, 2005), allowing their incorporation into portable XRFs. An important difference between X-ray tubes and radioactive sources is that X-ray tubes produce a continuum of X-rays across a broad range of energies. This continuum is weak compared to the characteristic X-rays, but can provide substantial excitation since it covers a broad energy range. However, one issue in using an X-ray tube source is the resulting background in the spectrum near the analytic X-ray lines from scatter by the sample. For this reason a filter is often used between the X-ray tube and the sample to suppress the continuum radiation while passing the characteristic X-rays from the anode; these filters are incorporated into the XRF unit. Miniature X-ray tubes permit simultaneous analysis of 20 to 25 elements; they also generally provide lower detection limits as compared to isotope systems for most metals. Additionally, the testing time does not increase with an X-ray tube, because the source does not decay. Typically, the testing speed after 4 or 5 years is the same as

Table 2.10 Isotope and Tube Based Sources for FP–XRF

Developer	Technology	Element range	Excitation Source:	Cost of the instrument
Oxford	HorizonPbi[a]	Pb	Cd^{109} 20 mCi	Only available in France
Niton	Xli/p 300	Pb	Cd^{109} 40 mCi	$17,000[b]
Oxford	XMET 5000/5100	S–U	Ag anode, ≤ 45 keV	$30,000-40,000[c]
Niton	Niton XL3t 600	K–U	Au anode, ≤ 50 keV	$37,000[b]
Innov-X Systems, Inc	LBP4000	Pb	Ag anode, 10-25 keV	$23, 220[d]
Spectro	SPECTRO xSORT	S–U	W anode, ≤ 40 keV	$34,536[e]

[a]: Only available in France

[b] The quotation from Niton

[c] The quotation from Oxford

[d] The quotation from Innov-X Systems, Inc

[e] The quotation from Spectro

when the analyzer's tube was new. While, in addition to the loss in analytic capabilities, radioisotope based units must eventually be replaced for sources. However, with a maximum output of 50 keV (Table 2.10), none of the handheld X-ray tube instruments found for this work can produce X-rays with sufficient energy to excite the K shell X-rays of lead. This K shell excitation is needed for lead-based paint buried beneath more recent coatings (Martin and Sackett, 2005). Because of the inconclusive range of X-ray tube-based XRF analyzers at and around the lead concentration of 1.0 mg cm^{-2} – the Federal standard for residential or occupied properties (U.S. EPA, 2003) – users run the risk of obtaining an inconclusive lead concentration in lead-based paint. With the ability to measure both L and K shell fluorescent lead X-rays, a radioisotope-based instrument can reliably test the lead even in the densest substrates and deeply buried or shielded paint. Given HUD's determination (HUD, 2003) that X-ray tube-based instruments provide inconclusive results as often as 16% of all samples and that these instruments can provide results with a false-positive rate of 2.5% and a false-negative rate of 1.9%, radioisotope-based instruments are needed to accurately identify and quantify lead in lead-based paint.

With the exception of Pb, X-ray tube sources are appropriate for all Resource Conservation and Recovery Act (RCRA) metals and Zn, as these have the capability of providing faster results in detecting a wider range of metals in the sample. On the other hand, a radioisotope-based instrument can provide deeper and multilayer detection for Pb.

Isotope based FP-XRF has been used by a number of researchers for determining Pb in paint. A study was conducted by Daniels et al. (2001) to demonstrate the effectiveness of a wet abrasive blasting technology to remove lead-based paint from

exterior wood siding and brick substrates as well as to evaluate the effectiveness of two waste stabilization technologies to treat the resulting blast media (coal slag and mineral sand) paint debris. The technology efficacy was determined by the use of an XRF analyzer with the capability of both L - and K-shell excitation for Pb using a radioisotope source. To detect the relationship between lead levels on painted surfaces and percent lead in the particles aerosolized during lead abatement, Choe et al. (2002) used a FP-XRF instrument (NITON-700, NITON Inc., Bedford, MA) to measure lead levels. Experiments were performed in the University of Cincinnati Environmental Test Chamber using wood doors painted with lead-based paint. While a good relationship (r^2 = 0.83) was found between the XRF readings and the percent lead in the particles aerosolized during dry scraping, no significant relationship was found for wet scraping (r^2 = 0.09) or dry machine sanding (r^2 = 0.002). Clark et al. (2005) used FP-XRF to determine environmental lead concentrations and distribution in the environment by studying Pb concentrations in paint, dust, air, soil, and other bulk samples near several industries that used lead and in the residential environments of children with very high blood lead levels.

Field investigations have benefited from the XRF instrument in various modes from safety monitoring to site screening. Kilbride and Poole (2006) detected total concentrations of Cu, Pb, As, Cd, Zn, Fe, Ni, and Mn for 81 soil samples using two types of FP-XRF systems: isotope (Niton Xli with sources Cd^{109} and Am^{241}) and an X-ray tube source (Niton XLt 700 series). Metal concentrations were statistically compared with analytical results from aqua regia digestion followed by inductively coupled plasma optical emission spectrometry (ICP-OES) analysis. The ability of each FP-XRF

instrument to produce comparable analytical results was assessed by linear regression, where a strong relationship was found for Fe analysis (r^2>0.89) with the X-ray tube instrument and for Fe, Cu, Pb, Zn, Cd, and Mn (r^2>0.88) with the isotope source-based instrument. Particle size did not influence the FP-XRF analyzer performance. Radu and Diamond (2009) used the XLp 703 Cd^{109} source analyzer and the XLt 793 miniaturized X-ray tube for thin sample and bulk homogenized (soil) sample analysis. A good correlation between total metals from digested samples analyzed by flame atomic absorption spectroscopy (AAS) and the tube-based XRF technique was achieved (r^2 values for Pb, As, Cu, and Zn were 0.995, 0.991, 0.959, and 0.843, respectively).

Markey et al. (2008) found that lead concentrations in soil obtained by FP-XRF protocol Method 6200 (U.S. EPA, 1998) are highly correlated (r^2 = 0.9764 – 0.992) with laboratory results using digestion followed by AAS (Table 2.11). One reason strong correlations were observed was that samples were homogenous, fine-grained, and dry; good correlations are generally observed for such samples (Kirtay et al., 1998; Clark et al., 1999). Binstock et al. (2009) evaluated the lead concentrations in soil with FP-XRF and digested samples followed by ICP-AES around housing where LBP was applied to exterior surfaces. Statistical analysis (i.e., sign test, Wilcoxon signed rank test, and paired t-test) indicated no difference (r^2 = 0.98 – 1.00) between the measurements. The results indicate that both the isotope and the X-ray tube FP-XRF instruments are effective tools for rapid, quantitative assessment of soil metal contamination and for monitoring the efficacy of remediation strategies.

Air quality monitoring has involved traditional high-volume air sampling for particulates and volatilized lead when studying LBP removal from bridges with abrasive

Table 2.11 Correlation between Metal Concentrations in Soil Measured by FP-XRF and that Found through Digestion Followed by AA and ICP

Sample Type	Metal concentration by XRF (ppm)				Metal concentration by AA or ICP (ppm)				r^2 value	Reference
	Pb	As	Zn	Cd	Pb	As	Zn	Cd		
Marine sediment	0.70	–	0.87	–	–	–	–	–	–	Kirtay et al. (1998)
Soil	750 - 882	–	–	–	920 – 1,124	–	–	–	0.9764 – 0.992	Markey et al. (2008)
Soil	5,300 ± 300	370 ± 30	1,040 ± 60	–	5,000 ± 300	860 ± 60	930 ± 60	–	0.843 – 0.996	Radu and Diamond (2009)
Soil in the industrial land	2 – 74,356	2 – 3,920	35 – 60,820	12 - 613	5 – 40,398	2 – 5,646	3 – 25,389	0 - 447	0.26 – 0.93	Kilbride et al. (2006)

– not measured

blasting. To determine the airborne lead concentration in a worker's breathing zone at a lead abatement site, Morley et al. (1997) used closed-faced, 37-mm cassettes with pre-loaded 0.8 micron pore size filters to sample aerosolized particles during blasting. FP-XRF was used for analysis and compared with that of digested samples measured with the graphite furnace AAS. No significant difference was reported between the lead concentrations obtained by the two methods (p-value 0.72). As a result, NIOSH (1998) developed Method 7702 for the FP-XRF analysis of air samples on filters. In another similar study, Zamurs et al. (1998) compared results of traditional laboratory filter analysis for lead by using ICP versus FP-XRF; results indicated that the latter effectively measured concentrations. In fact, a linear relationship between XRF and ICP measurements of digested samples was developed for air samples and the results showed a strong correlation (r^2 = 0.95). Such a relationship can be used to compare lead concentrations determined by FP-XRF analysis with lead limits established for workers in bridge-cleaning activities.

Overall, XRF has been widely applied in such applications as air monitoring of particles (Morley et al., 1997; Zamurs et al., 1998), dust samples (Zamurs et al., 1998), soil samples (Clark et al., 1999), and paint (Daniels et al., 2001). XRF has been proven effective in on site analysis as demonstrated by correlations between field and laboratory results. However, based on the literature, studies to date have not been conducted on correlating field results to lab analyses based on the U.S. EPA TCLP (U.S. EPA, 1992).

2.3.2 Field Portable Spectrophotometer

UV-visible spectrophotometry is commonly used for lead Pb(II) analysis because of its simplicity, precision, accuracy, low cost, and sensitivity. The Standard Method (SM) 3500-Pb D (Eaton et al., 2005) is a dithizone ($C_{13}H_{12}N_4S$) method initially developed for wastewater analysis using a spectrophotometer. Specifically, the dithizone method is designed for determining lead in water and wastewater. The DithiVer Metals Reagent is a stable powder form of dithizone. Lead ions in a basic solution react with dithizone is used to form a pink to red lead-dithizonate complex, which is extracted with chloroform. Extracted samples are then measured in the spectrophotometer at 515 nm. While a number of companies manufacture spectrophotometers for lead analyses, the Hach DR 2800 is the only field portable instrument that meets the U.S. EPA approved Method 8033 (Eaton et al., 2005) (which is equivalent to the SM 3500-Pb D). As a result, field detection of lead concentrations in wash water or wastewater is possible. Hach DR 2800 can detect lead concentrations as low as 3 to 300 μg L^{-1}.

The Hach portable spectrophotometer has been used for on-site applications as a field portable tool. Kucukbay et al. (2007) investigated chemical and physical parameters of the water and sediment samples taken from Karakaya Dam Lake during the four seasons. Constituents measured included Fe, Cu, Pb, Mn, Cd, Ca, NO_2^--N, NH_3-N, PO_4^{3-}, organic substances, and total filterable residues using standard reagents kits for the HACH DR 2010 spectrophotometer.

In addition to the in-situ analysis, leaching studies are effective methods to investigate contaminant mobility in the paint waste.

2.4 Leaching Studies and Waste Classification

While understanding metal distribution and techniques applied for the paint waste analysis are important, most critical is the metal mobility, which affects the waste classification and disposal. Toxicity characteristic leaching procedure (U.S. EPA, 1992) and multiple extraction procedure (U. S. EPA, 1986; 2004) are short-term and long-term leaching studies that simulate landfill conditions for waste classification. Sequential extraction (SE) focuses on resolving phases trace metals are associated within the waste, which supports modeling efforts.

2.4.1 Paint Waste Classification with TCLP

LBP is technically defined as having a minimum of 0.5% (5,000 ppm) by weight lead or when assessing surfaces, greater than 1.0 mg/cm^2 Pb (HUD, 2003; U.S. EPA, 1995). For non-residential LPB waste, the U.S. EPA TCLP (U.S. EPA, 1992) must be conducted on a representative sample to determine if the wastes are characteristically hazardous (Table 2.12). Specifically, wastes with a TCLP concentration less than the lead toxicity characteristic (TC) limit of 5 mg/L may be disposed at a Class I or II Municipal Solid Waste Landfill (MSWLF) or a construction and demolition (C&D) landfill. On the other hand, wastes with TC lead concentrations greater than 5 mg/L (Table 2.13) must be managed as a hazardous waste and disposed at an U.S. EPA RCRA permitted treatment, storage, and disposal (TSD) facility (U.S. EPA, 1998).

In 2004, the Minnesota Department of Transportation (Mn/DOT, 2004) designed guidelines and procedures to comply with Minnesota Air Quality and Waste Management regulations for the removal of paint on steel bridge structures. Specifically,

Table 2.12 Types of Landfills[a]

Types of landfill	Description of landfill	Acceptable waste	Determination of lead level
C&D	Construction, demolition, and land-clearing debris landfill; least protective landfill: no liners, and no groundwater monitoring	Residential LBP waste	Analyze paint using digestion for total lead analysis or by XRF
MSWLF (Subtitle D)	Municipal solid waste landfill: synthetic liner and leachate collection system	Residential LBP waste. Hazardous wastes from "conditionally exempt small quantity generators" if acceptable under their special waste plan.	TCLP
Subtitle C[b]	Hazardous waste landfill	Paint residue with toxicity concentration >5.0 mg/l for Lead (Table 2.13)	TCLP

a: U.S. EPA, (2003) Disposal of Residential Lead-Based Paint Waste, Final Rule http://www.epa.gov/wastes/nonhaz/municipal/landfill/pb-paint.htm

b: Disposal in a Subtitle C landfill does not apply to waste generated by construction or demolition activities conducted on a household or residence.

Table 2.13 Characterization Limits of the RCRA Metals and Zinc in Waste

Metal	Waste code	MCL[1] (µg/l)	TC[2] (mg/l)
As	D004	10	5
Ba	D005	2000	100
Cd	D006	5	1
Cr	D007	100	5
Pb	D008	TT[b] Action Level=15	5
Hg	D009	2	0.2
Se	D010	50	1
Ag	D011	100[a]	5
Zn		5000[a]	NA

[1] MCL: Maximum Contaminant Level, the highest level of a contaminant that is allowed in drinking water. U. S. EPA (2009)
http://www.epa.gov/safewater/contaminants/index.html#mcls

[2] TC level: Maximum Concentration of Contaminants for the Toxicity Characteristic.
U. S. EPA (1992), Toxicity characteristic leaching procedure (TCLP), SW-846 Method 1311Fenderal Register, 55(March 29), Washington, DC.

a. SDWR: Secondary drinking water regulations.

b. Lead and copper are regulated by a treatment technique that requires systems to control the corrosiveness of their water. If more than 10% of tap water samples exceed the action level, water systems must take additional steps. For copper, the action level is 1.3 mg/L, and for lead is 0.015 mg/L.

XRF was designated as an effective technique to determine the presence of lead in paint for steel bridge structures prior to blasting. For paint with greater than or equal to 0.5% (5,000 ppm) by weight or 0.5 mg/cm^2, the blasting residue will be sent to a laboratory and analyzed with the TCLP to determine waste classification. The residue can then be transported to an appropriate TSD facility. Daniels et al. (2001) studied the effectiveness of two stabilization technologies, Blastox and PreTox 2000 fast dry, on paint waste generated from a wet abrasive blasting technology. Even with the stabilization technology, paint debris was still classified as a hazardous waste based on the TCLP test ([Pb] > 5 mg/L).

As discussed earlier, a number of factors affect contaminant behavior which in turn affects leaching. Wadanambi et al. (2008) used the TCLP and the synthetic precipitation leaching procedure (SPLP) to examine leaching from LBP, where samples were obtained from a military barrack at Fort Ord, California (LBP-A) and a can of metal primer that contained red lead pigment (LBP-B). Results revealed that leached concentrations were dependent on pH as using the TCLP (pH $\leq$ 5.51) they were 5 - 25 times greater than those observed using the SPLP (pH $\geq$ 5.65). In addition, the substrate impacted the degree to which leaching occurred: drywall > wood > steel > concrete. Yet, the average lead concentration leached for all substrate conditions except concrete exceeded the TC limit for Pb (5 mg/L); the most significant factor was that of pH.

With TCLP, wastes are classified as hazardous or non-hazardous. However, this procedure requires collecting representative samples in the field, conducting the TCLP study in the lab, and analyzing samples with either inductively coupled plasma mass spectrometry (ICP-MS) or AAS. Therefore this method requires lengthy periods of time

and effort. Should an onsite classification method be feasible, significant time and costs may be saved.

2.4.2 Correlations Observed between XRF Results and TCLP or SPLP Analysis

A number of studies have found correlations between the TCLP test results and total concentrations of lead (Cao et al., 2003; Sun et al., 2006; Isaacs, 2007). Cao et al. (2003) found a linear relationship between total Pb (from digestion) and TCLP-Pb when studying the weathering of lead bullets and their environmental effect at outdoor shooting ranges. To assess the toxicity of heavy metals in contaminated soils located in a lead–zinc mine, Sun et al. (2006) measured concentrations of Cu, Zn, Pb, and Cd in soils. The resulting correlation between extractable Pb by TCLP test and total Pb measured by ICP-MS on digested samples was statistically significant ($r^2 > 0.96$). Isaacs (2007) studied lead leaching from soils and observed a significant correlation between TCLP results and total lead measured by ICP-MS on digested soil samples less than 75 μm ($r^2 = 0.82$, $P << 0.001$, $n = 13$).

NJDEP (2008) provided guidance for the use of the SPLP procedure to develop site-specific impact to ground water soil remediation standards (Figure 2.1). A linear regression was developed between contaminant concentrations in soil and leachate. Similarly, Florida Department of Environmental Protection (FDEP) (2009) provided guidance intended to address application of SPLP results in establishing site-specific regulatory limits for lead in soil. Specifically, paired results for total soil contaminant concentrations versus SPLP for each sampling location were obtained. To ensure lead concentrations would be below the groundwater cleanup target level (GCTL)

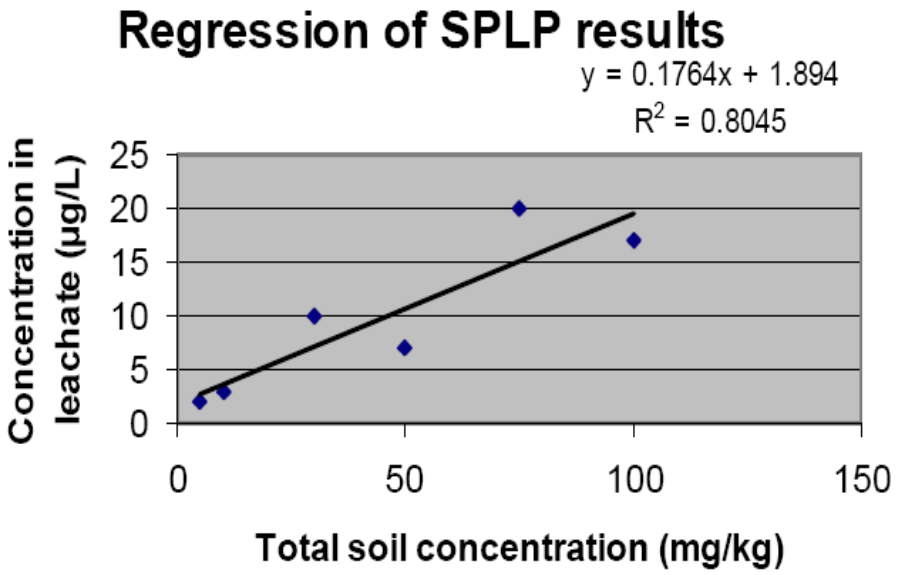

Figure 2.1 Relationship between contaminant concentration in soil and in leachate. Source: (NJDEP, 2008)

(drinking water standard), which is 15 μg/L in Florida, the estimated threshold based on the set of soil sampling data was approximately 250 mg/kg (Figure 2.2). This limit has since (FDEP, 2009) been recommended to guide remedial actions or design a risk-based approach to prevent groundwater contamination above drinking water standards. Clearly, because reliable correlations have been found between the total and leachable metal concentrations, the potential to perform direct, in situ hazardous waste classification of paint waste exists. As such, leaching studies may not be necessary and use of the FP-XRF instruments may be further advanced. In this work, a correlation between concentrations measured with FP-XRF and TCLP was investigated to achieve in situ hazardous waste classification.

However, a number of studies found that the presence of iron greatly reduced metal leaching from paint (Appleman, 1992; Bernecki et al., 1995; Smith, 1993) and other wastes (Cornelis et al., 2008; Kendall, 2003; Komárek et al., 2013). Smith (Smith, 1993) reported TCLP (U. S. EPA, 1992) results from LBP where leached concentrations of Pb averaged 70 mg L^{-1}. After the use of steel grit in removing paint, concentrations decreased to less than 5 mg L^{-1} (U. S. EPA, 1992). Bernecki et al. (Bernecki et al., 1995) hypothesized that iron reduced the lead in the paint waste to the less soluble metallic form. Yet the study did not include analyses to evaluate lead speciation. Other mechanisms may be more plausible such as sorption of Pb to iron oxides formed on the steel surfaces (Cornelis et al., 2008; Komárek et al., 2013; Zhou and Haynes, 2010). Iron oxide coatings are important interfaces affecting the fate of the trace metals because of their high surface area, strong affinity for metals, and the large sorption capacity (Cornell and Schwertmann, 1996). Cornelis et al. (Cornelis et al., 2008) reviewed the leaching

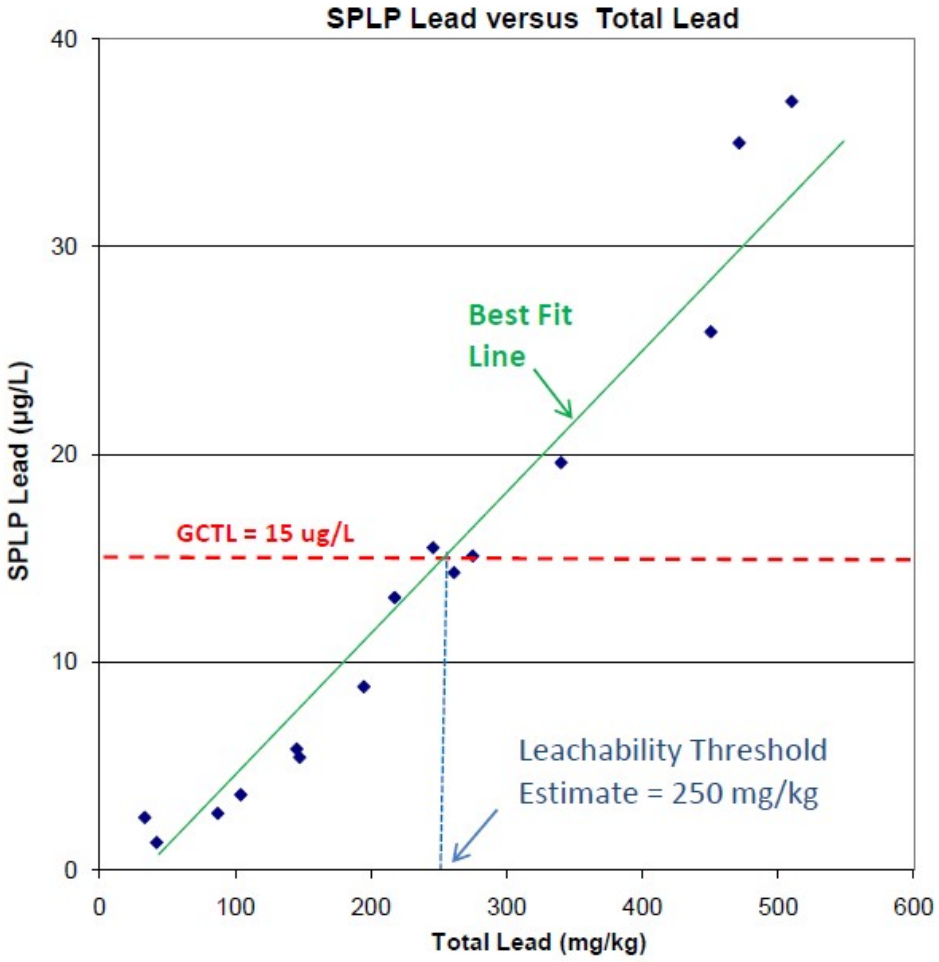

Figure 2.2 Relationship between the SPLP lead and total lead in the soil. Source: (FDEP, 2009).

mechanism of metal species in alkaline solid wastes including incinerator bottom ash, fly ash, and metallurgical slags. They found that adsorption to amorphous Fe and Al oxides is significant in weathered wastes and consequently reduced metal concentrations in the leachate. Nonetheless, because steel grit is used as abrasive blasting material during bridge rehabilitation, lead and other metals will be sequestered during the leaching procedure. Therefore, the long term mobility of the paint waste is investigated in this research using multiple extraction procedure (Esakku et al., 2008; Townsend et al., 2004) and the phases metals are associated with are addressed with sequential extraction (Davranche and. Bollinger, 2000; Pagnanelli et al., 2004).

2.4.3 Methods Used to Address the Long-term Metal Mobility of Trace Metals

MEP (U.S. EPA, 1986) was designed to simulate leaching of waste from repetitive events of acid rain in a landfill. The method is intended to simulate 1,000 years of freeze and thaw cycles and prolonged exposure to a leaching medium. This method involves an initial extraction with an acetic acid (CH_3COOH) solution (the pH of the solution maintained less than 5 through addition of 0.5 N CH_3COOH) (Method 1310B) (U. S. EPA, 2004) and then at least nine successive extractions with a synthetic acid rain solution (sulfuric/nitric acid [H_2SO_4/HNO_3] adjusted to an initial pH 3). Each extraction is conducted for 24 hours under completely mixed conditions. The repetitive extractions reveal the leachable concentrations in a simulated natural environment. One advantage of the MEP over the TCLP is that the MEP gradually removes excess alkalinity in the waste. Therefore, the leaching behavior of metal contaminants can be evaluated as a function of decreasing pH, which increases the solubility and mobility of metal cations.

A limitation of the MEP method is the lack of the mechanistic information on how the metal contaminant is associated with the solid. In a number of studies, the MEP test has been applied to investigate the long-term mobility of the waste. Esakku et al. (2008) assessed the leaching potential of select metals comparing total acid digestion (AD) with the MEP, TCLP, and a Canadian equilibrium leach test (ELT) (Environmental Canada and Alberta Environmental Centre [ECAEC], 1986). Results from the MEP approach revealed that leaching increased one to two orders of magnitude as compared to the TCLP. In addition, the extraction efficiency decreased in the following order: MEP > TCLP > ELT. To assess the toxicity and long-term stability, Shanmugamathan et al. (2008) conducted the TCLP and MEP on copper slag samples from an Indian copper plant. Results revealed that although the leachable metal concentrations (Pb and Zn) from the MEP test are greater than those from TCLP, the leached concentrations over the nine extraction cycles did not exceed the TC levels for the target metals. Based on these results, Shanmugamathan et al. concluded that the metals in the slag are not labile and would not be expected to leach under acid rain conditions.

While TCLP and MEP simulate leaching under landfill conditions, SEP subjects a sample to an extractant where a phase is dissolved. This extraction provides an estimate of the potential phases metals may be associated within the system (Tessier et al., 1979; Quevauviller, 1998; Filgueiras et al., 2002). SEP was developed in the 1970s for studying metal behavior (Gibbs, 1973; Shuman, 1979; Stover et al., 1976; Tessier et al., 1979). The number of steps and operationally defined phases in SEP schemes vary between three (Quevauviller et al., 1994; Rauret et al., 1999; Silviera and Sommers, 1977) and nine (Krishnamurti and Naidu, 2000, 2002; Miller et al., 1986b; Heron et al., 1994)

according to preferences and purpose. One of the more commonly used procedures (Tessier et al., 1979) isolates how the metal is associated with mineral, organic, and residual phases. Five fractions of increasing stability are isolated in the procedure: ion exchangeable, carbonates, adsorbed to iron and manganese oxides, bound to organic matter, and residuals, with estimated uncertainties up to 10%. Another procedure is the BCR which was developed by the Standards, Measurements, and Testing (SM&T) programme (Rauret et al., 1999). The procedure isolates three metal fractions, acid extractable (exchangeable and bound to carbonates), reducible (bound to iron and manganese oxides), and oxidizable (bound to sulfides and organics) (Rauret et al., 1999; Kartal et al., 2006). Sutherland and Tack (2002) found uncertainty in an optimized BCR procedure is typically 15%. The main difference between Tessier and BCR is that the former was designed to extract elements from specific phases, including exchangeable, carbonates, oxides, and sulfides/organic matter. The BCR method was not designed to attack specific phases, but rather to examine the potential for trace metal release under environmental conditions (ion exchange, reduction, and oxidation).

2.5 Modeling Applied for Metal Mobility

Because steel grit is used as abrasive blasting material during bridge rehabilitation, lead and other metals will be sequestered during the leaching procedure. Therefore, a more complex model is needed to address this condition. Modeling metal leaching and mobility have traditionally involved mechanistic models, such as the diffuse layer model (DLM) (Dzombak and Morel, 1990) applied when iron oxides are significant. Other theoretical and empirical models have also been invoked in a number of studies. Because

of the need to use field-based data in addressing waste classification, a statistical modeling is introduced and reviewed with principal components analysis (PCA).

Metal leaching from waste occurs primarily by two mechanisms (a) surface reactions (adsorption/desorption and/or surface precipitation) from the associated matrix, and (b) precipitation/dissolution. A number of researchers have demonstrated that the metal sorption to the Fe and Mn oxides is the rate limiting step for metal leaching from soil and cement-based solidified wastes (e.g., Tiruta-Barna et al., 2001; Karamalids and Voudrias, 2008; Dijkastra et al., 2009). Surface complexation models have successfully described metal leaching from the heterogeneous iron oxide surface, such as soil (Vithanage et al. 2013; Jing et al., 2006), steel slag (Apul et al. 2005), and weathered waste (Meima and Comans, 1997; 1998; Kendall, 2003). Kendall (2003) applied diffuse layer model (DLM) to investigate the potential leachability of Pb, Cu, and Zn from the foundry sand wastes. Comparing precipitation and sorption modeling with experimental data, Kendall further demonstrated that sorption is a more significant factor over the pH range of 3 to 8. Furthermore, by using DLM, Vithanage et al. (2013) successfully modeled Sb(V) adsorption on the heterogeneous iron-oxide-rich red earth soils. In addition to adsorption/desorption, Meima and Comans (1997; 1998) and Apul et al. (2005) found that surface coprecipitaion may also play an important role in metal leaching. Mechanistic models (such as DLM) provide a mathematical form of the equilibrium reaction based on mass balances of the species present and surface charge effects (Bradl, 2004). However, because this approach requires water chemistry conditions and species present, mechanistic models in general are more complex. Therefore, both mechanistic and empirical modeling are considered when addressing experimental data (e.g., Sauvé et

al., 2000; Lofts et al., 2004).

The empirical model is a posteriori form observed from adsorption data. For determining a good fit of experimental data a mathematical form is chosen that is as simple as possible and the number of adjustable parameters is kept at a minimum. Simple empirical models may be extended by considering additional mechanisms such as competition for sorption sites or heterogeneity of solid phase (Bradl, 2004). A number of researchers have used the theoretically-based Langmuir (e.g., Pierce and Moore, 1980; Padmanabham, 1983; Jackson and Inch, 1989; Kooner, 1993; Kanungo, 1994; Lee et al., 1996; 1998; Sauvé et al., 2000) and empirical Freundlich models (e.g., Dzombak and Morel, 1986; Mishra and Tiwary, 1995; 1998; Mishra et al., 1997; Christophi and Axe, 2000; Vaishya and Gupta, 2004) to describe equilibrium adsorption (Figure 2.3).

Because of the heterogeneity of the paint waste, one approach considered is based on the Freundlich isotherm (Eq. (1)):

$$\text{(adsorbed metal)} = K\,(\text{dissolved metal})^{n} \qquad (1)$$

where K is a function of adsorption energy and temperature and is a measure of adsorptive capacity; n determines intensity of adsorption. Several studies (Mcbridge et al, 1997; Sauve et al., 2000; Lofts et al., 2004) have introduced multivariate regression equations to predict Freundlich parameters K and dissolved concentrations from bulk soil properties. Buchter et al. (1989) measured Freundlich parameters (K and n) for 11 different soils and 15 trace elements. They also explored the correlation of Freundlich parameters with select soil properties and found that pH, cation-exchange capacity (CEC), and iron/aluminum oxide concentrations were the most important factors that correlated

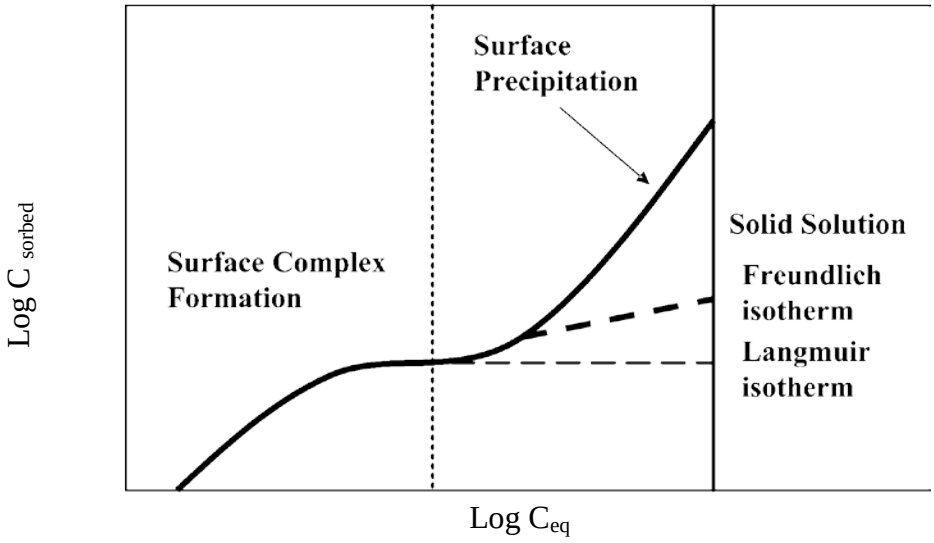

Figure 2.3 Classification of adsorption isotherms, adopted from Bradl and Hubbard (2002).

with K. Sauve et al. (2000) modeled the dissolved concentration of Cd, Cu, Ni, Pb, and Zn in soil solutions from a variety of contaminated soils. They found that K was dependent on pH, total metal concentrations (for Zn and Pb) (Eq. (2)), and soil organic material (for Cd, Cu, and Ni) (Eq. (3)). They further developed the model (Eq. (4)) for system studied. However, in these models, Sauve et al. (2000) did not include the specific oxides or clays in the soil.

$$\text{Log } K = a + b \cdot pH + c \cdot \log(\text{total metal}) \quad (2)$$

$$\text{or Log } K = a + b \cdot pH + c \cdot \log(\text{soil organic material}) \quad (3)$$

$$\text{Log (dissolved metal)} = a + b \cdot pH + c \cdot \log(\text{total metal}) + d \cdot \log(\text{soil organic material}) \quad (4)$$

Necessary variables in such regressions are the soil pH and the geochemically active species, which involves exchange with the soil solution and hence controls the dissolved concentration. The following general expression highlights important conditions:

$$\text{Log (dissolved metal)} = a + b \cdot pH + c \cdot \log(\text{total metal}) + d \cdot \log(\text{binding sites}) \quad (4)$$

The objective of this study is to use metal concentrations obtained with the FP-XRF to predict metal leaching and namely waste classification for the paint waste. From the preliminary results (Chapter 6), iron oxides in the paint waste were observed to be important surfaces for controlling the degree of metal leaching from the paint waste. Therefore, total Fe is applied and reflects the presence of iron oxides in the model. A fraction of metal was also observed to be associated with carbonates in the paint waste, which may be due to the application of calcite ($CaCO_3$) (12% by wt in the paint waste; Chapter 6) as an extender (supplementary pigments) in the paint. In fact, the dissolution of calcite ($CaCO_3$) will also affect the pH of the system during the leaching procedure. Consequently, total Ca is expected to be an important variable in the model. Other groups

of metals such as Zn and Ti present at elevated concentrations in the paint waste may be important variables in the model accounting for their potential influence on metal leaching in competitive adsorption and their function as binding site.

Based on the above discussion, metal leaching (the release of trace metal cations or anions into the aqueous phase) is expected to depend on a number of variables including (a) total metal concentration; (b) $CaCO_3$; (c) Fe concentration; and, (d) other groups of metals such as Zn and Ti present at elevated concentrations. The modeling approach to predict trace metal leaching in paint waste involved a statistical analysis as follows:

(i) Multivariate regression is tested in the first step of modeling.

$$\text{Leached metal} = a + b\cdot(\text{total Ca}) + c\cdot(\text{total Fe}) + d\cdot(\text{metal}_{i,\text{total}}) + e\cdot(\text{metal}_{i+1,\ \text{total}}) + \ldots + n\cdot(\text{metal}_{n,\ \text{total}})$$

(ii) Box-Cox transformation (Kutner et al., 2005) is applied according to the residual analysis if necessary, where leached metal y is transformed to y^{λ}:

$$(\text{Leached metal})^{\lambda} = a + b\cdot(\text{total Ca}) + c\cdot(\text{total Fe}) + d\cdot(\text{metal}_{i,\text{total}}) + e\cdot(\text{metal}_{i+1,\ \text{total}}) + \ldots + n\cdot(\text{metal}_{n,\ \text{total}})$$

(iii) Transformed models:

$$\text{Log (leached metal)} = a + b\cdot\log(\text{total Ca}) + c\cdot\log(\text{total Fe}) + d\ \log(\text{metal}_{i,\text{total}}) + e\cdot\log(\text{metal}_{i+1,\ \text{total}}) + \ldots + n\cdot\log(\text{metal}_{n,\ \text{total}})$$

where leached metal is in mg L^{-1}, a-n are coefficients determined using regression with appropriate data sets, and total metal is in mg kg^{-1} based on FP-XRF. The adsorption capacity is a function of iron oxides in the paint waste, which is represented by total Fe in the equation. Total Ca represents the calcite ($CaCO_3$) applied in the paint, which may also

affect the pH (and alkalinity) during leaching, and $Me_{i,total}$ represents the other groups of metals in the paint waste that may affect the metal leaching.

However, if all the potential variables are considered, there will be more than ten variables in the model. Therefore, it is necessary to sort the samples based on the factors that affect the metal leaching significantly. In this study, PCA was applied to identify the important factors and the potential variables in the model. PCA is a classical technique based on linear algebra. The analysis involves a mathematical procedure that transforms a number of possible correlated variables into a smaller number of uncorrelated variables called principal components (PCs) (Torrecilla et al., 2009), which are linear combinations of the original variables. The principal components account for as much of the variability in the data as possible, and each succeeding component accounts for as much of the remaining variability as possible. PCA is mainly used for key factors that explain the majority of variation within the data.

2.6 Summary of Literature

Studies of paints on bridges, buildings, and houses indicate that: 1. Lead in paint surface or subsurface layers exceed 5,000 ppm (mg/kg); 2. Zinc has been observed at elevated concentrations; 3. Cadmium is not routinely observed at detectable concentrations; and, 4. Selenium and silver were not generally used. During aging and weathering, paints tend to chalk, chip, flake, and otherwise deteriorate, resulting in an accumulation of lead and other contaminants in soils or surface water surrounding painted structures. Furthermore, during maintenance, reconstruction, rehabilitation, and demolition of bridges and other steel structures, solid waste and wash water are generated on-site. FP-XRF and portable

spectrophotometers maybe effective tools for assessing metal concentrations and characterizing waste as well as wash water. In addition, based on the literature review, reliable correlations have been found between the total and leachable metal concentrations in soil; the potential to perform direct, in situ hazardous classification of paint wastes exists. As such, leaching studies may not be necessary and use of the FP-XRF instruments may be further advanced. However, because steel grit is used as abrasive blasting material during bridge rehabilitation, lead and other metals will likely be sequestered during the leaching procedure. Therefore, the long term mobility of the paint waste is investigated in this research using MEP and sequential extraction procedure. Furthermore, modeling metal leaching and mobility have traditionally involved mechanistic models, such as the equilibrium DLM applied when iron oxides are significant. Other theoretical and empirical models have also been invoked in a number of studies. Because of the need to use field-based data in addressing waste classification, a statistical model using data from the FP-XRF is introduced with PCA. In the next section, the methodology is presented and followed by the associated results and discussion.

CHAPTER 3

OBJECTIVE AND HYPOTHESES

Based on the literature review, reliable correlations have been found between the total and leachable metal concentrations, the potential to perform direct, in situ hazardous classification of paint wastes exists. As such, leaching studies may not be necessary and use of the FP-XRF instruments may be further advanced. However, because steel grit is used as abrasive blasting material during bridge rehabilitation, lead and other metals will be sequestered during the leaching procedure. Therefore, a more complex model is needed to address this condition, where pH, iron concentrations, and metal concentrations will be addressed. Therefore, the objectives of this research are to:

- Evaluate the effectiveness of the FP-XRF to reliably characterize the hazardous nature of the paint waste.
- Quantify the degree to which steel grit remains with waste, which affects metal leachability.
- Investigate the short-term and long-term mobility of the trace metals from the waste by using TCLP, MEP, and SE.
- Evaluate the mechanisms responsible of metal leaching from the paint waste in the presence of steel grit during bridge rehabilitation.
- Develop a model that can predict the leachability of lead and other trace metals in paint waste from bridge rehabilitation using field portable techniques.

The following hypotheses are proposed:

- FP-XRF provides accurate concentrations for measuring the total metal and metalloid concentrations (RCRA metals as well as zinc and Fe) in paint waste; it can be used for more than screening.
- Because steel grit is used for blasting bridges to remove paint, metals such as Pb and Cr in the paint waste are sequestered by steel grit. Specifically, lead and other metals are sorbed to iron oxides formed on the steel grit surface.
- A model can be developed to predict the classification of a paint waste based on correlating data from laboratory studies and field portable analyses.

In the following chapters, methods to achieve the objectives and corresponding results are presented.

CHAPTER 4

SAMPLING APPROACH

In this chapter, quality assurance and quality control procedures (QA/QC) are reviewed first. Identification of the study sites is then reviewed in term of statistical number of representative bridges sampled and the representative number of samples from each bridge. Non-invasive analytical methodology is discussed and the NITON XLp-300 FP-XRF analyzer is involved. Lastly, the field sampling protocol is reviewed in terms of selecting representative samples of the paint and wash water from each bridge.

Based on sample size estimation and the project budget for travel, 24 bridges were randomly chosen from those have been repainted after 1989 (Figure 4.1). A total of four wash water samples, two filtered and two unfiltered, were collected from two random locations for each bridge site selected. Duplicate paint waste samples were collected from five random locations (or drums) for each bridge under rehabilitation and evaluated in this project.

4.1 Quality Assurance and Quality Control (QA/QC) Procedures

QA/QC procedures were based on Standard Methods for the Examination of Water and Wastewater (Eaton et al., 2005) as well as on the American Society for Testing and Materials (ASTM, 1990) methods. Milli-Q Type Π de-ionized water was employed in all experiments. All reagents were of certified analytical grade or trace metal quality. Glassware, plastic-ware, and associated materials were washed initially with a detergent, rinsed with tap water, and then with deionized water. For metals analysis, containers were

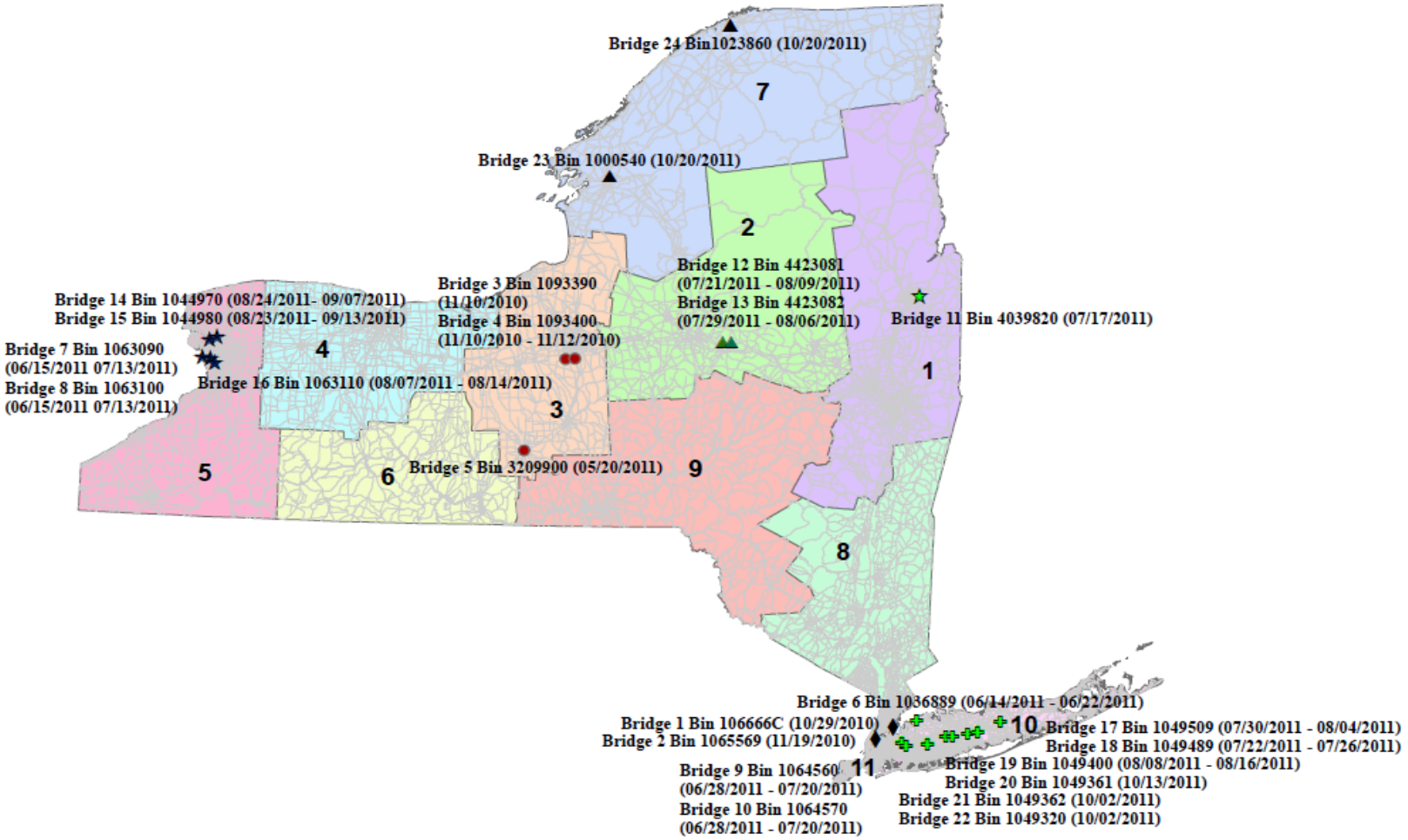

Figure 4.1 24 bridges under rehabilitation were selected between 2010 to 2011 from Regions 1, 2, 3, 5, 7, 10, and 11, where NYS are divided into 11 regions. All bridges in the study had been repainted at least once since 1989, when NYS prohibited the commercial use of LBP.

soaked in a 10% HNO_3 solution for 2 days when using glassware and 1 day for high density polyethylene (HDPE). Subsequently, all materials were rinsed in de-ionized water and stored in a particle-free environment. Paint samples were collected from bridge locations determined in the field. Tools were cleaned following QA/QC procedures. For each sample, new powder-free latex gloves (acid resistant) were worn to prevent cross contamination. Samples were stored in coolers maintained at a temperature of 4°C.

4.2 Sample Sites Estimation

Approximately 4,500 bridges are in need of rehabilitation in the New York. To obtain a statistically representative number of samples for the study, statistical methods were used for the approach using sample size estimation and a representative number of samples from each bridge was determined.

4.2.1 Sampling Theory

Sample size determination is an important step in planning a statistical study. One of the most popular approaches to sample-size determination involves applying hypothesis testing (Mathews, 2010; Ryan, 2013). The approach includes the following elements (Figure 4.2):

- Type I Error (α): Probability of rejecting the null hypothesis (H_0) when it is true. A Type I Error is the probability of alpha (α) in rejecting a true null hypothesis.
- Type II Error (β): Probability of not rejecting the null hypothesis (H_0) when it is false.
- Power = 1 - β: Probability of rejecting the null hypothesis when it is false.

		Hypothesis	
		H_0	H_1
Decision	H_0	Correct acceptance	Type II Error β
	H_1	Type I Error α	Correct rejection

$H_0: \mu \leq \mu_0$ $H_1: \mu > \mu_0$

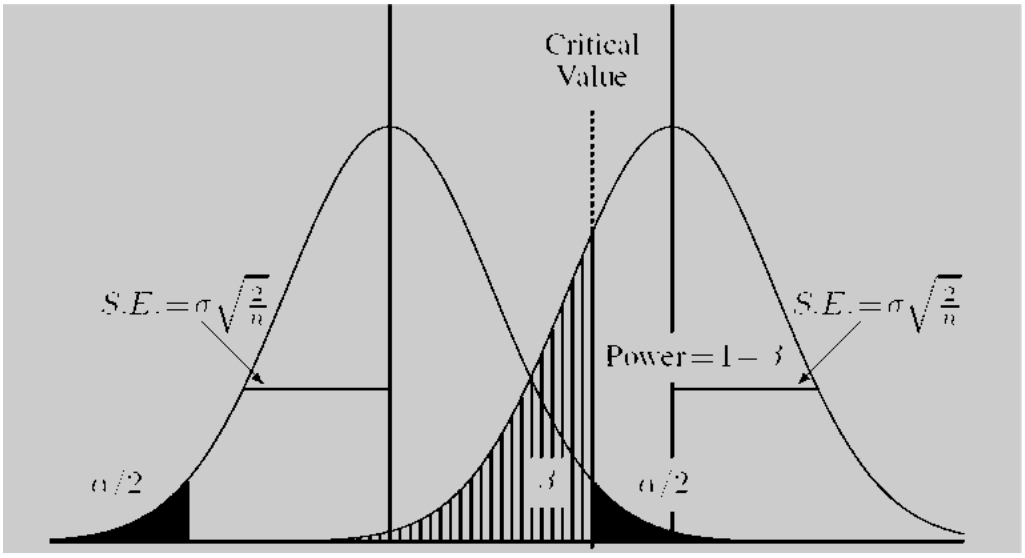

Figure 4.2 Type I Error (α), Type II Error (β) and sample size n.
(adopted from Belle, 2008)

- σ_0 and σ_1: Variances under the null and alternative hypotheses (may be the same).
- μ_0: Mean under the null and alternative hypotheses.
- μ_1: Mean under the expected data.
- n: Sample size.

A Correct Decision I occurs when we fail to reject a true null hypothesis; it has a probability of 1- α. A Correct Decision II occurs when we reject a false null hypothesis. The purpose of the experiment is to provide the occasion for this type of decision. The probability of this situation is 1- β and is known as the power of the statistical test. In other words, the ability of a test to reject null hypothesis when it is false (Figure 4.2).

For continuous measurements, the normal distribution is the default model, the hypotheses and expected data distributions are both normal and only differ by a shift in the mean. Specifically,

$$\bar{x} \propto N(\mu_0, \frac{\sigma^2}{n}) \quad \textbf{(5)}$$

$$\bar{x} \propto N(\mu_1, \frac{\sigma^2}{n}) \quad \textbf{(6)}$$

For a given test, α is assigned by the investigator in advance of performing the test. This value is a measure of the risk acceptable in rejecting a true null hypothesis. On the other hand, β may assume one of many values. Suppose we test the null hypothesis that some population parameter is less than or equal to some specified value, if H_0 is false and we fail to reject it, we commit a Type II Error. If the hypothesized value of the parameter is not the true value, the value of β (the probability of committing a Type II Error) depends on several factors (Mathews, 2010; Ryan, 2013): (1) the true value of the parameter of

interest, (2) the hypothesized value of the parameter, (3) the value of α, and (4) the sample size, n.

For a given hypothesis test we need to understand how well the test controls Type II Errors. If H_0 is in fact false, we would like to know the probability that we will reject it. The power of a test, designated 1- β is the probability that we will reject a false null hypothesis; it may be computed for any alternative value of the parameter about which we are testing a hypothesis. Therefore, 1- β is the probability that we will take the correct action when H_0 is false because the true parameter value is equal to the one for which we computed 1- β. For a given test we may specify any number of possible values of the parameter of interest and for each the value of 1- β is computed. The result is called the power function.

4.2.2 Sample Size

For a fixed Type I error (α), the goal of constructing and testing a hypothesis is to maximize power. Anderson-Cook and Dorai-Raj (2003) show how α, β, and power are related:

$$\text{Power} = P(\text{rejecting } H_0 \mid H_0 \text{ is false})$$

$$= \mathbf{P}\left(\frac{\bar{x} - \mu_0}{\sigma / \sqrt{n}} > t_a \,\middle|\, \mu = \mu_1 \right)$$

$$= \mathbf{P}\left(\bar{x} > \mu_0 + t_a \cdot \frac{\sigma}{\sqrt{n}} \,\middle|\, \mu = \mu_1 \right) \qquad (7)$$

$$= \mathbf{P}\left(\bar{x} - \mu_1 > \mu_0 - \mu_1 + t_a \cdot \frac{\sigma}{\sqrt{n}} \right)$$

$$= \mathbf{P}\left(\frac{\bar{x} - \mu_1}{\sigma / \sqrt{n}} > \frac{\mu_0 - \mu_1 + t_a \cdot \sigma / \sqrt{n}}{\sigma / \sqrt{n}} \right)$$

$$= \mathbf{P}\left(t > t_a - \frac{\mu_1 - \mu_0}{\sigma / \sqrt{n}}\right)$$

$$= \mathbf{P}\left(t > t_a - \frac{\Delta}{\sigma / \sqrt{n}}\right)$$

Power is affected by the following:

- Δ is the difference in means between the null and alternative distributions.
- n is the sample size.
- α is the probability (Type I error).

Based on the literature review developed earlier for this NYSDOT project (Chapter 2), most bridges built before 1978 applied lead based paint (Montgomery and Mathee, 2005; Falk et al., 2005; Kyger et al., 1999; Choe et al., 2002). Although the majority of the steel bridges in the New York State were constructed between 1950 and 1980, approximately 53% of these bridges have been rehabilitated and subsequently repainted after 1989 (Appendix A). As a result, lead concentrations in the paint waste are expected to be reduced. For wastes originating from abatement of non-residential structures, the U. S. EPA (1992) TCLP is used to determine waste TC concentrations (U. S. EPA, 1992). Based on resulting correlations, an objective of the project is predicting waste classification from the field data. For the purpose of determining a sample size, hypothesis testing is applied and the following assumption is used:

Bridges repainted after 1989 are tested with a one-sided test of H_0: $\mu_0 < 5$ mg/L versus H_1: $\mu_0 \geq 5$ mg/L (the mean of TCLP results is less than 5 mg/L versus greater than or equal to 5 mg/L). The hypothesis of interest will be the right-tailed hysteresis, which indicates that to reject null hypothesis, a sufficiently large sample size is needed to control the probability (power) 1- β that we will take the correct action

when H_0 is false. The purpose is to determine how large a sample (n) we need in order to realize that H_0 is false. The parameters include:

- N is 4,500 × 53% = 2,385 bridges (based on the data from NYSDOT, 53% of the bridges have been rehabilitated and subsequently repainted after 1989), large enough for continuous measurements in a Gaussian distribution (Navidi, 2006).
- Confidence intervals are typically stated at the 95% confidence level in applied practice (Zar, 1984). However, when presented graphically, confidence intervals can be shown at several confidence levels, for example 50%, 95% and 99%. In related statistical studies (Zhou et al., 2008; Lenth, 2001), the confidence level is generally targeted for 95%, which is therefore applied in this project.
- Type I Error is α, where α = 1- confidence level, which is 0.05 resulting in $t_{n,1-\alpha} = t_{n,0.95}$.
- To evaluate the lead-based paint removal waste stabilization technology, Daniels et al. (2001) apply the TCLP to assess the effectiveness of the technologies. In the study, the lead concentrations in the paint were greatly reduced by the stabilization technology: the TCLP the lead concentrations for the stabilized paint residue ranged from 0.2 – 52 mg/L. In our project, most bridges have been rehabilitated and subsequently repainted after 1989 (Appendix A), as such lead concentrations in the paint waste are expected to be reduced. Because of the similar work in this project, we assume a sample mean equivalent to that of the Daniels et al. study (2001), μ_1 = 13 mg/L.
- The studies (Daniels et al., 2001; Wadanambi et al., 2008) have shown standard deviations (SD) in the TCLP concentration ranging from 2.1 – 17.6. The average

standard deviations (SD) of the each series of data were calculated as 8.6 and 13.4 mg/L, respectively. In this project, 13.4 mg/L is assumed as the SD.

- For a given test we may specify any number of possible values of the parameter of interest (e.g.α) and for each the value of 1- β is computed. Lenth (2001) applied a range of β values to obtain a series of sample sizes. In this report, sample values of β are proposed to be 1%, 2.5%, 5%, 10%, and 20% resulting in powers, 1-β, of 80%, 90%, 95%, 97.5%, and 99%.

Because $\Delta = \mu_1 - \mu_0$, which is determined by the data (for the null hypothesis $\mu_0 < 5$ mg/L, we assume $\mu_0 = 4$ mg/L; $\mu_1 = 13$ mg/L) obtained from the previous assumption and α is fixed at 0.05, sample size n is obtained based on the following equation.

Power = P (rejecting $H_0 \mid H_0$ is false)

$$= \mathbf{P}\left(\frac{\bar{x}-\mu_0}{\sigma/\sqrt{n}} > t_a \,\middle|\, \mu=\mu_1\right) = \mathbf{P}\left(\bar{x} > \mu_0 + t_a \cdot \frac{\sigma}{\sqrt{n}} \,\middle|\, \mu=\mu_1\right) = \mathbf{P}\left(\bar{x}-\mu_1 > \mu_0-\mu_1+t_a\cdot\frac{\sigma}{\sqrt{n}}\right)$$

$$= \mathbf{P}\left(\frac{\bar{x}-\mu_1}{\sigma/\sqrt{n}} > \frac{\mu_0-\mu_1+t_a\cdot\sigma/\sqrt{n}}{\sigma/\sqrt{n}}\right) = \mathbf{P}\left(t > t_a - \frac{\mu_1-\mu_0}{\sigma/\sqrt{n}}\right) = \mathbf{P}\left(t > t_a - \frac{\Delta}{\sigma/\sqrt{n}}\right)$$

Therefore, applying α = 0.05, with varying Power = 1 - β, we generate a series of required sample sizes for bridges repainted after 1989 (Table 4.1). The larger the power, the more likely we will take the correct action when H_0 is false. Based on sample size estimation and the project budget for travel, 24 bridges were randomly chosen from those that have been repainted after 1989 (Table 4.1; Figure 4.1).

4.2.3 Representative Number of Samples from Each Bridge

Based on the above discussion, 24 bridges under rehabilitation which includes repainting

were sampled for wash water and paint waste. U.S. EPA (2003) recommends collecting two (potentially contaminated) samples to characterize threats and incidents to drinking water supplies. Therefore, in this protocol, considering the dissolved and total lead concentrations in wash water, a total of four samples, two filtered and two unfiltered, were collected from two random locations for each bridge site selected (Appendix A).

To achieve the objective of the sampling program in determining classification of waste as hazardous, the U.S. EPA (1990) has deemed that a single representative sample is sufficient. The regulations (U. S. EPA, 1990) do not directly specify what constitutes a sufficient number of samples to classify a solid waste as nonhazardous. However, for a petition to reclassify (delist) a listed hazardous waste, which includes a determination that the listed hazardous waste is not a characteristic hazardous waste (a "nonhazardous" classification), the regulations (U.S. EPA, 2006) require that at least four representative samples sufficient to represent variability or uniformity of the waste must be tested. Because the hazardous nature is not identified for the bridges that have undergone rehabilitation after 1989, at least four representative samples are needed conservatively.

Therefore, duplicate paint waste samples were collected from five random locations (or drums) for each bridge under rehabilitation and evaluated in this project, which reflects the paint waste from the bridges rehabilitated after 1989 (Appendix A).

Table 4.1 Sample Size for Bridges Repainted after 1989 (one-sided alternative hypothesis, Type I Error, $\alpha = 0.05$)

Type II Error β	Power = 1 – β	Numerator for sample size
0.5	0.5	8
0.2	0.8	15
0.15	0.85	17
0.1	0.9	20
0.075	0.925	22
0.05	0.95	24

4.3 Bridge Sampling

Protective gloves and clothes were worn during sampling and the general safety plan (NYSDOT, 2008) was adhered to at all times.

4.3.1 Wash Water Sampling Procedure

For each bridge site selected, a total of four wash water samples, two filtered and two unfiltered, were collected from two different locations. The water samples were obtained by immersion of the Nalgene® HDPE containers (1 L) into the wash water where water was allowed to run slowly into the bottle until almost full (≥ 0.75 L). The pH measurement in the field was determined with the Hach sensION 1 portable pH meter and adjustment to a pH less than 2 was accomplished using 0.1 N nitric acid (HNO_3) (Eaton et al., 2005). For dissolved lead analysis, filtration was conducted with sterilized disposable syringe filters (0.45 μm nylon membrane filters) before acid adjustment. Samples were subsequently sealed and stored for transport to the NJIT Metals Lab as described below in Section 4.3.3.

4.3.2 Paint Waste Sampling

Samples were collected in situ as well as brought back to the NJIT Metals Lab for further analysis. Duplicate paint waste samples were collected from five random locations/drums for each bridge site selected. The paint samples were obtained by using trowels where the sampled material was stored in HDPE containers that preserved the integrity of the sample. All sample bottles were labeled with the bridge bin number, the date, region, location, and bridge ID (e.g., Bin 106666C / 10/29/2010 / Region 11 / Bruckner Expressway / 11-1a).

4.3.3 Sample Preservation and Sample Storage

All sample bottle caps were sealed tightly then taped and placed into zip lock bags. For purposes of returning samples to the NJIT Metals Lab, samples were temporarily preserved in a cooler maintained at 4°C immediately upon collection. At NJIT, samples were stored in a refrigerator; preserved samples were stored up to 6 months at approximately 4 °C (U.S. EPA, 2007).

CHAPTER 5

LAB METHODOLOGY

In this section, methods used for investigating metal concentrations and distribution, characterization, metal mobility, and modeling are presented. Laboratory quality assurance and quality control procedures (QA/QC) were based on the American Society for Testing and Materials methods (American Society for Testing and Materials, 1990) Standard Methods for the Examination of Water and Wastewater (Eaton et al., 2005). All reagents were of certified analytical grade or trace metal quality. Containers were soaked in a 10% HNO_3 solution for 48 hours when using glassware and 24 hours for Nalgene® high-density polyethylene (HDPE) containers, then rinsed in Millipore-Q water, dried, and stored in a particle-free environment before use.

5.1 Total Metal Concentrations in Paint Waste and Wash Water

In the past few decades, the durability of paint applied on steel substrates has improved with the increasing usage of zinc-rich primer (Del Amo et al., 2003; Nishimura et al., 2000) and an epoxy topcoat (Borst et al., 2004; Edavan and Kopinski, 2009; Marchebois et al., 2004). Organic binders such as silicone resin (Borst et al., 2004) have also been used to reinforce corrosion resistance. Paint applied on steel surfaces has demonstrated long term corrosion resistance at approximately 22 years (half-life 11.4 years (Borst et al., 2004)). Based on the historical records (Appendix A; Table A2), bridge rehabilitation projects occur at a frequency ranging as great as 20 years reinforcing the corrosion resistance of paint coatings. Therefore the longevity of a paint formulation was not of

focus for this research. To investigate the metal concentrations and distribution in the paint waste, the application of the NITON XLp-300 series and NITON XL3t-600 series FP-XRF is presented for quantifying RCRA metals (i.e., As, Ba, Cr, Cd, Pb, Hg, Se, and Ag) along with iron and zinc in paint waste samples.

5.1.1 Analysis with NITON XLp-300 Series FP-XRF

The in situ analysis of bridge paint was conducted with a NITON XLp-300 FP-XRF analyzer, where rapid analysis was accomplished for lead assessment in units of mg/cm^2. Briefly, after self-calibration, the Pb paint mode with K-shell and L-shell detection was selected on the analyzer. When the screening results were stable, the instrument provided the lead concentrations in units of mg/cm^2. This analyzer has a 40 mCi cadmium-109 radioisotope source, which excites characteristic X-rays of the test sample. X-ray emission from a ^{109}Cd source occurs at approximately 22.5 and 88.1 keV (Table 5.1), which therefore excites the K shell fluorescent X-rays of lead. Because the excitation energy is approximately four times greater than the lower energy L shell, the resulting penetration through overlying paint layers is much greater, which enables measurement of lead in subsurface paint layers. Using an algorithm that combines both the L-shell and K-shell readings provides accuracy and precision for measuring Pb in surface or subsurface paint layers.

5.1.2 Analysis with Niton XL3t 600 FP-XRF

To investigate the metal distribution in the paint waste, RCRA metals (i.e., As, Ba, Cr, Cd, Pb, Hg, Se, and Ag) along with iron and zinc were analyzed with the

Table 5.1 Parameter for Two Types of FP-XRF

Type of XRF	Isotope-based FP-XRF XLp 300A	X-ray tube-based FP-XRF XL3t 600
Metals detected	Pb in paint mode	P, S, Cl, K, Ca, Sc, Ti, V, Cr, Mn, Fe, Co, Ni, Cu, Zn, As, Se, Rb, Sr, Zr, Mo, Ag, Cd, Sn, Sb, I, Ba, Hg, Tl, Pb, Th, U*
Excitation energy	22.5 keV and 88.1 keV	≤ 50 keV
Excitated shell	Both L and K shells	L shell only
Incorrect result		20.4% for lead
Source	^{109}Cd (22.5 KeV, 88.1 KeV)	50 keV Miniature Au Anode X-ray tube
Precision		False negative result for Pb
Limits of detection		See Tables 5.2 and 5.3
Cost of the instrument	17,000.00 41,000.00 (bundled price)	37,000.00

* – the elements are listed in order of increasing atomic number.

Source: Thermo Fisher Scientific**,** The Importance of excitation sources for X-ray fluorescence (XRF) analyzers in lead paint measurement.

NITON XL3t-600 series FP-XRF following EPA Method 6200 (U. S. EPA, 1998) using either Soil Mode (metal concentrations < 2% by wt) (Table 5.2) or Mining Mode (metal concentrations ≥ 2% by wt) (Table 5.3). The paint samples were loaded into 12 ml sample holders (SC-4331) and covered with transparent membranes. Sample analysis was carried out for 180 s. The XL3t-600 FP-XRF frame was used to support the analyzer during the detection procedure for continuous analysis. The instrument combines advanced electronics and a 50 keV X-ray tube. It is important to note that both Soil Mode and Mining Mode combine fundamental parameters (FP) mode with compton normalization (for background matrix automatic correction), which provides improved accuracy for samples ranging from less than 2% by wt to greater than 2% by wt. membranes. After the self – calibration, sample analysis was carried out for 180 s (Appendix B). The XL3t-600 FP-XRF frame was used to hold the analyzer during the detection procedure. The X-ray tube-based instruments provided however inconclusive results for Pb as often as 16% of all samples (HUD, 2003). False-positives hve been documented at 2.5% and false-negatives at 1.9% of all samples (HUD, 2003). Therefore for Pb analysis, radioisotope-based instruments that can excite both the K-shell and L-shell electrons penetrating further into the paint sample were needed to accurately identify and quantify lead in lead-based paint. For this purpose as described above, the NITON XLp-300 series lead-in-paint FP-XRF analyzer was used (Table 5.2).

Table 5.2 NITON XRF- XL3t 600 Limits of Detection for Contaminants using Soil Mode (mg/kg)

Metal	SiO_2[a] (interference free) (mg/kg)	SRM[a] (typical soil matrix) (mg/kg)
Arsenic	9	11
Barium	90	100
Cadmium	10	12
Chromium	65	85
Lead	8	13
Mercury	7	10
Selenium	6	20
Silver	10	10
Zinc	15	25

[a]The chart above details the sensitivity, or limits of detection (LOD) of Soil Mode for the XL3t 600 Series analyzer, specified for both SiO_2 matrix and a typical Standard Reference Material (SRM). The unit has a 50 keV miniature X-ray tube and multiple primary filters.

[b]Detection limits are specified following the U.S. EPA protocol of 99.7% confidence level. Individual limits of detection (LOD) improve as a function of the square root of the testing time. The LODs are averages of those obtained using bulk analysis mode on NITON XL3t 600 analyzers at testing times of 60 seconds per sample.

Table 5.3 NITON XRF- XL3t 600 Limits of Detection for Contaminants using Mining Mode (mg/kg)

Time	**60s filter**			
Matrix[a]	**Al-based matrix**	**Ti-based matrix**	**Fe-based matrix**	**Cu-based matrix**
Chromium	200	500	110	100
Iron	75	300	N/A	75
Pb	20	20	75	50
Selenium	N/A	20	20	25
Silver	N/A	N/A	N/A	N/A
Zinc	30	40	60	300

N/A = Not applicable

[a]The chart above details the sensitivity, or limits of detection (LOD) of Mining Mode for the XL3t 600 Series analyzer, specified Al-based matrix, Ti-based matrix, Fe-based matrix, and Cu-based matrix. The unit has a 50 keV miniature X-ray tube and multiple primary filters.

[b]Detection limits are specified following the U.S. EPA protocol of 99.7% confidence level. Individual limits of detection (LOD) improve as a function of the square root of the testing time. The LODs are averages of those obtained using bulk analysis mode on NITON XL3t 600 analyzers at testing times of 60 seconds per sample.

5.1.3 Wash Water Analysis

For the dissolved lead analysis, because the sample had been filtered through the 0.45 μm glass fiber filters before acid adjustment, the subsequent analysis was conducted directly using the Hach field spectrophotometer. Briefly, the DithiVer metals reagent (a stable powder form of dithizone, $C_{13}H_{12}N_4S$) reacted with lead ions in an alkaline solution to form a pink to red lead-dithizonate complex, which was extracted with chloroform. Extracted samples were then measured in the spectrophotometer at 515 nm. For total lead analysis, the samples were digested using EPA SW-846 digestion Method 3010A (U.S. EPA, 2004). Specifically, 100 ml water samples were treated with repeated addition of nitric acid and then heated until the sample was light in color or stabilized. After cooling to room temperature, 10 ml of hydrochloric acid (1:1) was added and the solution was then filtered through a 0.45 μm glass fiber filters, diluted to 100 ml with de-ionized water, and prepared for Pb analysis.

5.2 Characterization of the Paint Waste

Toxicity of metals strongly depends on their speciation in the paint waste. In this study, analysis was conducted using x-ray diffraction (XRD) and field emission scanning electron microscopy (FE-SEM) with energy dispersive x-ray spectroscopy (EDX) to investigate metal mineral forms, association, and surface morphology. The results from this study provide fundamental knowledge on the characterization of paint waste and valuable information for subsequent leaching studies.

5.2.1 X-Ray Diffraction (XRD) Analysis

Toxicity of metals strongly depends on their speciation in the paint waste. To investigate the metal forms, mineralogy was assessed using PANalytical Empyrean XRD system with a detection limit of approximately 1% by wt (Quinn, 2013). The paint waste samples were loaded in the sample holder with the back filling technique. Diffraction data were obtained by step-scans using Cu K-α radiation generated at 45 kV and 40 mA scanning from 10° to 100° 2θ. The (hkl) planes corresponding to peaks were calculated and compared with the standard powder diffraction file (PDF) (JCPDS, 1998). Primary minerals in the paint waste were evaluated in this analysis. To assess minerals of Pb, Cr, and iron oxides present and formed on the steel grit surface, PANalytical Empyrean x-ray diffraction (XRD) system was applied on the samples with the greatest concentrations of Pb, Cr, and Fe. In the interest of assessing iron oxide minerals formed on the steel grit surface, samples with the greatest concentrations of Fe were applied. Steel grit was separated from the paint waste using a magnetic bar. Fe oxide minerals were selected based on thermodynamic stability in the paint waste. Further identification was conducted by the comparing each of the diffractograms to the powder diffraction database. To isolate iron oxides formed on the steel grit surface, background subtraction (i.e., SiO_2 (silica), Zn (spelter), and Fe (martensite)) and normalization was conducted. Based on the peak and area analysis, semi-quantitative results were obtained on the composition of iron oxide.

5.2.2 Field Emission Scanning Electron Microscopy (FE-SEM) along with Energy Dispersive X-ray Micro Analyzer (EDX) Analysis

The structure of the iron oxides on the steel grit surface was investigated by FE-SEM (a resolution of 2.5 nm at 5 kV, 1.2 nm at 20 kV; and 3 nm at 1 kV). The LEO 1530 FE-SEM equipped with EDX (Inca series 200) was utilized to investigate the surface morphology and metal association with the iron oxide surface in the paint waste. For the FE-SEM, samples were coated under high vacuum with a layer of carbon using an Edward's 12E6/1266 coating unit. To avoid the effect of carbon coating, uncoated samples were prepared for EDX analysis for evaluating the surface composition of the steel grit such as Fe, and O.

5.3 Metal Mobility Studies

To investigate the leaching behavior of trace metals (such as Pb and Cr) from bridge paint waste, short-term (TCLP) and long-term leaching (MEP) studies were applied. Furthermore, sequential extraction (SE) procedure was conducted to evaluate the phases trace metals are associated with in paint waste.

5.3.1 Leaching with the TCLP

To investigate the hazardous nature of the paint waste, samples from 24 bridges were studied using the U. S. EPA Standard Method TCLP (U. S. EPA, 1992). This procedure is applied to simulate landfill conditions where the pH is lowered and volatile fatty acids (acetic acid, propionic acid, and butyric acid) are generated (Martel et al., 1997). In NYS, steel grit is blasted onto the bridge in a closed system to remove paint. As a result, the particle size of the paint waste is less than 9.5 mm and neither crushing nor grinding is

needed for the TCLP study. The procedure was performed in triplicate following U. S. EPA Standard Method 1311 (U. S. EPA, 1992) (Figure 5.1). Extractions were carried out with 20:1 extraction fluid to solid ratio in 2 L HDPE bottles at 30 ± 2 rpm for 18 hr. The pH was measured, and the extract was filtered, acidified, and analyzed with ICP-MS for the eight RCRA metals along with Fe and Zn (U. S. EPA, 2007).

5.3.2 Leaching with the MEP

MEP (U.S. EPA, 1986) was applied to address the long-term mobility of trace metals and associated metalloids in the paint wastes. This method was applied to simulate leaching of waste from repetitive events of acid rain in a landfill. In the interest of identifying the most significant impact from the five paint samples collected from each bridge, the sample with the greatest lead concentration was used. The procedure (Figure 5.2) was conducted on duplicate samples from the 24 bridges with an extraction period of 10 days where samples were collected once every 24 hours resulting in 480 samples. This method involves an initial extraction with an acetic acid (CH_3COOH) solution (the pH of the solution was maintained less than 5 through addition of 0.5 N CH_3COOH) (Method 1310B) (U. S. EPA, 2004) and then at least nine successive extractions with a synthetic acid rain solution (sulfuric/nitric acid [H_2SO_4/HNO_3] adjusted to an initial pH 3.0 ± 0.2). Each extraction was conducted for 24 hours under completely mixed conditions.

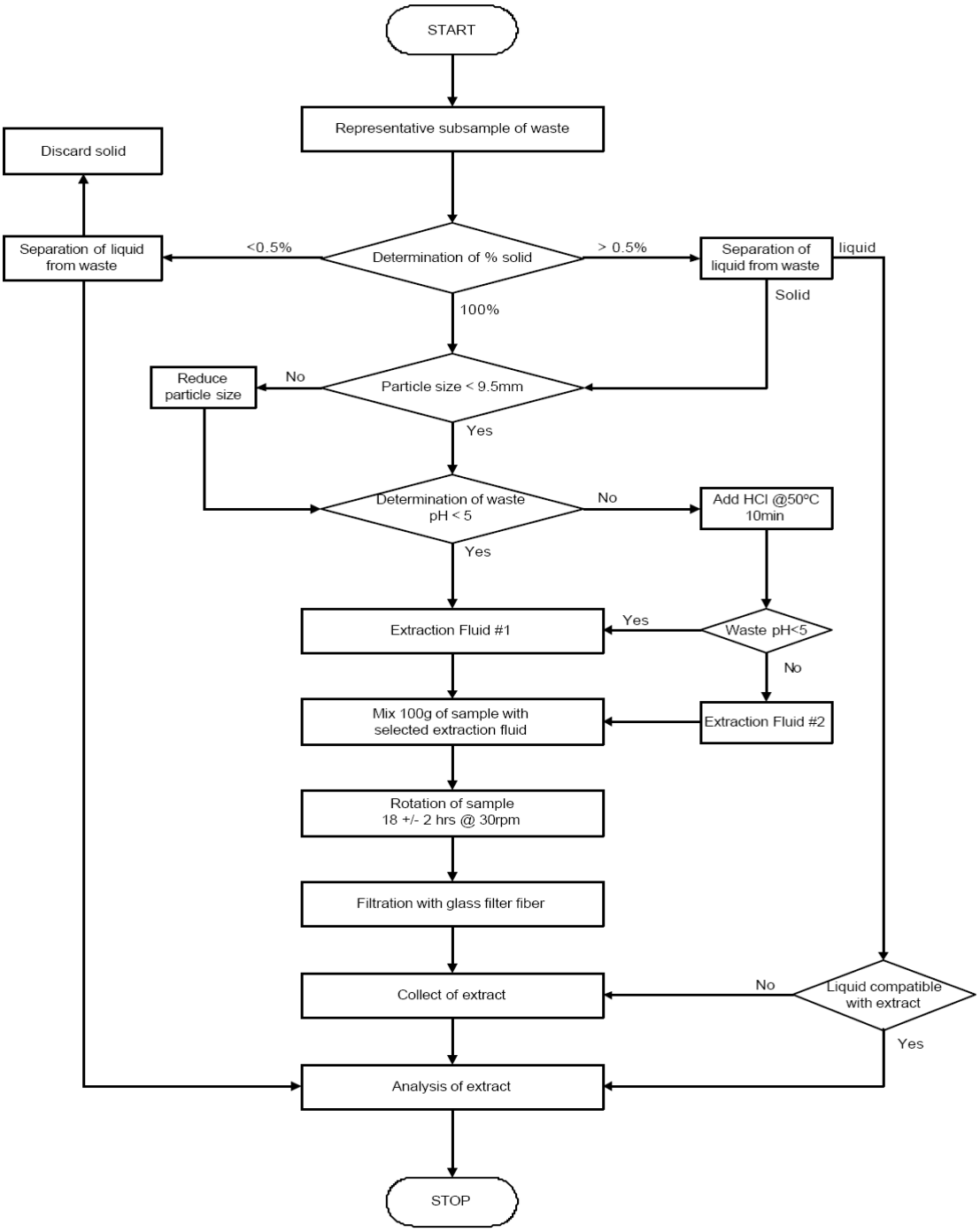

Figure 5.1 Flow Chart of TCLP Test Procedure (Method1311) (U. S. EPA, 1992).

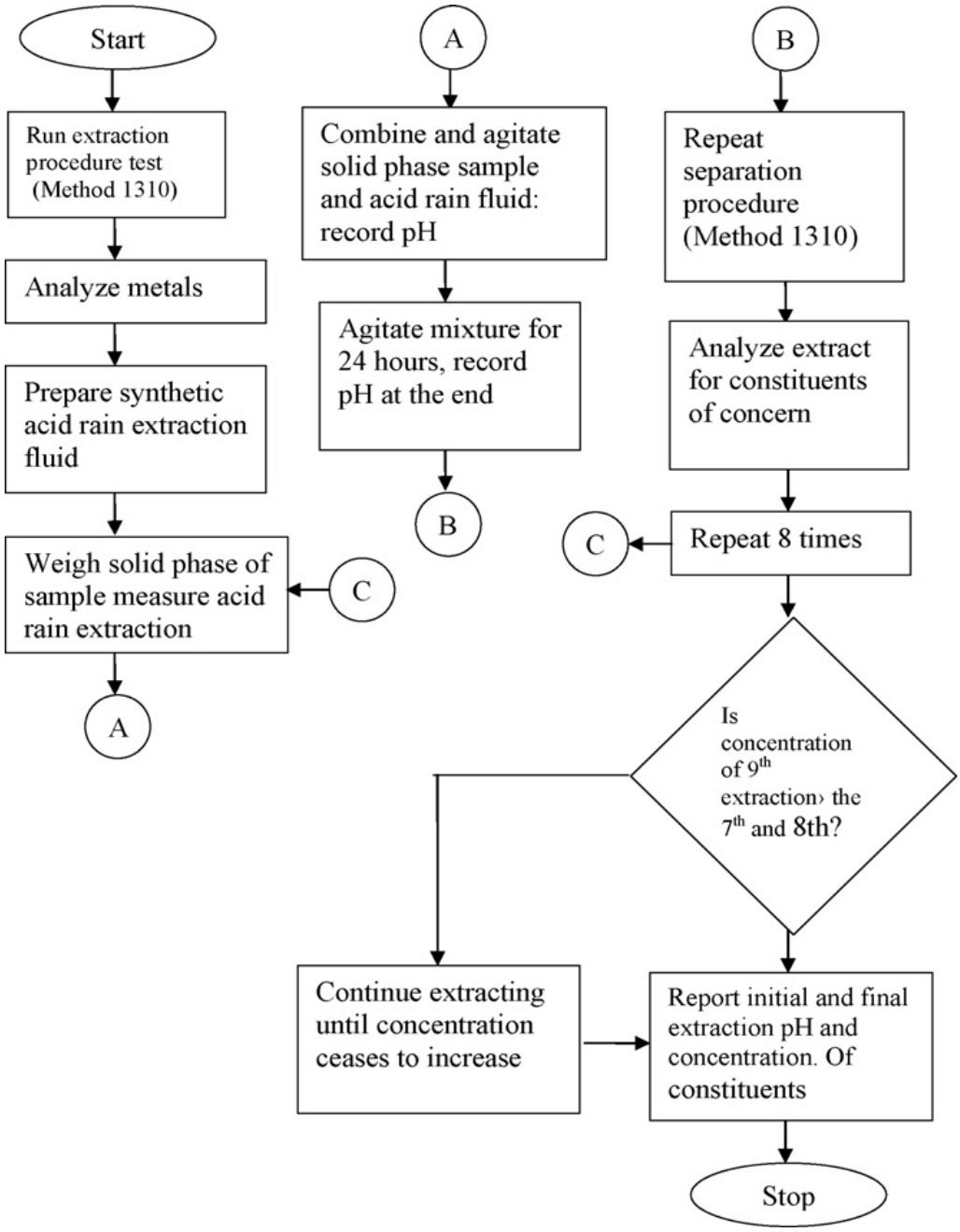

Figure 5.2 Flow Chart of the MEP Test Procedure (Method1320) (U. S. EPA, 1986).

The pH was measured, and the extract was filtered, acidified, and analyzed for metals and metalloids using ICP-MS (U. S. EPA, 2007). Remaining solids collected on the filter were used for successive extractions that simulate acid rain conditions (Method 1320) (U.S. EPA, 1986). The repetitive extractions reveal the leachable concentrations in a simulated landfill. One advantage of MEP over the TCLP is that it gradually removes excess alkalinity in the waste. Therefore, the leaching behavior of potential contaminants can be evaluated as a function of decreasing pH, which increases the solubility and mobility of metal cations. A limitation of batch and semibatch experiments including the MEP method is the lack of the mechanistic information on how the contaminant is associated with the paint waste.

5.3.3 Sequential Extraction Procedure (SEP)

While MEP and TCLP simulate leaching under landfill conditions, SE provides an estimate of the potential phases metals may be associated within the system (Filgueiras et al., 2002; Quevauviller, 1998; Tessier et al., 1979). To compare the results with other similar studies (i.e. (Davranche and Bollinger, 2000; Pagnanelli et al., 2004), extractions were conducted with the Tessier's five step procedure (Tessier et al., 1979). SE was carried out in duplicate on three samples collected from Regions 3, 10, and 11, where elevated trace metals were observed. Specifically, extractions were performed in 40 ml Sorvall® polypropylene centrifuge tubes using an end-over-end shaker rotated at 30 rpm. Between successive extractions, separation of extract from residue was carried out by centrifugation at 3,000g for 20 min. The supernatant was decanted into Naglene® HDPE bottles, acidified to pH less than 2, and refrigerated until analysis with ICP-MS. The

residues were washed with deionized water, centrifuged for 20 min, and the supernatant discarded. In Step 1, extraction for the exchangeable fraction in paint waste involved 1 M magnesium chloride ($MgCl_2$, pH 7.0) with continuous agitation; this contribution is not expected to be significant with paint waste. In the second step, carbonates were extracted with 1 M sodium acetate (CH_3COONa) adjusted to pH 5.0 with acetic acid (CH_3COOH). Continuous agitation was maintained. In Step 3, a 0.04 M hydroxylammonium chloride ($NH_2OH•HCl$) in 25% (v/v) acetic acid (CH_3COOH) solution was used to extract the fraction adsorbed to iron and manganese oxide phases from remaining residue. This step was performed at 96 ± 3°C with agitation for 6 h to reinforce the complete dissolution of the iron oxides. The hypothesis in this study is that metals in the paint waste interact with the iron oxides on the steel grit surface. Thus, this phase is expected to be significant. In Step 4, residue from Step 3 was treated at 85 ± 2 °C for 2h with 0.02 M HNO_3 and 30% H_2O_2 (adjusted to pH 2 with HNO_3). A second 3 ml aliquot of 30% H_2O_2 (pH 2 with HNO_3) was added with another 3 h of heating. After cooling, samples were diluted with 3.2 M ammonium acetate (CH_3COONH_4) solution in 20% (v/v) HNO_3. This step in the extraction is used for isolating the organic fraction. The concentration associated with the residue from Step 5 was calculated using a mass balance along with concentrations found in Steps 1, 2, 3, and 4 along with the initial total concentration from FP-XRF. The residual is assumed to represent the metals associated with minerals in the paint more difficult to digest including SiO_2 and TiO_2 (Barnes and Davis, 1996).

5.4 Modeling for the Metal Leaching

5.4.1 Surface Complexation Model

Based on the results from sequential extraction along with leaching studies, adsorption/desorption and dissolution/precipitation models were applied to consider plausible processes. Because ferrihydrite is a dominant sorbent (discussed in Chapter 7) and because of its significant adsorbent characteristics including a large surface area and high affinity for metal ions, this oxide surface was used in modeling sorption (Apul et al., 2005; Kendall, 2003). The hydrous ferric oxide (HFO) surface has low-affinity and high-affinity sites (Dzombak and Morel, 1990), represented as $Fe^{W}OH$ and $Fe^{S}OH$, respectively. The weak-affinity site density of 0.2 mol/mol Fe and the high-affinity site density of 0.005 mol/mol Fe were used in this study (Apul et al., 2005; Dzombak and Morel, 1990; Meima and Comans, 1998). Dominant surface complexes with ferrihydrite have been shown to include $FeOPb^{+}$, $FeOCrOH^{+}$, $FeOHBa^{2+}$, and $FeOZn^{+}$, (Dzombak and Morel, 1990; Jing et al., 2006; Kendall, 2003).

In this study, two models were trialed to describe the metal leaching over the pH of 4.5 to 7. Sorption onto the ferrihydrite surface was considered using the surface complexation diffuse layer model (DLM) coupled with 2-p*K* formalism. Surface acid - base reactions and equilibrium constants used in the DLM are from the compilation of studies reviewed in Dzombak and Morel (1990). Inputs such as background analyte, adsorbate, and sorbent concentrations were based on the TCLP leaching experiments, XRF analyse, and sequential extraction results (details in Chapter 7). An ionic strength of 0.1 was applied in the calculations to simulate the leaching condition considered. The second modeling approach involved precipitation/dissolution. Barnes and Davis (1996) demonstrated

$PbCO_3$ (cerrusite) (pH < 8) and $Pb_3(OH)_2(CO_3)_2$ (hydrocerussite) (pH ≥ 8) as the dominant Pb minerals in lead-based paint. In fact, the primary lead compound used in paints was white lead ($2PbCO_3 \cdot Pb(OH)_2$) with concentrations as great as 40% by wt of dry paint (Gooch, 1993). Lead chromate (chrome yellow $PbCrO_4$) was used in (colored) paint at 5 to 7% (Clark, 1976), while lead tetraoxide (red lead Pb_3O_4, Pb_2O_4, $PbO_2 \cdot 2PbO$) was also a component of paints (Clark, 1976; Gooch, 1993). Boy et al. (1995) found $Cr(OH)_3$ (chrome oxide green) as the dominant phase when they investigated chromium stabilization in paint waste with Portland cement and blast furnace slag. Jing et al. (2006) further demonstrated that $Cr(OH)_3$ and $Ca_2Cr_2O_5$ were the dominant phases when they evaluated Cr leaching behavior in the solidified soil. In this research, the solubility of the following minerals was considered: $PbCrO_4$ (lead chromate), Pb_3O_4 (red lead**),** $PbCO_3$ (cerrusite), $Pb(OH)_2$, $Pb_3(OH)_2(CO_3)_2$ (hydrocerussite), PbO (litharge), $Cr(OH)_3$ (or Cr_2O_3 chrome oxide green), Barite ($BaSO_4$), witherite ($BaCO_3$), $ZnCO_3$, and ZnO. Based on their use in paint formulations and thermodynamic stability (Baes and Mesmer, 1976; Ball and Nordstrom, 1991; Marani et al., 1995; Schecher and McAvoy, 1992; Stumm and Morgan, 1996), the following minerals were applied in this study: $PbCO_3$ (pK_{so} = 13.13) (Benjamin, 2002), $Pb_3(OH)_2(CO_3)_2$ (pK_{so} = 45.46) (Benjamin, 2002), $Cr(OH)_3$ (or Cr_2O_3) (pK_{so} = 33.13) (Benjamin, 2002), $BaSO_4$ (pK_{S0} = 8.29) (Benjamin, 2002), and ZnO (pK_{so} = 6.12) (Benjamin, 2002) (Appendix D).

5.4.2 Principal Component Analysis (PCA)

PCA is used to identify and reduce the dimensionality of data, from which a model is developed to predict metal leaching and therefore classification of the paint waste. The

analysis involves a mathematical procedure that transforms a number of potentially correlated variables into a smaller number of uncorrelated variables (principal components (PCs)) (Torrecilla et al., 2009), which are linear combinations of the original variables. The eigenvalues are used to determine the percentage as well as cumulative percentage of variances, where PCs with eigenvalues greater than 1 are selected (Kaiser, 1960). The eigenvalues reflect the quality of the projection from the N-dimensional initial table to a lower number of dimensions. The PC with the greatest eigenvalue is considered the most significant. The eigenvalues and the corresponding factors are sorted by descending order to the degree to which the initial variability is represented (converted to %). In this study, correlation-based PCA (Torrecilla et al., 2009) was applied to understand variables (i.e., As, Ba, Cr, Cd, Fe, Pb, Hg, Ag, Se, Zn, Ti, and Ca) that play a significant role in addressing total variances in the statistical model.

5.4.3 Statistical Modeling for Field Characterization of Waste Classification

Based on the PCA analysis, leaching data were subjected to multivariate statistical analyses to evaluate the effect of statistically significant variables on metal leaching. Multivariate statistical approaches such as multiple linear regression analysis (MLRA) were used to determine the significance of specific parameters among the datasets. The total metal concentrations from FP-XRF analysis were applied as inputs in the leaching models. The coefficients a-n in the model were determined by the significance of the p-value for each coefficient.

5.5 Summary

In summary, a suite of analyses were applied in this research. Metal concentrations in paint waste and wash water were evaluated by FP-XRF and field spectrophotometer. XRD and FE-SEM analyses were applied to investigate the mineralogy and morphology of the paint waste. Leachable and extracted metal concentrations were obtained by TCLP, MEP, and SE. In addition, to understand the mechanism responsible for metal leaching, mechanistic modeling (surface complexation DLM along with precipitation/dissolution modeling) was applied to support PCA of data obtained with FP-XRF. As a result, multiple linear regression analysis was employed to model the metal leaching from bridge paint waste in the presence of steel grit.

CHAPTER 6

METAL CONCENTRATIONS AND DISTRIBUTION IN PAINT WASTE GENERATED DURING BRIDGE REHABILITATION IN NEW YORK STATE

In this section, results are presented for the metal concentration, distribution, and association in the bridge paint waste. Pb concentrations in bridge wash water are reviewed as well. The results from this section provide fundamental knowledge on the characterization of paint waste and valuable information for subsequent leaching studies.

6.1 Metal Distribution in the Paint Waste (XRF Analysis)

The variability charts reflect the significant variability in metal concentrations across a single bridge (Appendix E). For example at Bridge 2-1, Pb variability ranged from 43% to 127% by wt, while Zn varied from 0.2 to 10% by wt. For the 24 bridges studied throughout NYS, one sample per bridge cannot adequately describe metal concentrations. In addition, the t-test was applied on the samples that are sorted by region . No significant difference was observed for metal concentrations between the regions studied (Region 2 and 5; Region 1, 3, 7, 10, and 11). This result indicated metal concentrations were not distributed as function as a region. Concentrations of most metals in paint ranged over several orders of magnitude (Table 6.1): 5 to 168,090 mg kg^{-1} for Pb, 49,367 to 799,210 mg kg^{-1} for Fe, and 27 to 425,510 mg kg^{-1} for Zn. Other elemental compound of As, Ba, Cr, Cd, Se, and Ag were also detected (Table 6.1): less than 11 (detection limit) to 12,678 mg kg^{-1} for As, less than 100 (detection limit) to

Table 6.1 Quartile Distribution of Trace Metals in Paint Waste from NYS (n = 117)

Metal	Metal concentrations (mg kg^{-1})									
	As	**Ba**	**Cr**	**Cd**	**Fe**	**Pb**	**Hg**	**Se**	**Ag**	**Zn**
Mean	2,906	6,431	3,018	53	244,929	46,060	73	18	28	85,530
Minimum	BDL	BDL	21	BDL	49,367	5	BDL	BDL	BDL	27
25^{th} percentile	541	2,797	490	6	133,125	9,058	BDL	BDL	BDL	32,233
Median	1,866	5,785	2,455	49	245,820	45,870	BDL	BDL	29	51,467
75^{th} percentile	5,280	9,410	5,268	88	329,765	73,693	BDL	20	48	85,458
Maximum	12,678	16,319	10,192	248	799,210	168,093	528	195	133	425,507

BDL refers to below detection limit.
Detection limits (mg kg^{-1}) for this study: As = 11, Ba = 100, Cd = 12, Cr = 85, Pb = 13, Se = 20, Ag = 10, Fe = 75, Zn = 25, Hg = 10.

16,319 mg $kg^{-1}$for Ba, 21 to 10,192 mg kg^{-1} for Cr, less than 12 (detection limit) to 248 mg kg^{-1} for Cd, less than 20 (detection limit) to 195 mg kg^{-1} for Se, and less than 10 (detection limit) to 133 mg kg^{-1} for Ag. Although used before 1992 as a preservative to control bacteria, mildew, and other fungi (U. S. EPA, 1990; 2000), Hg was only observed in three bridges up to 528 mg kg^{-1}. The observed Pb concentrations (Figure 6.1) are a consequence of its wide application as a corrosion inhibitor in paint before the 1980s (Gooch, 1993; Strivens and Lambourne, 1999). Even though rehabilitation and subsequent repainting were conducted more than once since 1989 for bridges studied in NYS, 94 out of 117 paint samples exhibited lead concentrations greater than 5,000 mg kg^{-1}, which is the an action limit from HUD (NIOSH, 1992). The elevated Fe found in samples is from a number of sources: 10 - 15% by wt of black iron oxide (Fe_2O_3 [synthetic]+ MnO_2 [pyrolusite]) is used in the paint (Boxall and Von Fraunhofer, 1980), rust forms on the bridge as well, and the most significant source appears to be the steel grit blasting abrasive (Appleman, 1992; 1997). Although contractors use a magnetic separation process to remove steel grit from paint waste, the blasting abrasive agent is not entirely removed. Typically steel (cast steel) grit is comprised by wt of Fe (> 96%), C (< 1.2%), Mn (< 1.3%), Si (< 1.2%), Cr (< 0.25%), Cu (< 0.25%), and Ni (< 0.2%) (Dunkerley et al., 1978). In New York, steel grit is typically used as the blasting abrasive (NYSDOT, 2008). Other abrasives used throughout the country include black beauty (a mixture of Fe oxide, Al oxide, Ca oxide, and silicon dioxide), boiler slag, sand, furnace slag, aluminum oxide, and garnet (Iowa Department of Transportation (IADOT), 2006; Minnesota Department of Transportation (MnDOT), 2004; U.S. EPA, 1997). The observed Zn reflects the increasing usage of Zn primer on the bridges (Strivens and Lambourne, 1999; Turner and Sogo, 2012).

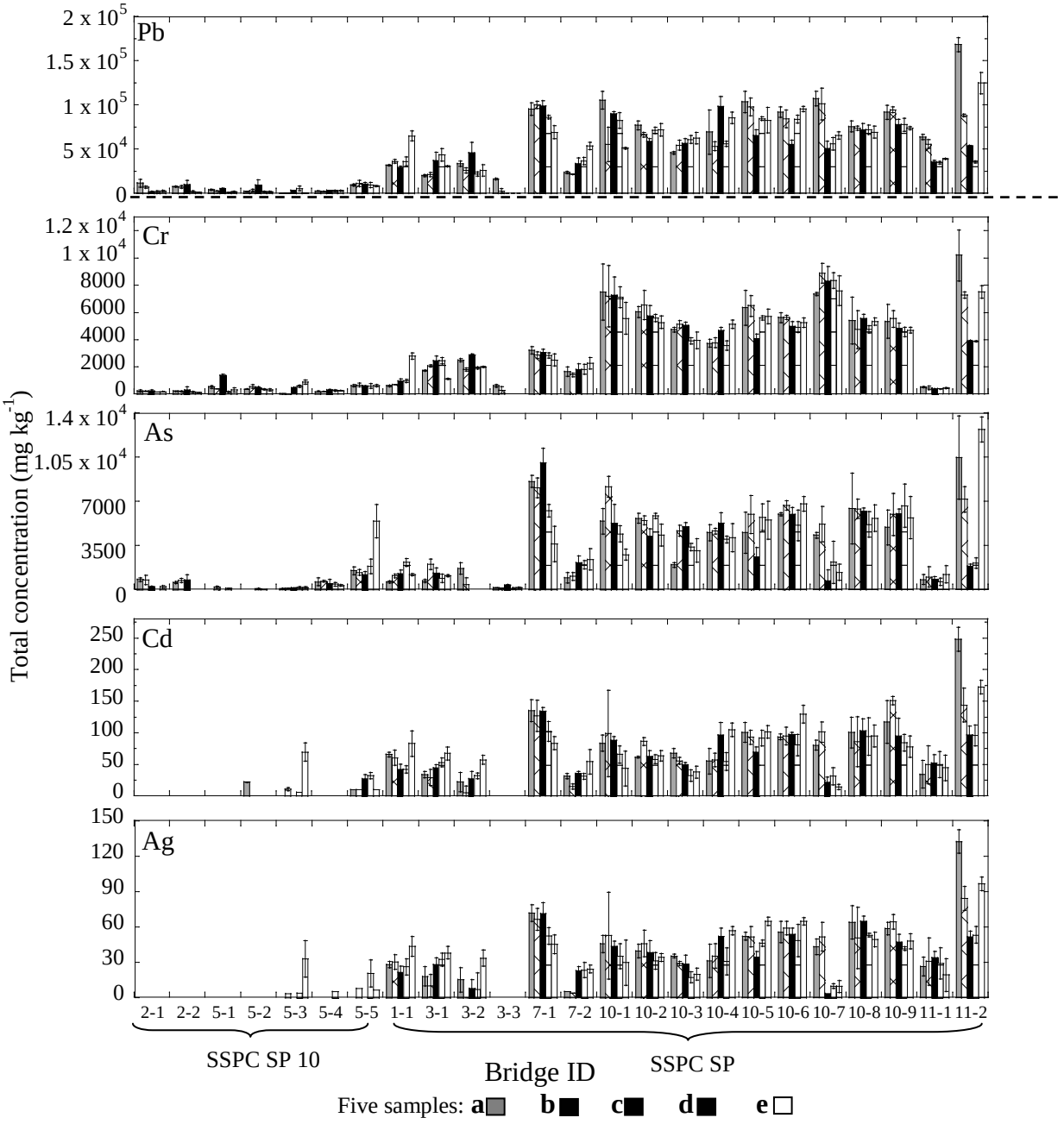

--- LBP is defined as paint with Pb concentrations greater than 0.5 % by wt (5000 mg kg $^{-1}$) (HUD, 2003).

Figure 6.1 Total concentrations of Cr, Pb, As, Cd, and Ag in paint are shown as a function of the five locations for bridges in Regions 1, 2, 3, 5, 7, 10, and 11 using NITON XL3t-600 series FP-XRF. Mode was used for sample with metal concentrations greater than 2 % by wt, while Soil Mode was applied for samples with concentrations less than 2 % by wt. Bridge ID represents the region number and bridge sampled in this region. All bridges sampled were rehabilitated after 1989. Blasting standard SSPC SP 10 was applied for bridges in Regions 2 and 5, while SSPC SP 6 were used for bridges in Regions 1, 3, 7, 10, and 11.

Overall, concentrations of Pb and Zn are consistent with the similar studies (Table 6.2) (Bernecki et al., 1995; Brumis et al., 2001; Mielke and Gonzales, 2008; Mielke et al., 2001), whereas Fe concentrations obtained in this study are greater than that observed by Bernecki et al. (1995) and Turner and Sogo (2012) (Table 6.2). The results are attributed to the elevated steel grit concentrations remaining in the paint waste, which to some extent dilutes the presence of other metals (such as Pb and Zn) in the paint. As, Cr, and Cd are consistent with or greater than the concentrations in the residential paint (Brumis et al., 2001; Mielke et al., 2001; Turner and Sogo, 2012). Because most work has focused on Pb, an analysis of Ba, Se, Ag, and Hg concentrations in paint waste has seldom been reported (Conroy et al., 1996; Mielke et al., 2001)

Interestingly, concentrations of Pb, As, Cd, Cr, and Ag in the paint waste samples follow a similar trend, while Zn, Hg, and Se appear to follow a consistent trend (Figures 6.1 and 6.2). Furthermore, greater Pb, As, Cd, Cr, and Ag were observed in waste from bridges in Regions 1, 3, 7, 10, and 11, and lower concentrations of these metals were detected in Regions 2 and 5. These results may be attributed to the paint formulation that includes pigments and extenders as well as the surface preparation methods applied on the bridges (discussed below in Section 6.2).

6.2 Statistical Analysis of the Metal Distribution and Association

To further investigate the metal distribution and association, correlations were evaluated between metals in the paint waste. Pearson's correlation matrix (Table 6.3) indicated that Pb correlated with As ($R^2 = 0.78$), Cr ($R^2 = 0.73$), Cd ($R^2 = 0.88$), and Ag ($R^2 = 0.67$) (Table 6.3). Trends with strong correlation coefficients were observed between Cd and

Table 6.2 Metal Concentrations in Paint Used on Surface Structures

Sources	Concentration of Metals in paint by dry weight (ppm)										Reference
	Pb	Hg	As	Cd	Cr	Se	Ag	Ba	Zn	Fe	
1 µm bridge paint particle	895,000	–	–	–	–	–	–	–	–	21,000	Bernecki et al., (1995)
55 µm bridge paint particle	28,000	–	–	–	–	–	–	–	868,000	30,000	
270 µm bridge paint particle	331,000	–	–	–	–	–	–	–	50,000	44,000	
Western span of the San Francisco-Oakland Bay Bridge.	42,000	–	< 500	< 2.0	< 1,900	–	–	–		–	Brumis et al. (2001)
New Orleans houses	112 – 256,797	–	–	7 - 439	2 - 417	–	–	–	52 – 98,056	–	Mielke et al. (2001)
Exterior house paint	464 – 317,151	0.8– 214.0	–	–	–	–	–	–	–	–	Mielke and Gonzales (2008)
Interior house paint	24 – 63,313	0.03– 39.2	–	–	–	–	–	–	–	–	
Exterior urban paints	4.5 - 36,900	–	BDL - 3.26	BDL – 1.00	1.9 - 775	–	–	–	39 - 23,500	196 – 54,500	Turner and Sogo (2012)
Paint waste	5 – 168,090	BDL – 527	BDL – 12,678	BDL– 248	21 – 10,192	BDL – 195	BDL – 132	BDL – 16,319	27 – 425,510	–	This study

BDL refers to below detection limit

Detection limits (mg kg^{-1}) for this study: As = 11, Ba = 100, Cd = 12, Cr = 85, Pb = 13, Se = 20, Ag = 10, Fe = 75, Zn = 25, Hg = 10.

– refers to not reported

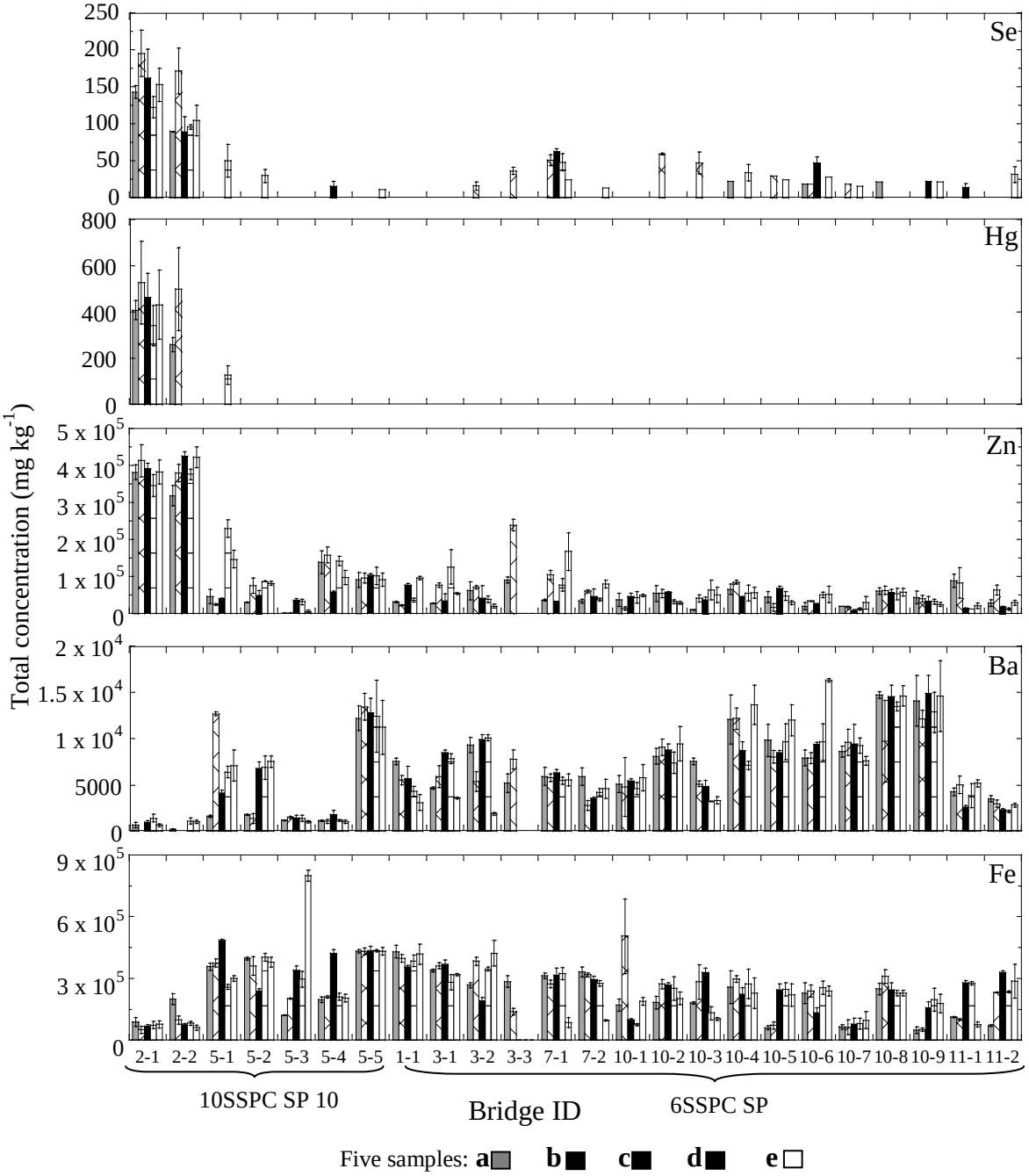

Figure 6.2 Total concentrations of Se, Hg, Zn, Ba, and Fe in paint are shown as a function of the five locations for bridges in Regions 1, 2, 3, 5, 7, 10, and 11 using NITON XL3t-600 series FP-XRF. Mining Mode was used for sample with metal concentrations greater than 2 % by wt, while Soil Mode was applied for samples with concentrations less than 2 % by wt. Bridge ID represents the region number and bridge sampled in this region. All bridges sampled were rehabilitated after 1989. Blasting standard SSPC SP 10 was applied for bridges in Regions 2 and 5, while SSPC SP 6 were used for bridges in Regions 1, 3, 7, 10, and 11.

Ag (R^2 = 0.95) as well as As and Cd (R^2 = 0.72) (Table 6.3). Furthermore, correlations were observed between Hg and Se (R^2= 0.99), Hg and Zn (R^2= 0.94), and Se and Zn (R^2= 0.76). Similar results have been reported by Bhuiyan et al. (2011), where they observed correlations between Pb and Cd (R^2 = 0.64); As and Cr (R^2 = 0.63); and, Pb and Cr (R^2 = 0.51). As a result of their findings, Bhuiyan et al. (2011) hypothesized that the paint industry may be one of the sources of contamination in the water distribution system in Dhaka, Bangladesh. In our study, the paint applied in NYS has a similar composition to that found by Turner and Sogo (2012), where As, Cr, Cd, Pb, Fe, and Znwere observed in the exterior urban paints in UK. On the other hand, correlations were not observed between Pb, Fe, and Zn concentrations (R^2 < 0.11, Table 6.3) suggesting unique sources in the paint waste. The composition of paint waste is complex and heterogeneous because of the historical application of the pigments and subsequent incomplete paint removal. To identify possible factors that affect the distribution of trace elements in the paint waste, PCA was applied.

PCA showed essentially two main constituent axes with eigenvalues greater than 1 (Table 6.4), together explaining 77.4% of the data variance. The first eigenvalue of 6.63 represents 55.3% of the total variability. This result demonstrates that if the data were illustrated with one axis, 55.3% of the total variability in the data can be explained. Correlations greater than 0.70 (Table 6.4) are considered to demonstrate significant influence. The first PC (axis) revealed strong relationships with the associated total concentration present in the waste (e.g., As, Cr, Cd, Pb, and Ag) (Table 6.4). These results are attributed to the paint formulation and the surface preparation standard applied to the bridges. The Society for Protective Coatings (SSPC) surface preparation standard

Table 6.3 Coefficient Determination (R^2) for RCRA Metals, as well as Iron and Zinc.

	Pb	Ba	Cr	Cd	Ag	Hg	Se	As	Fe	Zn
Pb	1.0									
Ba	0.17	1.0								
Cr	**0.73***	0.17	1.0							
Cd	**0.68**	0.02	0.33	1.0						
Ag	**0.67**	0.03	0.31	0.95	1.0					
Hg	0.11	0.60	0.07	0.0	0.0	1.0				
Se	0.33	0.40	0.30	0.10	0.085	**0.99**	1.0			
As	**0.78**	0.10	0.56	0.72	0.72	0.28	0.17	1.0		
Fe	0.056	0.0004	0.091	0.063	0.033	0.82	0.29	0.024	1.0	
Zn	0.14	0.10	0.18	0.011	0.0082	**0.94**	**0.76**	0.11	0.086	1.0

* – R^2 greater than 0.65 is highlighted as significant number.

Table 6.4 Principal Component Loadings of Total Metals and pH in the Paint Waste Samples

Variable	PC 1	PC 2
As	0.829	-0.433
Ba	0.658	0.429
Ca	0.655	-0.165
Cd	0.877	-0.342
Cr	0.854	-0.432
Fe	0.375	0.705
Pb	0.863	-0.448
Hg	**-0.698**	-0.477
Ag	0.886	-0.358
Se	**-0.787**	-0.518
Ti	0.297	0.665
Zn	**-0.851**	-0.418
Eigenvalue	6.63	2.64
Proportion	0.553	0.22
Cumulative	0.553	0.773

Correlation value greater than 0.70 are highlighted

SP-6 (Commercial Blast Cleaning) (NYSDOT, 2008) has been applied on bridges in New York State prior to 2006, where paint and rust from steel were removed to a remaining residual of 33% of the total removal area. After 2006, SSPC SP-10 (Near White Blast Cleaning) has been required in the blasting procedure (NYSDOT, 2008) for all regions in NY SP-10 restricts the visible residue remaining on the bridge surface to 5% of the total removal area (The surface preparation methods mentioned here refer to the ones applied in the previous rehabilitation, which determined the residual waste remaining on the bridge). Consequently, for the 24 bridges studied, 99% of the paint samples from the bridges blasted to SSPC SP-6 (Regions 1, 3, 7, 10, and 11) revealed Pb concentrations greater than the HUD limit of 5,000 mg kg^{-1} (NIOSH, 1992), while 37% of the paint samples from the bridges blasted with SSPC SP-10 (Regions 2 and 5) exhibited Pb concentrations greater than 5,000 mg kg^{-1} (Figure 6.1; Table 6.1). The second PC (axis) (Table 6.4) in PCA revealed the influence of Fe in the paint waste demonstrating that it is an important factor impacting metal distribution. Because of the varying concentration of steel grit remaining in sample, 5% to 80% by weight, RCRA metals in the paint waste vary as well

While understanding the total metal distribution and its association in the paint waste are important, most critical is the metal form which affects its potential mobility upon disposal. Toxicity of metals is dependent on the chemical form in the paint waste.

6.3 Mineralogy of Paint Waste (XRD Analysis)

XRD results revealed the presence of pigment minerals used before 1989 when lead-based paint was prohibited in NYS (NYSDOT, 1988) (Figure 6.3). Pb and Cr occurred with similar trends in the paint waste (Figure 6.3). Specifically, Pb was speciated as lead

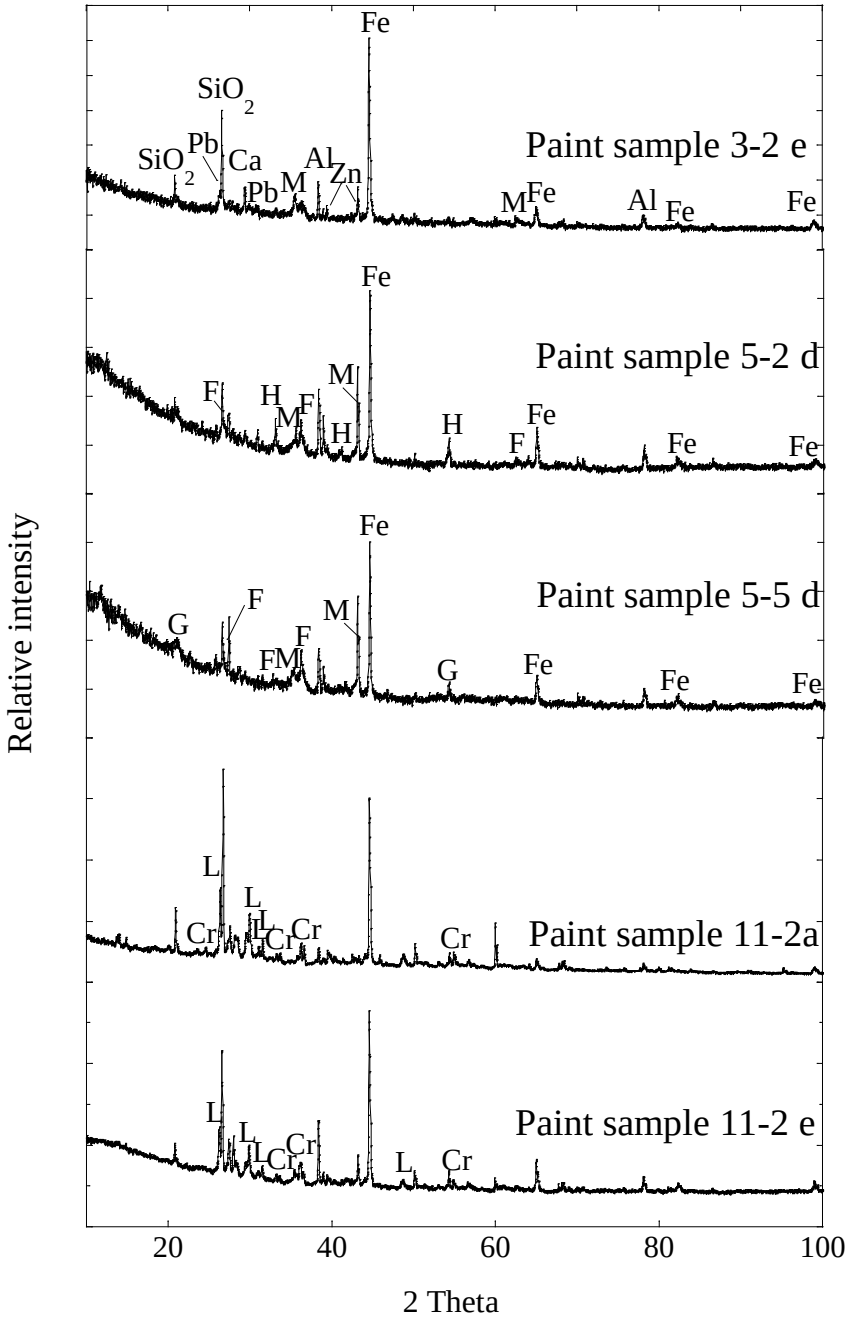

Fe – Fe SiO_2 – SiO_2 Ti – TiO_2 Ca – $CaCO_3$ Al - Al
Pb – Pb_3O_4 L – $PbCrO_4 \cdot PbO$ Cr – Cr_2O_3 M – magnetite [Fe_3O_4]
H – hematite [Fe_2O_3] F – ferrihydrite [$5Fe_2O_3 \cdot 9H_2O$] G – goethite [FeO(OH)]

Figure 6.3 XRD analysis of the primary minerals, Pb, Cr, and iron oxides in paint waste samples from Regions 3, 5, and 11.

tetraoxide (Pb_3O_4) and in association with Cr(VI) as crocoite ($PbCrO_4$). These results are expected as lead tetraoxide (or red lead Pb_3O_4, Pb_2O_4, $PbO_2{\cdot}2PbO$) and lead chromate ($PbCrO_4{\cdot}PbO$) are reported to be the most widely used corrosion-inhibiting pigments on metal structures painted before the 1980s (Gooch, 1993; Strivens and Lambourne, 1999) (Table 2.2). Lead chromate ($PbCrO_4$) was the dominate Cr mineral applied for bridge paint (Winchester, 1988) although Cr has also been applied as Cr_2O_3 (Figure 6.3). The presence of Cr_2O_3 is partly attributed to the application of chromium oxide green (Cr_2O_3) in paint providing a green pigment (Strivens and Lambourne, 1999). Degradation (reduction) of the pigment itself is another important explanation (Monico et al., 2011). Reduction of $PbCrO_4{\cdot}PbO$ to the trivalent state (Cr_2O_3) in paint has been studied by others (Erkens et al., 2001; Monico et al., 2011; Somme-Dubru et al., 1981). The redox process is induced by heat, UV-visible light, contaminants, and SO_2 (Erkens et al., 2001; Somme-Dubru et al., 1981). Monico et al. (2011) reported approximately two-thirds of chromate yellow pigment ($PbCrO_4{\cdot}PbO$) in paintings from the 1910s was reduced to Cr(III) compounds such as $Cr_2O_3{\cdot}2H_2O$, in some cases correlated to the presence of Ba (sulfate) and/or to that of aluminum silicate compounds. Nonetheless, the presence of Pb was consistent with Cr (Figure 6.3).

Iron oxides observed in the paint waste included ferrihydrite (5Fe2O3·9H2O or $Fe_5HO_8{\cdot}4H_2O$), magnetite (Fe_3O_4), goethite (α-FeO(OH)), and hematite (Fe_2O_3) (Figure 6.3). These oxidation products are formed on the steel grit surface (Hartley and Lepp, 2008; Jambor and Dutrizac, 1998; Müller and Pluquet, 1998). Iron oxides (11% by wt) (Table 6.5) have been studied extensively on the steel surfaces (Cornelis et al., 2008; Komárek et al., 2013; Zhou and Haynes, 2010) because of its role in metal sequestration

Table 6.5 Primary Component of the Paint Waste Samples from XRD Analysis.

Bridge Sample ID	Major minerals in paint waste (% by wt)							Total
3-2 e	Al (32)	Fe(23)	Magnetite (Fe_3O_4) (23)	Quartz (SiO_2) (15)	$CaCO_3$ (7)			100
5-2 d	Fe (26)	Quartz (SiO_2) (27)	Rutile (TiO_2) (16)	$CaCO_3$ (12)	Hemetite (Fe_2O_3) (11)	Zn (8)		100
11-2 a	Quartz (SiO_2) (70)	Phoenicochroite (Pb_2OCrO_4) (11)	Rutile (TiO_2) (10)	Cr_2O_3 (9)				100
11-2 e	Quartz (SiO_2) (37.6)	Al (25.7)	Fe (14.9)	Rutile (TiO_2) (8.9)	Phoenicochroite (Pb_2OCrO_4) (5)	Calcite 5	Zn (3)	100

Detection limit of XRD system is approximately 1% by wt (Quinn, 2013).

in soils. Iron oxides particularly the amorphous metastable mineral ferrihydrite is an important sorbent in the environment because of its high surface area, strong affinity for metals, and an abundance of binding sites. Consequently, the presence of iron oxides may have a significant effect on contaminant mobility from the paint waste.

In addition to the Pb, Cr, and Fe minerals, the paint waste throughout NYS revealed SiO_2 (silica), Fe (martensite) (Society of Automotive Engineers (SAE) 2006), TiO_2 (rutile), Al (bauxite), $CaCO_3$ (calcite), and Zn (spelter)/ZnO (zincite) (Figure 6.3, Tables 6.5 and 6.6). Generally, the composition of a paint can be described as the carrier (continuous phase) and pigment (discontinuous phase) (Lambourne and Strivens, 1999). The former includes binders (i.e., polymer chains such as long chain carboxylic acids and alkyd resins) and solvents (e.g., ether [-C-O-C]), while the latter is composed of extenders (or supplementary pigment, i.e., TiO_2 and $CaCO_3$), primary pigments (fine particle organic or inorganic, i.e., lithopone [ZnS mixed with $BaSO_4$]), and additives (minor components) (Bentley, 1998; Clark, 1976).

6.4 Morphology of Paint Waste (FE-SEM Analysis)

Morphologically the paint particles exhibit an irregular topography ranging from 0.05 to 1 mm (Figure 6.4) and angular shape steel grit residue (Figure 6.4) with diameters of 0.3 to 1 mm (Figure 6.4). In this study, EDX observations of Si, Ti, Ca, and Al correlated with Pb and Cr (Figure 6.4) (Table 6.5), which is consistent with the findings from other studies (Franquelo et al., 2012; Turner and Sogo, 2012). Minerals such as $CaCO_3$ and SiO_2 may affect the metal mobility. For example, Andra et al. (2011) found that Ca was an important factor in the mobilization of Pb from alkaline soils in San Antonio, TX. The

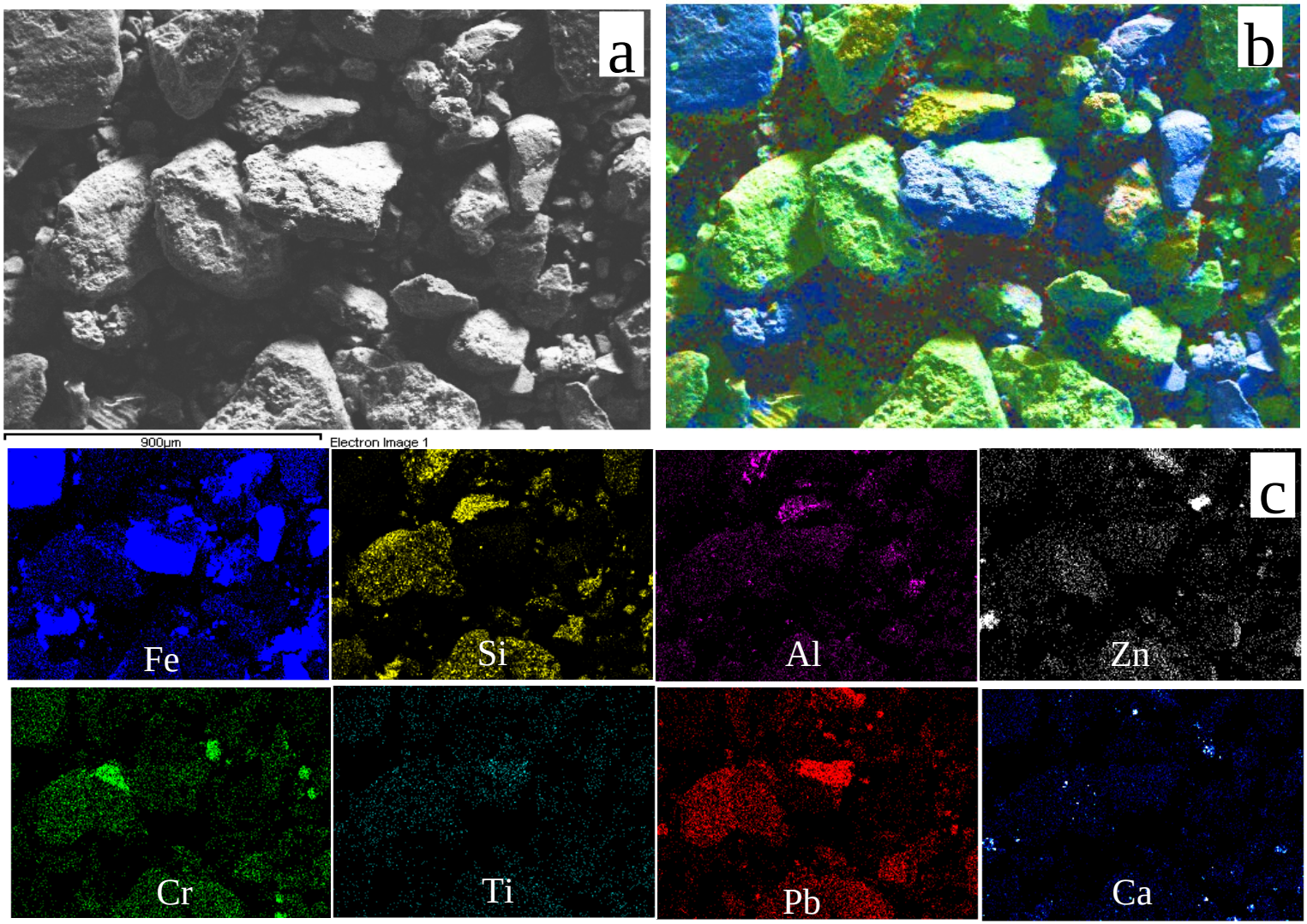

Figure 6.4 FE-SEM images and EDX mapping on the paint waste sample. (a) FE-SEM image; (b) Blue particles represent the steel grit; green particles present the paint in the waste sample; (c) EDX mapping on paint waste sample from Region 7 (color images in mapping represent the corresponding elements).

Table 6.6 Summarized XRF and XRD Results

Identified matrix phases from XRD	**Metal - bearing phases in paint waste**	
	XRF elements	**Miner minerals measured from XRD***
Quartz (SiO2),	Pb	Lead tetroxide [Pb_3O_4]
Rutile (TiO2)		$Pb_2(CrO_4)O$
Calcite (CaCO3)	Cr	Cr_2O_3
Al (bauxite)	Zn	Zinc oxide [ZnO]
Fe (martensite)		Zinc chromates [$ZnCr_2O_4$]
Zn (spelter)	Fe	Magnetite [Fe_3O_4)
		Geothite [FeO(OH)]
		Hematite [Fe_2O_3]
		Ferrihydrite ($5Fe_2O_3 \cdot 9H_2O$)
	Ba	$BaSO_4$,
		[(Ba,Pb)SO_4],

* Metals (such as As, Cd, and Ag) at levels less than 1 % by wt were not detectable by XRD.

release of the $CaCO_3$ from paint waste does not directly affect the metal mobility. However, its dissolution results in an increase in pH. Therefore, although elevated metals were observed, the presence of a number of minerals in the paint waste, including iron oxide (ferrihydrite ($5Fe_2O_3 \cdot 9H_2O$ or $Fe_5HO_8 \cdot 4H_2O$), magnetite (Fe_3O_4), goethite (α-FeO(OH)), and hematite (Fe_2O_3)), calcite ($CaCO_3$), and (SiO_2) silica, affect the potential mobility of metals in the paint waste.

6.5 Lead Concentrations in Bridge Wash Water

Dissolved Pb concentrations ranged from 2.5 µg/L to 410 µg/L (Figure 6.5), while total Pb concentrations were observed from 33 to 5,700 µg/L (Figure 6.6). Variability in dissolved Pb and total Pb was observed throughout the regions (Figures 6.5 and 6.6), and can be attributed to a number of factors including high pressure wash intensity and duration of application. The total lead concentrations are as great as 10 times the dissolved lead concentrations. On average, 84% of total lead concentrations in bridge wash water are in the particulate form. In general, Pb concentrations in the wash water samples from Region 5 were less than those from Regions 3 and 10 (Figures 6.5 and 6.6). The results are consistent with trends found from analyzing metal concentrations in the paint waste. Because surface preparation standard SSPC SP-6 (Commercial Blast Cleaning) (NYSDOT, 2008) was applied to the bridges, as great as 33% of paint remained on the bridge (NYSDOT, 2008). During high-pressure wash, the water impinges on the existing paint and exposed steel surfaces, removing weakly held material, which is carried off by the wash water. Therefore, the wash water generated is

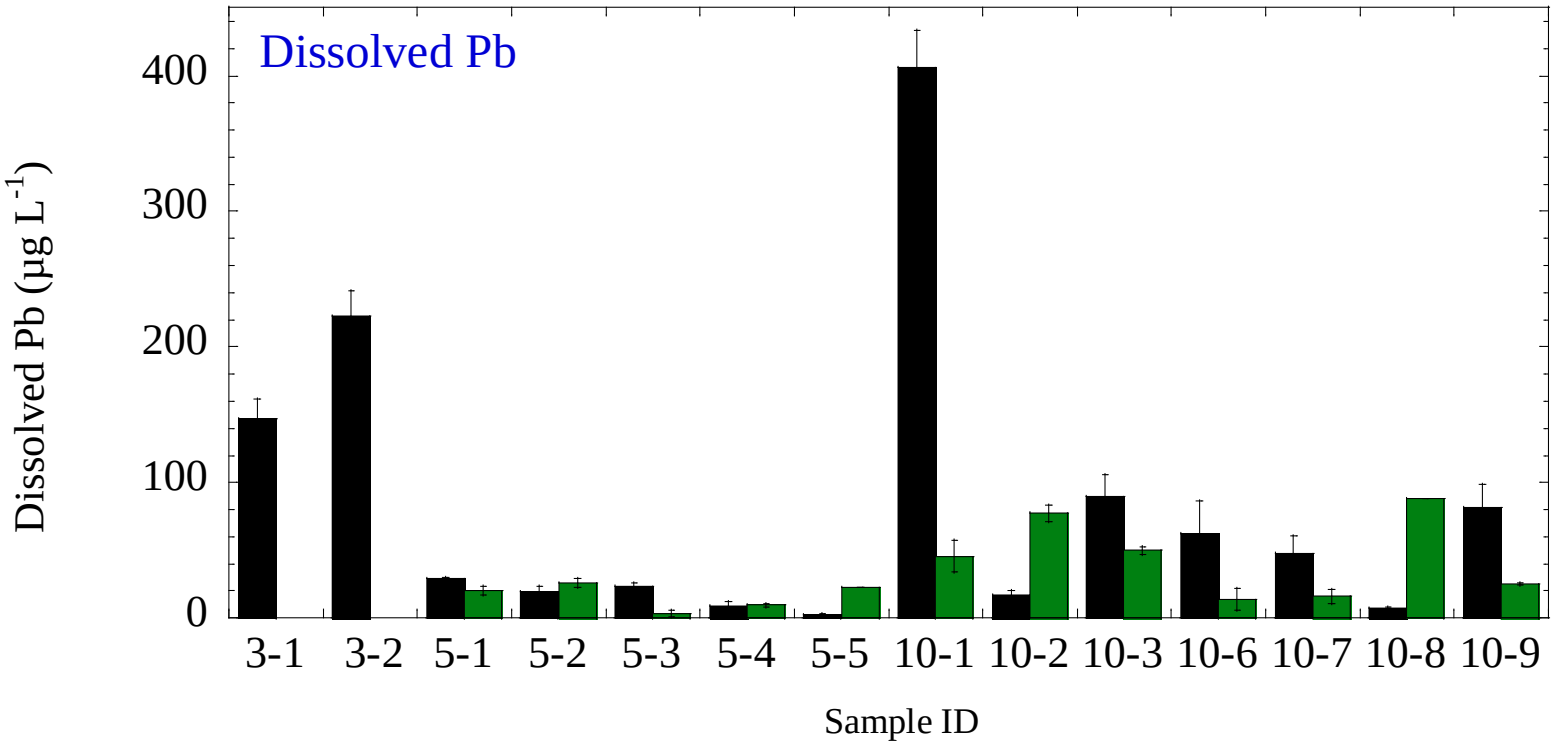

Figure 6.5 Dissolved Pb concentrations are shown as a function of the two locations for the 14 bridges sampled using the Hach field spectrophotometer. One sampling location was available for Bridges 3-1 and 3-2. All bridges sampled were rehabilitated after 1989.

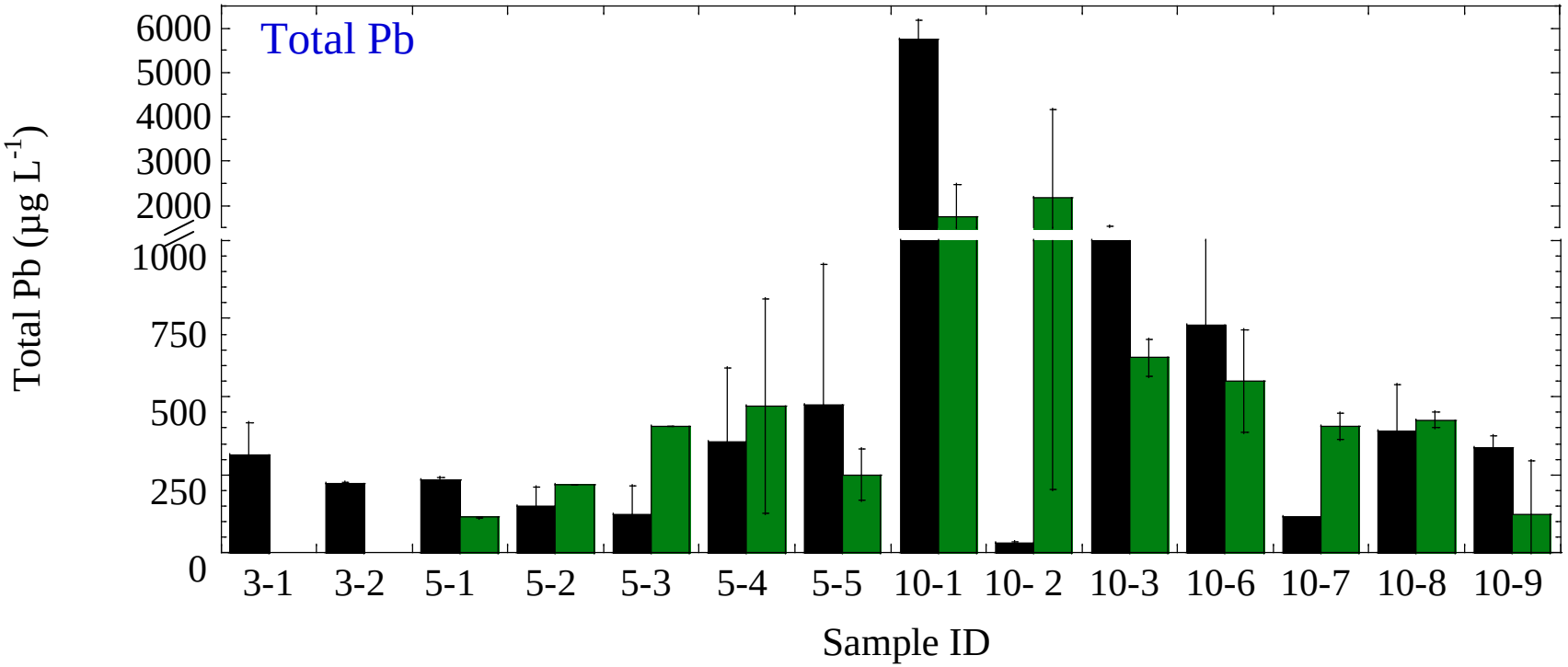

Figure 6.6 Total Pb concentrations are shown as a function of the two locations sampled for the 14 bridges using the Hach field spectrophotometer. One sampling location was available for Bridges 3-1 and 3-2. All bridges sampled were rehabilitated after 1989.

contaminated with lead paint debris. The wash water concentrations are lower than those observed by Hopwood et al. (2003), where they attempted to apply a geotextile fabric to filter wash water from bridges undergoing maintenance prior to its release. Hopwood et al. reported dissolved lead concentrations ranged from less than detection to 5,500 µg/L while total lead concentrations were observed from 2,300 to 130,000 µg/L during high pressure (3,000 to 10,000 psi) washing. After filtration, dissolved lead concentrations were reduced to less than detection to 4,100 µg/L, while total lead concentrations ranged from 2,000 to 22,000 µg/L. On the other hand, results from this study are comparable with those obtained by Davis and Burns (1999) where the effect of acid rain on LBP structures was investigated. Results revealed that the total lead concentrations in the runoff from structures followed the order of wood 2.6 - 380 µg/L, brick 3.3 - 240 µg/L, and cement 2.0 - 110 µg/L. The lead concentrations depended on the age of the paint and condition of deterioration. In our study, Bridge 10-1 (Figure 6.5) exhibited the greatest dissolved lead concentration of 410 µg/L and total lead concentration of 5,700 µg/L. These results were consistent with the elevated lead concentrations observed using FP-XRF on the paint waste samples from Bridge 10-1.

Generally, wash water is filtered before discharged into a sewer or through runoff if determined hazardous (Appleman, 1997). States set their own standard for determining whether wash water is hazardous. Pennsylvania DOT requires a series of handling and disposal conditions for wash water including water collection, filtration of paint chips or particles, and water characterization; Massachusetts Turnpike set 100 ppm Pb as the criterion for wash water. In NYS, special collection requirements exist for washing a structure over a public water supply, where wash water over a body of water is required

to be collected and diverted to the adjoining land mass (NYSDOT, 2008). In this study, all samples revealed dissolved lead concentrations less than 1,000 µg/L; 89% of the samples were observed from non-detectable to 90 µg/L. Four of the samples showed total lead concentrations greater than 1,000 µg/L; 85% of the samples ranged from non-detectable to 750 µg/L. Dissolved lead and lead contaminated paint particulates in wash water are transported either directly or indirectly to surface water through storm drains. Lead contaminated paint particles will continue to dissolve as they are being transported, releasing lead into solution. The dissolution rate can be enhanced by complexing ligands commonly found in natural waters, such as humic acid (Guy and Chakrabarth, 1976) and chloride (Davis and Barnes, 1996). The mobility of metals in the environment is a function of their speciation. In addition to the wash water, metals may be mobilized through rainfall, and urban stormwater runoff is considered to be a major source of metals to surface waters. Therefore, although lead concentrations were investigated in the bridge wash water during high pressure wash, the results suggest potential for rainwater contamination from the bridge paint surface as well.

The surface water quality standard in New York State is 50 µg L^{-1} for Pb, where the surface water used as drinking water source; as low as 8 µg/L is applied for the saline surface water where there is fish, shellfish, and wildlife propagation and survival (NYSDEC, 1999). Ground water quality standard in NYS is 25 µg L^{-1} for Pb (NYSDEC, 1999). 35% of the samples revealed dissolved lead concentrations greater than the surface water quality standard 50 µg L^{-1}, while 96% of the samples were observed total lead in wash water greater than 50 µg L^{-1}. These results suggest that bridge wash water

containing lead or paint solids may be collected, properly treated, and discharged to a permitted location to prevent surface water or ground water pollution.

6.6 Summary

XRF results indicate that although the 24 bridges studied to date have been repainted after 1989, lead-based paint was not entirely removed. Eighty percent of paint waste samples exhibited lead concentrations greater than 5,000 mg kg^{-1}. The elevated iron concentrations are present from the application of steel grit used to remove paint. Other compounds of As, Ba, Cd, Hg, Se, and Ag were observed in paint as pigments and preservatives as well. Pb concentrations were observed to correlate with As (R^2 = 0.78), Cd (R^2 = 0.73), Cr (R^2 = 0.88), and Ag (R^2 = 0.67), while other relationships were observed between Hg and Se (R^2= 0.99), Hg and Zn (R^2= 0.94), and Se and Zn (R^2= 0.76). The trends were found across all the regions in NYS indicating consistent application of these metals as pigments and extenders in paint composition. XRD results further revealed pigments used before 1989 such as Pb_3O_4, $PbCrO_4 \cdot PbO$, and Cr_2O_3. Primary minerals in the paint waste are SiO_2 (silica), Fe (martensite), TiO_2 (rutile), Al (bauxite), $CaCO_3$ (calcite), and Zn (spelter)/ZnO (zincite). FE-SEM/EDX results further demonstrated that Si, Ti, Ca, and Al are associated with Pb and Cr. Despite the elevated metal concentrations observed, the presence of a number of minerals in the paint waste, such as iron oxides, $CaCO_3$, and SiO_2 may play important roles in reducing metal mobility from the waste.

Dissolved Pb concentrations in bridge wash waster ranged from 2.5 µg L^{-1} to 410 µg L^{-1}, while total Pb concentrations were observed from 33 to 5,700 µg L^{-1}. The total

lead concentrations were as great as 10 times the dissolved lead concentrations. In general, Pb concentrations in wash water samples from Region 5 were less than those from Regions 3 and 10. The results were consistent with trends found from analyzing metal concentrations in the paint waste. Results revealed dissolved lead concentrations less than 1,000 µg L^{-1}; 89% of the samples were observed from non-detectable to 90 µg L^{-1}. Four of the samples revealed total lead concentrations greater than 1,000 µg L^{-1}; 85% of the samples ranged from non-detectable to 750 µg L^{-1}. Based on the surface water quality standards, results in this study suggest that bridge wash water containing lead or paint solids may require collection, treatment, and discharge to a permitted location to prevent surface water or ground water pollution.

CHAPTER 7

METAL LEACHING FROM THE BRIDGE PAINT WASTE IN THE PRESENCE OF STEEL GRIT

In this section, short-term and long-term leaching studies were conducted to investigate the leaching behavior of trace metals (such as Pb and Cr) from bridge paint waste. Coupled with sequential extraction (SE), this section focuses on resolving phases trace metals are associated with in paint waste. The oxide mineralogy in the paint waste and results obtained may be used in developing predictive models for metal leaching as well as in addressing disposal and management of paint waste.

7.1 Short-term Leaching (TCLP)

The TCLP results (Figure 7.1; Appendix C) revealed that leached metal concentrations in the extracts ranged from less than 0.0005 (detection limit) to 1.46 mg L^{-1} for Pb, less than 0.0007 (detection limit) to 9.52 mg L^{-1} for Cr, and less than 0.0004 (detection limit) to 9.60 mg L^{-1} for Ba. Concentrations observed were less than the TC levels (for Pb 5 mg L^{-1}, Cr 5 mg L^{-1}, and Ba 100 mg L^{-1}), with the exception of three samples exhibiting Cr concentrations greater than the TC of 5 mg L^{-1} (U. S. EPA, 1992). These results were one to two orders of magnitude lower than the other similar studies (Table 7.1), where leaching was observed as great as 587 mg L^{-1} for Pb and up to 44.7 mg L^{-1} for Cr (Boy et al., 1995; Halim et al., 2003; Martel et al., 1997; U.S. EPA, 1998; Wadanambi et al., 2008)

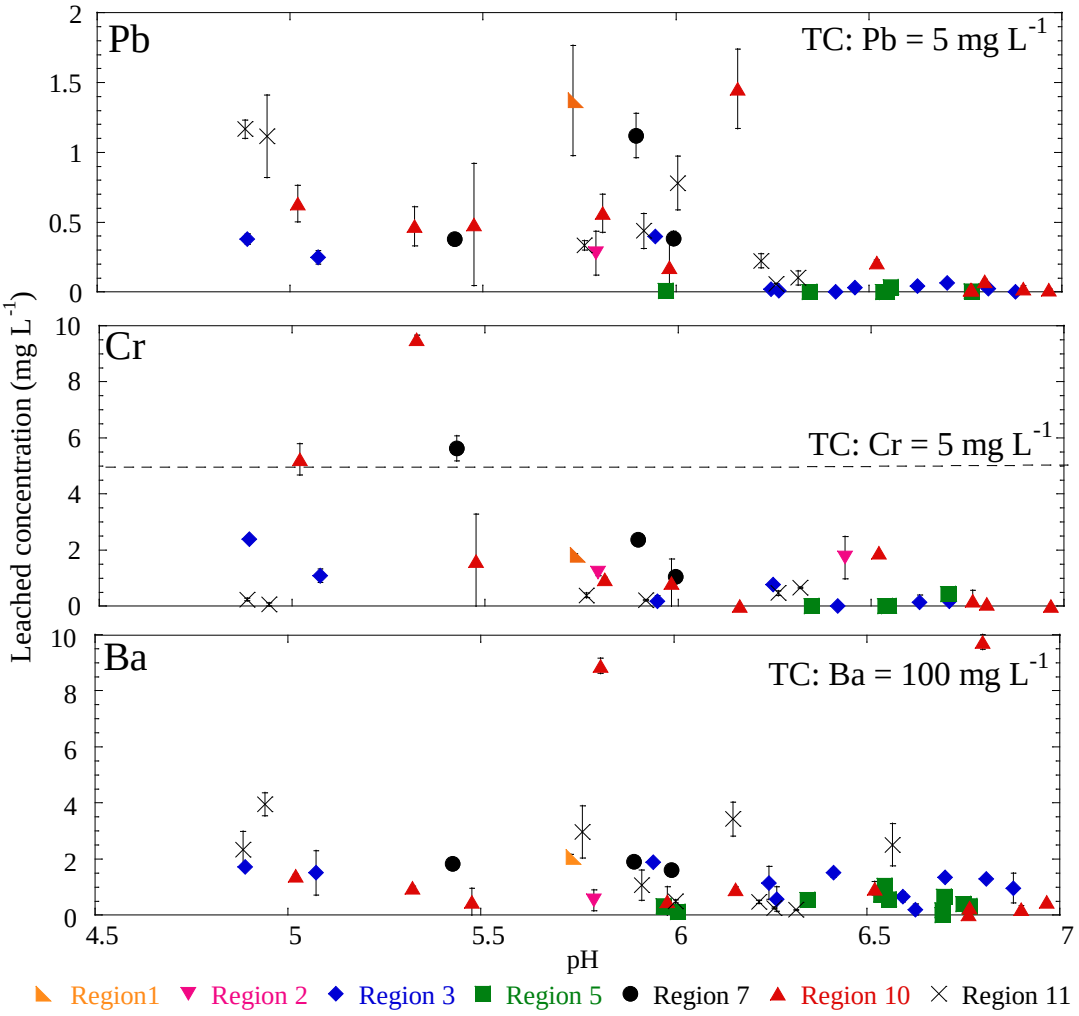

Figure 7.1 Leaching results from TCLP for Pb, Cr, and Ba as a function of pH after 18 hours with 0.05 M ionic strength. Samples are extracted using Fluid #1 (0.1 N CH_3COOH, which has been adjusted with NaOH to an initial pH of 4.93 ± 0.05) or Fluid #2 (0.1 N CH_3COOH, which has an initial pH of 2.88 ± 0.05) based on the alkalinity of the waste material. TC: Toxicity characteristics.

Table 7.1 TCLP (mg L^{-1}) Results from Lead-Based Paint (LBP) or Other Waste Studies.

Sample	Ba	Cr	Pb	Zn	Fe	References
Paint wastes associated with plastic media	0.55 – 0.74	16.32 – 44.73	<0.066	–	–	Boy et al. (Boy et al., 1995)
LBP	–	–	28.3 – 36.7	–	–	Martel et al. (Martel et al., 1997)
LBP debris			0.05 – 72.8			U.S. EPA (U.S. EPA, 1998)
LBP	–	–	205 – 587	–	–	Wadanambi et al. (Wadanambi et al., 2008)
Paint waste with stabilizer			0.2 – 52			Daniels et al. (Daniels et al., 2001)
Waste foundry sand associated with hydrous ferric oxide (HFO)			0.4 – 9.0	132 – 141	BDL –213	Kendall (Kendall, 2003)
Paint waste associated with steel grit*	BDL – 9.6	BDL – 9.52	BDL – 1.46	BDL – 1307	BDL – 3275	This study

BDL refers to below detection limit
– refers to not reported
*Detection limits (mg L^{-1}) for this study: Ba = 0.0004, Cr = 0.0007, Pb = 0.0005, Fe = 0.0025, Zn = 0.001.

(Table 7.1). The leaching results for Pb, Cr, and Ba (Figure 1) showed trends as a function of pH, where the leached metal concentrations decreased as the pH increased from 4.5 to 7. Similar results have been reported by many researchers (Boy et al., 1995; Kendall, 2003; Martel et al., 1997), where metal leaching was observed to be pH dependent.

From earlier studies (Chapter 6), elevated metal concentrations were observed in the waste. For example, Pb was detected ranging from 5 to 168,090 mg kg^{-1}, Cr from 21 to 10,192 mg kg^{-1}, and Ba from less than detection limit (100 mg kg^{-1}) to 16,319 mg kg^{-1} (Chapter 6). Yet the leached metal concentrations were less than the TC levels (Figure 1). One explanation for the leached concentrations observed can be attributed to the use of iron-based abrasives in the paint removal process. The typical steel (cast steel) grit applied is composed by wt of Fe (> 96%), C (< 1.2%), Mn (< 1.3%), Si (< 1.2%), Cr (< 0.25%), Cu (< 0.25%), and Ni (< 0.2%) (Dunkerley et al., 1978). Earlier studies (Chapter 6) demonstrated that as great as 80% by wt of the paint waste is comprised of steel grit. Therefore, surface interactions between metals and the steel grit surface likely play an important role in metal mobility and leaching. These interactions involve potentially a number of mechanisms: Iron oxides form on the steel grit surface (Apul et al., 2005; Jambor and Dutrizac, 1998; Stipp et al., 2002). The surface charge on the iron oxides arises from deprotonation and protonation of potential determining $MOH_2^{0.5+}$ and $MOH^{0.5-}$ groups (Haynes, 1982; Zhou and Haynes, 2010) (Figure 7.2). This surface becomes increasingly negatively charged as the hydroxide ion activity (and pH) increases and becomes more positively charged as pH decreases; the surface charge is developed with respect to the oxide zero point of charge (ZPC)

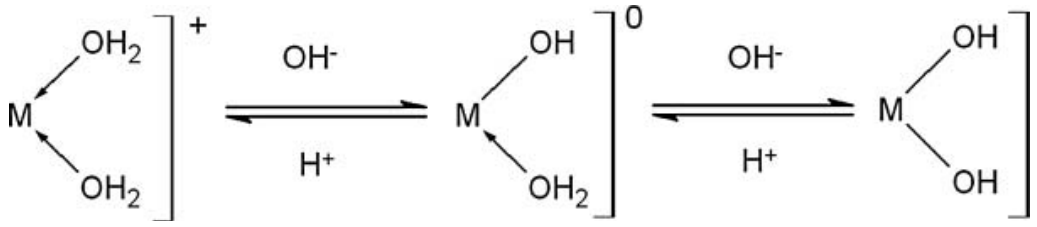

Figure 7.2 Schematic diagram of the pH-dependent charge on an amphoteric metal oxide surface (Haynes, 1982; Zhou and Haynes, 2010).

(i.e., pH_{ZPC} = 7.8 − 8.8 for ferrihydrite, pH_{ZPC} = 6.5 - 7.9 for magnetite (Cornell and Schwertmann, 1996; Illés and Tombácz, 2003)). Cations desorb as the pH decreases and anions are released as the pH increases. The trend observed in this study is consistent with cation sorption (Pb^{2+}, $Cr(OH)^{2+}$, Ba^{2+}) to the iron oxides formed on the steel grit surface, where a fraction of sorbed metals desorb during leaching (Strawn and Sparks, 1999; Swift et al., 1991). Given the potentially significant surface interactions between trace metals and the iron oxide surface, reduced concentrations observed in leaching are likely due to the presence of iron oxides. Therefore, we hypothesize that iron oxides form on the steel grit surface. Metals in the paint waste interact with the iron oxide surface through sorption/desorption and/or dissolution/precipitation processes at the aqueous-solid interface.

Cr is a RCRA metal where the hexavalent form is of significant toxicity (Boy et al., 1995). Cr is introduced in paint as Cr_2O_3 and CrO_4^{2-} (Doroszkowski et al., 1999). Reduction of Cr(VI) to Cr(III) has been observed under acidic conditions (pH < 7) (Weng et al., 2001; Weng et al., 1996) as well as with reducing agents Fe(II) or zero valent iron (Du et al., 2012; Peterson et al., 1996; Peterson et al., 1997). Hexavalent chromium may be reduced to trivalent chromium in the presence of ferrous iron (magnetite) or zero-valent (steel grit) iron under acidic conditions. Therefore, Cr(III) is expected to be the dominant speciation in the leaching procedure.

Although the metal mobility and speciation were investigated by TCLP (Appendix C), the 18-h leaching procedure is likely insufficient for evaluating the long-term behavior of paint waste. Therefore, to understand the long-term stability of paint waste and address its disposal, MEP was applied in this study.

7.2 Long-term Leaching (MEP)

Concentrations measured in extracts from the MEP experiments where either greater than or equal to that observed in the TCLP (Appendix C). In the first day of extraction, the greatest concentrations of metals leached were observed (Figure 7.3; Appendix C). From the second to fourth day of extraction, leached concentrations decreased as function of extraction time (Figure 7.3). The leached metal increased from the fourth to eighth day and decreased again from eighth to tenth day. Specifically, the first day of extraction resulted in leached concentrations as great as 22.6 mg L^{-1} for Pb, 0.064 mg L^{-1} for Cr, and up to 6.6 mg L^{-1} for Ba (Figure 7.3). From the second to fourth day of extraction, leached concentrations were observed from below detection level (BDL) (< 0.0005) to 2.04 mg L^{-1} for Pb, BDL (< 0.0007) to 0.04 mg L^{-1} for Cr, and 0.03 to 0.3 mg L^{-1} for Ba (Figure 7.3; Appendix C); the reduced leaching was observed with increasing time. These results are attributed to the continuum of sorption reactions between specific adsorption and surface precipitation/coprecipitation:

$$S-OH + Me^{2+} + H_2O \leftrightarrow S-O-MeOH_2^{+} + H^{+}$$ (Bradl, 2004; Dzombak and Morel, 1990)

$$S-O-MeOH_2^{+} + Me^{2+} + H_2O \leftrightarrow S-O-MeOH_2^{+} + Me(OH)_{2(s)} + 2H^{+}$$ (Bradl, 2004)

The adsorption process may be followed by surface precipitation reactions (Zhou and Haynes, 2010). Initial surface precipitates may exhibit a disordered lattice (amorphous) and therefore are metastable. Over time, the solid slowly converts to the more stable, less reactive, crystalline form, which has a lower solubility.

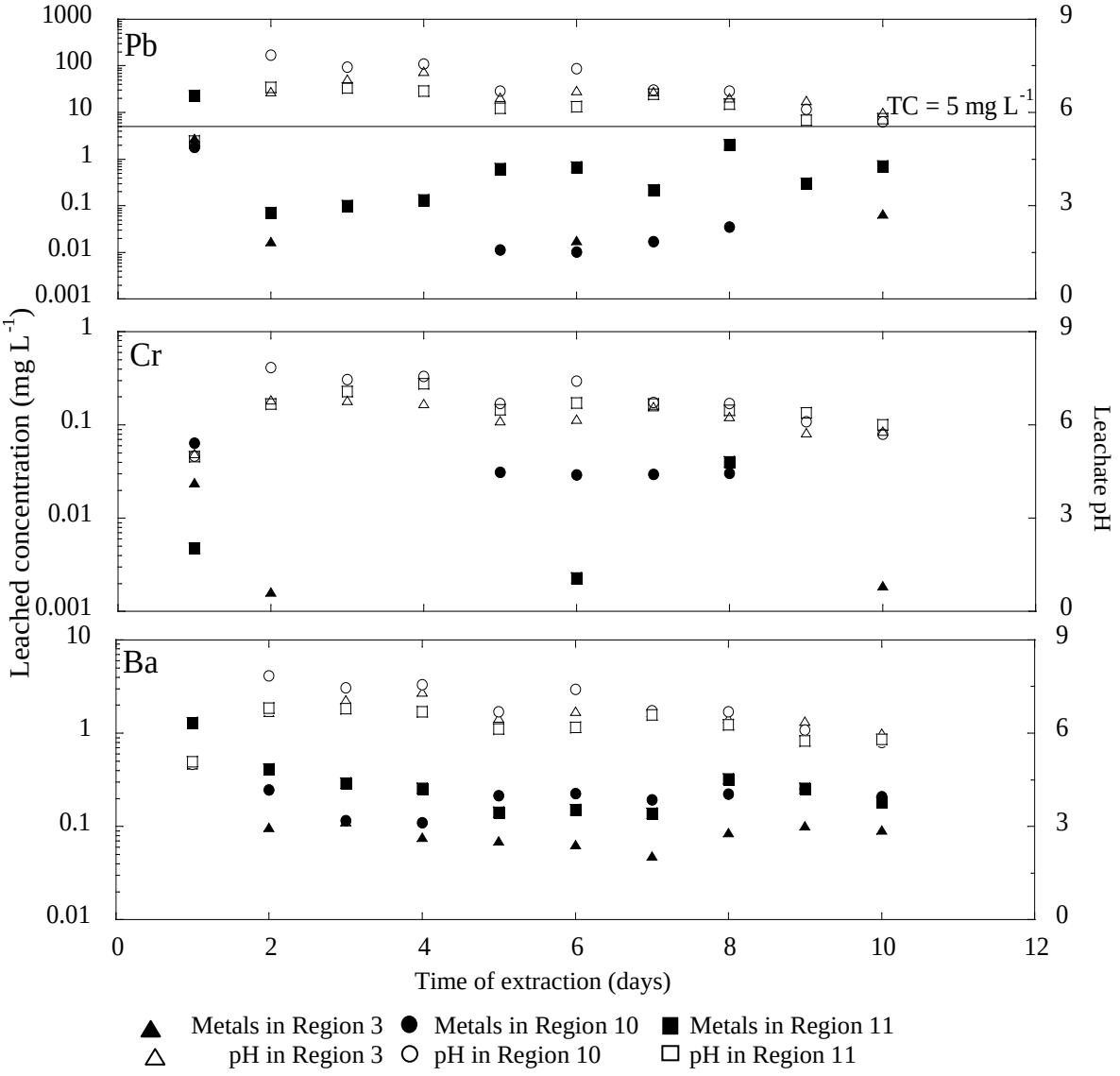

Figure 7.3. Leaching concentrations of Pb, Cr, and Ba from MEP are shown as a function of 10 days of extractions. The first extraction is performed with a pH of 5.0 followed by the subsequent nine successive extractions using the initial pH of 3.0 ± 0.2 that simulate acid rain conditions.

Interestingly, MEP results revealed increased Pb, Cr, and Ba concentrations in the leachate for pH greater than 7 as compared to second and third day of extraction. Increased Pb concentrations were observed over pH 7.0 to 7.5; Cr leaching increased over pH 6.5 to 8.5, and increased Ba concentrations were observed over pH 6.8 to 9.5. These results are consistent with that observed by Townsend et al. (Townsend et al., 2004b), where they applied MEP to evaluate the leaching of arsenic, chromium, and copper from chromated copper arsenate (CCA)-treated wood. Results may be explained in part by metal complexation with organic ligands dissolving from the paint. Trace metals such as Pb and Cr complex with both low molecular weight organic ligands (i.e., citrate, acetate, and formate) and high molecular weight organic ligands (i.e., long chain carboxylic acids). At higher pH conditions, these organics dissolve along with the bound metals such as Pb and Cr(III) (Halim et al., 2004). Aqueous complexation increased trace metal mobility in the leachate for pH greater than 7 (Bradl, 2004).

Although increased leaching was observed in long-term studies, 19 of 24 samples revealed that the TC level was not exceeded. A significant fraction of the trace metals is still associated with the solid phase. To investigate the forms metals are associated within the paint waste and further address the long-term mobility, sequential extraction was conducted.

7.3 Metal Association with Paint Waste (SE)

In the first and second steps of sequential extraction, the exchangeable and carbonate fractions (Figure 7.4) showed by wt 5.25 to 6.84% Pb (% refers to the extracted concentration over the total concentration), 4.27 to 4.73% Cr, 0.47 to 0.63% Ba, and 4.99

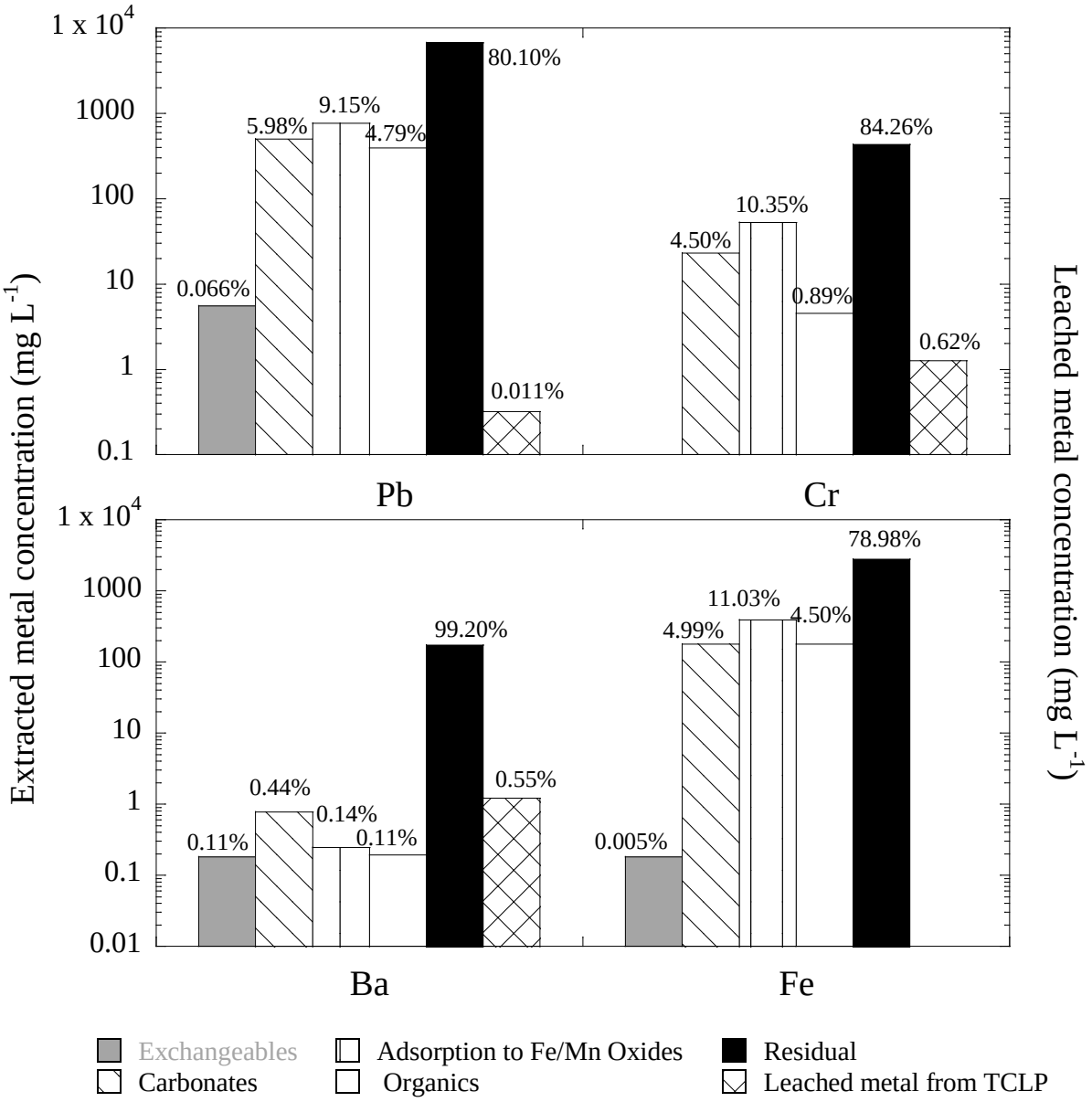

Figure 7.4 Mass balances of selective sequential extraction fractions for Pb, Cr, Ba, and Fe.

to 5.07% Fe. This phase represents metals and metalloids that are exchangeable and weakly bound (i.e., PbO pK_{SO} =12.72 at 25°(Baes and Mesmer, 1976); ion-exchangeable Fe(II) (Heron et al., 1994)) as well as dissolution *of* carbonate minerals (i.e., $Pb_3(OH)_2(CO_3)_2$ pK_{S0} = 45.46 (Baes and Mesmer, 1976)); Pb_3CO_3 pK_{S0} = 13.13(Baes and Mesmer, 1976); and $CaCO_3$ pK_{S0} = 8.36 (Benjamin, 2002), where Pb and Cr are associated with $CaCO_3$). During the leaching experiments, these forms are expected to be released in the aqueous phase. The relatively low concentrations of Pb, Cr, Ba, and Fe observed are consistent with other studies (Funatsuki et al., 2012; Pueyo et al., 2003).

In the third step of the extraction (pH 3 and 0.04 M NH_2OH•HCl in 25% [v/v] CH_3COOHa), metals associated with iron and manganese oxides phases are extracted and resulted in 6.48 to 11.82% Pb, 5.87 to 14.84% Cr, 0.09 to 0.20% Ba, and 7.84% to 14.22% Fe (12.46 to 22.61% as iron oxides) (Figure 7.4). This fraction relates to metal (Pb, Cr, and Ba) complexation with iron oxides (Davranche and Bollinger, 2000), which was observed at 11 % by wt with XRD (discussed below in Section 3.4). The elevated iron oxide minerals phase (11 % by wt) (Figure 7.4) are important surfaces for trace metal sorption of, for example, Pb and Cr. The degree of metal affinity for iron oxides observed in this extraction followed the trend of Pb ≈ Cr > Zn > Ba> As. Again, the presence of iron oxides formed on the steel grit provided a sink for the Pb and other metals in paint waste. The leached concentrations are consistent with the exchangeable, carbonates, and sorbed fractions found through sequential extraction (Figure 7.4). One limitation in this step is that NH_2OH·HCl extraction efficiency for well-crystallized (or synthetic) iron oxides is reported at less than a 30% recovery (La Force and Fendorf, 2000). Thus, amorphous iron oxide was extracted in this step. Metals extracted from this phase may re-

adsorb to unextracted materials (Hass and Fine, 2010; Howard and Shu, 1996). For example, metal released from iron oxides may be re-adsorbed by organics that have not yet been extracted (Howard and Shu, 1996). Therefore, the extracted metals in this step may underestimate the importance of this phase.

The fourth extraction step using nitric acid (0.02 M HNO_3) and hydrogen peroxide (30% H_2O_2) followed by ammonium acetate (NH_4Ac) (pH 2) resulted in leaching of Pb 4.01 to 5.39%, Cr 0.12 to 1.65%, Ba 0.05 to 0.17%, and Fe 3.86 to 6.13% (Figure 7.4). This fraction reflects metals organically bound. Because the paint composition (Doroszkowski et al., 1999), this phase is expected. In the paint formulation, greater than 60% by wt is composed of organic solvents, while approximately 10% pigments and additives are applied (Clark, 1976). The inorganic pigment in paint is primarily made up of compounds such as Pb_3O_4, Cr_2O_3, and Fe_2O_3 (Doroszkowski et al., 1999), along with polymer to produce a homogenous viscous fluid.

The remaining or residual fraction involves for example metals substituted into a mineral lattice structure. This fraction is not expected to be mobilized in the environment or under landfill conditions. In this study, sequential extraction helps to better understand the phases where metals such as Pb and Cr may be associated with in the waste. Using a mass balance, approximately 80% of Pb, 85% of Cr, 99% of Ba, and 80% of Fe (Figure 7.4) are associated with the residual phase. A number of phases play roles in trace metal interactions and behavior: minerals in the paint (i.e., SiO_2), iron oxide coatings on the steel grit surface, and other pigment matrices (such as TiO_2), which are more difficult to digest (Barnes and Davis, 1996). These results are similar to other studies, where Pb overall exhibited the greatest mobility as compared to other trace metals (La Force and

Fendorf, 2000). The degree of mobilization in this extraction followed the trend of Pb > Cr > Ba. Steel grit, comprised of approximately 96% iron, undergoes corrosion/oxidation resulting in iron oxide coatings (Hartley and Lepp, 2008; Jambor and Dutrizac, 1998; Müller and Pluquet, 1998). Ferrihydrite is one of the most widespread form of iron oxides (Jambor and Dutrizac, 1998; Komárek et al., 2013) and can be characterized by the number of X-ray diffraction lines: typically two-line ferrihydrite exhibits little crystallinity while six-line ferrihydrite is more crystalline. Specifically, two-line ferrihydrite (bulk composition $5Fe_2O_3 \cdot 9H_2O$) is a poorly crystalline Fe(III) oxyhydroxide occurring as small (2-4 nm) spherical particles that aggregate in the environment (Jambor and Dutrizac, 1998). This form of iron oxides was shown to effectively reduce bioavailability of metal contaminants (Hartley and Lepp, 2008) and immobilize metals in sediment (Müller and Pluquet, 1998). Given the importance of iron oxides coated steel, further characterization was applied.

7.4 Iron Oxide Minerals

The accumulation and leaching behavior of trace metals at the interface of Fe-based surfaces is strongly influenced by the iron oxide mineralogy. In the interest of assessing minerals of Fe in the paint waste, samples with the greatest concentrations were applied. Diffractograms revealed 2θ peaks at 44.7, 65.0, 82.3, and 99.1 (Figure 7.5), which correspond to (110), (200), (211), and (220) crystal planes for Fe. Several minor peaks (Figure 4) reflected the presence of amorphous iron oxides, which is due in large part to the steel grit. The broad peaks between 2θ values of 33.1 to 36.2 indicate the presence of ferrihydrite, which will crystallize over time to other thermodynamically stable Fe(III)

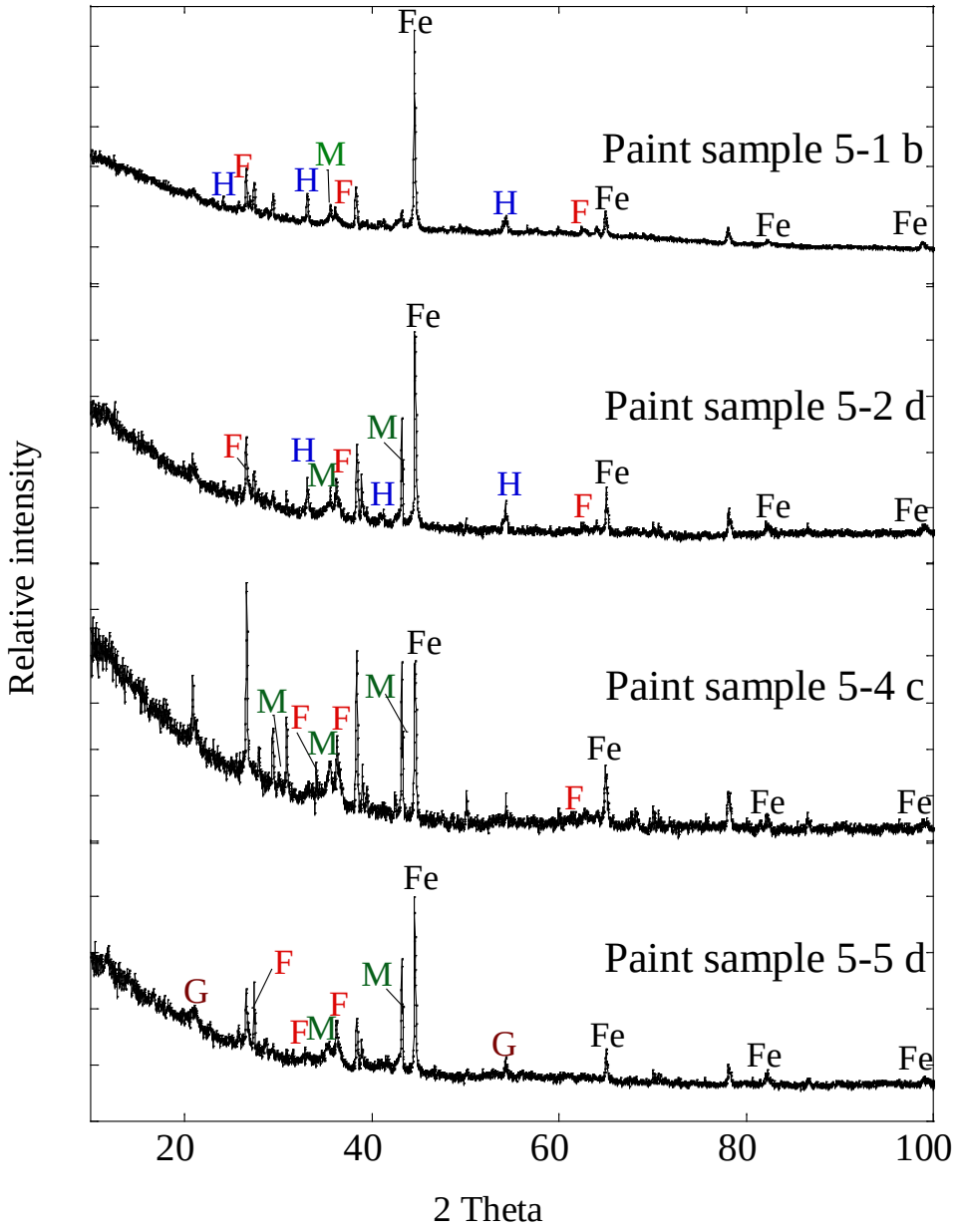

Fe – Fe,
M – magnetite [Fe_3O_4]
H – hematite [Fe_2O_3]
F – ferrihydrite ($5Fe_2O_3 \cdot 9H_2O$)
G – goethite FeO(OH)

Figure 7.5 XRD patterns of iron and iron oxides in paint waste samples from Region 5.

oxides, goethite (α-FeO(OH); $K_{sp} = 10^{-41}$ (Das et al., 2011)) and hematite (α-Fe_2O_3; $K_{sp} = 10^{-43}$ (Das et al., 2011)) at neutral pH (Jambor and Dutrizac, 1998) (Figure 7.5). In this study, steel grit particles were observed to be present at diameters less than 1 mm (Chapter 6). Fe (as martensite(Sae Specification, 2006)) was observed as great as 45% by wt using XRD. Given their significant surface area, iron oxide concentrations were as great as 11% by wt in the paint waste samples based on the peak area in the diffractogram (Figure 7.5). These oxide coatings provide an important sink for the trace metals attenuation.

7.5 Future Implication of the Paint Waste Management

The presence of the iron oxides formed on the steel grit in the paint waste may have an environmental advantage in reducing contaminant mobility. When the waste materials are landfilled, surface interactions between trace metals (such as Pb and Cr) and iron oxide coatings can drastically reduce leachate concentrations. A number of transportation agencies (i.e., NYSDOT, (NYSDOT, 2008); Minnesota Department of Transportation (MnDOT), (Minnesota Department of Transportation (MnDOT), 2004) apply a conservative approach by assuming all waste generated from bridges rehabilitated before 1988 or with lead concentrations greater than 5,000 ppm as hazardous material. The findings in this study indicate that the paint waste from bridges may be characterized as non-hazardous material and disposed at a municipal solid waste (MSW) landfill or a construction and demolition (C&D) landfill. Consequently, the associated costs will be reduced.

7.6 Summary

In summary, although elevated metals were observed in the paint waste, 48 out of 51 samples passed the TCLP test. In MEP studies addressing long-term leaching behavior, 19 out of 24 samples revealed concentrations less than the TC level. These observations suggest that metals are sequestered through interactions with the steel grit surface, resulting in reduced leachable concentrations (less than the TC limit). Sequential extraction revealed that trace metals were found at lower fractions in exchangeable and carbonate forms, while greater contributions of these metals were associated with iron oxides. Yet, the largest fraction, greater than 80%, was associated with the residual phase. XRD analysis corroborated that iron oxides formed on the steel grit surface providing an important interface for trace metals. The presence of the iron oxides in the paint waste may have an environmental advantage in considering contaminant mobility.

CHAPTER 8

TRACE METAL LEACHING MECHANISMS FROM BRIDGE PAINT WASTE IN THE PRESENCE OF STEEL GRIT.

Iron oxide was observed to be an important surface for the cations and anions in the paint waste. In this chapter, we investigated the structure of the iron oxide coating formed on the steel grit surface and the potential bonding structure of metals. Furthermore, modeling of the ions in aqueous, sorbed, and precipitated phases was used to consider whether surface complexation or precipitation controls metal leaching.

8.1 The Structure of the Iron Oxides Formed on the Steel Grit Surface

XRD results indicated the presence of ferrihydrite (60% by wt) ($5Fe_2O_3 \cdot 9H_2O$ or $Fe_5HO_8 \cdot 4H_2O$), magnetite (7.1%) (Fe_3O_4), goethite (22%) (α-FeO(OH)), and hematite (11%) (Fe_2O_3) on the steel grit surface (Appendix E) (Chapter 6). In this study, FE-SEM was applied to evaluate the morphology and surface composition of the steel grit particles. Spherical particle aggregates were observed (Figure 8.1) consistent of ferrihydrite ($5Fe_2O_3 \cdot 9H_2O$ or $Fe_5HO_8 \cdot 4H_2O$) (Das et al., 2011; Equeenuddin et al., 2010; Stipp et al., 2002). These aggregates ranged from 20 to 200 nm in diameter (Figure 8.1). In addition, Pb (0.09%) and Cr (0.08%) were associated with Fe (70.91% by wt) and O (23.79%) on the steel grit surface (Figure 8.1) indicating metal association with the iron oxide surface.

The formation of the iron oxide coatings has been observed by many researchers (De La Fuente et al., 2011; Kelly et al., 2007; Lu et al., 2011; Stipp et al., 2002).

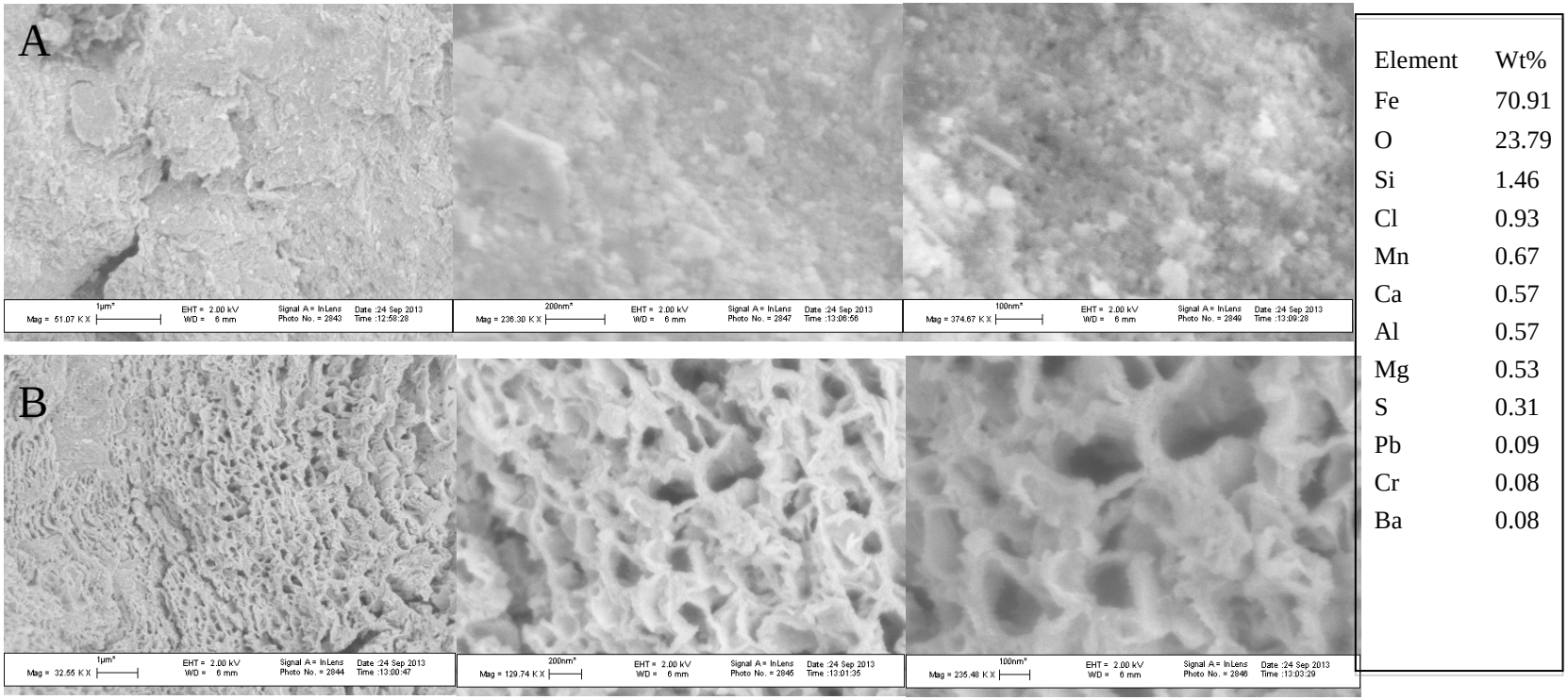

Element	Wt%
Fe	70.91
O	23.79
Si	1.46
Cl	0.93
Mn	0.67
Ca	0.57
Al	0.57
Mg	0.53
S	0.31
Pb	0.09
Cr	0.08
Ba	0.08

Figure 8.1 FE-SEM images on the steel grit surface of the paint waste sample.

Ferrihydrite and lepidocrocite are typical morphological structures on steel surfaces after exposure in the atmospheric (De La Fuente et al., 2011; El Hajj et al., 2013; Monnier et al., 2010). Lu et al. (Lu et al., 2011) hypothesized that Pb^{2+} was first adsorbed onto the nanometer-sized, metastable, iron oxyhydroxide polymers of 2-line ferrihydrite. As these nano-particles assembled into larger particles, Pb^{2+} was trapped in the iron oxyhydroxide structure and re-arranged on the iron oxide surface. On the other hand, ferrihydrite may gradually convert to the more crystalline and stable Fe(III) oxides goethite (α-FeO(OH); $K_{SO} = 10^{-41}$) (Das et al., 2011), hematite (α-Fe_2O_3; $K_{SO} = 10^{-43}$) (Das et al., 2011), and lepidocrocite (γ-FeOOH; $K_{SO} = 10^{-39}$) (Lu et al., 2011) at neutral pH (Jambor and Dutrizac, 1998)(Shaw et al., 2004). Nonetheless, ferrihydrite formed on the steel grit surface is not only metastable for long periods(Das et al., 2011; Lu et al., 2011) (e.g., Axe and Anderson (Axe and Anderson, 1995) observed the transformation of ferrihydrite to goethite and hematite in 14 weeks; 19% by wt of the initial ferrihydrite remained at room temperature and pH 6 after 970 days (Schwertmann and Murad, 1983)), it also provides an abundance of binding sites for trace metals in paint waste (Dzombak and Morel, 1990).

Based on the discussion in Section 7.3, greater contributions of metals (Pb, Cr, and Ba) were found with iron oxides, while less than 6.8% of Pb, Cr, and Ba were associated with the exchangeable and carbonate forms. The largest fraction, however, greater than 80%, was associated with the residual phase comprised of minerals in the paint including SiO_2 and TiO_2. Overall, the greatest fraction of mobilized metals (as great as 15% by wt) was associated with the iron oxide phase. Wadanambi et al. (2008) found that paint waste generated without the application of steel grit, resulted in Pb leaching as

great as 587 mg/L (27% by wt in the paint waste) (Wadanambi et al., 2008). In this study, because of the presence iron oxide in the paint waste, redistribution of metals occurs from exchange sites to specific sorption sites, resulting in greater fraction of mobilized metals associated with the iron oxide phase. Therefore, leaching of the trace metals from the paint waste may be controlled by the iron oxide surface. Sorption is an important process that is responsible for metal leaching.

In general, metal adsorption on iron oxides is a two-step process - a fast initial uptake followed by a slower sorption process that has been attributed to processes including surface precipitation (or coprecipitation) (Lu et al., 2011; Vithanage et al., 2013) and surface diffusion along pore surfaces (Fan et al., 2005; Xu et al., 2006). X-ray absorption near edge structure (XANES) and x-ray absorption fine-structure (XAFS) analyses of Pb(II) - sorbed to amorphous iron oxide surfaces revealed that Pb(II) ions form mononuclear bidentate edge sharing surface complexes on FeO_6 octahedra with two Fe atoms located at approximately 3.34 Å (pH > 4.5) (Dyer et al., 2003), Pb–O distance of 2.25–2.35 Å, and Pb–Fe distances of 3.29–3.36 (3.65–3.76) Å (Dyer et al., 2003; Xu et al., 2006). The adsorption of a Cr(III) atom onto goethite or HFO occurs via the formation of inner-sphere surface complexes (Manceau et al., 1992; Peterson et al., 1997). Cr(III) atoms are surrounded by three metal (Fe or Cr) shells at 3.00–3.05, 3.40–3.46, and 3.94–4.03 Å, consistent with a mixed α- and γ-MeOOH (coprecipitation for Cr) local structure (Me represents Fe or Cr) (Manceau et al., 1992; Peterson et al., 1997).

To better understand the metal behavior and the adsorption effect in the paint waste, adsorption and desorption edges for Pb and Cr were investigated.

8.2 Leaching and Desorption Process

In this study, greater than 99.95% of Pb is associated with paint waste, while 96% of Cr is sequestered in the leaching procedure (Figure 8.2). Paint waste with elevated Fe concentrations (and consequent iron oxides) revealed lower metal leaching (Figure 8.2) suggesting metal sorption to iron oxides is a dominant mechanism responsible for metal leaching. For example, bridge paint samples in Region 5, where Fe was observed as great as 80% by wt, revealed less than 0.004% by wt of Pb and 0.07% by wt of Cr released/leached.

In addition, adsorption and desorption results for Pb and Cr (Figure 8.2) showed trends as a function of pH, where the released/leached metal concentrations decreased as the pH increased from 4.5 to 7. Similar results have been reported by many researchers (Boy et al., 1995; Kendall, 2003; Martel et al., 1997), where metal leaching was observed to be pH dependent. The surface charge of iron oxides is a function of pH, with an increasingly net negative charge as the pH increases above the zero point of charge. The trend observed in this study is consistent with cation sorption (Pb^{2+} and $Cr(OH)^{2+}$) to the iron oxide formed on the steel grit surface, where a fraction of sorbed metals desorb during leaching (Strawn and Sparks, 1999; Swift et al., 1991). To further investigate plausible processes, adsorption/desorption and precipitation/dissolution modeling were applied.

8.3 Mechanistic Modeling of Metal Leaching

Based on the above discussion, bidentate surface complexes are assumed in this study, where $FeOH^0$ represents a surface hydroxyl group and the surface reaction for either

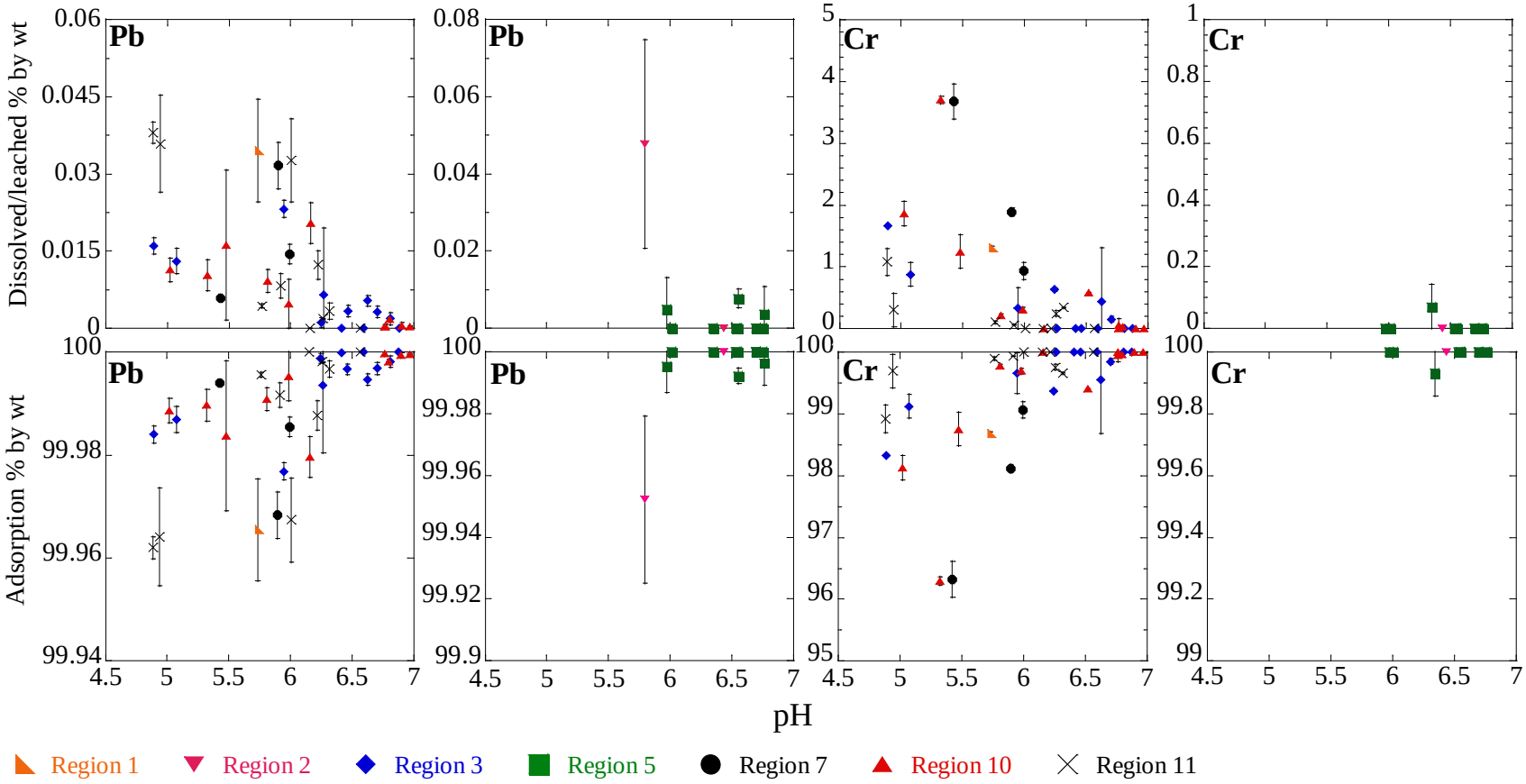

Figure 8.2 Adsorption edges for Pb and Cr from the paint waste are shown after 18 hours of equilibration with 50g L^{-1} paint waste in Fluid #1 (0.1 N CH_3COOH, which has been adjusted with NaOH to an initial pH of 4.93 ± 0.05) or Fluid #2 (0.1 N CH_3COOH, which has an initial pH of 2.88 ± 0.05) based on the alkalinity of the waste material. Ionic strength = 0.1 M.

Pb^{2+}, $Cr(OH)^{2+}$, Ba^{2+}, or Zn^{2+} (Me) on HFO is the following:

$$\equiv Fe-OH^{0}+Me^{2+} = \equiv Fe-OMe^{+}+H^{+} \qquad \log K_{Me} \text{ (Dzombak and Morel, 1990)}$$

In our study, non-detectable to 0.048% by wt of the total Pb leached from the paint waste for the pH range of 4.5 to 7 (Table 8.1; Figure 8.3). Although XRD analysis reveals the presence of $PbCrO_4$ and Pb_3O_4 in the paint waste (Chapter 6), these forms of Pb are associated with residual phase. Based on lead solubility (Appendix D), $PbCO_3$ (cerrusite) is considered as the dominant solid for pH less than 8, while $Pb_3(OH)_2(CO_3)_2$ (hydrocerussite) controls the solubility for pH greater than or equal to 8. This result is consistent with that found by Barnes and Davis (Barnes and Davis, 1996). However, the precipitation simulation did not capture the leaching data from TCLP procedure and overestimated the dissolved lead in the solution. The diffuse layer model (log K_{Me} = 4.65 for Pb) (Dzombak and Morel, 1990) captured 90% of the data within the 95% confidence level, suggesting that sorption to the iron oxides plays an important role in Pb leaching. Interestingly, leaching from pH 4.5 to 5.5 resulted in less desorption than that obtained from adsorption modeling with DLM. This result is likely attributed to the continuum of sorption reactions between specific adsorption and surface precipitation/coprecipitation of the Pb mineral occurring on the steel grit surface, which is in agreement with previous studies of weathered steel slag by Apul et al (Apul et al., 2005).

$$S-OH+Me^{2+}+H_2O \leftrightarrow S-O-MeOH_2^{+}+H^{+} \quad \text{(Bradl, 2004; Dzombak and Morel, 1990)}$$

$$S-O-MeOH_2^{+}+Me^{2+}+H_2O \leftrightarrow S-O-MeOH_2^{+}+Me(OH)_{2(s)}+2H^{+} \qquad \text{(Bradl, 2004)}$$

Initial surface precipitates may exhibit a disordered lattice (amorphous) and therefore are metastable. Over time, as these nano-particles assemble into larger particles, metals are

Table 8.1 Total Concentration, Boundary Conditions, and Leached Concentrations Used in Surface Complexation Modeling

	Pb			Cr			Ba			Zn		
	mean	**mini**	**max**	**mean**	**min**	**max**	**mean**	**min**	**max**	**mean**	**min**	**max**
Total Concentrations in the paint (mg/kg)[a]	4.6×10^{4}	5	1.7×10^{5}	3,018	21	1×10^{4}	6,600	228	1.6×10^{4}	1.3×10^{5}	1.3×10^{4}	1.1×10^{6}
Leached concentrations over TCLP procedure (M or mol/L)	1.4×10^{-6}	BDL[b]	1.0×10^{-5}	1.5×10^{-5}	BDL	1.8×10^{-4}	1.0×10^{-5}	BDL	7.1×10^{-5}	0.0066	3.1×10^{-4}	0.02
Desorbed metal concentrations over TCLP procedure (% of total metal)	0.011	BDL	0.048	0.62	BDL	3.7	0.55	BDL	2.1	11.72	0.41	53.5

a: The values are based on results from XRF.

b: BDL refers to below detection limit.

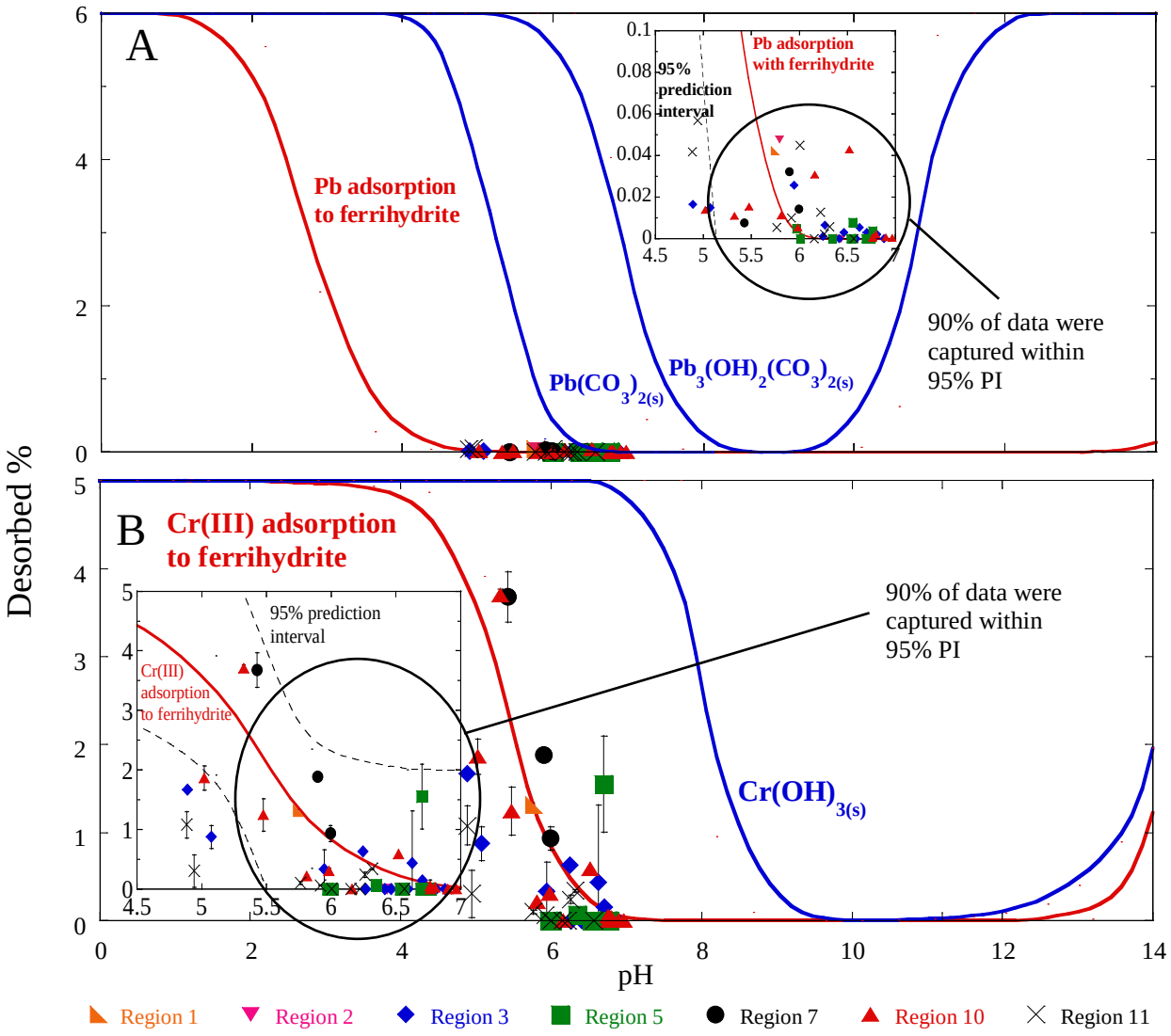

Figure 8.3 Desorbed Pb (A) and Cr (B) in the presence of steel grit associated with paint waste as a function of pH after 18 hours using the TCLP. Cr_T = 1.8×10^{-4} M, Pb_T = 1.0×10^{-5} M, Fe_T = 0.07 M, ionic strength = 0.1 M, surface area = 600 m^2/g, K_{MePb} = $10^{4.65}$(Dzombak and Morel, 1990), K_{MeCr} = $10^{2.11}$(Dzombak and Morel, 1990), $K_{soPbCO3}$ = $10^{-13.13}$ (Benjamin, 2002), $K_{so\ Pb3(OH)2(CO3)2}$ = $10^{-45.46}$ (Benjamin, 2002), and $K_{soCr2O3}$ = $10^{-33.13}$ (Benjamin, 2002).

trapped in the iron oxide structure and re-arranged on the steel grit surface (Lu et al., 2011). The oxides slowly converts to the more stable, less reactive, crystalline form, which has a lower solubility. These results are consistent with that observed by Apul et al. (Apul et al., 2005) and Meima and Comans (Meima and Comans, 1998) where they found both adsorption and coprecipitation are important processes that affect Pb leaching from the incinerator bottom ash and steel slag.

Similar with the Pb work, precipitation modeling of the TCLP results overestimated the dissolved concentrations in the system. Although the chromium hydroxide $Cr(OH)_3$ (or Cr_2O_3) was observed in paint waste (Chapter 6) based on its solubility (Appendix D), $Cr(OH)_3$ may influence metal leaching for pH greater than 6.8 (Figure 8.3). The desorbed Cr decreased as pH increased from 4.5 to 7 and the adsorption simulation captured 90% of the desorption data within the 95% confidence interval. The DLM model adequately predicted the observed leaching (Figure 8.3) in the paint waste suggesting sorption/desorption from the iron oxide surface as the dominant process. This result is similar to that found by Jing et al. (Jing et al., 2006) where leaching behavior of Cr was mainly controlled by the adsorption on iron oxides in the solidified soil. In addition, the trend is consistent with the trivalent Cr leaching (i.e., cation adsorption/desorption). In this study, Cr(III) is expected to be the dominant species, although a small fraction of Cr(VI) maybe exist in the leachate. Cr is introduced in paint as Cr_2O_3 and CrO_4^{2-} (Doroszkowski et al., 1999). Reduction of Cr(VI) to Cr(III) has been observed under acidic conditions (pH < 7) (Chowdhury et al., 2012) as well as with reducing agents Fe(II) or zero valent iron (Chowdhury et al., 2012; Du et al., 2012; Stipp et al., 2002). Hexavalent chromium may be reduced to trivalent chromium in the presence

of ferrous iron (magnetite) ($Cr^{6+} + 3Fe^{2+} \rightarrow Cr^{3+} + 3Fe^{3+}$) or zero-valent (steel grit) iron under acidic conditions. Therefore, Cr(III) is expected to be the dominant speciation in the system. Compared to Pb, Cr (as great as 9.52 mg/L or 3.7% by wt) leached to a greater degree than lead (0.048% by wt for Pb). Because of the difference between Pb and Cr surface complexation constants $K_{MePb} = 10^{4.65} > K_{MeCr(III)} = 10^{2.11}$ (intrinsic constant) (Dzombak and Morel, 1990) these results are expected.

Several possible mechanisms described the Ba leaching in the system. Although adsorption occurs on the steel grit iron oxide surface, precipitation of Ba as $BaSO_4$ occurs in the system. Ba has been and is currently used as an extender (Strivens and Lambourne, 1999) in paint. $BaSO_4$ is the primary form applied in paint and XRD results demonstrated that barite ($BaSO_4$) was the dominant form in the system (Chapter 6). In addition, Ba may coprecipite with Sr in the system. Sr is used as pigment in paint (such as strontium aluminate) and is observed from non-detectable to 2,137 mg/kg in this study. A number of researchers (e g., Cravotta, 2008; Mudd et al., 2004) have reported that coprecipitation between Ba and Sr affect Ba leaching from the weathered solid waste. In this study, both sorption and precipitation modeling captured a portion of the leaching data (Figures 8.4 and 8.5). Because of the heterogeneity of solid phase in paint sample, both sorption (including adsorption and coprecipitation Ba-Sr) and precipitation are important processes that affect Ba leaching from the waste. These results are in agreement with previous modeling studies of the leaching behavior of Ba in soils (Dijkstra et al., 2009) and coal ash (Mudd et al., 2004).

Although sorption of Zn may also occur on the steel grit iron oxide surface, coprecipitation has been observed for Zn and HFO

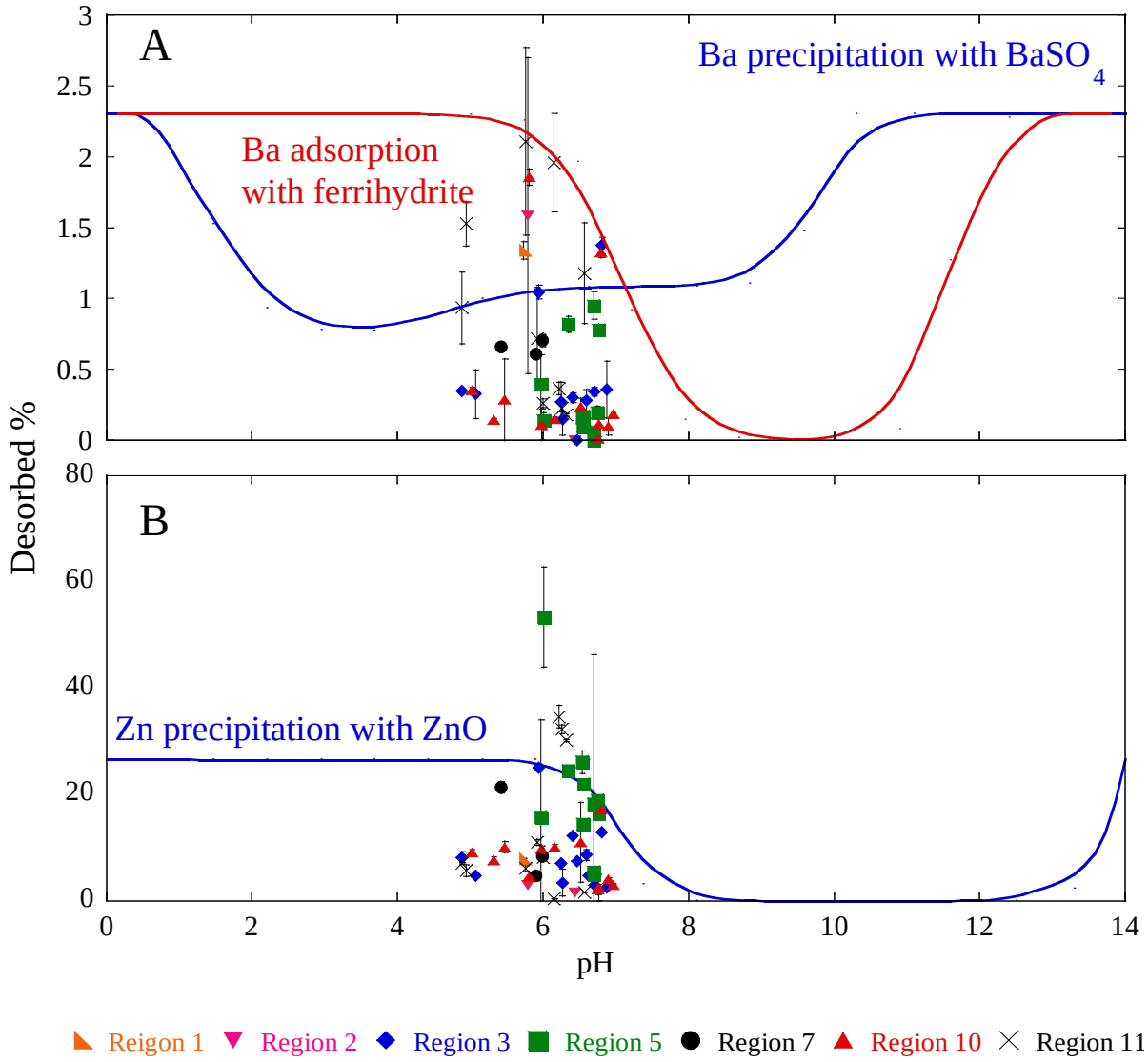

Figure 8.4 Desorbed Ba (A) and Zn (B) in the presence of steel grit associated with paint waste as a function of pH 0 to 14 after 18 hours using the TCLP. $Ba_T = 3.2\times10^{-5}$, $Zn_T = 0.02$, $Fe_T = 0.07$ M, ionic strength = 0.1 M, surface area = 600 m^2/g, $K_{MeBa} = 10^{5.46}$ (Dzombak and Morel, 1990), $K_{MeZn} = 10^{3.49}$ (Dzombak and Morel, 1990), $K_{soBaSO4} = 10^{-9.86}$ (Benjamin, 2002), and $K_{soZnO} = 10^{-16.12}$ (Benjamin, 2002).

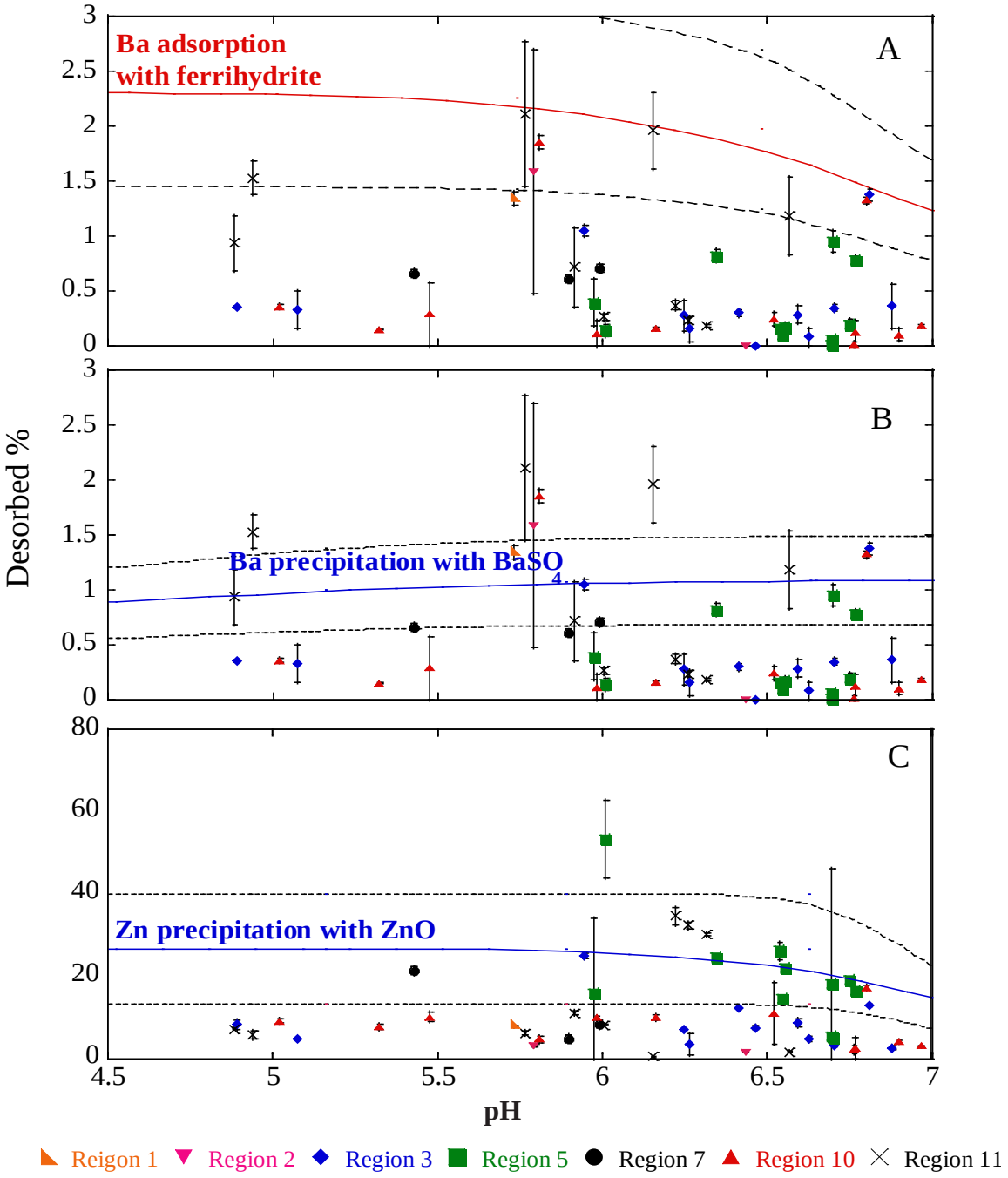

Figure 8.5 Desorbed Ba (A, B) and Zn (C) in the presence of steel grit associated with paint waste as a function of pH 4.5 to 7 after 18 hours using the TCLP. $Ba_T = 3.2\times10^{-5}$, $Zn_T = 0.02$, $Fe_T = 0.07$ M, ionic strength = 0.1 M, surface area = 600 m^2/g, $K_{MeBa} = 10^{5.46}$ (Dzombak and Morel, 1990), $K_{MeZn} = 10^{3.49}$ (Dzombak and Morel, 1990), $K_{soBaSO4} = 10^{-9.86}$ (Benjamin, 2002), and $K_{soZnO} = 10^{-16.12}$ (Benjamin, 2002). The dash line represents the 95% prediction interval.

(Crawford et al., 1997; Trivedi et al., 2001). In addition, ZnO, observed with XRD (Chapter 7), is the precipitated in the paint waste. In addition to ZnO, other zinc minerals, such as $ZnCrO_4$ and ZnS applied in paint, may limit the dissolution of Zn and subsequently control the upper limit of Zn concentrations in the system. In this study, Zn leaching was observed as great as 50% of the total Zn in the paint waste (Table 8.1). Sorption modeling underestimated the Zn leaching, while precipitation modeling overestimated the dissolved Zn from paint. Therefore, both sorption (including adsorption and coprecipitation Zn/HFO) and precipitation are important processes that affect Zn leaching from the waste.

8.4 Summary

Overall, the DLM described leaching of Pb and Cr in the presence of the steel grit. Adsorption/desorption is likely the main mechanism responsible for the Pb and Cr leaching. For Ba and Zn, both sorption and precipitation are important processes supporting predictive mechanistic leaching from the waste. Nonetheless, ferrihydrite, the dominant phase on the steel grit surface, provides abundant binding sites for trace metals. Surface sorption and co-precipitation may lead to structural incorporation of sorbed metals. Consequently, removal of metals (such as Pb) by iron oxides in the environment may be permanent. The findings in this study may have positive implications for DOT agencies in addressing disposal and management of paint waste during bridge rehabilitation.

In fact, in addition to iron oxide, other minerals and phases in paint waste may also affect leaching, such as TiO_2. Therefore, a number of factors may affect metal

leaching behavior including total metal concentrations in the paint waste, dominant sorbents present, competing metal ions, and the pH of the system. To develop a practical model that can be used for in-situ characterization, Fe along with other minerals (metals) present at elevated concentration in the paint waste samples are expected to play important roles in the statistical model accounting for their potential influence on metal leaching. In the next chapter, PCA is invoked to address and support the analysis of significant variables. Consequently, statistically-based models for leaching from paint waste are developed.

CHAPTER 9

STATISTICAL MODEL DEVELOPMENT FOR METAL LEACHING FROM BRIDGE PAINT WASTE IN THE PRESENCE OF STEEL GRIT.

Mechanistic models provide a mathematical form of the equilibrium reaction based on mass balances of the species present and surface charge effects (Bradl, 2004). However, because this approach requires water chemistry conditions and species present, mechanistic models in general are more complex. Given that field data will be used to classify waste, statistical modeling is introduced into this study. Mechanistic modeling is used to support PCA of data obtained with FP-XRF. The statistical models formulated in this work are based exclusively on data collected from bridges undergoing rehabilitation where steel grit was used as the blasting material.

9.1 Principal Component Analysis (PCA)

In this study, applying PCA to the raw data showed essentially three main constituent axes with eigenvalues greater than 1 (Table 9.1), together explaining 85% of the data variance. The first PC represents 55.3% of the total variability and strong relationships with the associated total concentration present in the samples. The positive weights (i.e. As, Cr, Cd, Pb, and Ag) are associated with the bridge blasted with SSPC 6, while the negative weights (i.e. Hg, Se, and Zn) were related with the bridges applied with SSPC 10 during bridge rehabilitation. Surface preparation standard SSPC (The Society for Protective Coatings) SP-6 (Commercial Blast Cleaning) (NYSDOT, 2008) has been applied to bridges in New York State before 2006, where paint and rust from steel were removed to a remaining residual

Table 9.1 Principal Component Loadings of Total Metals in the Paint Waste Samples

Variable	PC 1	PC 2	PC 3
As	0.829	-0.433	-0.22
Ba	0.658	0.429	0.19
Ca	0.655	-0.165	0.672
Cd	0.877	-0.342	-0.243
Cr	0.854	-0.432	0.004
Fe	0.375	0.705	-0.437
Pb	0.863	-0.448	-0.027
Hg	**-0.698**	-0.477	-0.191
Ag	0.886	-0.358	-0.228
Se	**-0.787**	-0.518	-0.127
Ti	0.297	0.665	-0.156
Zn	**-0.851**	-0.418	-0.034
Eigenvalue	6.63	2.64	1.00
Proportion	0.553	0.22	0.076
Cumulative	0.553	0.773	0.849

Correlation value greater than 0.66 are highlighted

of 33% of the total removal area. After 2006, SSPC SP-10 (Near White Blast Cleaning) was required in the blasting procedure (NYSDOT, 2008) for all regions in NY. SP-10 restricts the visible residues remaining on the bridge surface to 5% of the total removal area. In this study, elevated total concentrations of As, Cd, Cr, Pb, and Ag were observed from bridges in Regions 1, 3, 7, 10, and 11, where the SSPC SP-6 blasting standard was applied. Greater concentrations of total Hg, Se, and Zn were related with the bridges in Regions 2 and 5, which were blasted with surface preparation standard SSPC SP-10 (Margrey, 2012) during rehabilitation. With the first PC, fifty-five percent of the total variability can be explained.

The second PC in PCA revealed the influence of Fe in the paint waste demonstrating that Fe is an important factor impacting model variability in paint waste. This result is attributed to the iron oxides formed on the steel grit surface, which provides a highly reactive surface for metal sorption in the system and further controls the degree of metal leaching from the paint waste. In addition to Fe, Ti was also observed to be an important factor in the paint waste based on PC2 (Table 9.1). This result is somewhat attributed to the application of TiO_2 as extenders in paint, which may provide sorption surface for trace metals as well. The third PC exhibited the effect of Ca in the paint waste. The observed behavior of Ca is consistent with Andra et al. (2011), where Ca was an important factor in the mobilization of Pb from alkaline soils in San Antonio, TX. The observed Ca is attributed to the application of calcite ($CaCO_3$) (12% by wt in paint waste, Chapter 6) as an extender (supplementary pigments) in the paint (Lambourne and Strivens, 1999). The release of the $CaCO_3$ from paint waste does not directly affect the metal leaching. However, the dissolution of the $CaCO_3$ results in an increase in pH during

the leaching procedure. Because metal leaching is a function of pH, dissolution of the $CaCO_3$ reflects this pH change and hence metal leaching. Therefore, $CaCO_3$ is expected to be an important factor in the leaching model.

Using PCA analysis, the most important factors accounting for total variability are the surface preparation standard (reflected in Table 9.1 (PC1)) and steel grit (iron) remaining in the paint waste (reflected in Table 9.1 (PC2)). Other factors such as Ti and Ca (reflected in Table 9.1 (PC2 and PC3)) also impact the variability in paint waste. These results are consistent with the correlations presented earlier in Chapter 6.2 and mechanistic processes identified in Chapter 8. Therefore, metal leaching (the release of trace metal cation or anion to the water phase) depends on (a) total metal concentrations; (b) $CaCO_3$ affecting the pH and alkalinity; (c) Fe oxides providing a highly reactive surface for metal sorption; and, (d) other groups of metals such as Zn and Ti in the paint waste.

To address the best-fit model of experimental data, the mathematical form should be chosen to be as simple as possible with the number of adjustable parameters at a minimum. Therefore, multiple regression analysis was applied in this study.

9.2 Statistical Modeling for Field Characterization of Waste Classification

Given an understanding of mechanistic processes along with a demonstrated analysis of variables through PCA, statistically-based models for leaching from paint waste are developed. In this study, MLRA was applied to establish a single correlation between a dependent and several independent variables. Metal leaching is the dependent variable and the metal concentrations from PCA are independent variables. The primary objective

of this analysis was to use independent variables capable of predicting the dependent variable leached metal concentration. Results from leaching studies (TCLP and MEP) (Chapter 7) were used to assess predicted values. Because the surface preparation standard was observed to be an important factor in PCA analysis, leaching results were sorted into groups with respect to the two methods: SSPC 6 and SSPC 10 (Table 9.2). The surface preparation methods mentioned here refer to the ones applied in the previous rehabilitation, which determined the residual waste remaining on the bridge.

Visually, the threshold in Fe concentrations is estimated from 17% to 24% by weight (Figure 9.1). Therefore, a range of threshold values at 1% intervals were tested to examine the significance of regression. Comparing the mean square errors (MSE) (regime 1 and regime 2) obtained from each threshold considered, the breakpoint (regime 1 and regime 2) with the smallest MSE was determined as the select threshold for this study. Consequently, two regime regressions were obtained with Fe concentrations ($\leq$ 20% or > 20% by wt) in the paint waste. A series of residual plots revealed the reasonableness of the two regime models (Appendix F). In addition, the Chow test (F test on extra sum of squares) (Chow, 1960) indicated that two regime models were more adequate compared to a simpler model (single regime) (Appendix F).

Based on the two regime models developed, one formulation with an indicator variable is presented as follows:

(iv) $Y = y_{1*}(1 - \lambda) + y_{2*}\,\lambda$ $\quad Fe \leq 20\%\ \lambda = 0$

$\quad Fe > 20\%\ \lambda = 1$”

λ is an indicator variable in the two regimes; y_1 and y_2 represent the two regime models derived from statistical analysis as follows:

Table 9.2 Sample Sorted with Respected to Surface Preparation Standard and Fe Concentrations

Region	Bridges	SSPC 6		SSPC 10
		Fe ≤ 20%	Fe > 20%	7 ≤ Fe ≤ 80%
Region 1`	1-1		√	
Region 2	2-1			√
	2-2			√
Region 3	3-1		√	
	3-2	√	√	
	3-3*	√	√	
Region 5	5-1			√
	5-2			√
	5-3			√
	5-4			√
	5-5			√
Region 7	7-1*	√	√	
	7-2	√		
Region 10	10-1*	√	√	
	10-2		√	
	10-3	√		
	10-4		√	
	10-5	√		
	10-6		√	
	10-7	√		
	10-8		√	
	10-9	√		
Region 11	11-1*	√	√	
	11-2*	√	√	

* Great variability of Fe concentrations were observed in different sampling locations.

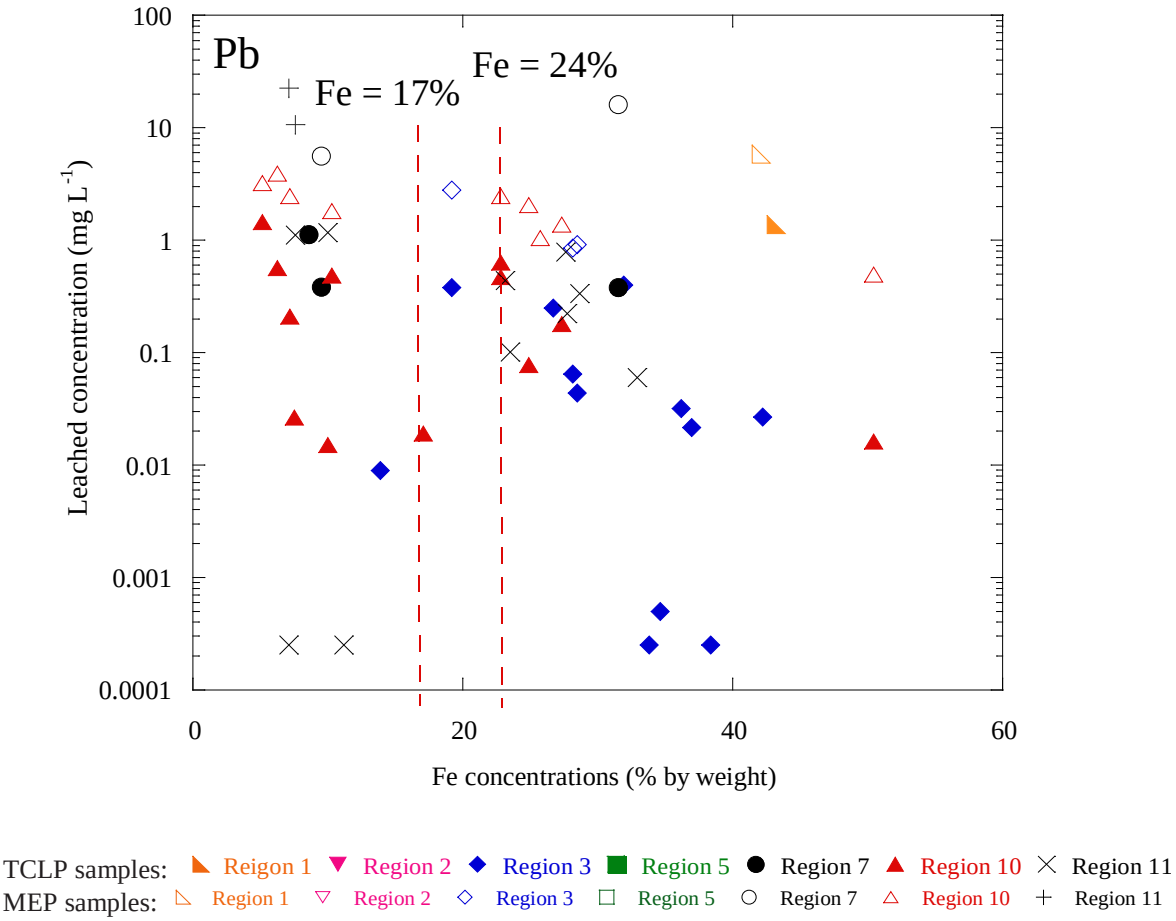

Figure 9.1 Leached Pb concentrations are shown as a function of total Fe (% by wt) concentrations in paint waste. The dash lines represent the threshold range observed in this study.

(v) Multivariate regression is tested in the first step of modeling.

$$\text{Leached metal} = a + b\cdot(\text{total Ca}) + c\cdot(\text{total Fe}) + d\cdot(\text{metal}_{i,\text{total}}) + e\cdot(\text{metal}_{i+1,\text{total}}) + \ldots + n\cdot(\text{metal}_{n,\text{total}})$$

(vi) Box-Cox transformation (Kutner et al., 2005) is applied according to the residual analysis if necessary, where leached metal y is transformed to y^{λ}:

$$(\text{Leached metal})^{\lambda} = a + b\cdot(\text{total Ca}) + c\cdot(\text{total Fe}) + d\cdot(\text{metal}_{i,\text{total}}) + e\cdot(\text{metal}_{i+1,\text{total}}) + \ldots + n\cdot(\text{metal}_{n,\text{total}})$$

(vii) Transformed models:

$$\log(\text{leached metal}) = a + b\cdot\log(\text{total Ca}) + c\cdot\log(\text{total Fe}) + d\log(\text{metal}_{i,\text{total}}) + e\cdot\log(\text{metal}_{i+1,\text{total}}) + \ldots + n\cdot\log(\text{metal}_{n,\text{total}})$$

where leached metal concentrations are in mg L^{-1}, a-n are coefficients determined using regression with appropriate data sets (Appendix F), and total metal is in mg kg^{-1} based on FP-XRF. The adsorption capacity is a function of iron oxides in the paint waste, which is represented by total Fe in the equation. Total Ca represents the calcite ($CaCO_3$) applied in the paint, which may also affect the pH (and alkalinity) during leaching. $Me_{i,total}$ represents other total metals in the paint waste that may affect the metal leaching. This last variable may be an artifact of the waste composition where a number of metals were observed to be present.

Specifically, for each model, the F-test (ANOVA), goodness of fit, and t-test were applied to evaluate the significance of regression, individual coefficients, and subset of coefficients (F-test) (Appendix F). Based on the PCA analysis, highly correlated metals were removed from the model to reduce the number of variables. The significance of a

restricted model was assessed using a partial F-test. Furthermore, a series of residual plots were applied to investigate the reasonableness of the restricted model (Appendix F).

The coefficient of determination, R^2 (Tables 9.3 and 9.4), is an estimate of the model fit in predicting observed leaching. The % variation of the data is explained by the best fit.

R^2 = sum of squares (regression) / sum of squares (total)

A P value of 5% or less is generally accepted as the point at which there is a 5% chance that the results would have been observed in a random distribution. In other words, the model is specified correctly with a 95% probability.

The statistical models developed for metal leaching demonstrated 96 percent of the data fall within the 95% confidence level for Pb (R^2 0.6 – 0.9, $p \leq 0.04$), Ba (R^2 0.5 – 0.7, $p \leq 0.1$), and Zn (R^2 0.6 – 0.7, $p \leq 0.08$) (Tables 9.3 and 9.4) (Figures 9.2 to 9.5). However, the regression model obtained for Cr leaching was not significant (R^2 0.3 – 0.5, $p \leq 0.75$) (Table 9.3) as the p value was observed as great as 0.75, suggesting the regression is not significant for Cr. Good correlations were observed between predicted and observed metal leaching for bridge samples blasted with SSPC 10 preparation (R^2 = 0.84 for Pb, R^2 = 0.70 for Ba, and R^2 = 0.71 for Zn) (Figures 9.2 to 9.5).

Compared to the bridges cleaned with SSPC 6, the bridges blasted using SSPC 10 revealed less leached metal concentrations. For example, leached Pb concentrations varied from less than 0.0005 (detection limit) to 0.83 mg L^{-1}, which are less than TC level of 5 mg L^{-1}. Similarly, these samples revealed less than 0.0007 (detection limit) to 0.98 mg L^{-1} for Cr, and less than 0.0004 (detection limit) to 1.06 mg L^{-1} for Ba; these fall below the TC level of 5 mg L^{-1} for Cr and 100 mg L^{-1} for Ba. Results indicate that the

Table 9.3 Statistical Analysis Results from Multivariate Regression of the Leached Metal Concentrations for Pb and Cr (mg L^{-1})

Metal	Surface preparation	Model used for prediction	Threshold	R^2	Number of Samples	Number of Observations[a]	Statistical Significance
Pb	SSPC 6	Pb leaching (mg L^{-1}) = 10 ^ [- 69.2 + 51.1λ - (5.9 - 6.5 λ) log (Fe mg/kg^{-1}) – (5.2 - 4.3 λ) log Cr (mg Kg^{-1}) + (15.4 - 11.2 λ) log Pb (mg Kg^{-1}) + (4.9 - 4.6 λ) log Ca (mg Kg^{-1}) + (4.9 - 4.2 λ) log Ti (mg Kg^{-1}) - (20.1-23.1 λ) log Ag (mg Kg^{-1}) + (16.4 - 20.7 λ) log Cd (mg Kg^{-1})	Fe ≤ 20% λ = 0	0.7	23	20	P = 0.04
			Fe > 20% λ = 1	0.6	32	28	P = 0.003
	SSPC 10	Pb leaching (mg L^{-1}) = exp [-5.1 + 0.00038 Pb (mg Kg^{-1}) + 0.000056 Ca (mg Kg^{-1}) – 0.000078 Ti (mg Kg^{-1})]		0.8	20	11	P = 0.004
Cr	SSPC 6	Cr leaching (mg L^{-1}) = 10 ^ (-5.8 + 33.1 λ + (0.91- 5.63 λ) log (Fe mg Kg^{-1}) – (3.77 + 2.34 λ) log (Cr mg Kg^{-1}) + (1.52 – 2.32 λ) log (Zn mg Kg^{-1}) - (3.89 – 4.17 λ) log (Ca mg Kg^{-1}) + (2.37+2.60 λ) log (Ti mg Kg^{-1}) –(8.24-8.24 λ) log (Cd mg Kg^{-1}) + (8.24-9.53 λ) log (As mg Kg^{-1}) - 0.80 λ log (Zn mg Kg^{-1}) +1.8 λ log (Pb mg Kg^{-1}) +1.3 λ log (Ag mg Kg^{-1}))	Fe ≤ 20% λ = 0	0.5	23	21	P = 0.19
			Fe > 20% λ = 1	0.3	32	20	P = 0.26
	SSPC 10	Cr leaching (mg L^{-1}) = 12.4 - 0.000022 Zn (mg Kg^{-1}) - 0.000032 Fe (mg Kg^{-1}) + 0.0077 Cr (mg Kg^{-1}) + 0.000053 Pb (mg Kg^{-1}) - 0.00020 Ca (mg Kg^{-1}) - 0.000038 Ti (mg Kg^{-1})		0.5	20	8	P = 0.75

a: The number reflects the samples above the detection limit

Table 9.4 Statistical Analysis Results from Multivariate Regression of the Leached Metal Concentrations for Ba and Zn (mg L^{-1})

Metal	Surface preparation	Model used for prediction	Threshold	R^2	Number of Samples	Number of Observations[a]	Statistical Significance
Ba	SSPC 6	Ba leaching (mg L^{-1}) = 11.9 - 10.3λ - (0.00046 - 0.00046 λ) Ba (mg Kg^{-1}) - (0.0000091 - 0.000010λ) Fe (mg Kg^{-1}) + (0.00047-0.00059 λ) Cr (mg Kg^{-1}) - (0.000038-0.000038λ) Pb (mg Kg^{-1}) – (0.00018 - 0.00015 λ) Ca (mg Kg^{-1}) + (0.00012-0.00015λ) Ti (mg Kg^{-1}) – (0.021-0.039 λ) Cd (mg Kg^{-1}) - 0.018 λ Ag (mg Kg^{-1})	Fe ≤ 20% λ = 0	0.5	23	22	P = 0.1
			Fe > 20% λ = 1	0.5	32	27	P = 0.02
	SSPC10	Ba leaching (mg L^{-1}) =[-0.66 - 2.18×10^{-5} Ba (mg Kg^{-1}) + 2.63×10^{-6} Zn (mg Kg^{-1}) + 3.37×10^{-6} Fe (mg Kg^{-1}) + 0.00011 Pb (mg Kg^{-1}) - 1.14×10^{-5} Ca (mg Kg^{-1}) - 0.0014 As (mg Kg^{-1})]$^{0.5}$		0.7	20	19	P = 0.01
Zn	SSPC 6	Zn leaching (mg L^{-1}) = 416 - 300 λ + (0.0019 + 0.0021λ) Zn (mg Kg^{-1}) – (0.017 - 0.014 λ) Pb (mg Kg^{-1}) – (0.061 - 0.0038 λ) Cr (mg Kg^{-1}) + (0.0068 - 0.011 λ) Ca (mg Kg^{-1}) + (0.025 - 0.016 λ) Ti (mg Kg^{-1}) + (5.0 -10.5 λ) Cd (mg Kg^{-1}) + (0.095-0.095 λ) As (mg Kg^{-1}) + (19.7 λ) Ag (mg Kg^{-1})	Fe ≤ 20% λ = 0	0.7	23	22	P < 0.003
			Fe > 20% λ = 1	0.6	32	29	P < 0.008
	SSPC 10	Zn leaching (mg L^{-1}) = [0.40 - 0.00050 Ba (mg Kg^{-1}) + 5.27×10^{-5} Zn (mg Kg^{-1}) + 4.79 Ag (mg Kg^{-1}) - 0.015 As (mg Kg^{-1})]^2		0.7	20	19	P = 0.001

a: The number reflects the samples above the detection limit

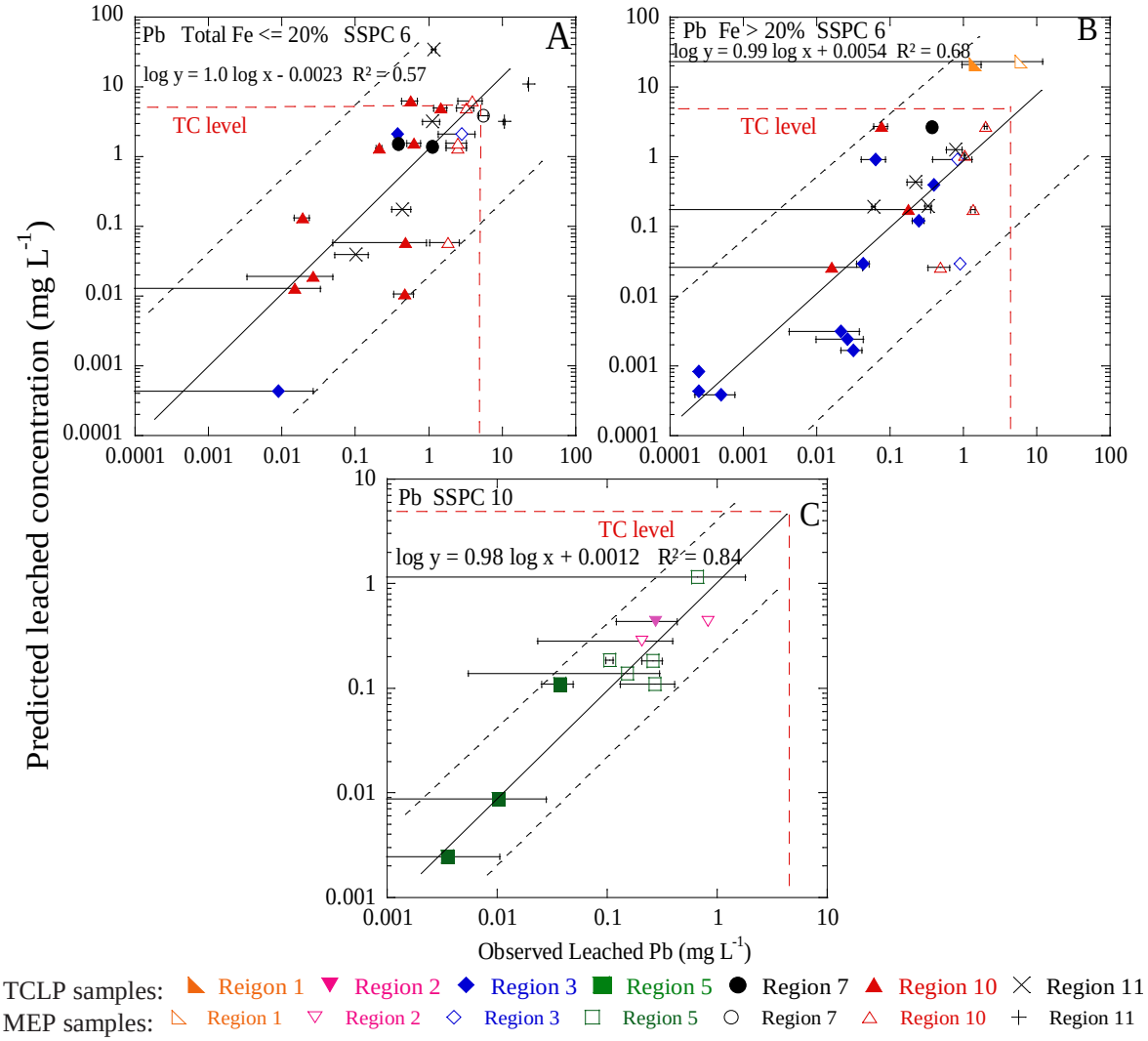

Figure 9.2 Comparison of the results from predicted and observed leached Pb concentrations. The samples represent the TCLP and first day of the MEP extraction conducted on the paint waste samples. Bridges were blasted to (A) surface preparation SSPC 6 with total Fe concentration less than or equal to 20% (% by wt), number of observations N = 20; (B) SSPC 6 with total Fe concentration greater than 20% (% by wt). N = 28; and (C) SSPC 10 N = 11. TC level for Pb is 5 mg L^{-1}. The dash line represents the 95% prediction interval.

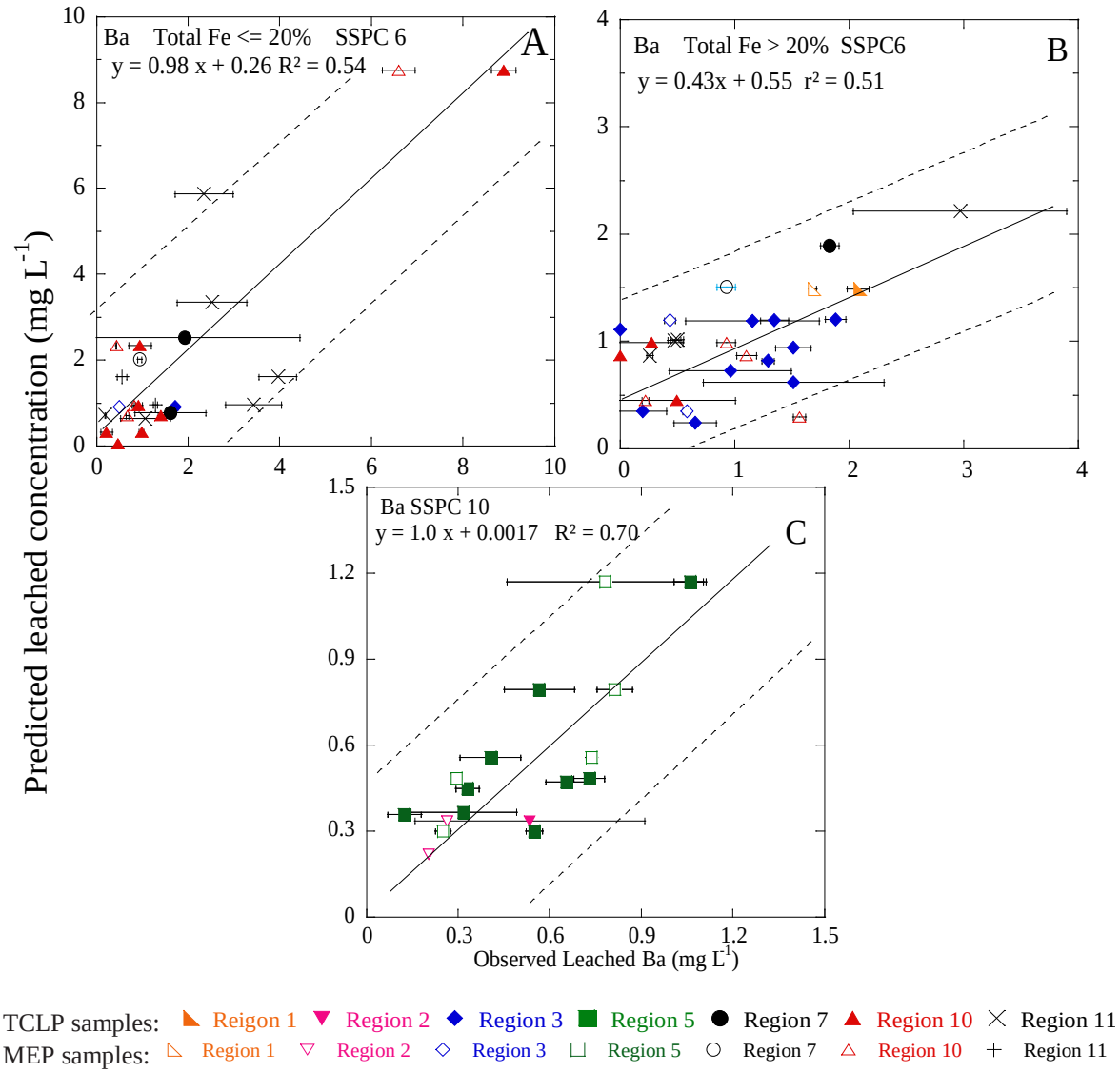

Figure 9.3 Comparison of the results from predicted and observed leached Ba concentrations. The samples represent the TCLP and first day of the MEP extraction conducted on the paint waste samples. Bridges were blasted to (A) surface preparation SSPC 6 with total Fe concentration less than or equal to 20% (% by wt), number of observations N = 22; (B) SSPC 6 with total Fe concentration greater than 20% (% by wt). N = 27; and (C) SSPC 10 N = 19. TC level for Ba is 100 mg L^{-1}. The dash line represents the 95% prediction interval.

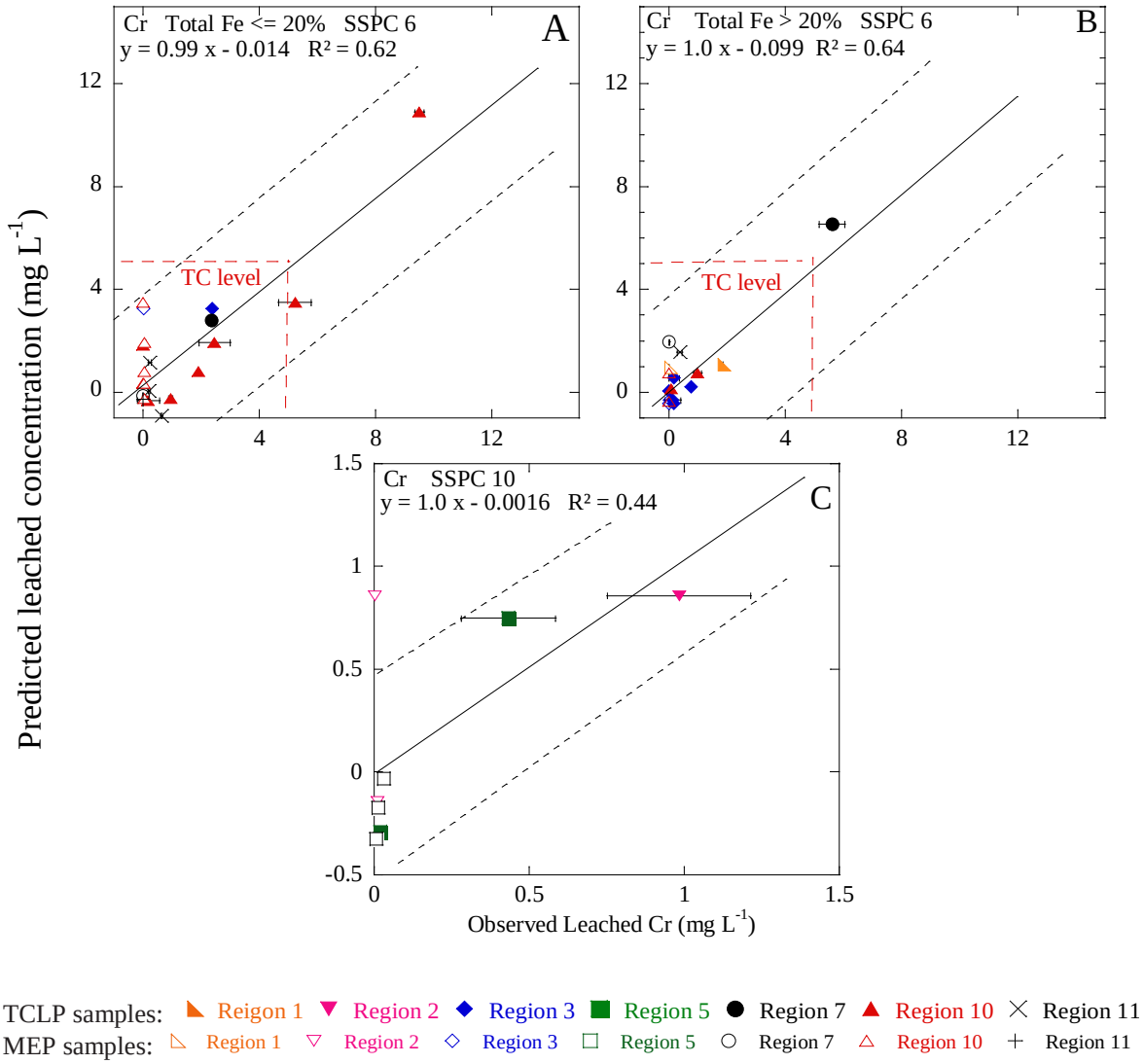

Figure 9.4 Comparison of the results from predicted and observed leached Cr concentrations. The samples represent the TCLP and first day of the MEP extraction conducted on the paint waste samples. Bridges were blasted to (A) surface preparation SSPC 6 with total Fe concentration less than or equal to 20% (% by wt), number of observations N = 21; (B) SSPC 6 with total Fe concentration greater than 20% (% by wt). N = 20; and (C) SSPC 10 N = 8. TC level for Cr is 5 mg L^{-1}. The dash line represents the 95% prediction interval.

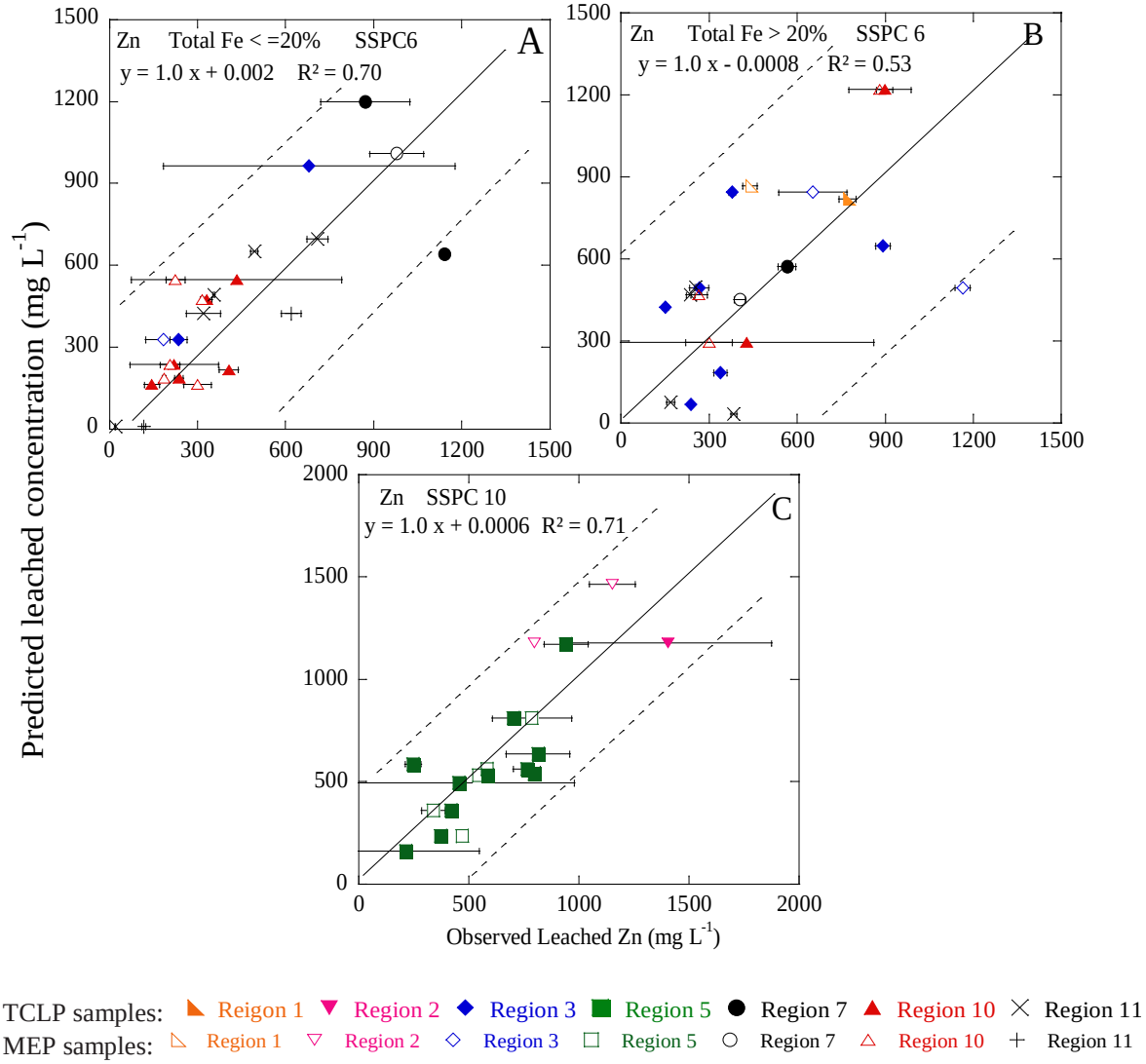

Figure 9.5 Comparison of the results from predicted and observed leached Zn concentrations. The samples represent the TCLP and first day of the MEP extraction conducted on the paint waste samples. Bridges were blasted to (A) surface preparation SSPC 6 with total Fe concentration less than or equal to 20% (% by wt), number of observations N = 22; (B) SSPC 6 with total Fe concentration greater than 20% (% by wt). N = 29; and (C) SSPC 10 N = 19. The dash line represents the 95% prediction interval.

paint waste from bridges cleaned with SSPC 10 is classified as non-hazardous material. For bridges cleaned with SSPC 6, 9% of the samples exhibited leached Pb concentrations greater than TC level of 5 mg L^{-1} (Figure 9.2), while 5% of the samples revealed leached Cr concentrations greater than TC level of 5 mg L^{-1} (Figure 9.4). Overall, 14% of the samples revealed metal leaching greater than TC levels, suggesting the hazardous nature for these samples. Most of the leaching data can be described adequately over a wide range of total metal concentrations. In contrast to the metals discussed above (Pb, Cr, and Ba), the bridge samples blasted using SSPC 10 revealed greater leached Zn concentrations (from 216 mg L^{-1} to 1405 mg L^{-1}) than the samples cleaned with SSPC 6 (129 mg L^{-1} to 1163 mg L^{-1}). These results are consistent with the increasing usage of zinc primer (ZnO, $Zn_3(PO_4)_2 \cdot 2H_2O$, and epoxy zinc rich primer) (80% zinc content dry) in bridges blasted using SSPC 10.

On the other hand, metal leaching is affected by total Fe concentrations in the paint waste, where iron oxides forms on the steel grit surface providing a reactive surface for metal sorption. In this study, metal leaching increased with decreasing Fe ($\leq$ 20% by wt) compared to that observed with relatively greater Fe concentrations (> 20%). This effect is supported by the model developed as well. A negative correlation was obtained between metal leaching (including Pb and Ba) and total Fe concentrations in the paint: metal leaching decreased as total Fe concentration increased in the samples (Tables 9.3 and 9.4). These results are consistent with the well-recognized importance of iron oxide in surface complexation with trace metals.

9.3 Summary

In this chapter, a statistically - based model was developed based on an understanding of mechanistic processes along with a demonstrated analysis of variables through PCA. These statistical models developed demonstrated 96 percent of the data falling within the 95% confidence level for Pb (R^2 0.6 – 0.9, $p \leq 0.04$), Ba (R^2 0.5 – 0.7, $p \leq 0.1$), and Zn (R^2 0.6 – 0.7, $p \leq 0.08$). However, the regression model obtained for Cr leaching is not significant (R^2 0.3 – 0.5, $p \leq 0.75$). The results in this study indicated that the paint waste from bridges cleaned with SSPC 10 may be for the most part classified as non-hazardous material, while 14% of the sample set would be classified as hazardous for the bridges blasted using SSPC 6. A practical advantage in applying models developed is the ability to estimate contaminant leaching from paint waste without additional laboratory studies including TCLP. Therefore, results of this work may assist in better understanding and predicting the mobility of trace metals as well as in addressing disposal and management of paint waste during bridge rehabilitation.

CHAPTER 10

CONCLUSION AND FUTURE WORK

XRF results indicated that although the 24 bridges studied to date have been repainted after 1989, LBP was not entirely removed. Eighty percent of paint waste samples exhibited lead concentrations greater than 5,000 mg kg^{-1}. The elevated iron concentrations are present from the application of steel grit used to remove paint. Other compounds of As, Ba, Cd, Hg, Se, and Ag were observed in paint as pigments and preservatives as well. Pb concentrations were observed to correlate with As (R^2 = 0.78), Cd (R^2 = 0.73), Cr (R^2 = 0.88), and Ag (R^2 = 0.67), while other relationships were observed between Hg and Se (R^2= 0.99), Hg and Zn (R^2 = 0.94), and Se and Zn (R^2= 0.76). The trends were found across all the regions in NYS indicating consistent application of these metals as pigments and extenders in paint composition.

However, although elevated metals were observed in the paint waste, leaching results from TCLP and MEP revealed only up to 22.6 mg L^{-1} for Pb and 9.52 mg L^{-1} for Cr. The relatively low concentrations observed are attributed to the use of iron-based abrasives (steel grit) in the paint removal process. Because steel grit is used for blasting bridges in NY to remove paint, metals such as Pb in the paint waste are sequestered by the elevated iron concentrations, which ranged from 5 - 80% by wt. As a result, metal concentrations in the leachate are less than the TC level. Sequential extraction demonstrated that less than 6.8% of Pb, Cr, and Ba were associated with the exchangeable and carbonate forms, while greater contributions were found with iron oxides. The largest fraction, however, greater than 80%, was associated with the residual phase comprised of minerals in the paint including SiO_2 and TiO_2. XRD analysis

corroborated that iron oxides formed on the steel grit surface provided an important interface for trace metals. The presence of the iron oxides in the paint waste may have an environmental advantage in considering contaminant mobility.

Ferrihyidrite was observed to be an important surface on the steel grit; spherical particle aggregates ranged from 20 to 200 nm in diameter. The DLM described leaching of Pb and Cr in the presence of the steel grit. Adsorption/desorption is likely the main mechanism responsible for the Pb and Cr leaching. For Ba and Zn, both adsorption and precipitation are important processes supporting predictive mechanistic leaching from the waste. Nonetheless, ferrihydrite, the dominant phase on the steel grit surface, provides abundant binding sites for trace metals. Surface sorption and co-precipitation may lead to structural incorporation of sorbed metals. Consequently, removal of metals (such as Pb) by iron oxides in the environment may be permanent. The findings in this study may have positive implications for DOT agencies in addressing disposal and management of paint waste during bridge rehabilitation.

Based on an understanding of mechanistic processes along with a demonstrated analysis of variables through PCA, statistically-based models for leaching from paint waste were developed. The results in this study indicated that the paint waste from bridges cleaned with SSPC 10 may be for the most part classified as non-hazardous material, while 14% of the sample set would be classified as hazardous for the bridges blasted using SSPC 6. Therefore, results of this work may assist in better understanding and predicting the mobility of trace metals as well as in addressing disposal and management of paint waste during bridge rehabilitation.

Future work associated with this research should include model validation in the

field. Because the models developed in this study are based on the collected samples from the 24 bridges in seven regions of NYS, bridge samples collected from other bridge regions or states are suggested for model validation. This research would be beneficial in addressing waste classification for other state DOTs working with similar structures and rehabilitation procedures. Additionally, addressing adsorption mechanisms on the iron oxide surface requires further work. The molecular interaction between trace metals and the iron oxide surface is not well understood yet and needs to be addressed for better description of natural systems. Therefore, techniques including x-ray absorption spectroscopy (XAS) can be applied to determine the structure of the iron oxides coating and the bonding structures of Pb and Cr as the representative metal contaminants in the paint waste. However, the composition of the paint waste is complex and heterogeneous; paint is mixed with the remaining steel grit during the bridge rehabilitation. Hence, separating the steel grit completely from the paint waste is difficult. In addition, the composition of organic and residual phases in the samples are various and not clear, therefore, XAS analysis of bonding structures of Fe and Pb in the paint waste would be challenging.

APPENDIX A

BRIDGES SAMPLED AND SAMPLE DETAILS

The detail information for bridge samples are presented below.

Table A.1 Bridges Sampled and Sample Details

Bridge number	Region	Bridge name and the location	Bin	Date rehabilitated	Date sampled	Wash water sample	Paint waste sample
1	11	Bruckner Expressway, Bronx	106666C		10/29/2010	0	10
2	11	Brooklyn-Queens Expressway(BQE) over Long Island Expressway (LIE), New York	1065569		11/19/2010	0	10
3	3	Route 5 over Roadway A, Syracuse,	1093390	10/20/2010-10/28/2010	11/10/2010	2[a]	10
4	3	Roadway C over Roadway A, Syracuse	1093400	11/03/2010-11/10/2010	11/10/2010-11/12/2010	2[b]	10
5	3	Ithaca	3209900		05/20/2011	0	4[c]
6	10	Rt 107 over Sea Cliff Ave, Sea Cliff	1036889	06/13/2011-06/22/2011	06/14/2011-6/22/2011	4	10
7	5	Virginia-Carolina ramp to I-190 Southbound, Buffalo	1063090	06/02/2011-7/10/2011	06/15/2011-7/13/2011	4	10
8	5	I-190 Southbound ramp to Virginia-Carolina, Buffalo	1063100	06/02/2011-7/10/2011	06/15/2011-7/13/2011	4	10

Bridge number	Region	Bridge name and the location	Bin	Date rehabilitated	Date sampled	Wash water sample	Paint waste sample
9	10	Rt 495 (Wesbound) Service Rd over Nicolls Rd, Queens	1064560	06/27/2011-07/ 22/2011	6/28/2011-07/20/2011	4	10
10	10	Rt 495 (Easbound) Service Rd over Nicolls Rd, Queens	1064570	06/27/2011-07/ 22/2011	6/28/2011-07/20/2011	4	10
11	1	Route 196 over Town Rd/Champlain Canal, Town of Kingsbury, Washington County	4039820		07/17/2011	0	10
12	2	Mainline Thruway over Mohawk River (W. B.), Herkimer County	4423081		07/21/2011 - 08/09/2011	0	10
13	2	Mainline Thruway over Mohawk River (E. B.), Herkimer County	4423082		07/29/2011 - 08/06/2011	0	10
14	5	Two-mile creek Road over I-290, Tonawanda	1044970		08/24/011-09/07/2011	4	10
15	5	East park drive over I-290, Tonawanda	1044980	08/23/2011-09/12/2011	8/23/2011-09/13/2011	4	10
16	5	Peace bridge plaza ramp to I-190 Southbound, Buffalo	1063110	07/17/2011-07/26/2011	08/07/2011 - 08/14/2011	4	10
17	10	Hawkins Ave over Rt 495, Ronkonkoma	1049509	07/25/2011-8/02/2011	07/30/2011 -8/04/2011	0	10

Bridge number	Region	Bridge name and the location	Bin	Date rehabilitated	Date sampled	Wash water sample	Paint waste sample
18	10	Ronkonkoma Ave over Rt 495, Ronkonkoma	1049489	07/18/2011-07/24/2011	07/22/2011-07/26/2011	0	10
19	10	Washington Ave over Rt 495, Ronkonkoma	1049400	08/05/2011-08/15/2011	08/08/2011-08/16/2011	4	10
20	10	Rt 495 (Eastbound) over Commack Rd, New York	1049361	10/05/2011-10/12/2011	10/13/2011	4	10
21	10	Rt 495 (Westbound) over Commack Rd, New York	1049362		10/02/2011	4	10
22	10	Bagatelle Rd over Rt 495, Huntington	1049320		10/02/2011	4	10
23	7	NYS Route 3 over Black River, Town of Rutland	1000540	10/05/2011	10/20/2011	0	10
24	7	NYS Route 37 over Big Sucker Brook, Village of Waddington, St.	1023860	10/05/2011	10/20/2011	0	10

a, b Only one location is available for wash water sampling in the bridge working site.
c Only two locations are available for paint waste sampling in the bridge working site.

Table A.2 Bridge Rehabilitation Information and Pigments Historically Used*.

Paint waste collected	Sample ID	SSPC standard applied	Year built	Year(s) repainted	Paint and pigment information
Region 1	1-1	SP 6	1938	1990,1991	NA
Region 2	2-1 2-2	SP 10	1955	1997	Organic zinc primer (80% zinc dry matter content), epoxy penetration sealer second coat, epoxy third coat, and polyurethane finish coat. Manufacture was Carboline.
Region 3	3-1 3-2	SP 6	1975	1991, 1999	NA
	3-3		1940	1991	
Region 5	5-1	SP 10	1972	2002	Low-gloss to flat-finish, micaceous iron oxides (MIO) pigmented, one component of polyurthane top coat. Manufacture was Xymax Coatings.
	5-2		1972	2002	
	5-3		1963	1998	NA
	5-4		1963	1998	
	5-5		1972	1992	
Region 7	7-1	SP 6	1948	1997	NA
	7-2		1957	1998	

Paint waste collected	Sample ID	SSPC standard applied	Year built	Year(s) repainted	Paint and pigment information
Region 10	10-1	SP 6	1953	1995	NA
	10-2		1970	1979, 1986, 1999	
	10-3		1970	1979, 1986, 1999	
	10-4		1967	1985, 1999	
	10-5		1967	1999	
	10-6		1964	1986, 1989	
	10-7		1963	1978, 1989, 1993, 1994	
	10-8		1963	1978, 1992, 1994, 1995	
	10-9		1963	1977, 1997	
Region 11	11-1	SP 6	1959	1996	NA
	11-2		1969	1990	

SP 6 – Commercial Blast Cleaning where paint and rust from steel were removed to a remaining residual of 33% per unit area of surface.
SP10 – Near White Blast Cleaning where paint and rust from steel were removed to a remaining residual of 5% per unit area of surface. SSPC SP-10 was required in NYS since 2006. However, some contractors have applied SP-10 to the bridges even before 2006.
NA– Historical records for the bridges are not available.
*– lead was discontinued for the bridges paint in New York State.

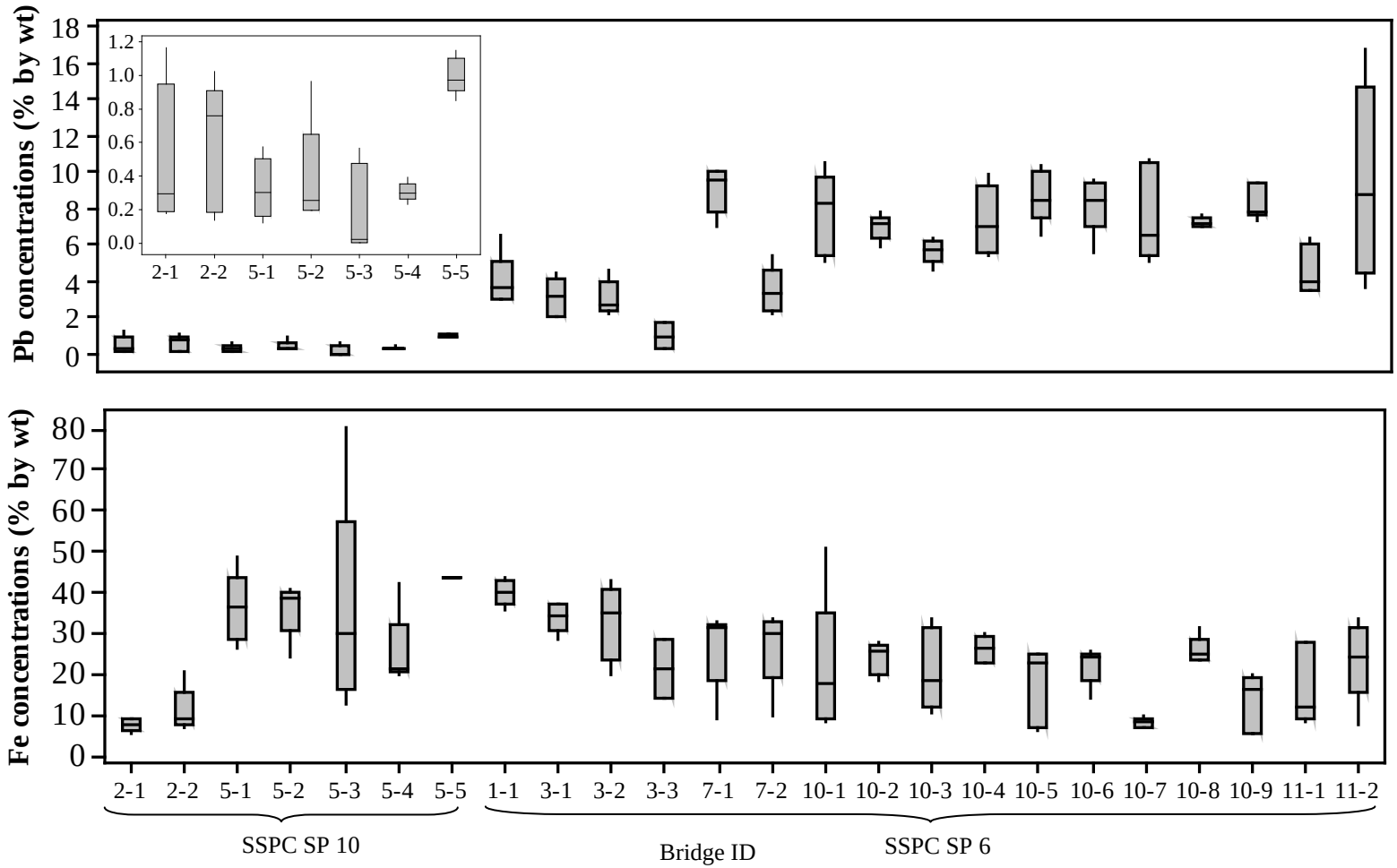

Figure A.1 Variability Charts for Pb and Fe are shown as a function of the bridges sampled in Regions 1, 2, 3, 5, 7, 10, and 11 using the NITON XL3t-600 series FP-XRF. The first and third quartiles are represented; the median is highlighted. The whiskers represent the minima and maxima.

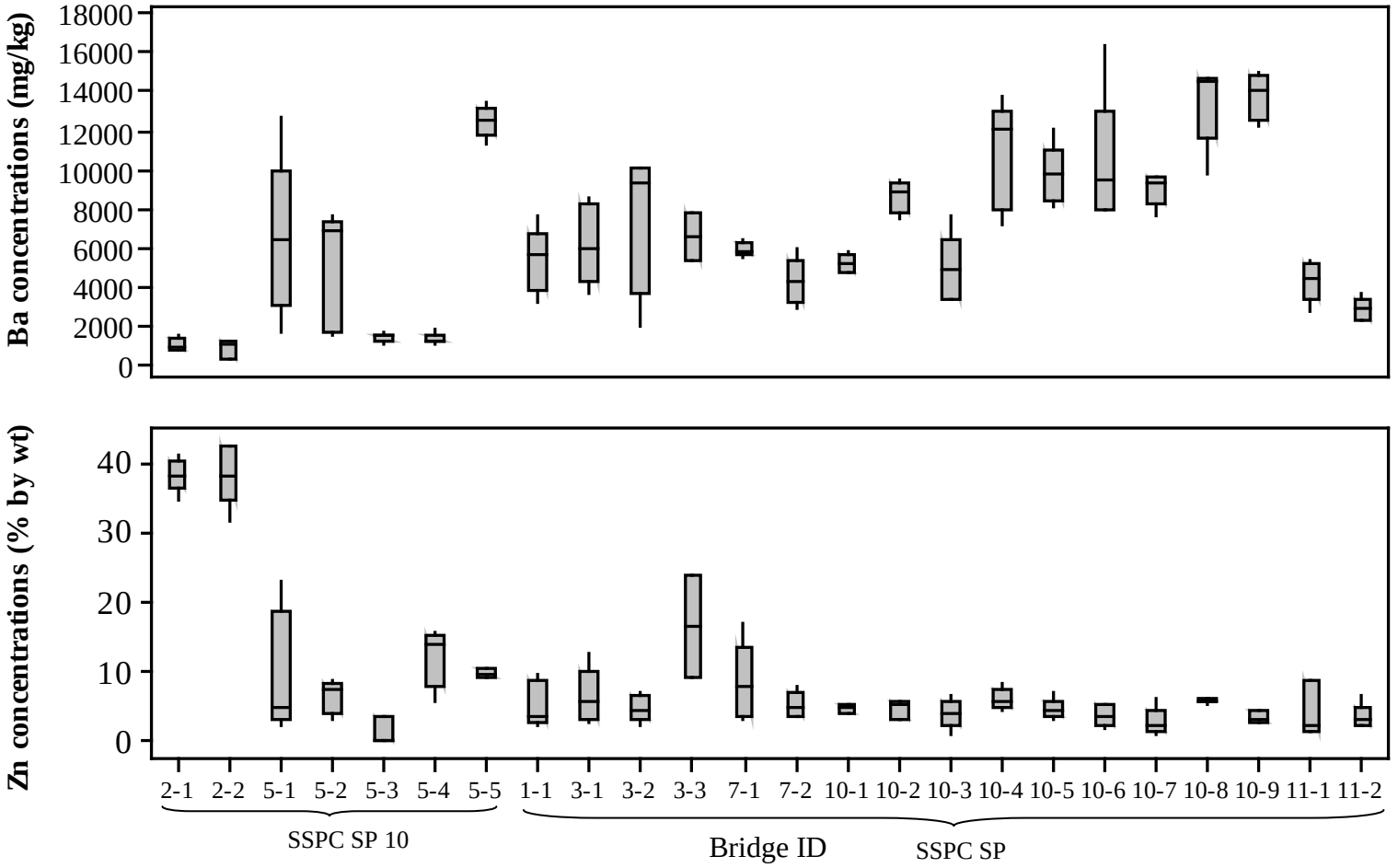

Figure A.2 Variability Charts for Ba and Zn are shown as a function of the bridges sampled in Regions 1, 2, 3, 5, 7, 10, and 11 using the NITON XL3t-600 series FP-XRF. The first and third quartiles are represented; the median is highlighted. The whiskers represent the minima and maxima.

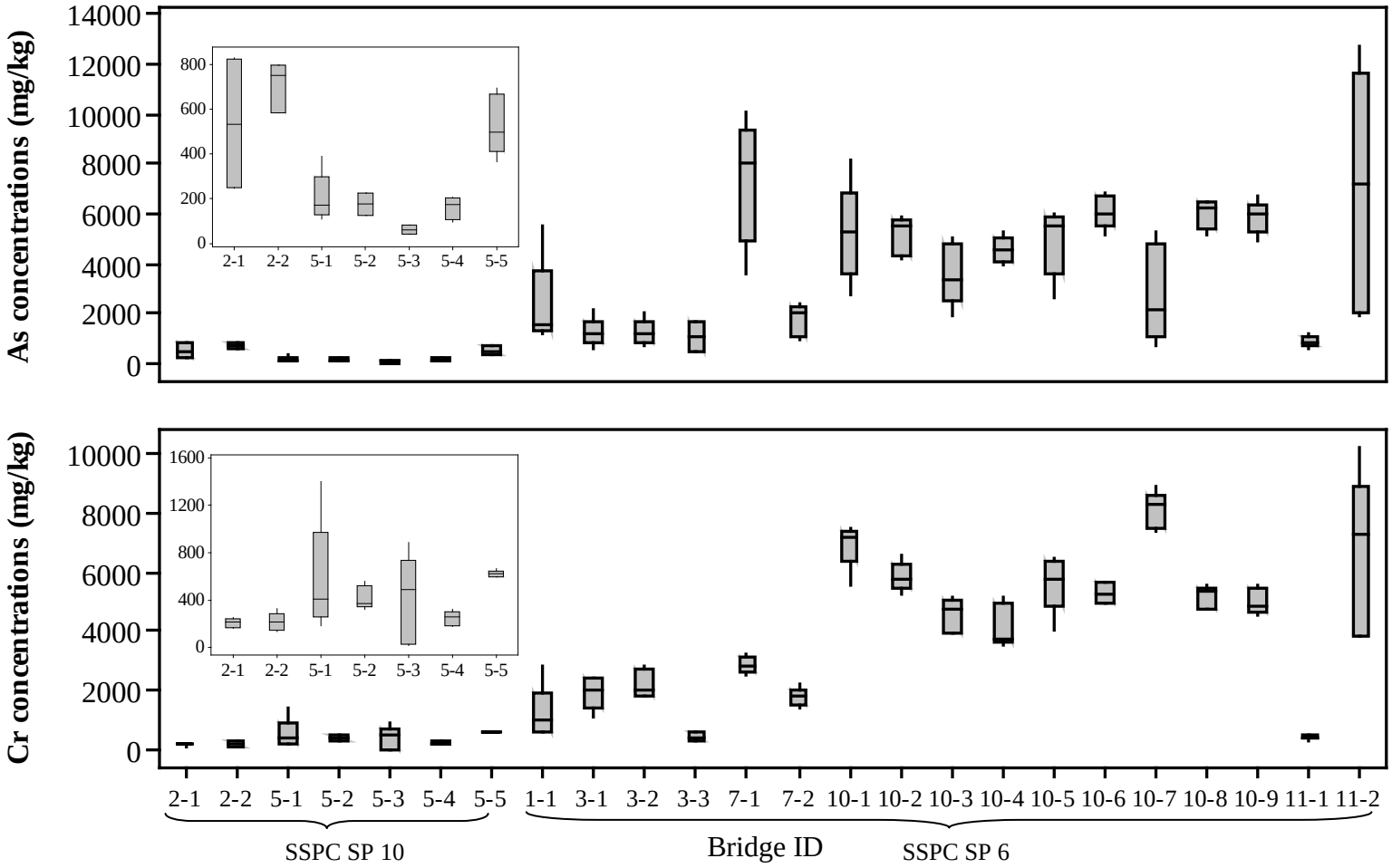

Figure A.3 Variability Charts for As and Cr are shown as a function of the bridges sampled in Regions 1, 2, 3, 5, 7, 10, and 11 using the NITON XL3t-600 series FP-XRF. The first and third quartiles are represented; the median is highlighted. The whiskers represent the minima and maxima.

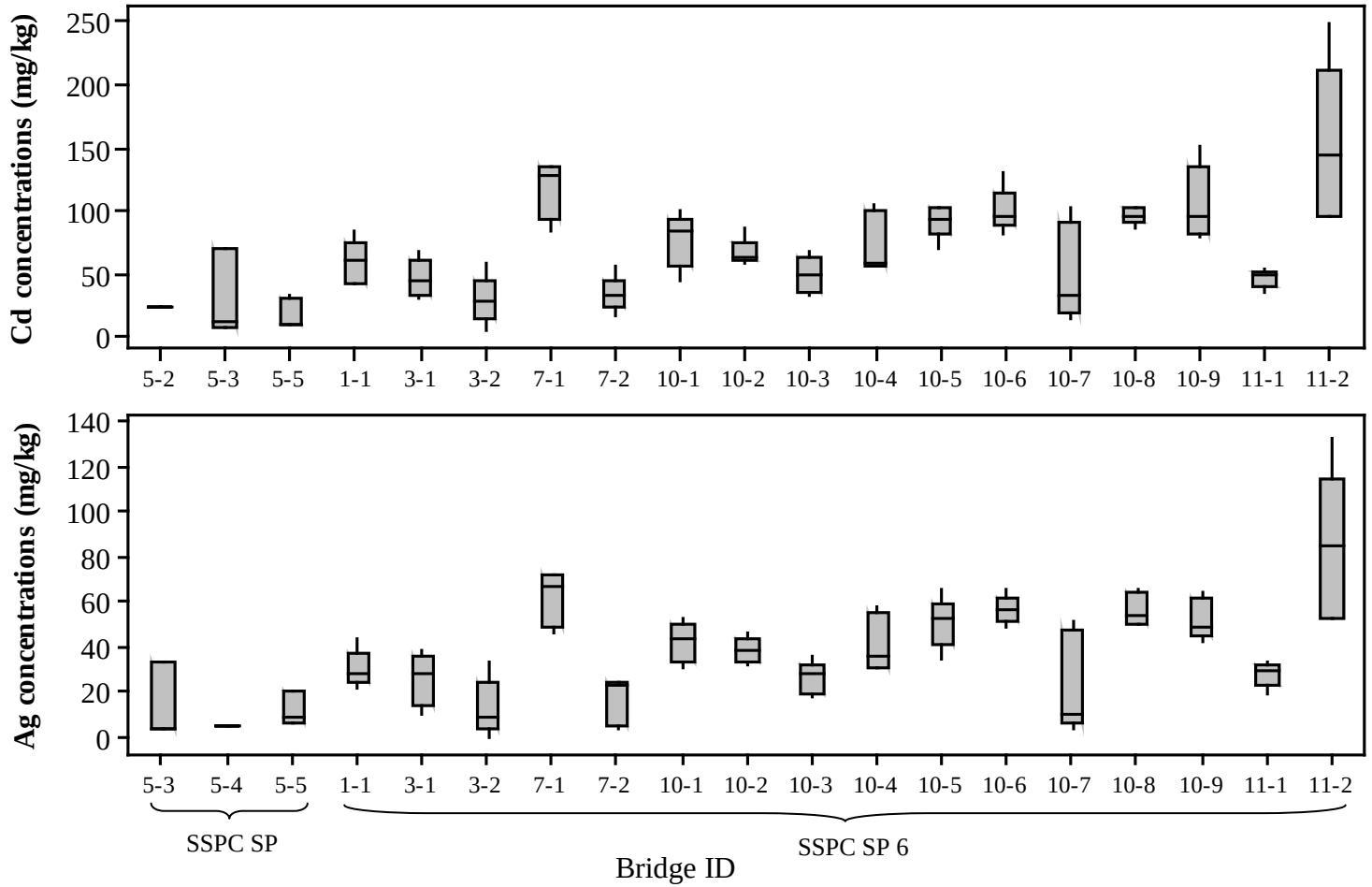

Figure A.4 Variability Charts for Cd and Ag are shown as a function of the bridges sampled in Regions 1, 2, 3, 5, 7, 10, and 11 using the NITON XL3t-600 series FP-XRF. The first and third quartiles are represented; the median is highlighted. The whiskers represent the minima and maxima.

APPENDIX B

PROTOCOL FOR IN SITE BRIDGE PAINT ANALYSIS USING FP-XRF

B1. Standard Operating Procedure (SOP) for NITON XLp-300 series Analyzer

1. Log on and calibration procedures

1.1 Log on procedures

(1) To turn on the instrument, depress on/off/escape button on the control panel for approximately 3 seconds (Figure B1), until you hear a beep.

(2) When the Logon screen (Figure B1) present, tap anywhere on this screen to continue.

(3) The Logon Screen will be replaced by a Warning Screen (Figure B1), advising that this analyzer produces radiation when the lights are flashing. This warning has to be acknowledged by selecting the “Yes” button before logging on (Selecting the “No” button will result in returning to the Logon Screen).

(4) The Virtual Numeric Keypad becomes available to log onto the analyzer (Figure B1). The temporary password assigned by default is 1-2-3-4, followed by the “E” key. After the log on procedures are completed, the word "USER" will appear on the bottom of the screen, then the Main Menu (Figure B2) will appear.

(5) After being powered on, the NITON 300 Series Analyzer will perform an internal re-calibration before an analysis is initiated. It is recommended to let the instrument warm up for ten minutes after start up, before testing is begun.

1.2 Instrument calibration

(1) To calibrate the instrument, select the Calibrate icon from the Utilities Menu (Figure B2). The analyzer is programmed to calibrate for a specific, predetermined period in order to ensure proper operation of the Niton XLp analyzer in the field.

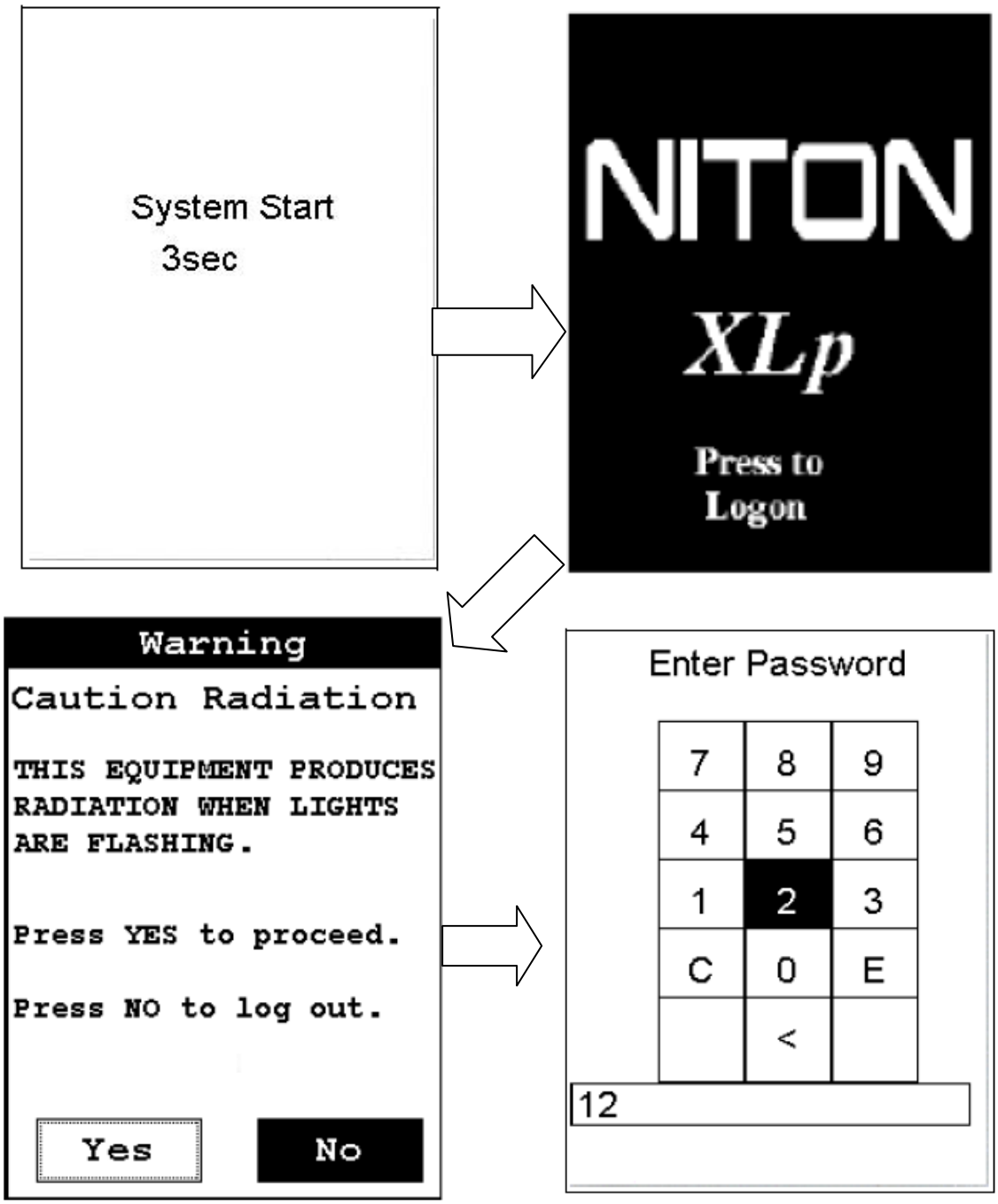

Figure B.1 Log on procedure for NITON XLp-300 series analyze

(2) After the calibration has finished, the calibration results will be displayed. Press the on/off/escape button or the Return icon to return to the Main Menu. In order to insure good test results, it is essential to calibrate Niton XLp300 Series Lead-based-Paint Analyzer daily.

(3) Note the "Res" figure displayed following the detector calibration. This number, usually < 500eV, is an evaluation of the detector resolution and should be consistent with past calibration results. This data will download as a stored reading if the user chooses to download readings, so it can be saved for tracking the instrument's performance.

(4) During analysis and detector calibrations, it is important to ensure that the analyzer is not exposed to strong electromagnetic fields, including those produced by computer monitors, hard drives, cellular telephones, walkie-talkies, etc. Keep a minimum two feet (0.7 meters) distance between the analyzer and electronic devices. Avoid any vibration, loud noise, strong electronic fields, or other possible interference when the analyzer is calibrating its detector.

2. Icon functions in the main menu

The Main menu is divided into 6 sub-menus (Figure B2):

- By selecting the **Mode** icon from the Main Menu screen, the analyzer will remember the last mode used on the analyzer, and will use that mode by default unless another mode is selected.
- By selecting the **Utilities** icon from the Main Menu screen, the Utilities Menu enables you to view analyzer specifications; set the date and time; and auto-calibrate the analyzer electronics and the touch screen display.

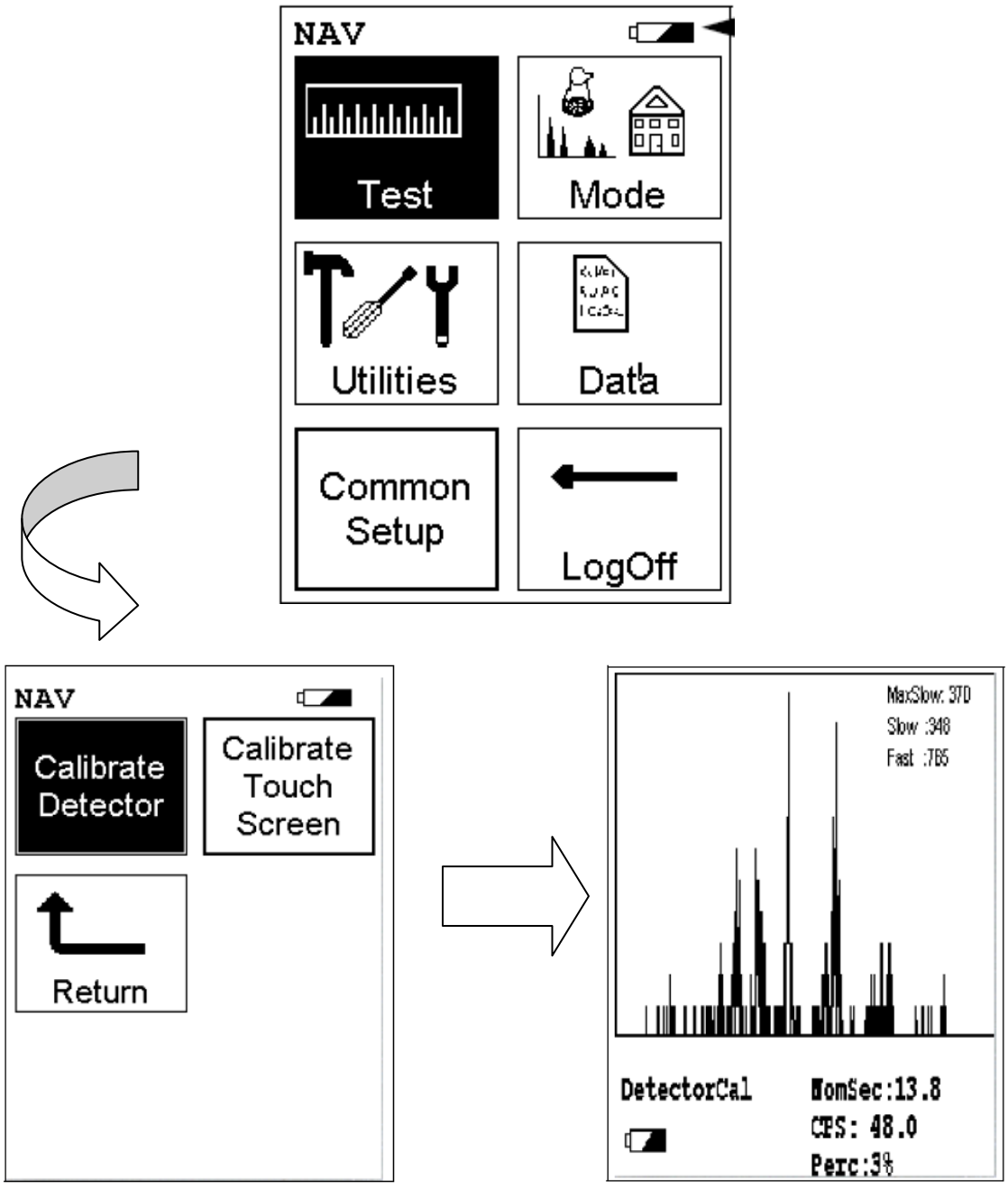

Figure B.2 Main menu for NITON XLp-300 series Lead-in-Paint analyzer and the analyzer calibration.

- By selecting the **Data** icon from the Main Menu screen, the Data Menu allows you to view readings, and allows you to view the alloy library and stored signatures.
- By selecting the **Common Setup** icon from the Main Menu screen, the Common Setup Menu allows you to turn on or off the liquid crystal display backlight, turn on or off the integrated bar code scan engine, to enable and configure source utilization, and to enable or disable the printer.
- By selecting the **Logoff** icon, the Logon Screen logs you out and allows you to login again, preventing casual unauthorized access to your analyzer.

3. Two modes for lead paint detection

There are two kinds of modes can be used for lead testing: Standard Mode and K+L Mode (Figure **B**3). The Standard Mode is a qualitative analysis designed for 95% confidence level as to whether the sample is above or below the Action Level. This mode tends to give very fast readings, because it terminates the test as soon as 95% confidence has been achieved. The Set Action Level Screen needs to be set for Standard Mode test. To change the preset Action Level to match the Action Level set by specific locality, select the "C" key from the Virtual Numeric Keypad to clear the current Action Level value, select the new Action Level value using the numeric keys, then select "E" to enter the new Action Level value (Figure B3). The Action Level will be changed to the new value. Then new Set Action Level Screen will be displayed. K+L Mode is a quantitative analysis which allows you to determine the statistical confidence of the

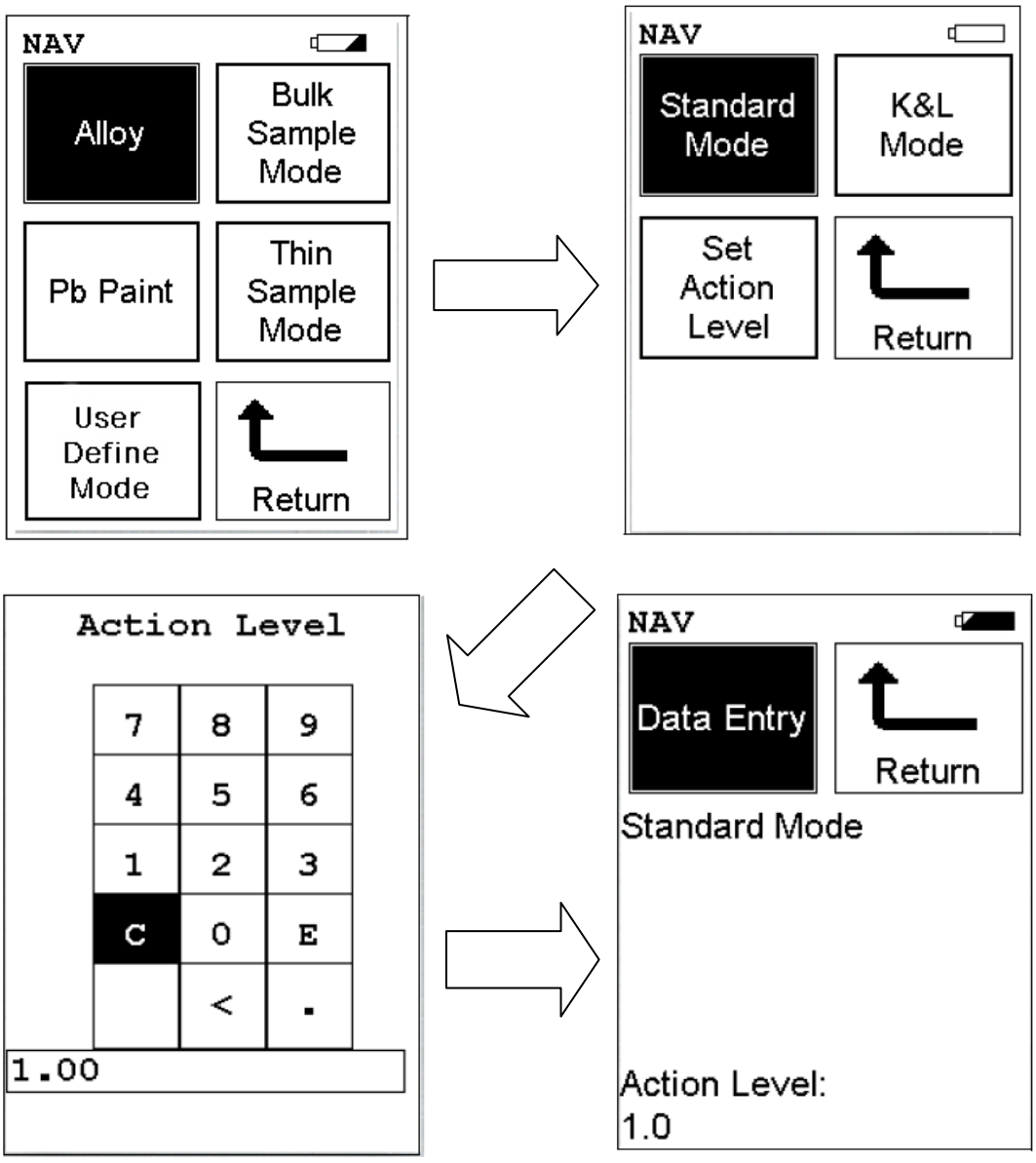

Figure B.3 The Pb Paint Mode Menu and Set Action Level

reading to a 95% Confidence Level while allowing you the flexibility of continuing the test for as long as you wish up to the (user-definable) maximum test time.

4. Data entry screens

Once Standard Mode or K+L Mode is selected, a sample test can be immediately initiated using the proper preconditions for operation. The data information entered will be associated with the next sample tested. By using The Data Entry Screens (Figure B4), the values for various parameters can be tracked by the system along with the actual analysis results. The data information can be input in several different fields, or categories, concerning the sample, in several different ways:

• Selecting the Menu Code Number will initiate a bar code scan to input pre-printed bar code parameter values

• Selecting the Drop-Down Menu Button will access the particular Drop-Down Menu for that parameter, allowing you to select the parameter value from a pre-determined list.

• Selecting the Keyboard button allows you to input a parameter value as required using the Virtual Keyboard.

These fields are saved along with the subsequent reading, and allow you to associate important information about the sample directly with the reading, so that you have a full description of the sample tied into the reading itself. These parameters all describe the particular test target to be analyzed. The location of the target in the site, the type of target, the surface and

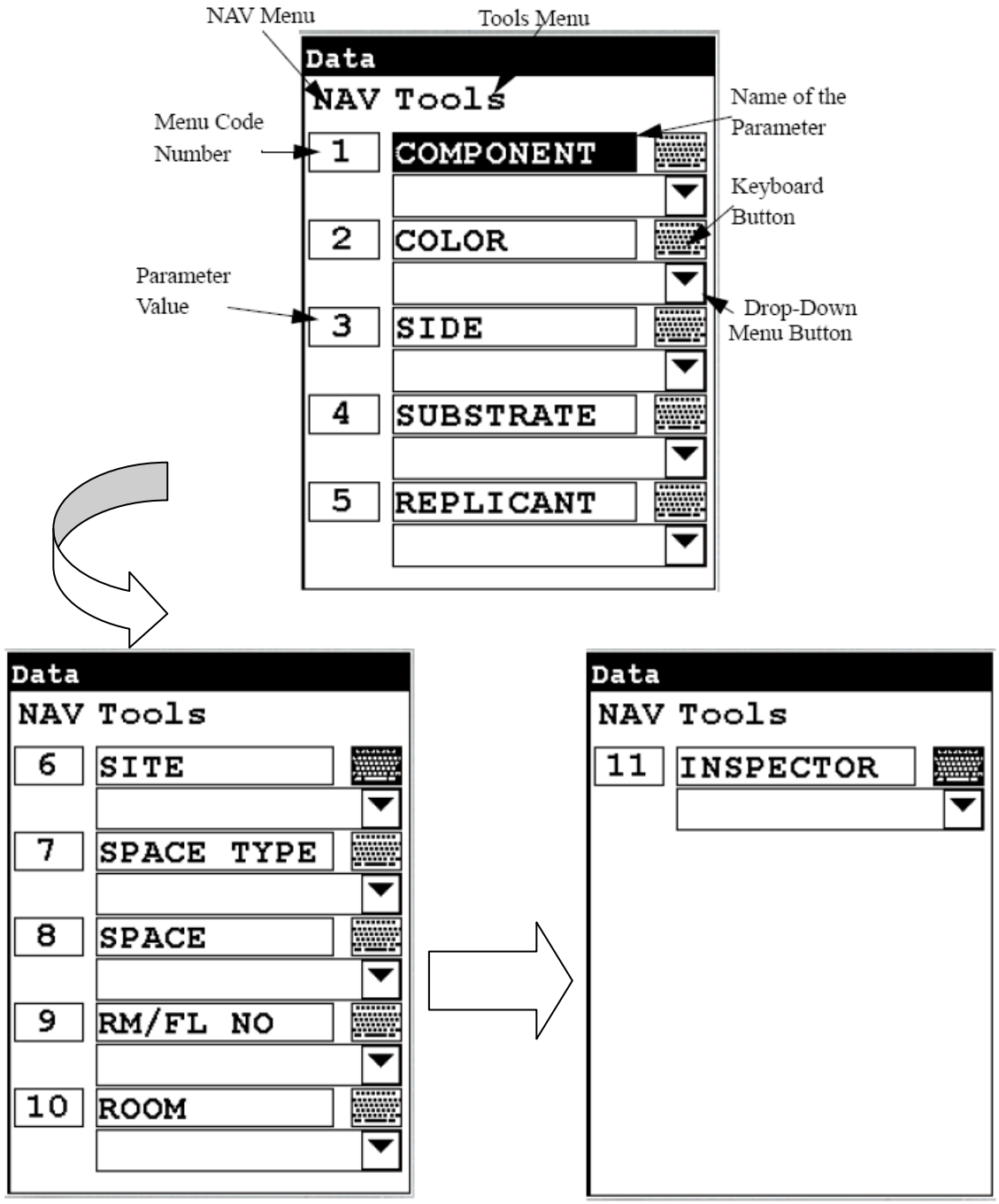

Figure B.4 Data input information

substrate, the condition of the surface, and the inspector performing the test are some of the parameters tracked by the analyzer.

5. Measurements

Five different methods of operation are used for taking a sample measurement. The analyzer will be configured to use one of those methods, depending on the regulatory requirements of the specific locality.

- Trigger-Only method. With the Trigger-Only method, you only need to place the measurement window close to the sample to be analyzed and pull the trigger for sample analysis to be initiated.
- Trigger-and-Proximity-Sensor method. With the Trigger-and-Proximity-Sensor method, you must place the measurement window against the sample to be analyzed to engage the proximity sensor on the front of the instrument, then pull the trigger for sample analysis to be initiated.
- Momentary-Trigger-Touch-and-Proximity-Sensor method. With the Momentary-Trigger Touch-and-Proximity-Sensor method, you must place the measurement window against the surface to be analyzed to engage the proximity sensor on the front of the instrument, then pull the trigger. The trigger may be released and the reading will continue until you release the proximity button, or other criteria (such as Max Time) are reached.
- Trigger-and-Interlock method. With the Trigger-and-Interlock method, you need to place the measurement window close to the sample to be analyzed, press and keep pressing the interlock button at the rear of the instrument with your free hand, then pull the trigger for sample analysis to be initiated.

- Trigger-Interlock-and-Proximity-Sensor method. With the Trigger-Interlock-and-Proximity-Sensor method, you must place the measurement window against the sample to be analyzed to engage the proximity sensor on the front of the instrument, press and keep pressing the interlock button at the rear of the instrument with your free hand, then pull the trigger for sample analysis to be initiated.

With any of these methods, analysis will stop if any one of the preconditions are violated. For example, with the Trigger-Interlock-and-Proximity-Sensor method, if the trigger or the Proximity Sensor or the Interlock is released, the reading will stop immediately, and the shutters will close.

6. Results

NITON Analyzer will display the Results Screen throughout the duration of each reading. The Results Screen is updated regularly throughout the reading. When the reading is complete, a final screen update will appear, and your NITON analyzer will display the final results of the measurement which has just been completed.

6.1 Standard mode testing results

Before the analyzer has reached a determination, the result will be shown as“Inconclusive”. The analyzer will beep twice when a result is reached then terminate the reading. The display will change from “Inconclusive” to show the result, either “Positive” for lead detected above the action level, or “Negative” for no lead or lead below the action level. The lead concentration is displayed in mg/cm^2.

6.2 K+L Mode testing results

The K+L Mode results screen will show the same basic display throughout the reading. The analyzer will beep twice to indicate it has reached a conclusion, and the result field will change from “Inconclusive” to “Positive” or “Negative”, but the reading will continue for as long as you the trigger continue to be hold down and the Proximity Sensor is depressed. The K+L results screen shows the reading results and error for both K and L-shell readings (Figure B5). The “Lead Detected in mg/cm^2 total” field (Figure B5) is the result of the judgment of the analyzer as to which reading, K or L-shell, best represents the true condition.

In the Standard mode / K+L Mode, the Depth Index (Figure B5) is a numerical value indicating the amount of non-leaded paint covering the lead (if any) detected by the analyzer:

- A Depth Index of less than 1.5 indicates a reading very near the surface.
- A Depth Index between 1.6 and 4.0 indicates a moderate depth.
- A Depth Index of greater than 4.0 indicates a deeply buried reading.

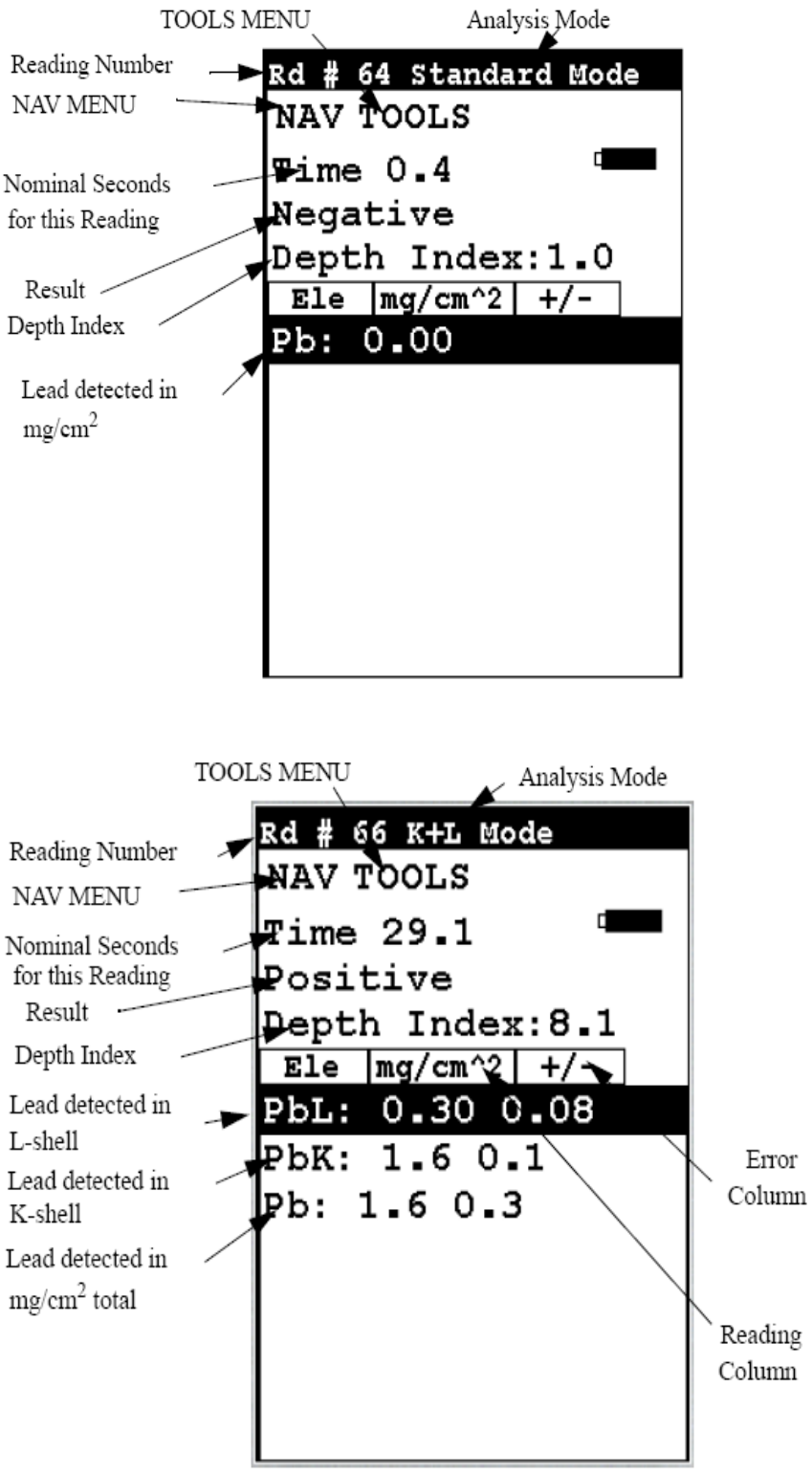

Figure B.5 Testing results under the Standard Mode and K+L Mode

B2 Standard Operating Procedure (SOP) for NITON XL3t-600 Series Analyzer

1. Log on and calibration procedures

Log on and calibration procedures for NITON XL3t-600 series analyzer (Figure B6) are the same as NITON XLp-300 series analyzer (part 1).

2. Icon functions in the main menu

Icon functions in the main menu for NITON XL3t-600 series analyzer (Figure B7) are the same as NITON XLp-300 series analyzer (part 2).

3. Standard Soil Mode or Mining Mode for the RCRA metals and zinc detection in the paint

To detect metal concentrations in the paint, simply select the Standard Soil Mode icon or Mining Mode Cu/Zn icon from the Bulk Analysis Menu (Figure B8).

4. Data entry screens

The function of the Data Entry Screens for NITON XL3t-600 series analyzer (Figure B9) is the same as NITON XLp-300 series analyzer (part 4).

5. Measurements

There are six different methods of operation for taking a sample measurement, and the analyzer will be configured to use one of those methods for samples, depending on the regulatory requirements of the specific locality.

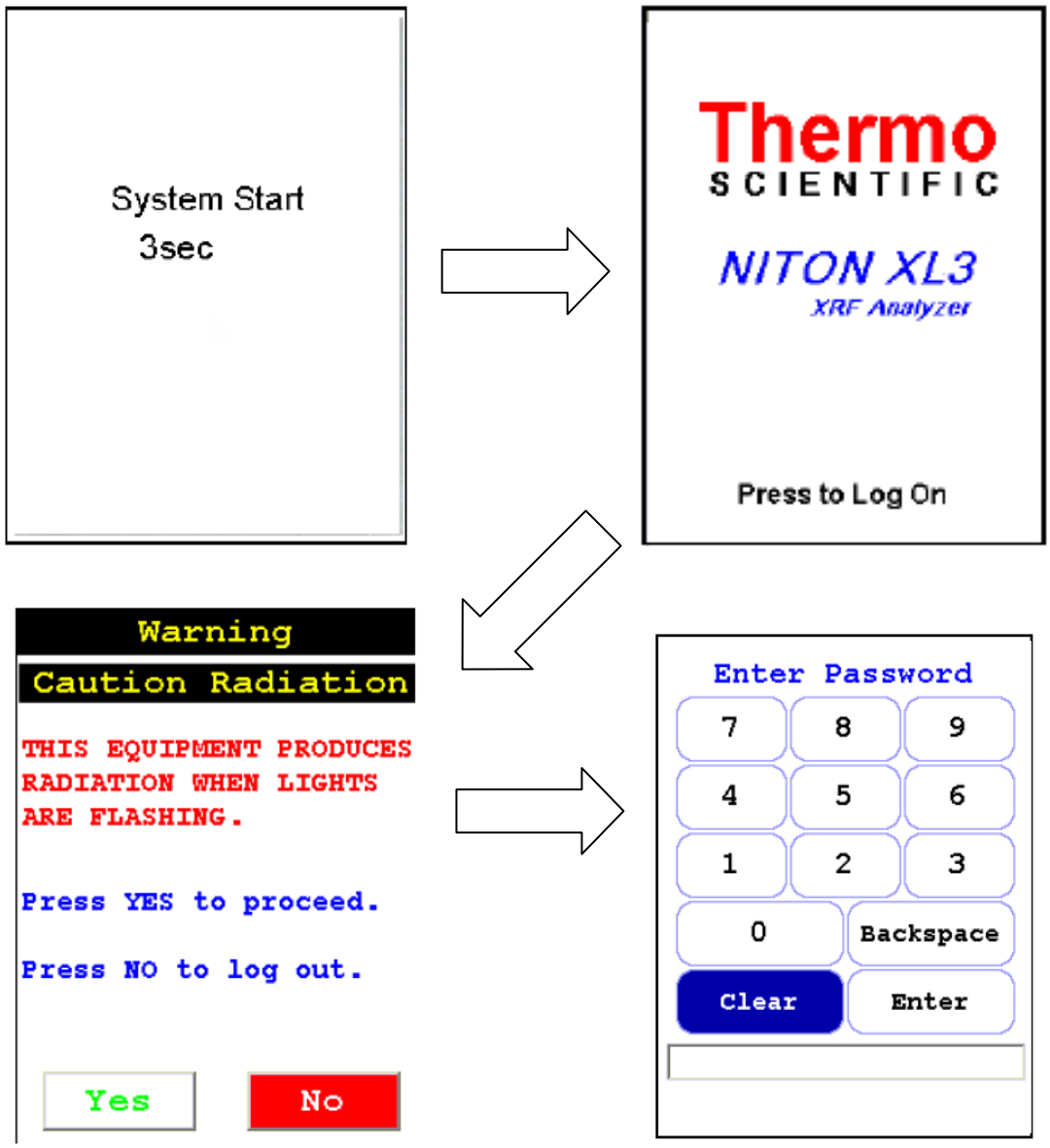

Figure B.6 Log on procedure for NITON XL3t-600 series analyzer

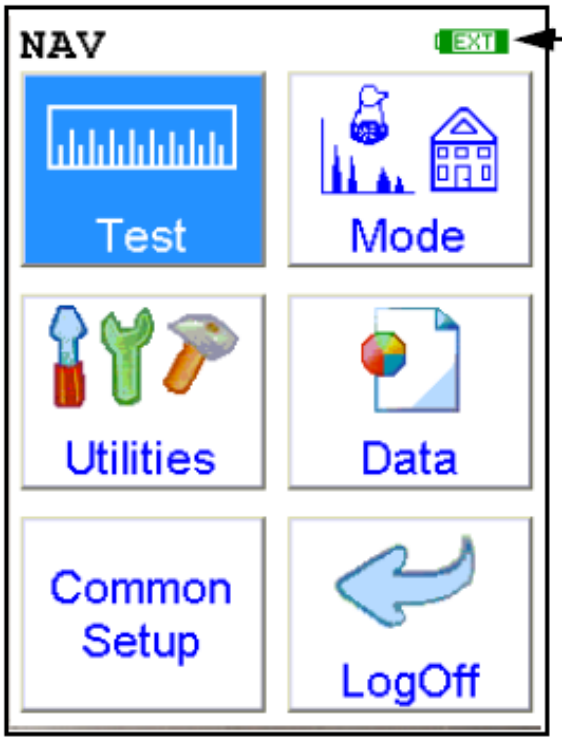

Figure B.7 Main menu for NITON XL3t-600 series analyze

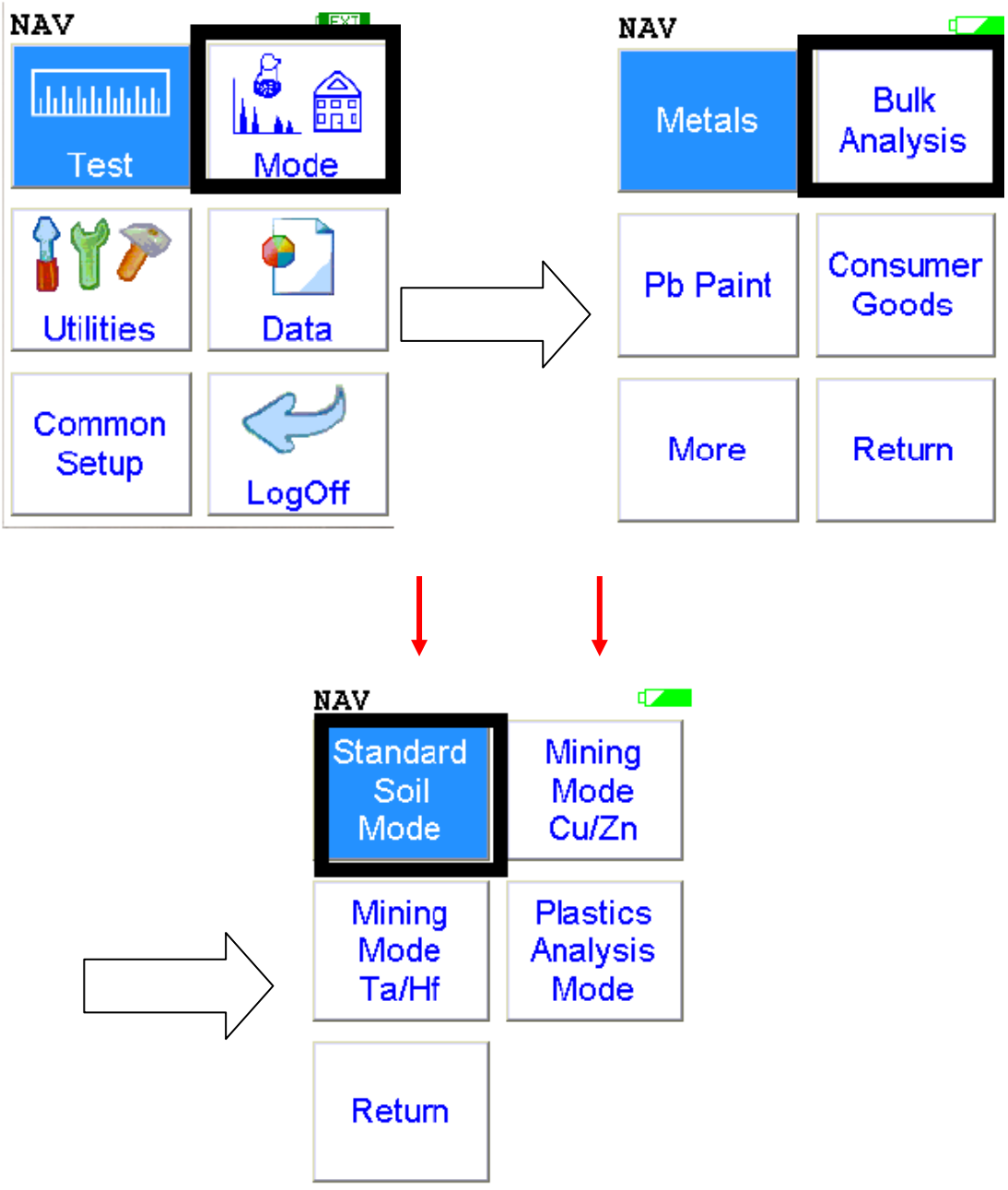

Figure B.8 Standard soil analysis mode

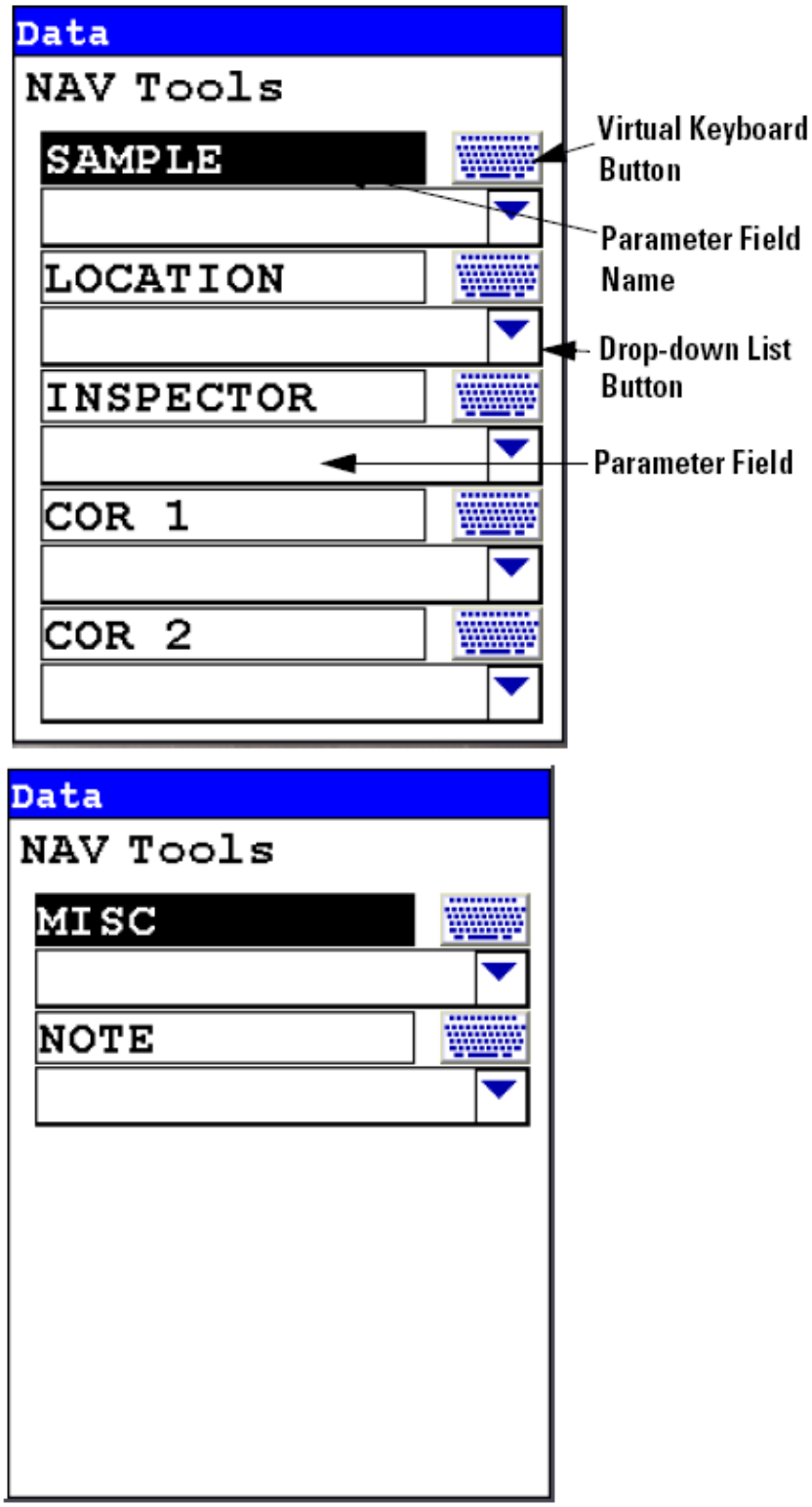

Figure B.9 Data input information for NITON XL3t-600 series analyzer

- Trigger-Only method. With the Trigger-Only method, you only need to place the measurement window close to the sample to be analyzed and pull the trigger for sample analysis to be initiated.

- Trigger-and-Proximity-Sensor method. With the Trigger-and-Proximity-Sensor method, you must place the measurement window against the sample to be analyzed to engage the proximity sensor on the front of the instrument, then pull the trigger for sample analysis to be initiated.

- Momentary-Trigger-Touch-and-Proximity-Sensor method. With the Momentary-Trigger-Touch-and-Proximity-Sensor method, you must place the measurement window against the surface to be analyzed to engage the proximity sensor on the front of the instrument, then pull the trigger. The trigger may be released and the reading will continue until you release the proximity button, or other criteria (such as Max Time) are reached.

- Trigger-and-Interlock method. With the Trigger-and-Interlock method, you need to place the measurement window close to the sample to be analyzed, press and keep pressing the interlock button at the rear of the instrument with your free hand, then pull the trigger for sample analysis to be initiated.

- Trigger-Interlock-and-Proximity-Sensor method. With the Trigger-Interlock-and-Proximity-Sensor method, you must place the measurement window against the sample to be analyzed to engage the proximity sensor on the front of the instrument, press and keep pressing the interlock button at the rear of the instrument with your free hand, then pull the trigger for sample analysis to be initiated.

- Easy Trigger method. With the Easy trigger method, you need only place the measurement window against the sample area and pull the trigger once to initiate a sample analysis. Your analyzer will continuously sample the backscatter, using a complex internal algorithm, to determine if the measurement window is against a sample or pointing to the empty air. If it finds that there is no sample directly against the measurement window, the analyzer will stop directing radiation through the window as soon as this determination is made.

With any of these methods, analysis will stop if any one of the preconditions are violated. For example, with the Trigger-Interlock-and-Proximity-Sensor method, if the trigger or the Proximity Sensor or the Interlock is released, the reading will stop immediately, and the X-ray tube will shut down.

6. Results

At the top are the elements detected in the sample; and underneath this, elements are below the detection limit (Figure B10). For an element to be detected by your analyzer in a given sample, the measured concentration of the sample must be at least three times the standard deviation of the measurement. This detection limit will depend on the composition of the sample. The measurement precision for each element displayed appears to the right of the measured concentration, under the heading "+/-". The precision of each measurement is two times the standard deviation (sigma). An element is classified as "detected" if the measured concentration (in ppm) is at least 1.5 times the precision. Detected elements are displayed in ppm, followed by the measurement precision. Non-detected elements are shown as < the detection limit (LOD) for that sample. The detection limit for a given element varies depending on the other elements in the matrix.

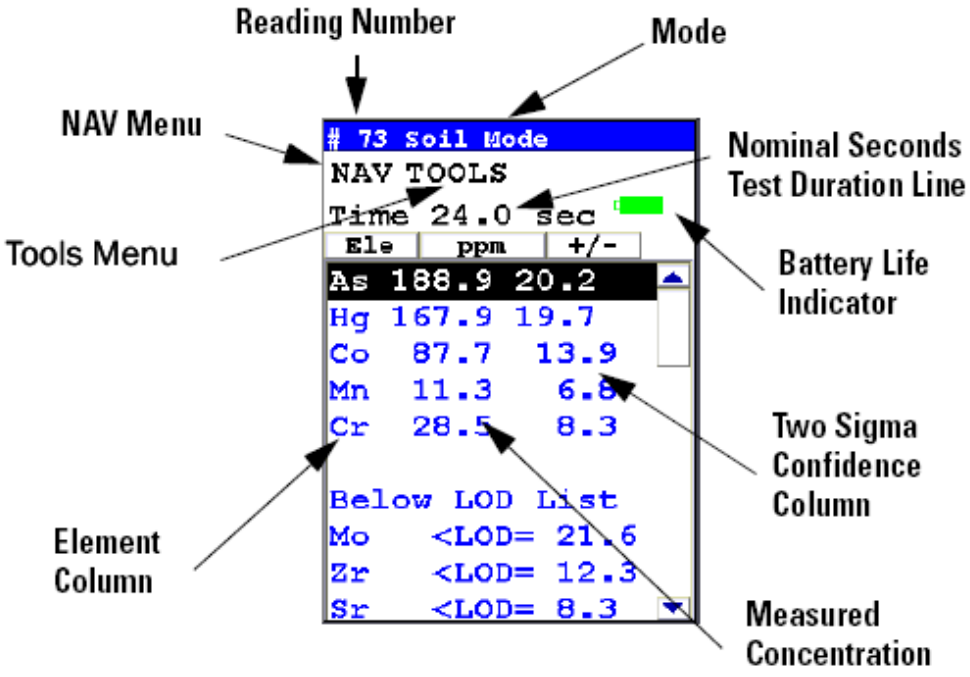

Figure B.10 The standard bulk measurement result scree

APPENDIX C

TCLP AND MEP RESULTS FOR THE 24 BRIDGES IN NEW YORK STATE

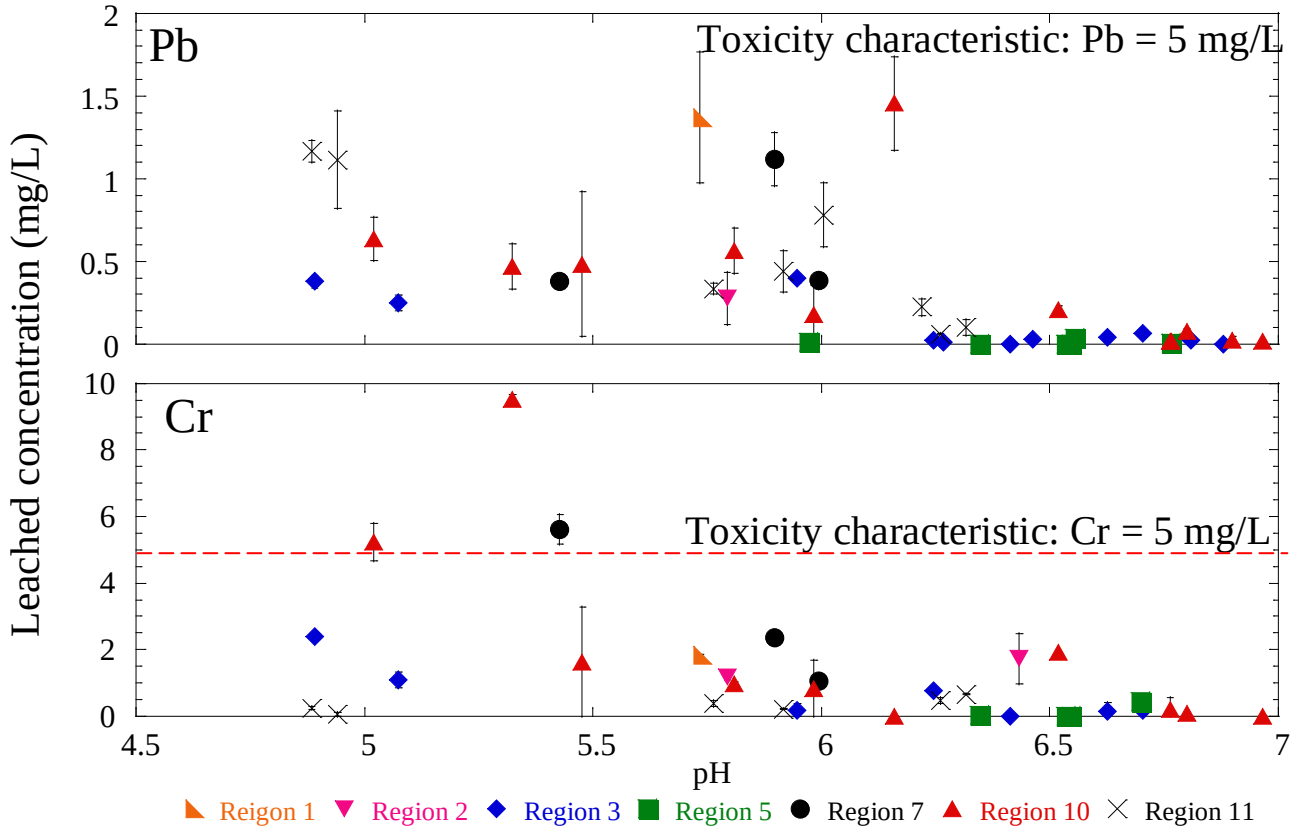

Figure C.1 Leaching results from TCLP for Pb and Cr as a function of pH after 18 hours with 0.05 M ionic strength. Samples are extracted using Fluid #1 (0.1 N CH_3COOH, which has been adjusted with NaOH to an initial pH of 4.93 ± 0.05) or Fluid #2 (0.1 N CH_3COOH, which has an initial pH of 2.88 ± 0.05) based on the alkalinity of the waste material.

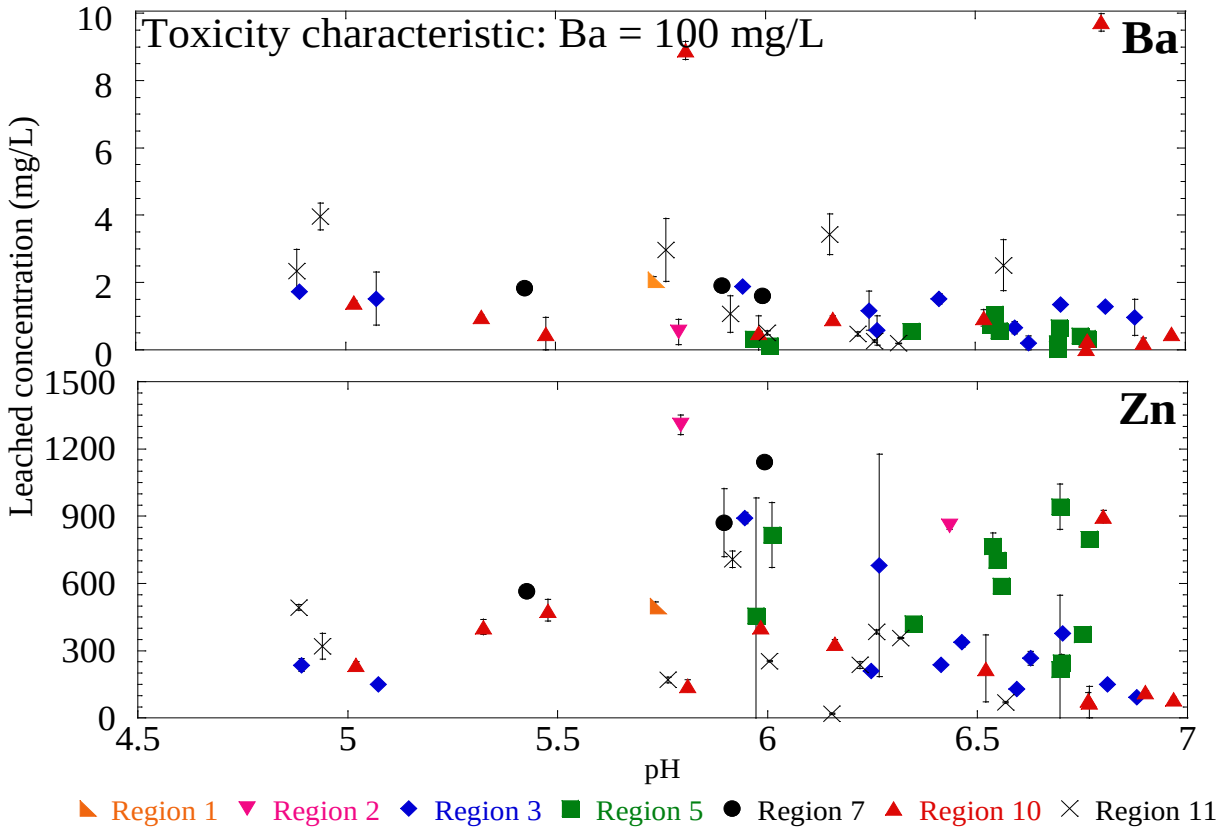

Figure C.2 Leaching results from TCLP for Ba and Zn as a function of pH after 18 hours with 0.05 M ionic strength. Samples are extracted using Fluid #1 (0.1 N CH_3COOH, which has been adjusted with NaOH to an initial pH of 4.93 ± 0.05) or Fluid #2 (0.1 N CH_3COOH, which has an initial pH of 2.88 ± 0.05) based on the alkalinity of the waste material.

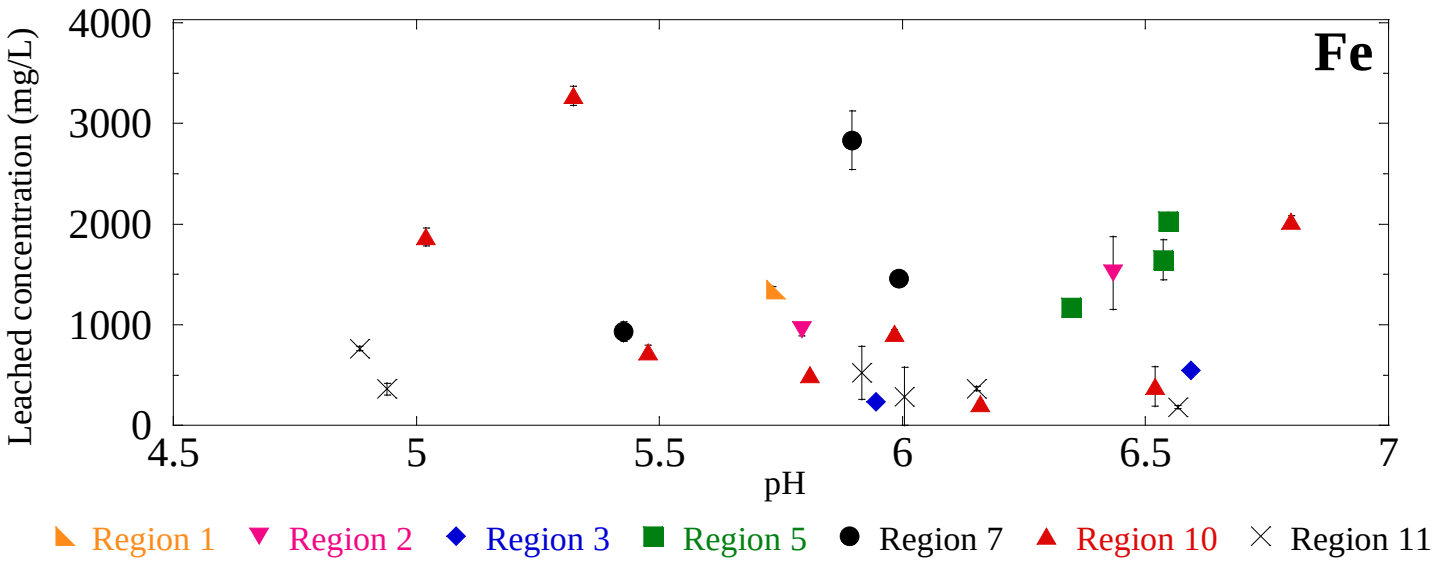

Figure C.3 Leaching results from TCLP for Fe as a function of pH after 18 hours with 0.05 M ionic strength. Samples are extracted using Fluid #1 (0.1 N CH_3COOH, which has been adjusted with NaOH to an initial pH of 4.93 ± 0.05) or Fluid #2 (0.1 N CH_3COOH, which has an initial pH of 2.88 ± 0.05) based on the alkalinity of the waste material.

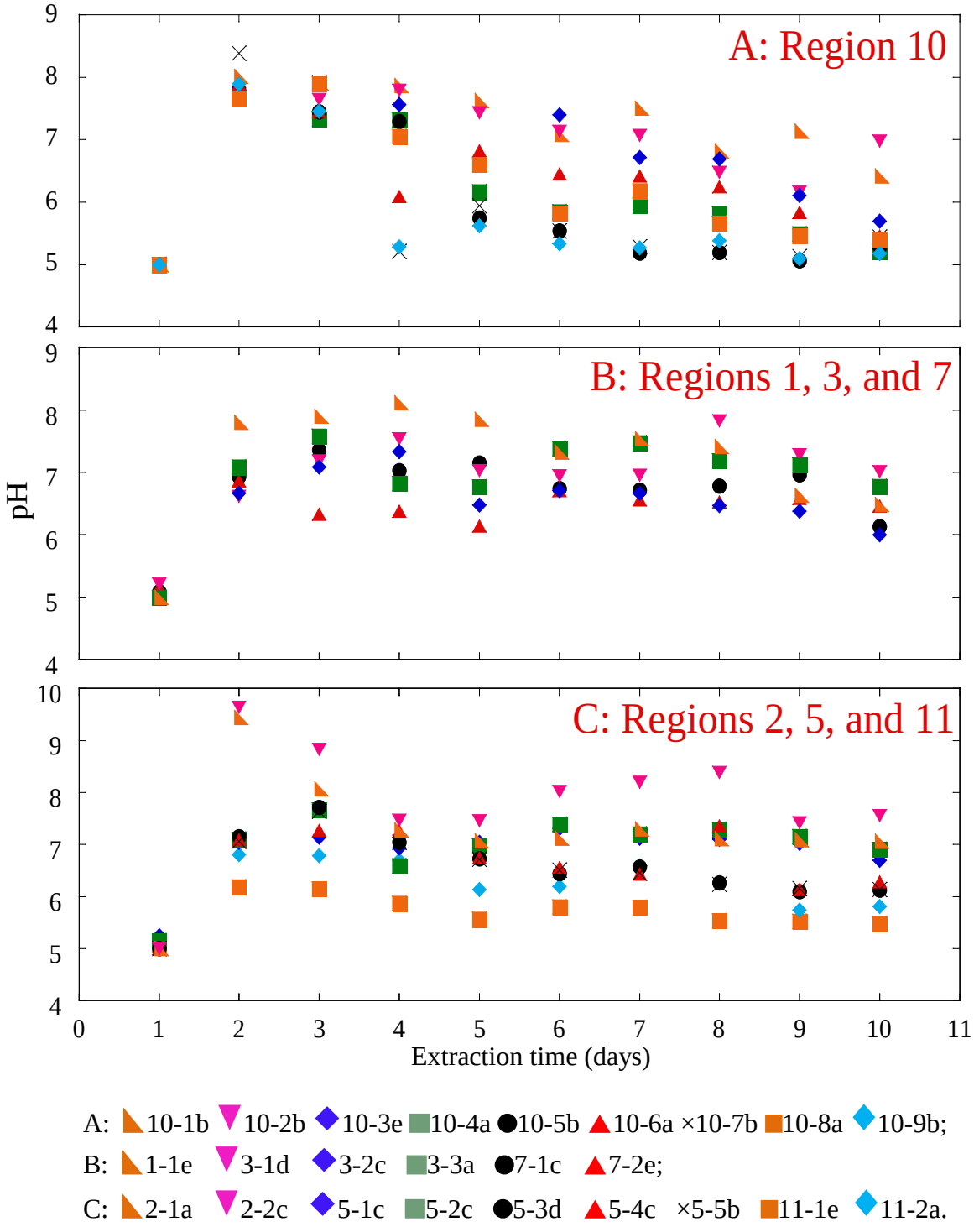

Figure C.4 pH from MEP are shown as a function of 10 days of extractions. The first extraction is performed with a pH of 5.0 followed by the subsequent nine successive extractions using the initial pH of 3.0 ± 0.2 that simulate acid rain conditions.

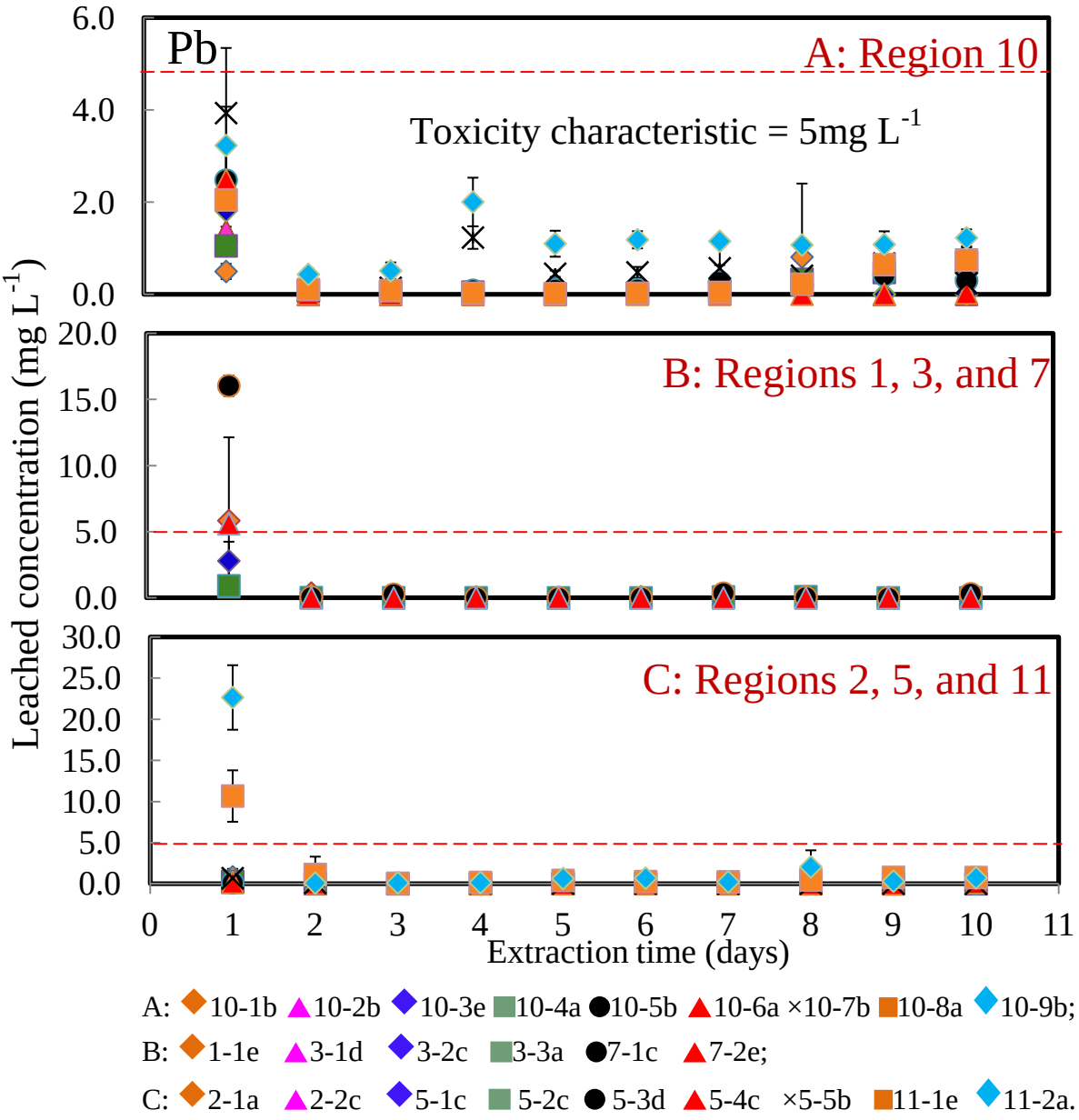

Figure C.5 Leaching concentrations of Pb from MEP are shown as a function of 10 days of extractions. The first extraction is performed with a pH of 5.0 followed by the subsequent nine successive extractions using the initial pH of 3.0 ± 0.2 that simulate acid rain conditions. Toxicity characteristic Pb = 5 mg L^{-1}.

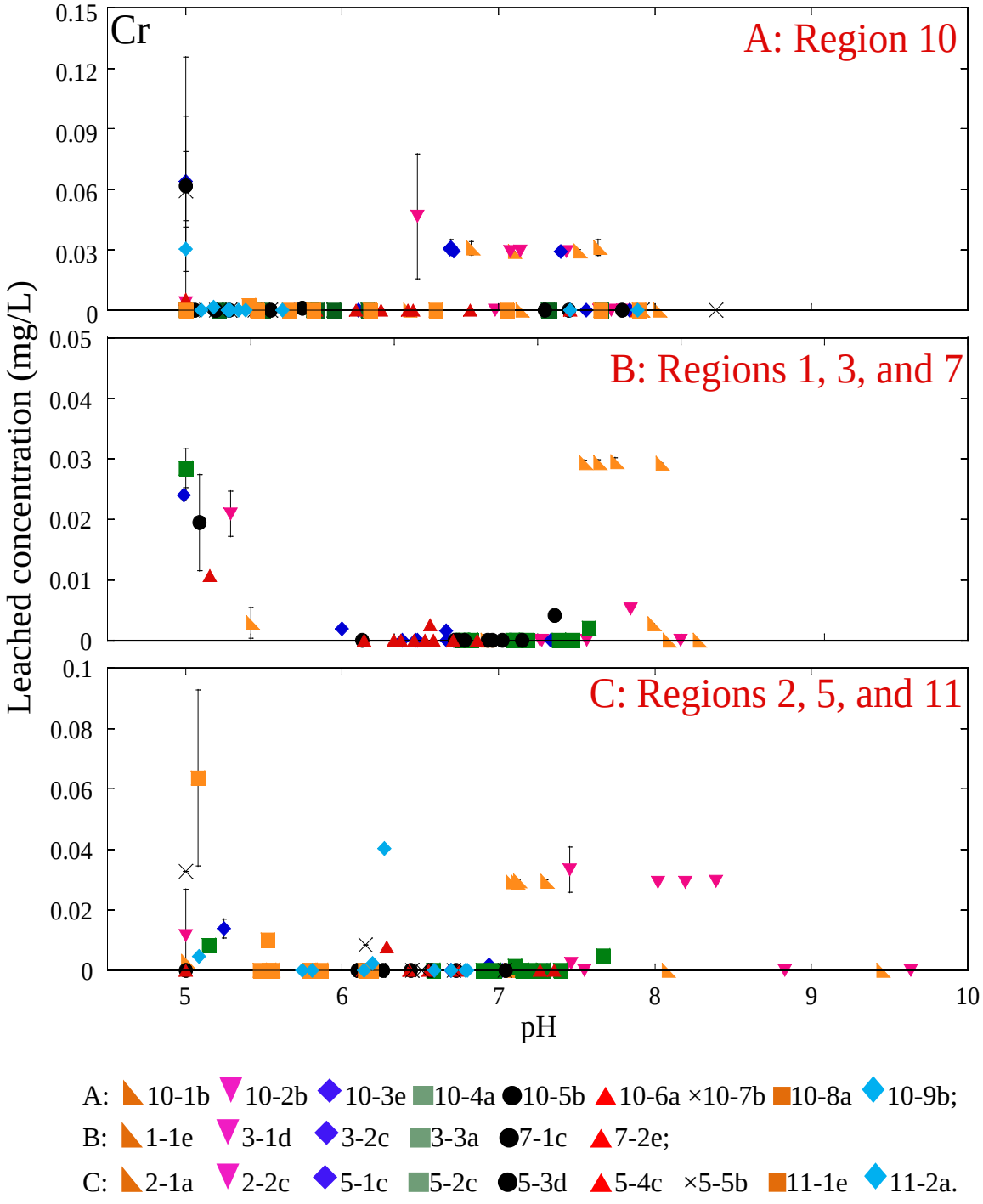

Figure C.6 Leaching concentrations of Cr from MEP are shown as a function of pH. The first extraction is performed with a pH of 5.0 followed by the subsequent nine successive extractions using the initial pH of 3.0 ± 0.2 that simulate acid rain conditions. Toxicity characteristic Cr = 5 mg L^{-1}.

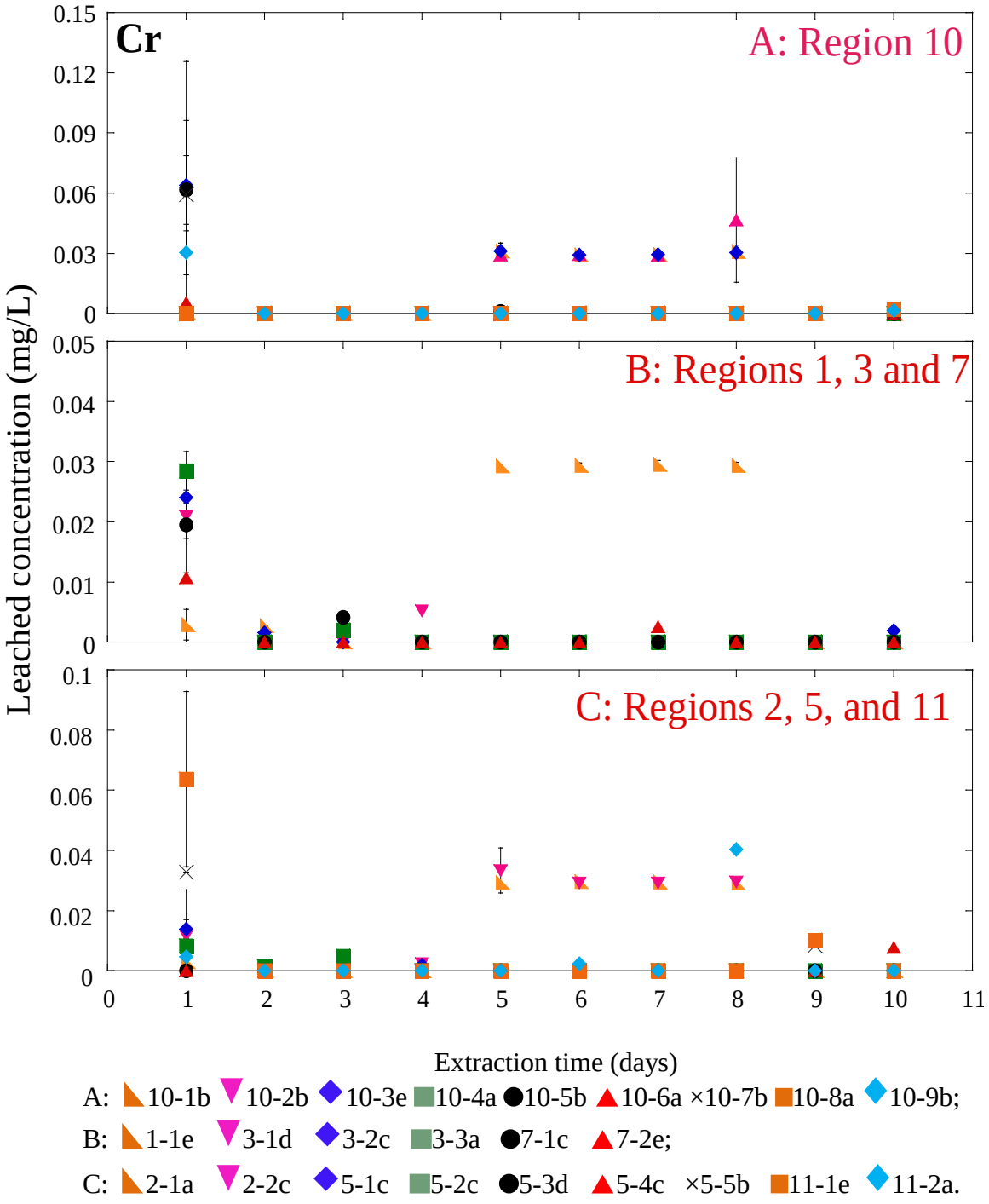

Figure C.7 Leaching concentrations of Cr from MEP are shown as a function of 10 days of extractions. The first extraction is performed with a pH of 5.0 followed by the subsequent nine successive extractions using the initial pH of 3.0 ± 0.2 that simulate acid rain conditions. Toxicity characteristic Cr = 5 mg L^{-1}.

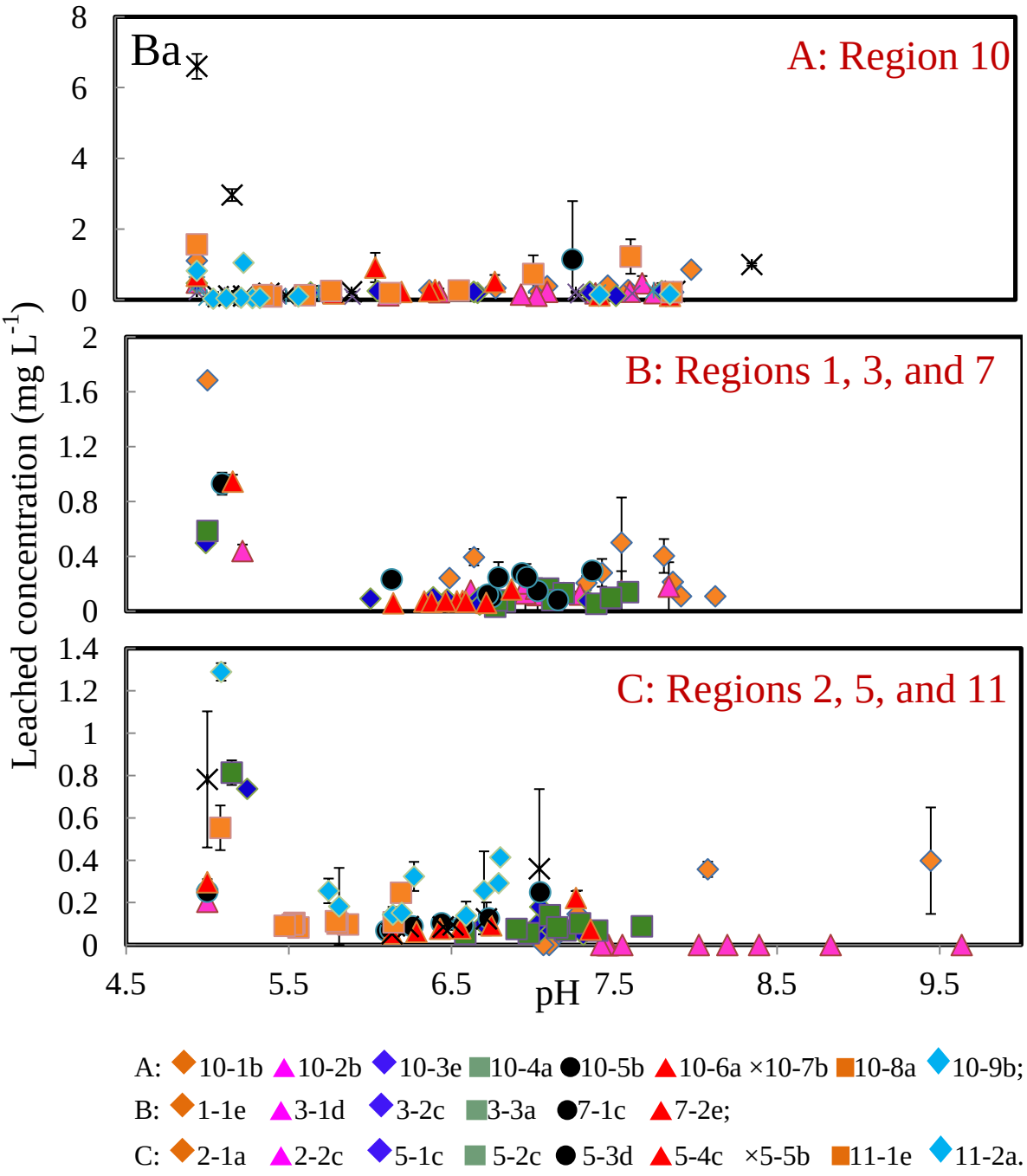

Figure C.8 Leaching concentrations of Ba from MEP are shown as a function of pH. The first extraction is performed with a pH of 5.0 followed by the subsequent nine successive extractions using the initial pH of 3.0 ± 0.2 that simulate acid rain conditions. Toxicity characteristic Ba = 100 mg L^{-1}.

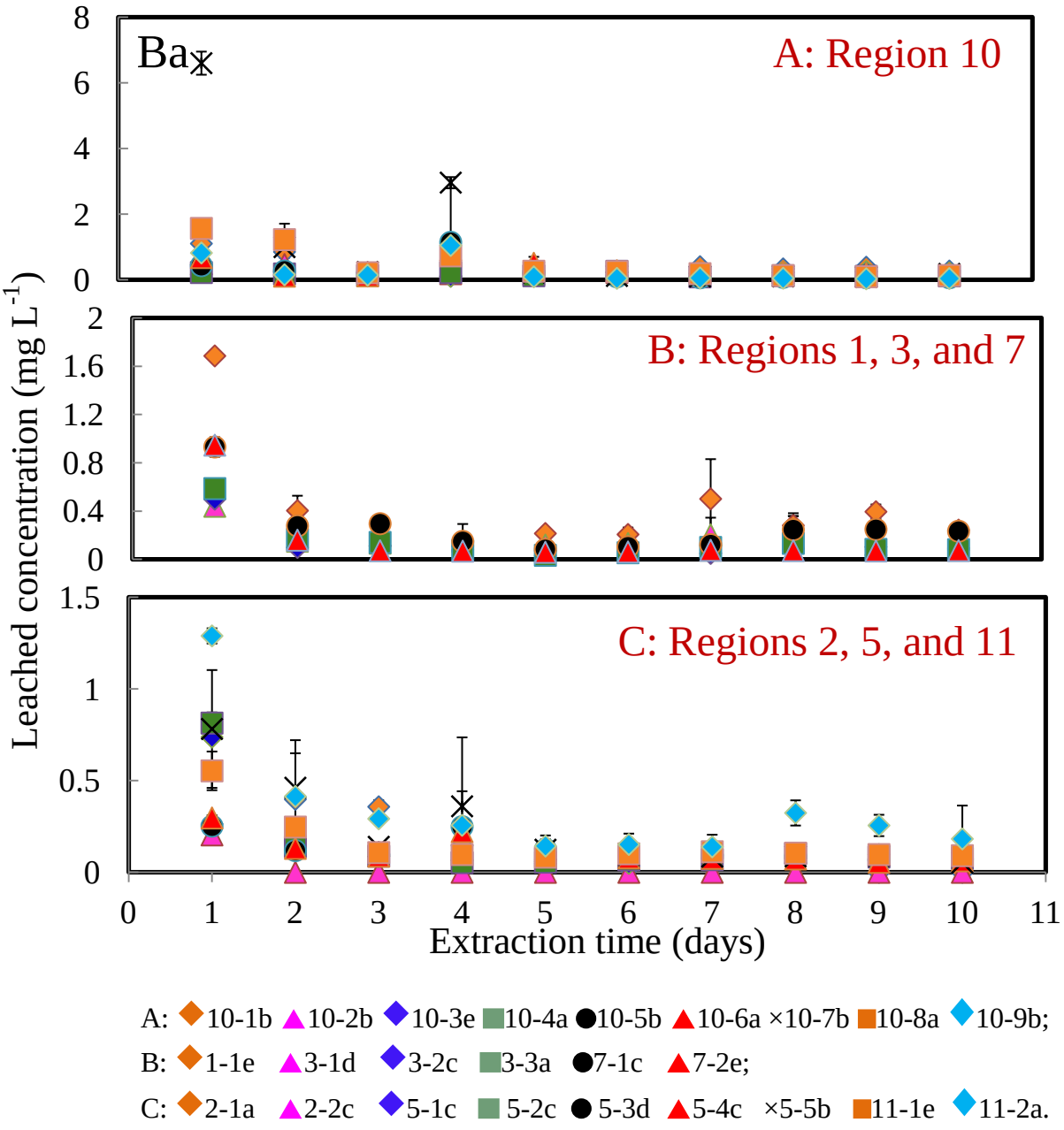

Figure C.9 Leaching concentrations of Ba from MEP are shown as a function of 10 days of extractions. The first extraction is performed with a pH of 5.0 followed by the subsequent nine successive extractions using the initial pH of 3.0 ± 0.2 that simulate acid rain conditions. Toxicity characteristic Ba = 100 mg L^{-1}.

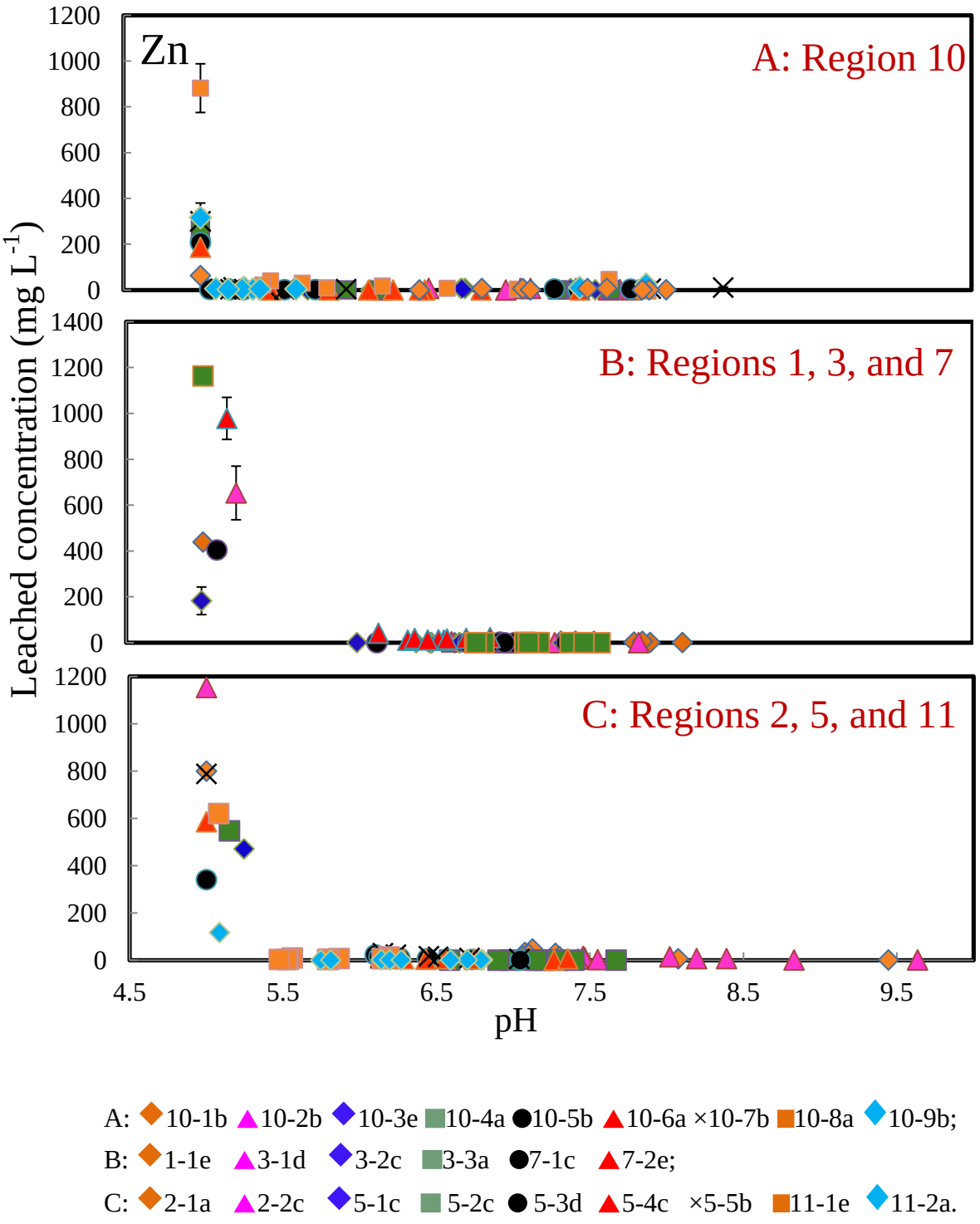

Figure C.10 Leaching concentrations of Zn from MEP are shown as a function of pH. The first extraction is performed with a pH of 5.0 followed by the subsequent nine successive extractions using the initial pH of 3.0 ± 0.2 that simulate acid rain conditions.

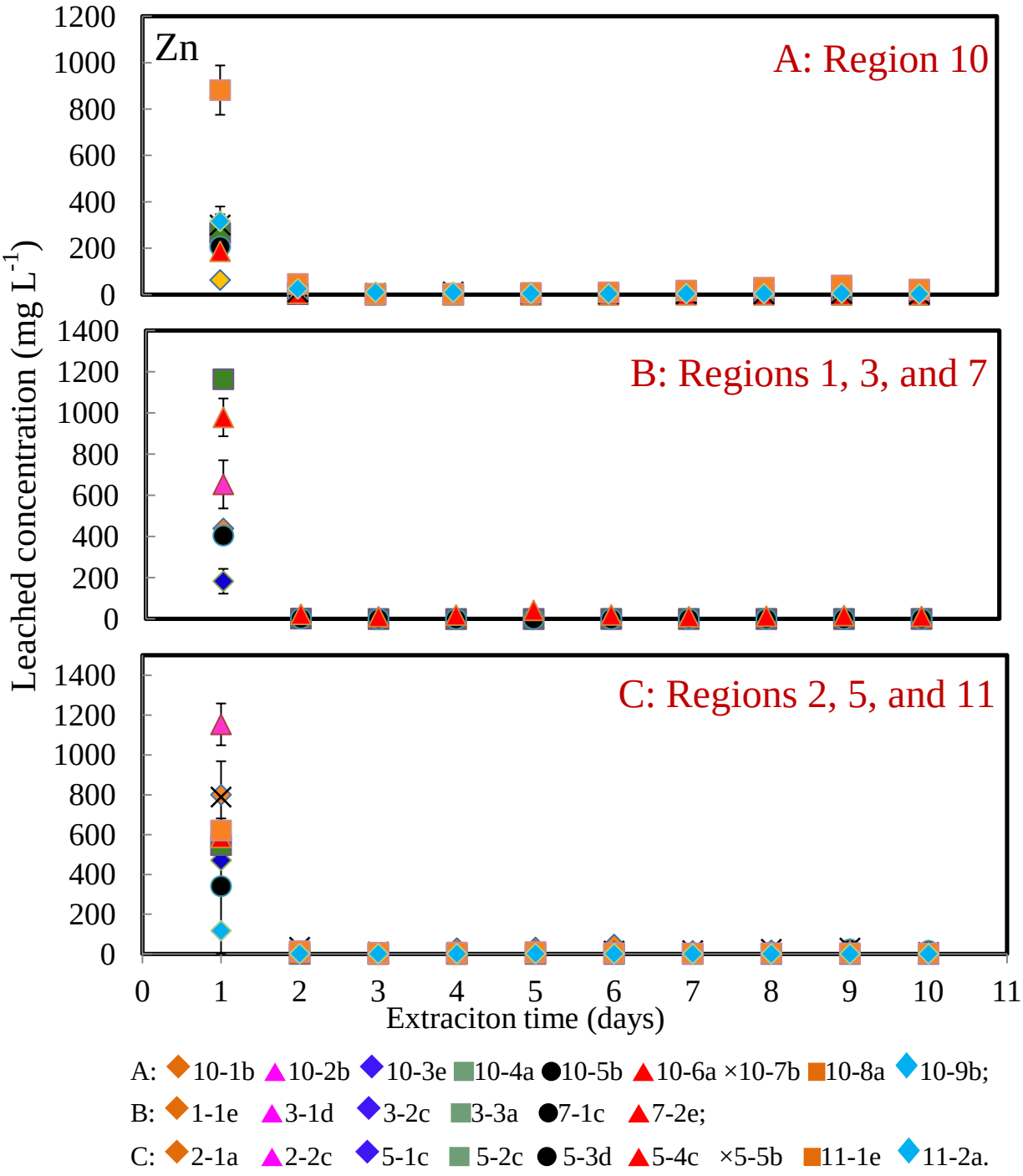

Figure C.11 Leaching concentrations of Zn from MEP are shown as a function of 10 days of extractions. The first extraction is performed with a pH of 5.0 followed by the subsequent nine successive extractions using the initial pH of 3.0 ± 0.2 that simulate acid rain conditions.

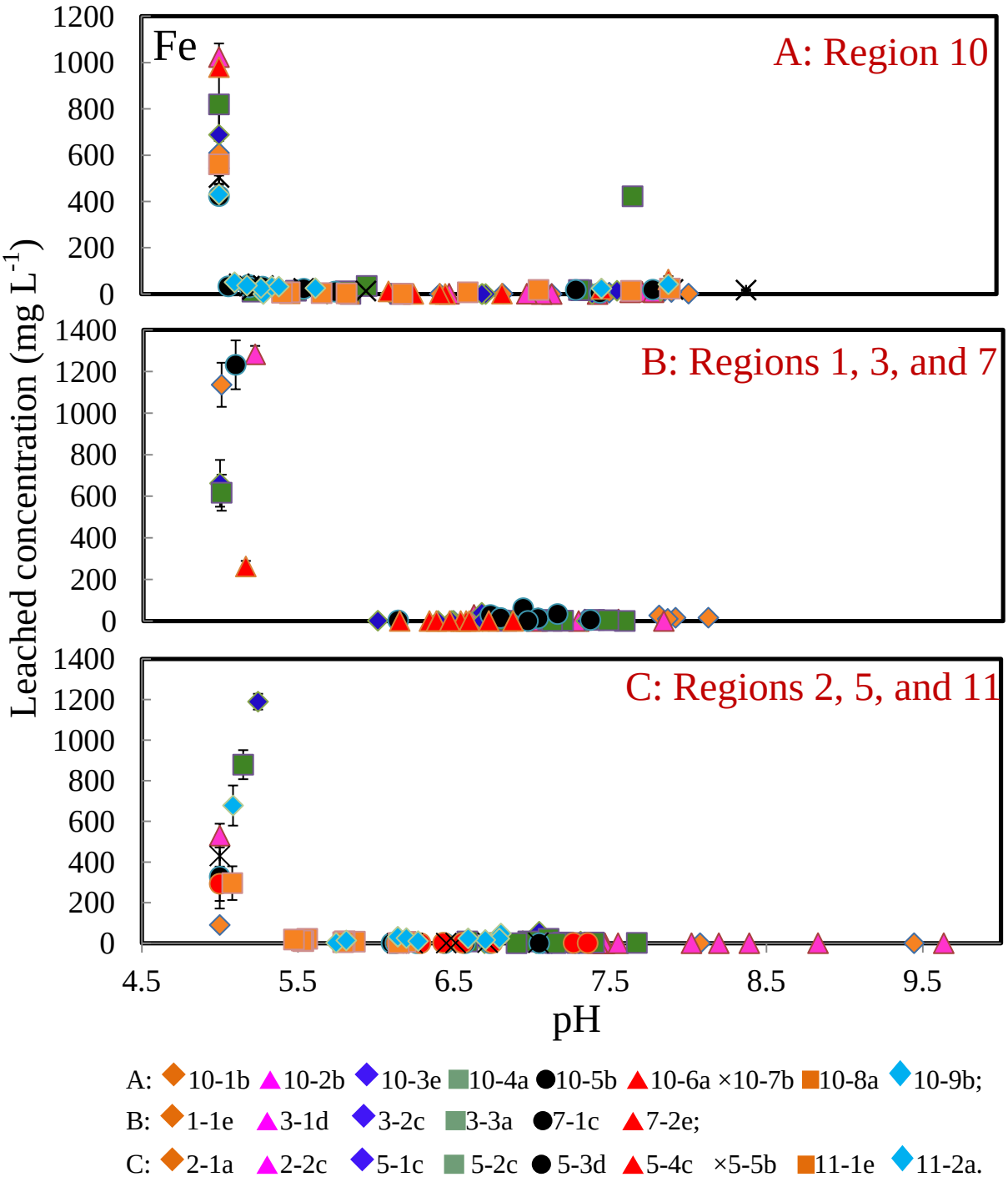

Figure C.12 Leaching concentrations of Fe from MEP are shown as a function of pH. The first extraction is performed with a pH of 5.0 followed by the subsequent nine successive extractions using the initial pH of 3.0 ± 0.2 that simulate acid rain conditions.

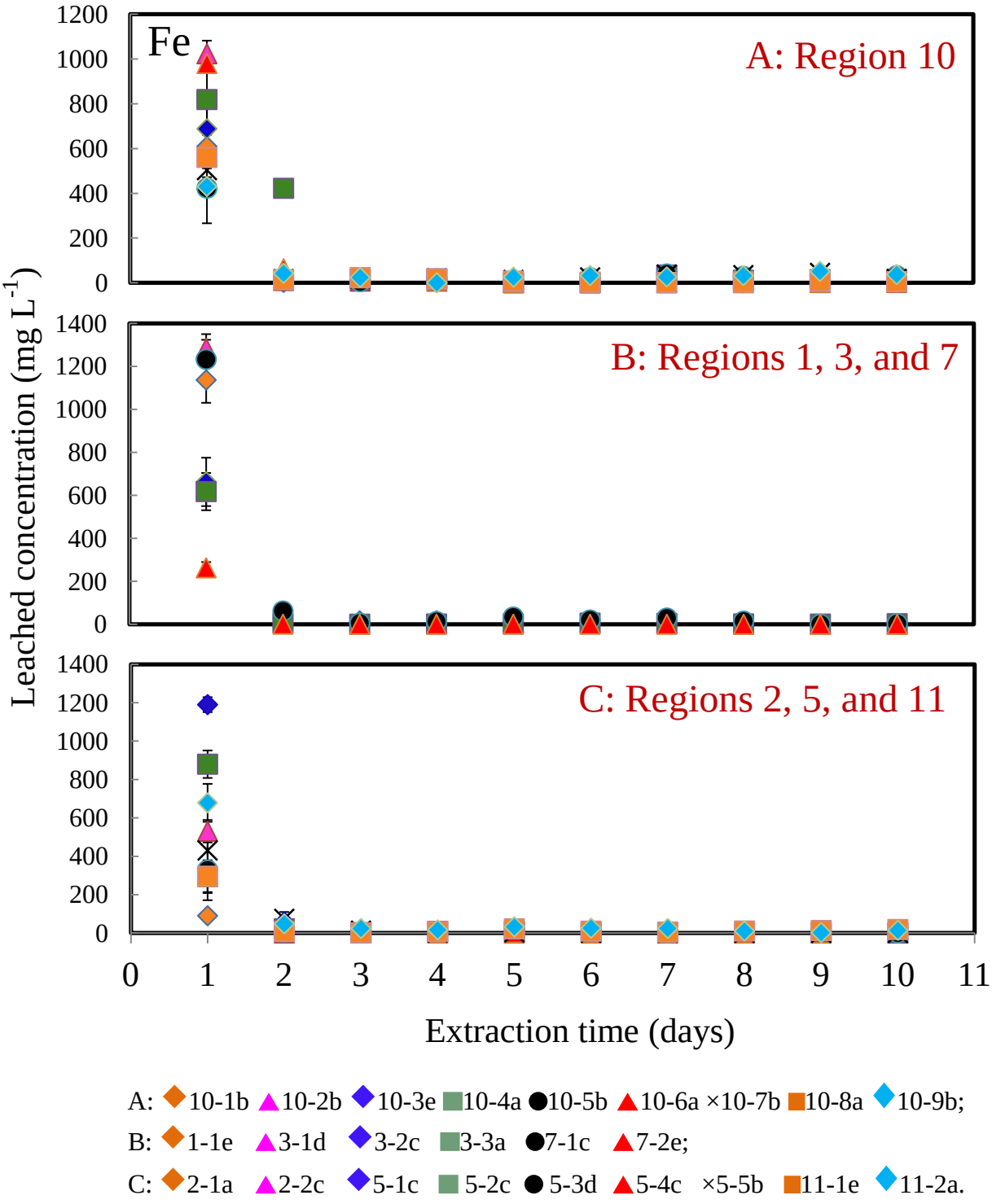

Figure C.13 Leaching concentrations of Zn from MEP are shown as a function of 10 days of extractions. The first extraction is performed with a pH of 5.0 followed by the subsequent nine successive extractions using the initial pH of 3.0 ± 0.2 that simulate acid rain conditions.

APPENDIX D

SOLUBILITY AND SPECIATION OF RCRA METALS, FE AS WELL ZN

The solubility and speciation diagrams of RCRA metals, Fe as well as Zn are presented below.

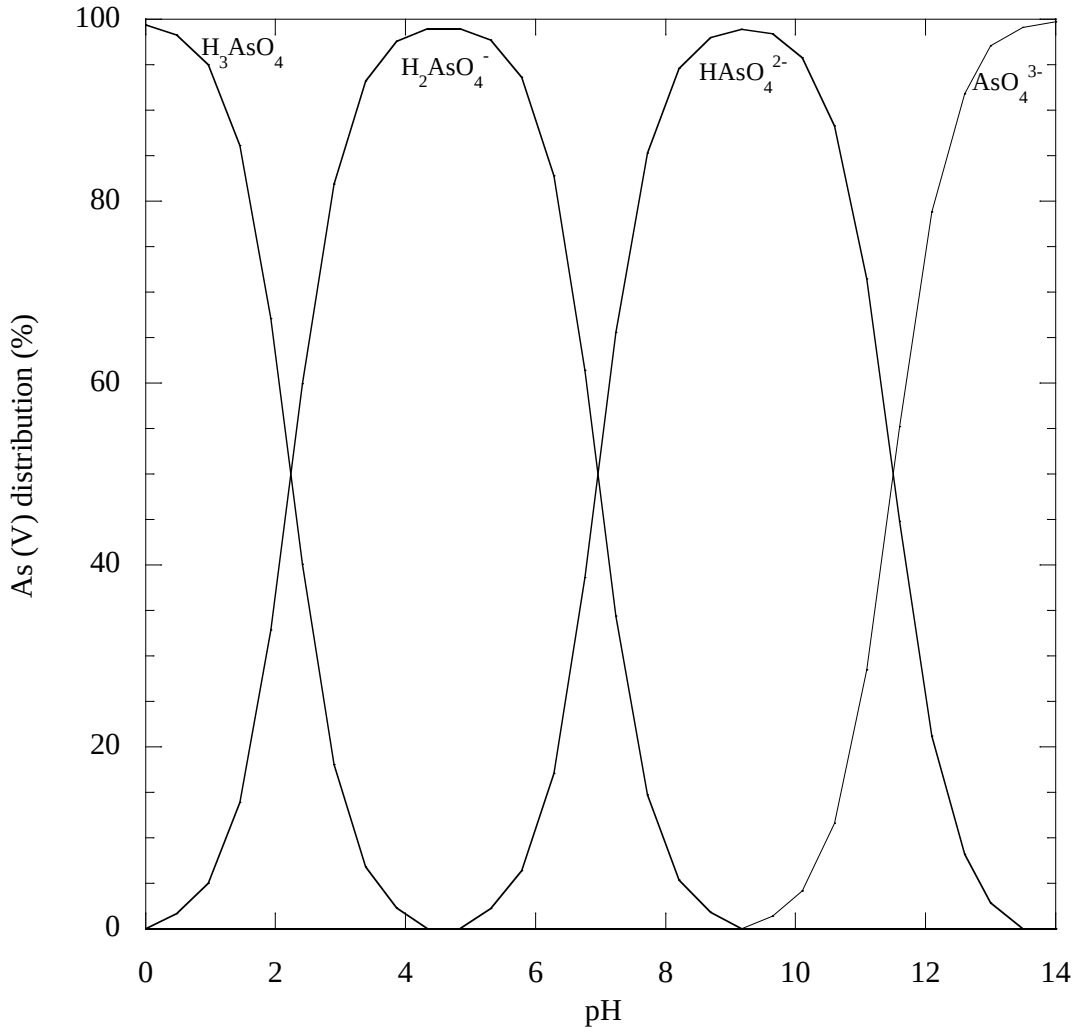

Figure D.1 As (III) speciation in the leaching studies of paint waste, CH_3COOH at 0.1 M, 298 K and open to atmosphere. All the speciation was computed using MINEQL$^+$. The total concentration of As leached was 8.9×10^{-6} M.

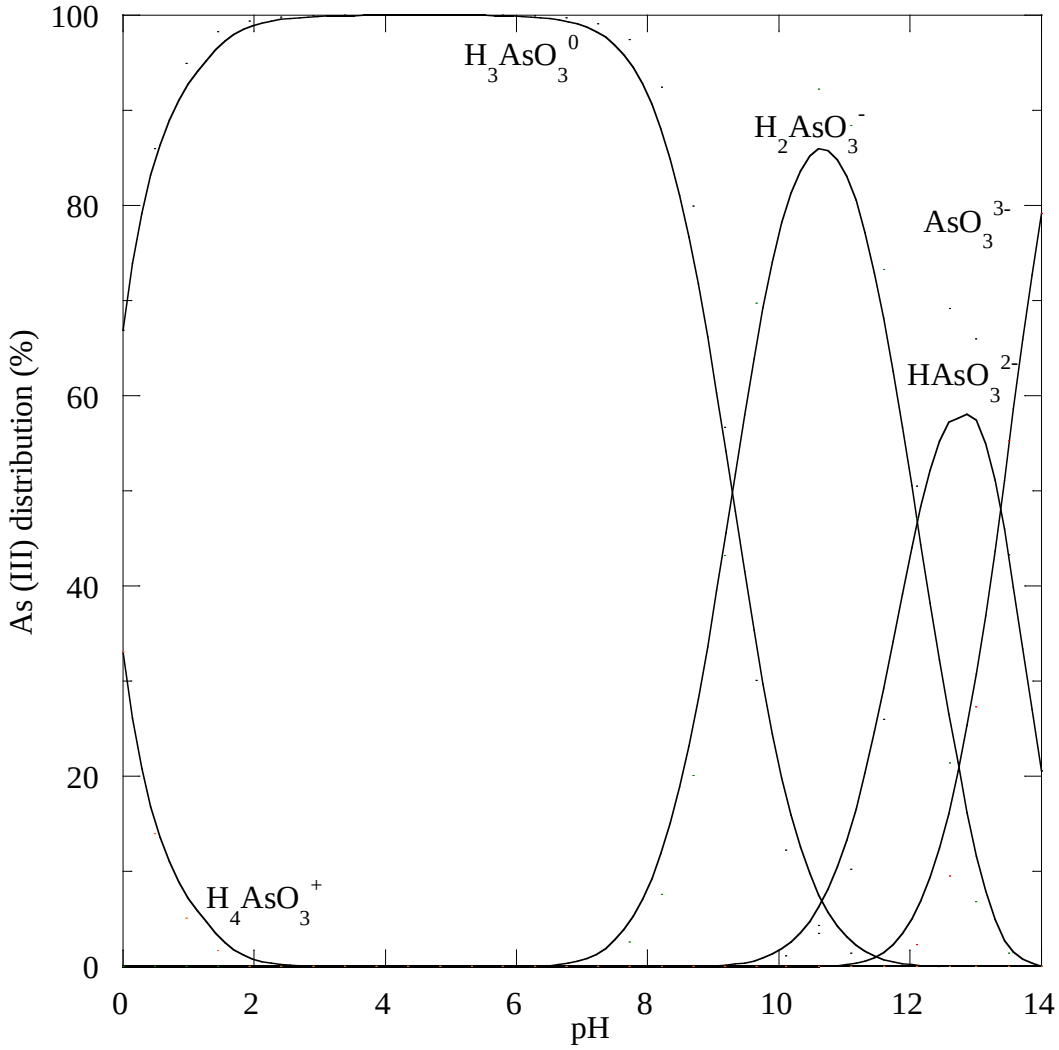

Figure D.2 As (VI) speciation in the leaching studies of paint waste, CH_3COOH at 0.1 M, 298 K and open to atmosphere. All the speciation was computed using MINEQL$^+$. The total concentration of As leached was 8.9×10^{-6} M.

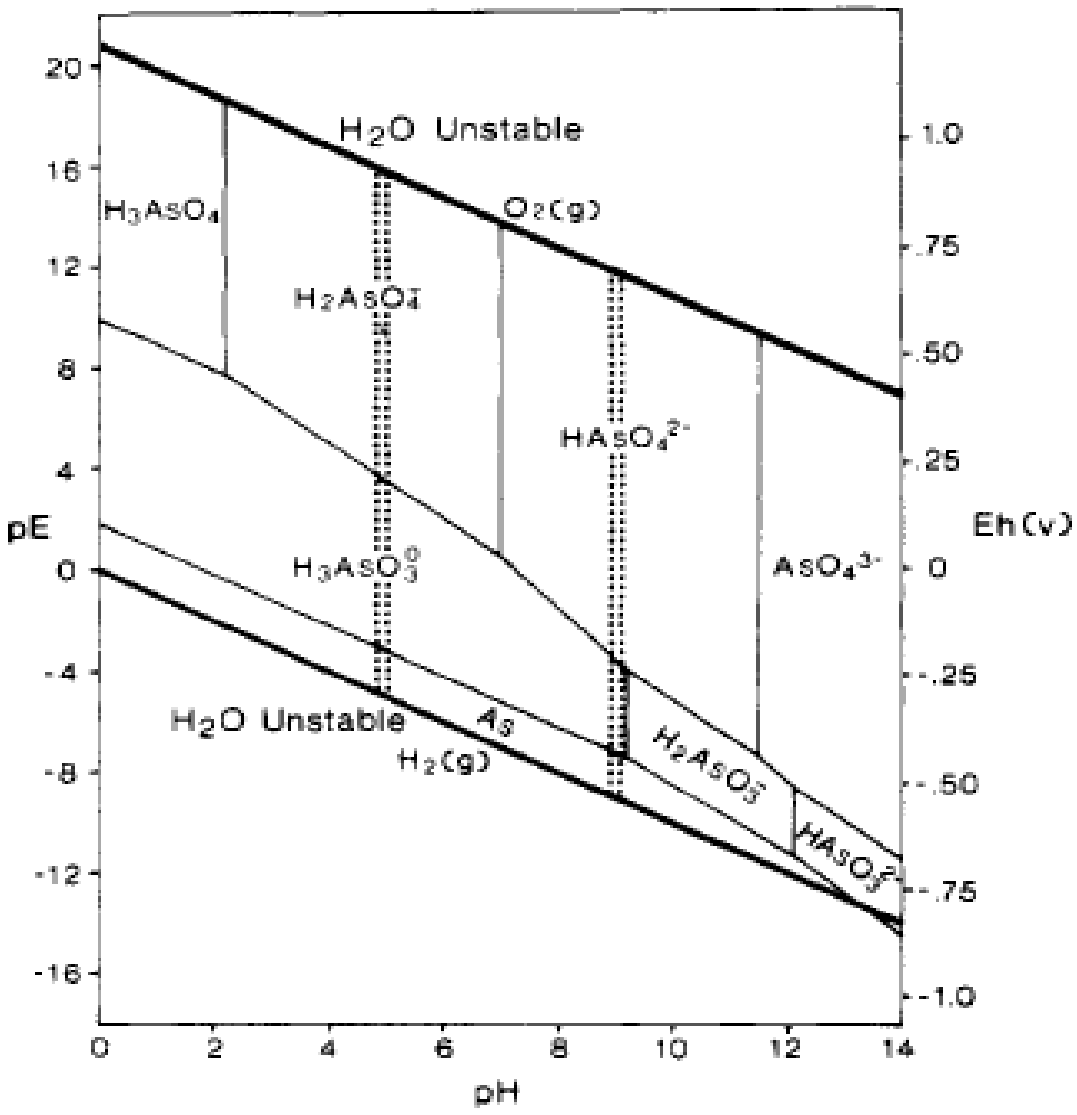

Figure D.3 The pE–pH diagram for As at 298 K, in an open system with total As 5.0×10^{-8} M from Cullen and Reimer (1989).

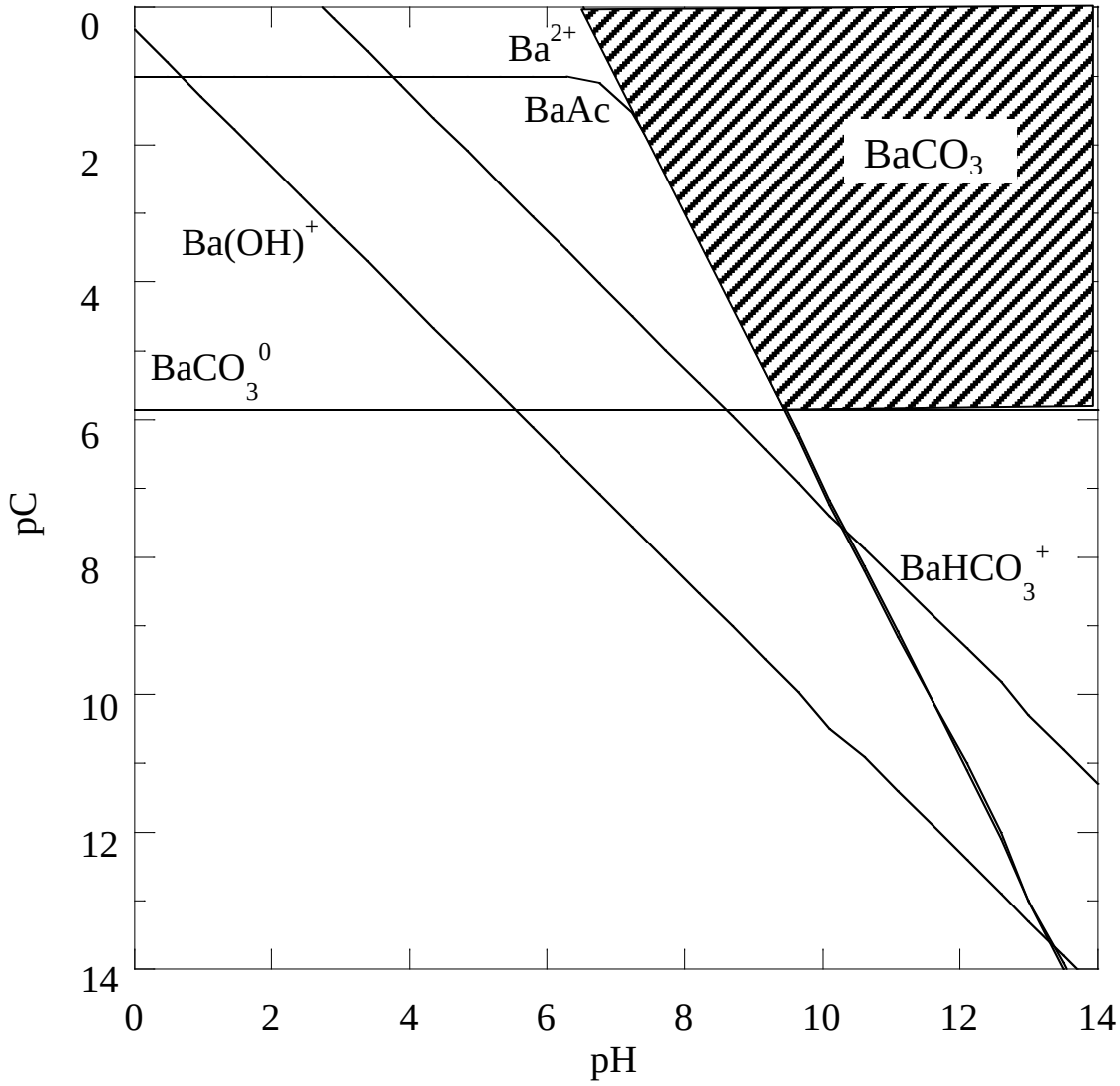

Figure D.4 Ba solubility in equilibrium with $BaCO_5$, CH_3COOH at 0.1 M, 298 K and open to atmosphere. All the speciation was computed using MINEQL$^+$.

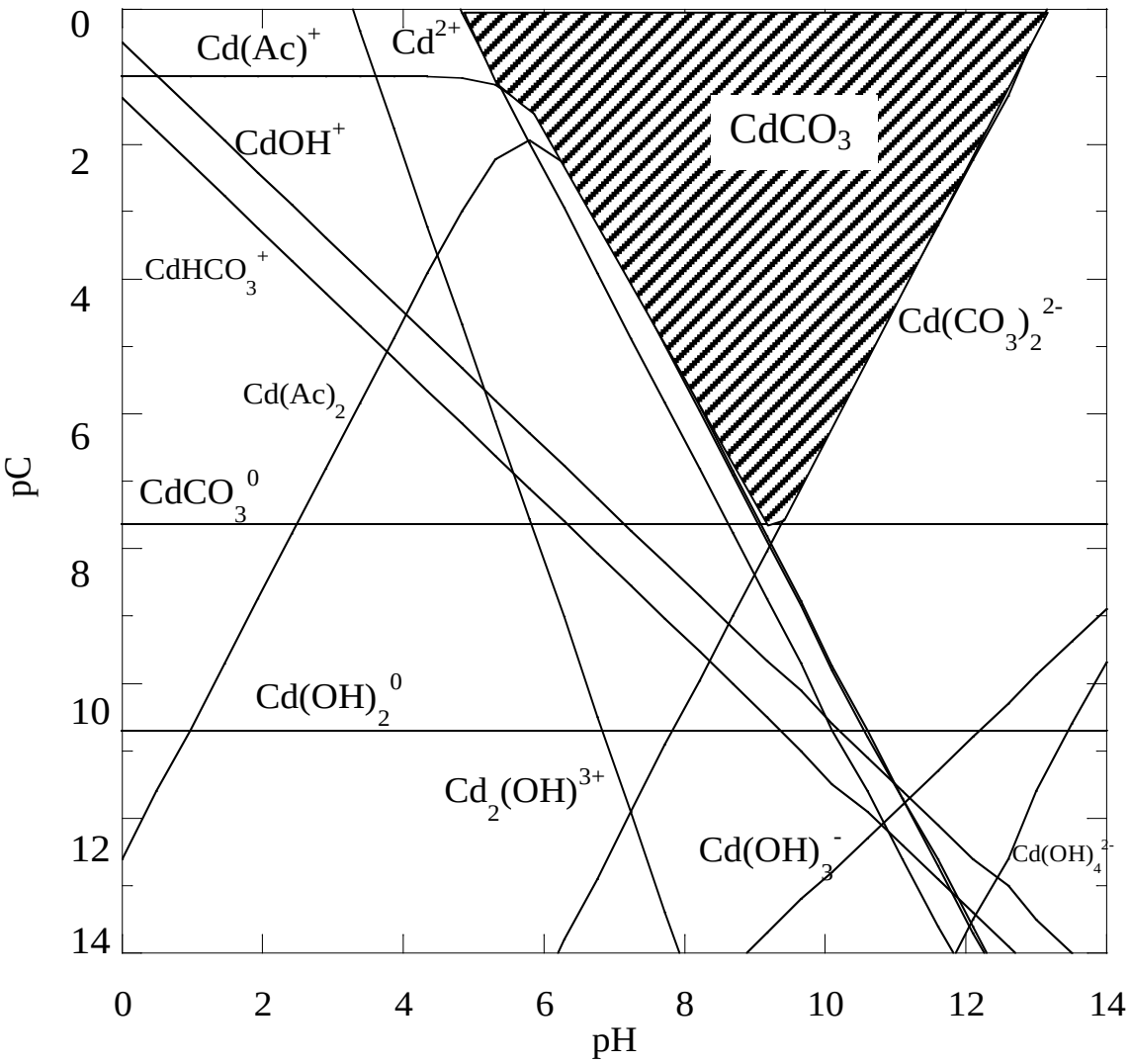

Figure D.5 Cd solubility in equilibrium with $CdCO_{5,}$ CH_3COOH at 0.1 M, 298 K and open to atmosphere. All the speciation was computed using $MINEQL^+$.

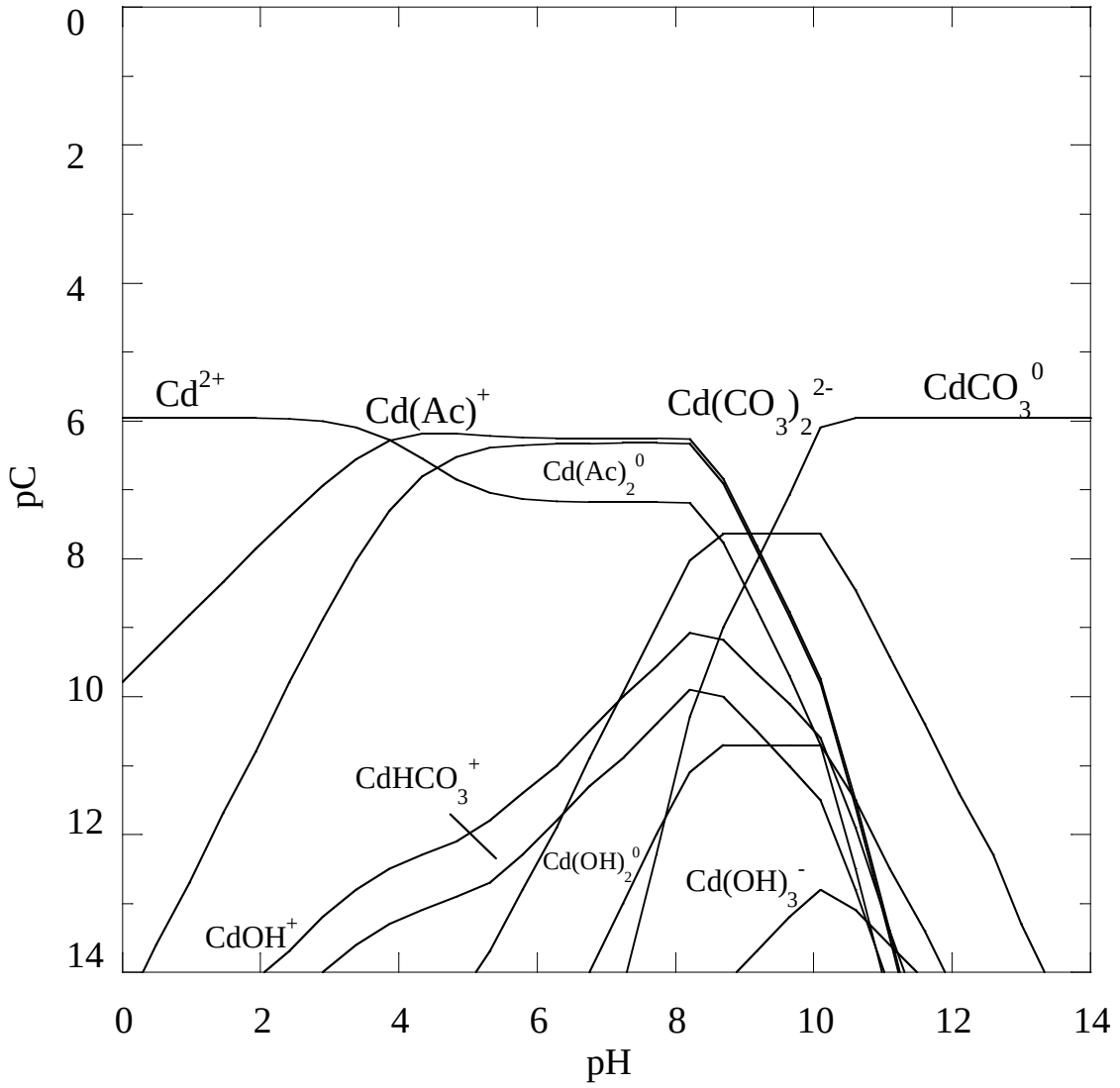

Figure D.6 Cd speciation in the leaching studies of paint waste, CH_3COOH at 0.1 M, 298 K and open to atmosphere. All the speciation was computed using MINEQL$^+$. The total concentration of Cd leached was 1.1×10^{-6} M.

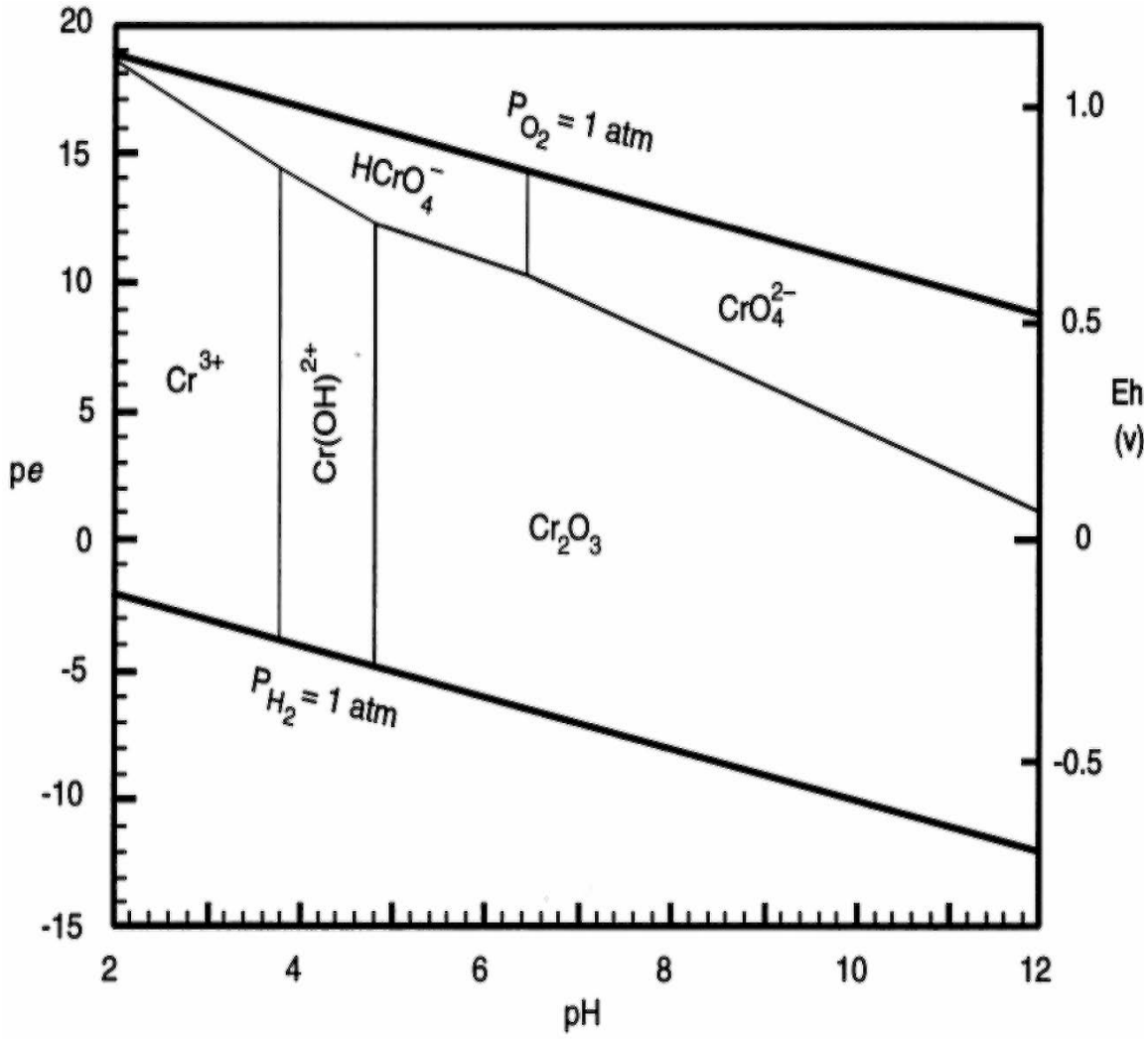

Figure D.7 The pE–pH diagram for Cr at 298 K, in an open system with total Cr 1.0×10^{-6} M from Rai et al. (1989).

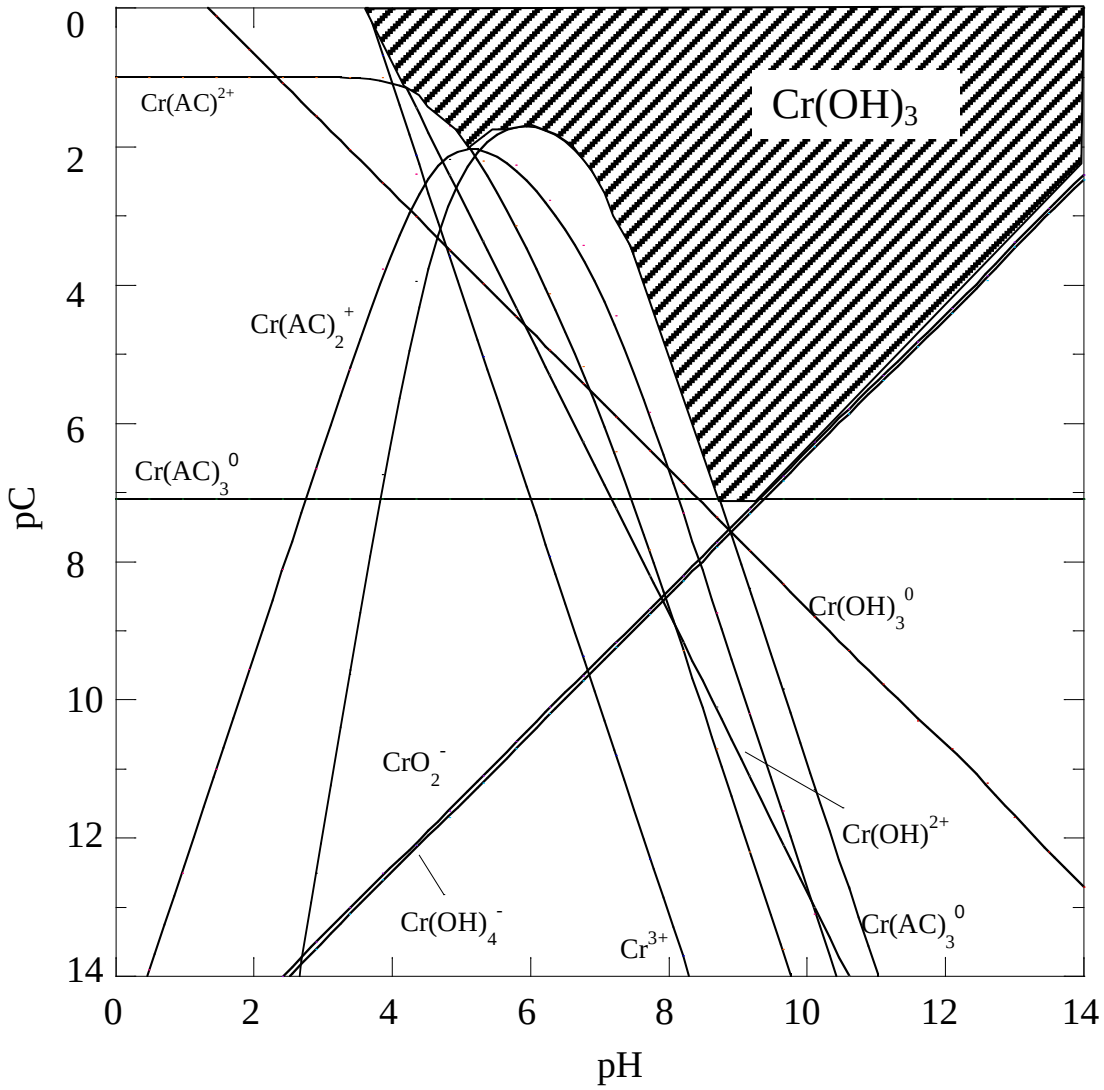

Figure D.8 Cr (III) solubility in equilibrium with $Cr(OH)_3$, CH_3COOH at 0.1 M, 298 K and open to atmosphere. All the speciation was computed using MINEQL$^+$.

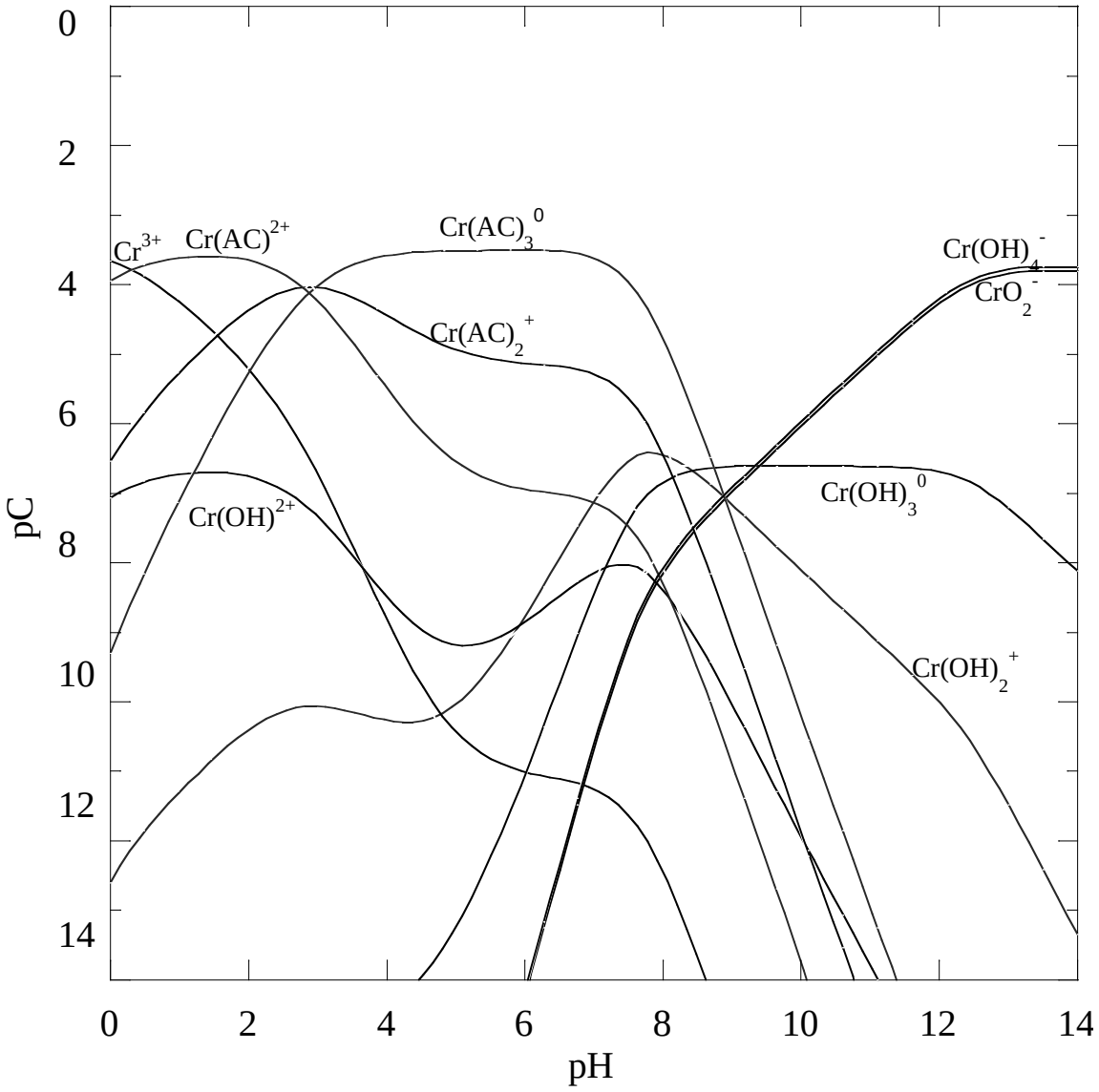

Figure D.9 Cr(III) speciation in the leaching studies of paint waste, CH_3COOH at 0.1 M, 298 K and open to atmosphere. All the speciation was computed using MINEQL$^+$. The total concentration of Cr leached was 1.8×10^{-4} M.

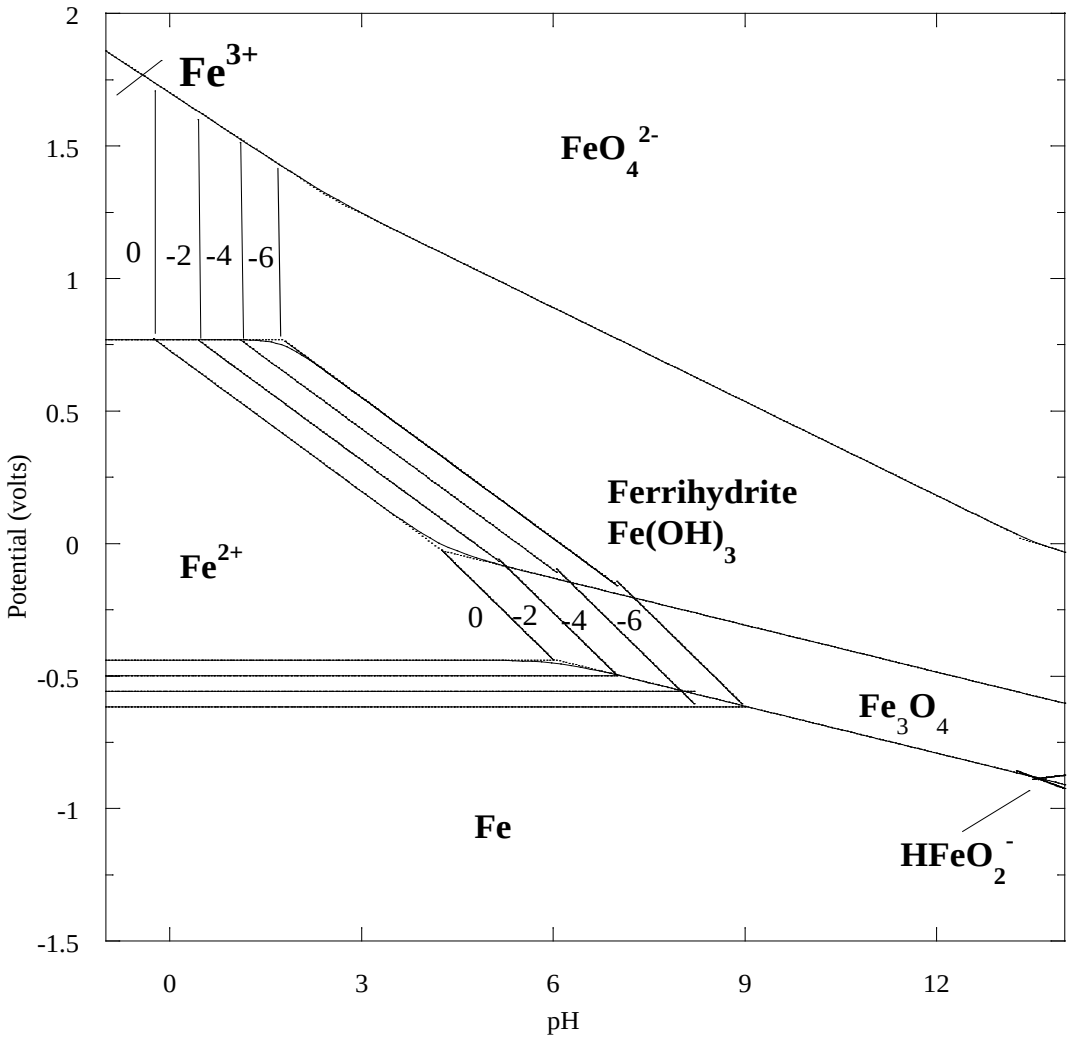

Figure D.10 Potential - pH equilibrium diagram of iron or steel considering four concentrations of soluble species (10^{0}, 10^{-2}, 10^{-4}, 10^{-6} M), four soluble species (Fe^{3+}, Fe^{2+} , FeO_4^{2-}, $HFeO_2^{-}$), and corrosion material ferrihydrite [$Fe(OH)_3$] at 298 K.

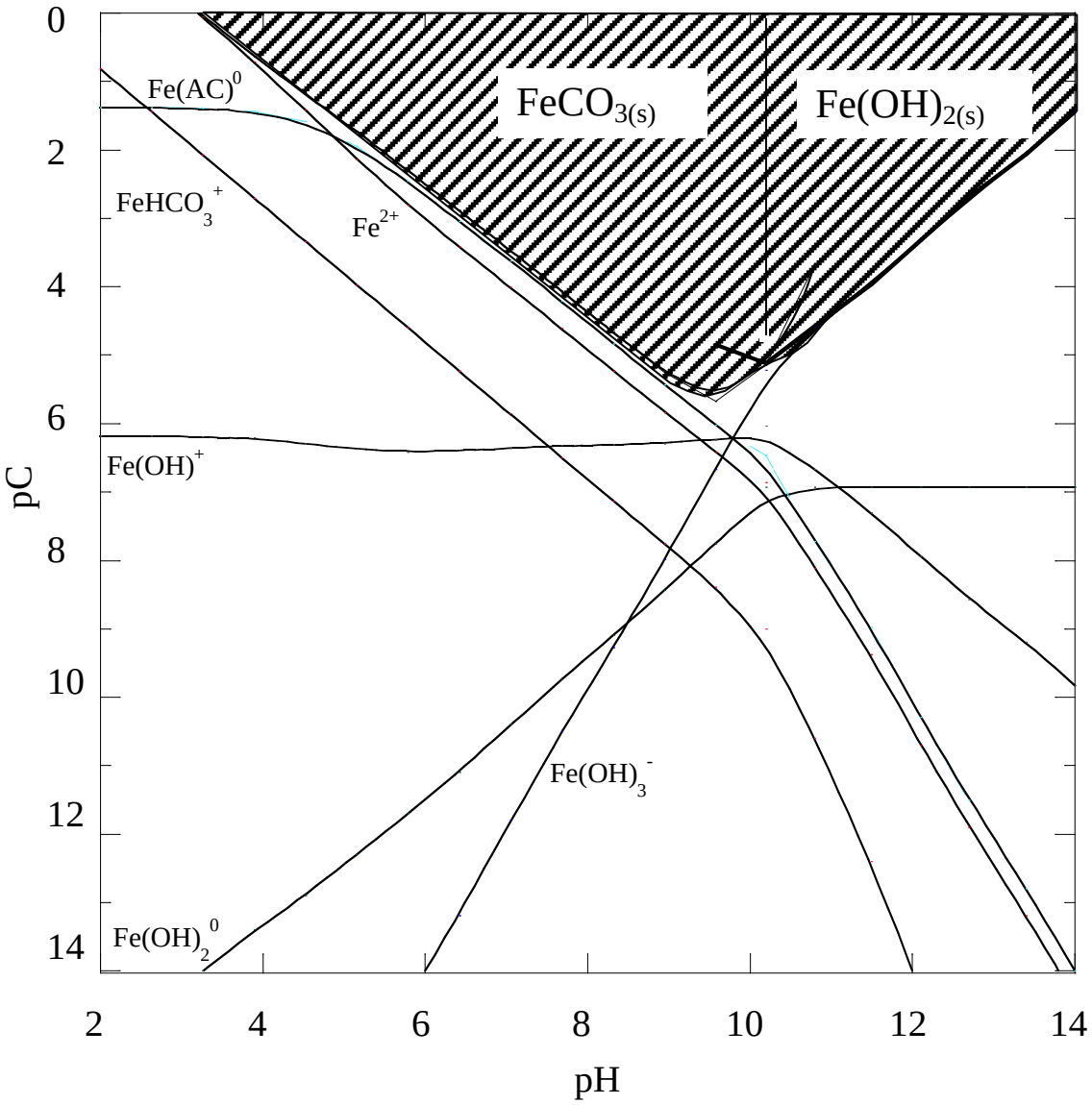

Figure D.11 Fe^{2+} solubility in equilibrium with $Fe(OH)_2$ and $FeCO_3$, CH_3COOH at 0.1 M, 298 K and open to atmosphere. All the speciation was computed using MINEQL$^+$.

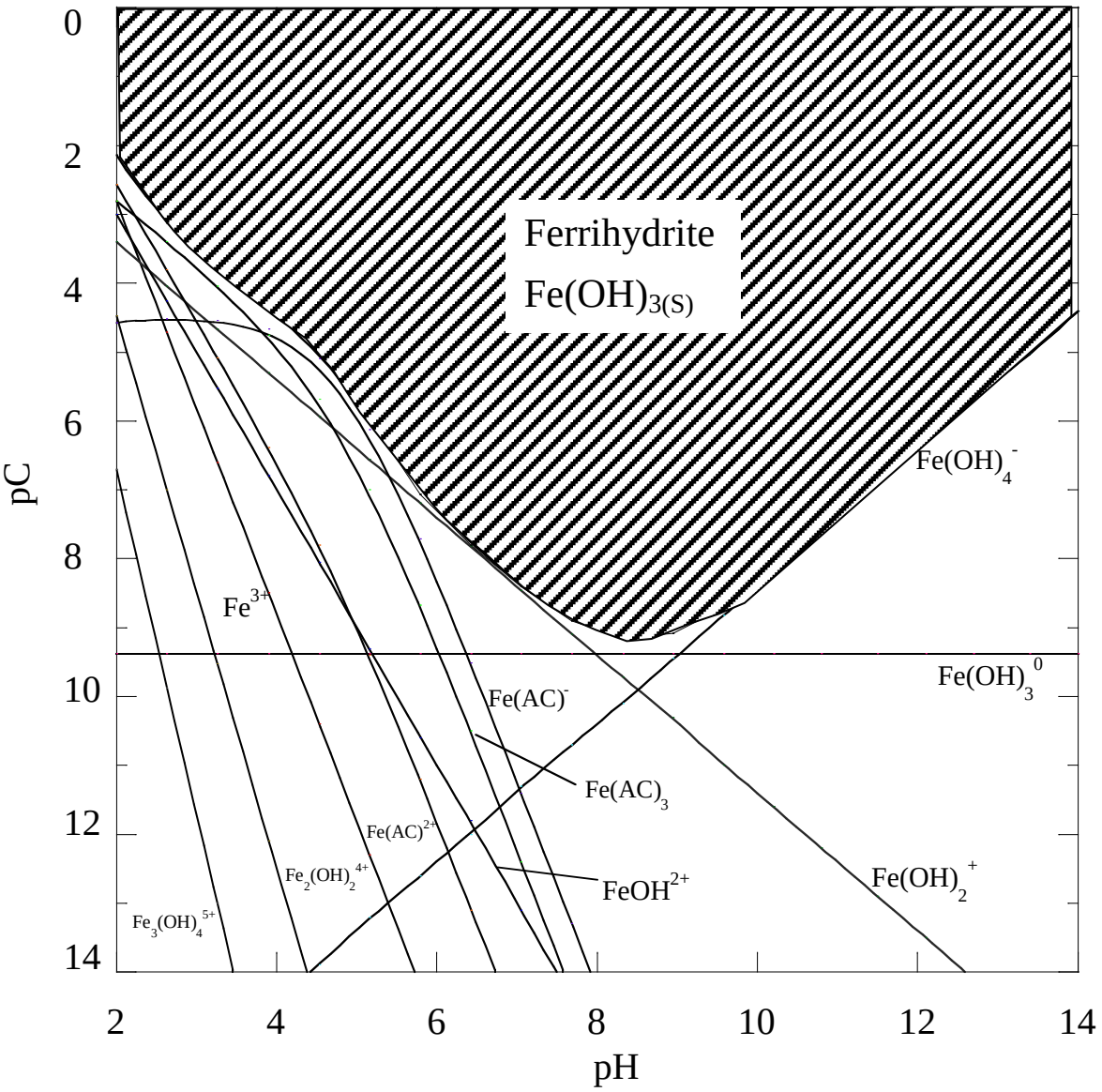

Figure D.12 Fe^{3+} solubility in equilibrium with Ferrihydrite [$Fe(OH)_3$], CH_3COOH at 0.1 M, 298 K and open to atmosphere. All the speciation was computed using MINEQL$^+$.

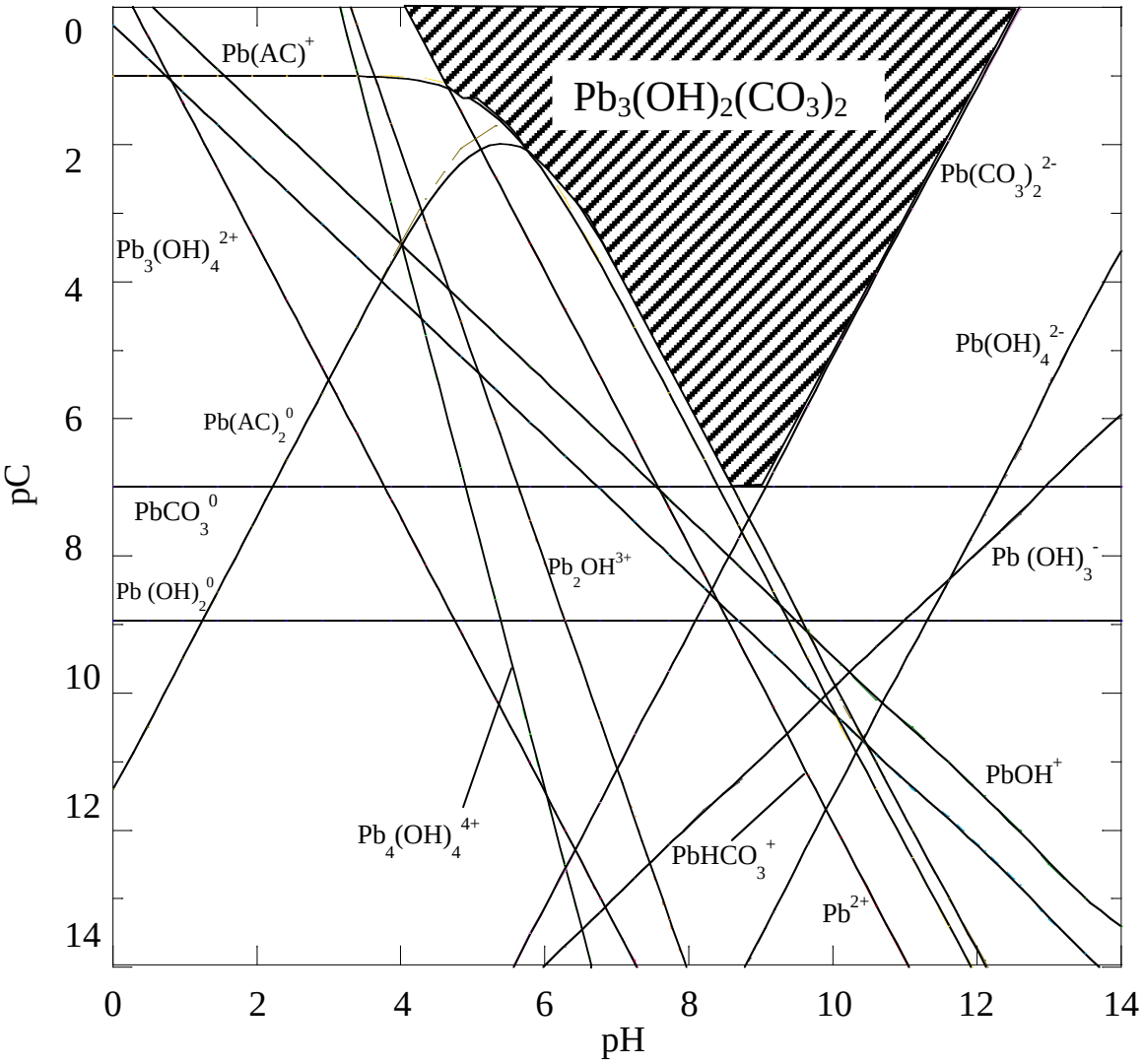

Figure D.13 Pb solubility in equilibrium with $Pb_3(OH)_2(CO_3)_2$, CH_3COOH at 0.1 M, 298 K and open to atmosphere. All the speciation was computed using MINEQL$^+$.

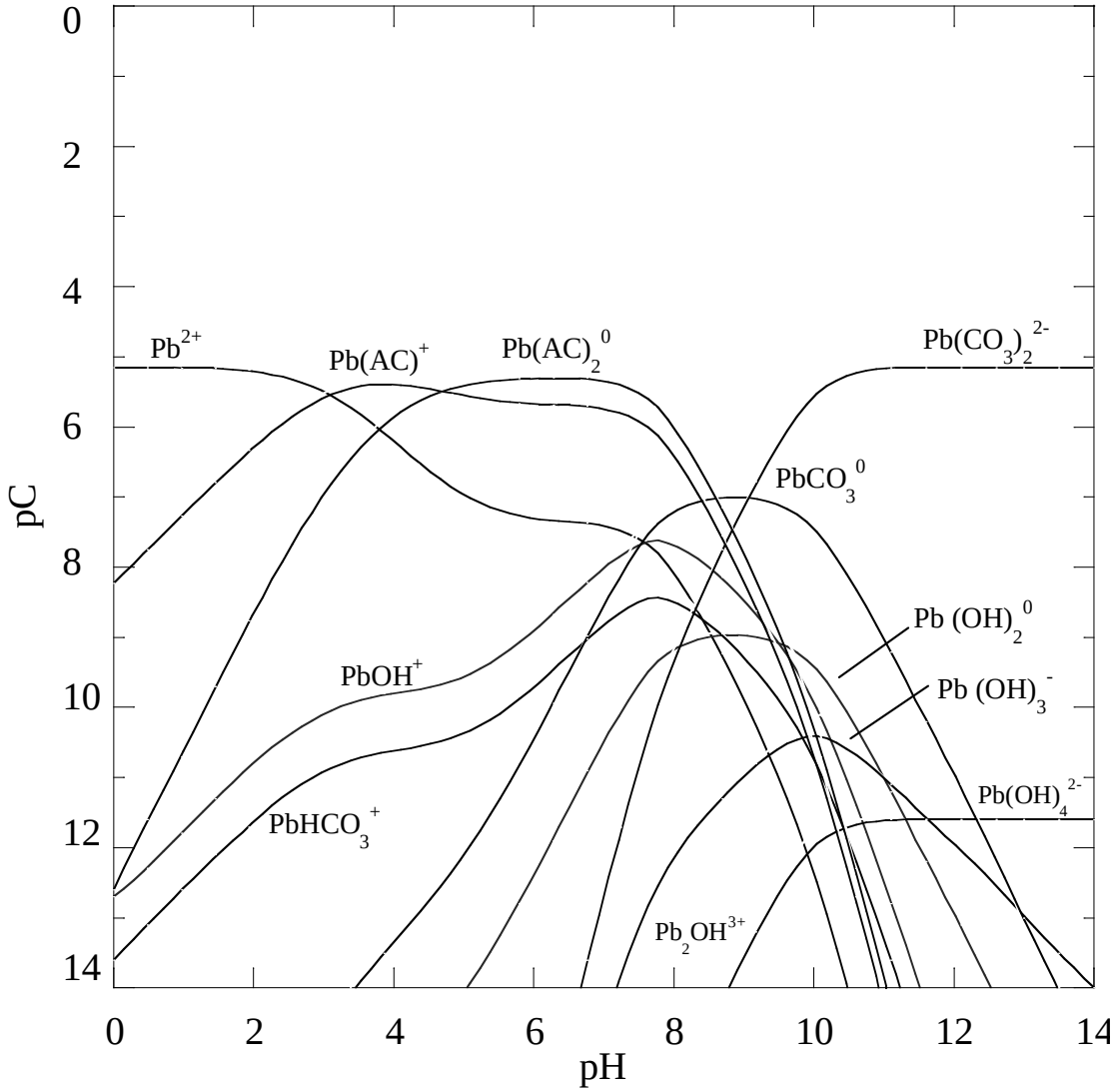

Figure D.14 Pb speciation in the leaching studies of paint waste, CH_3COOH at 0.1 M, 298 K and open to atmosphere. All the speciation was computed using MINEQL$^+$. The total concentration of Pb leached was 7.1×10^{-6} M.

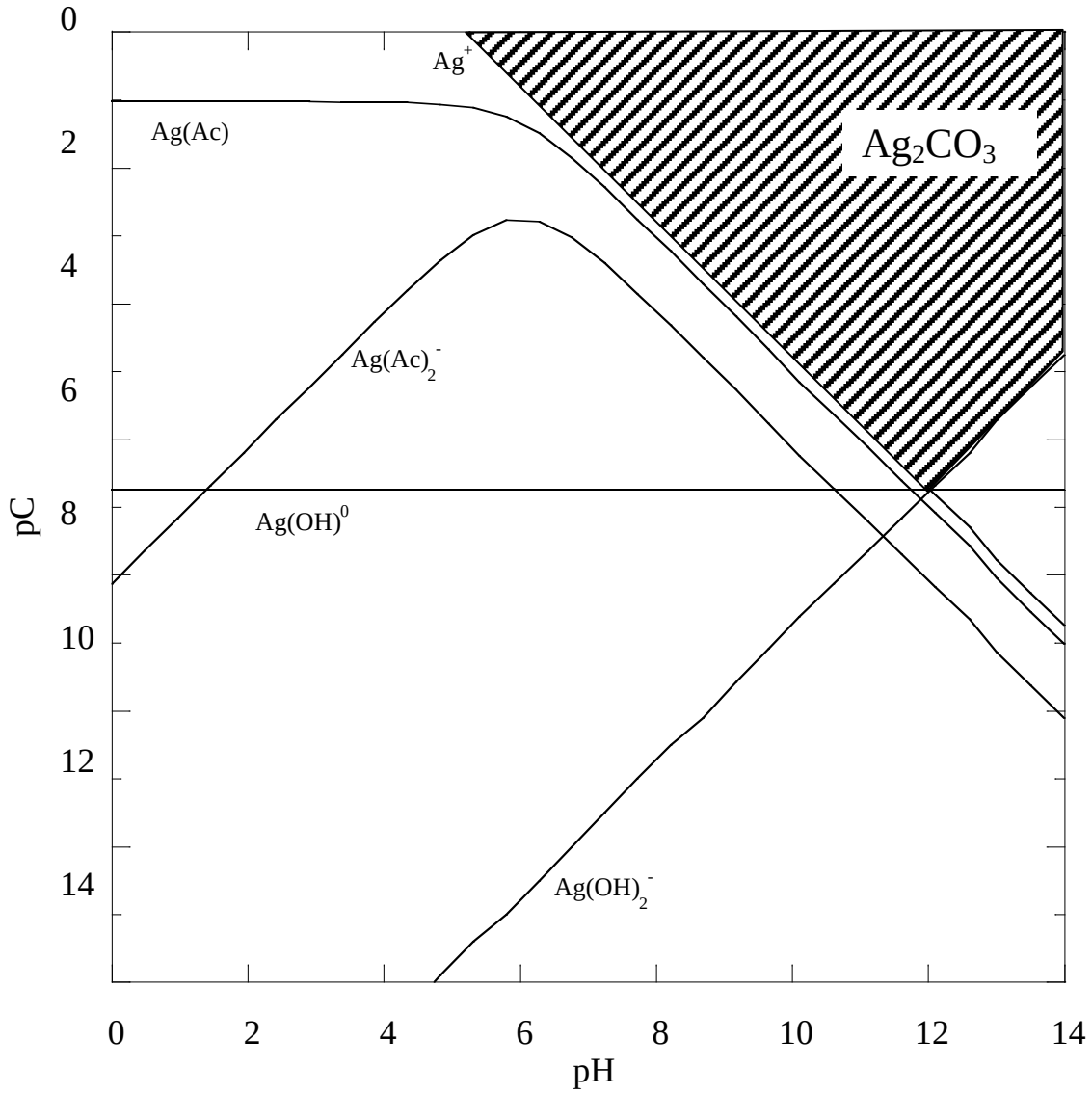

Figure D.15 Ag solubility in equilibrium with Ag_2CO_3, CH_3COOH at 0.1 M, 298 K and open to atmosphere. All the speciation was computed using MINEQL$^+$.

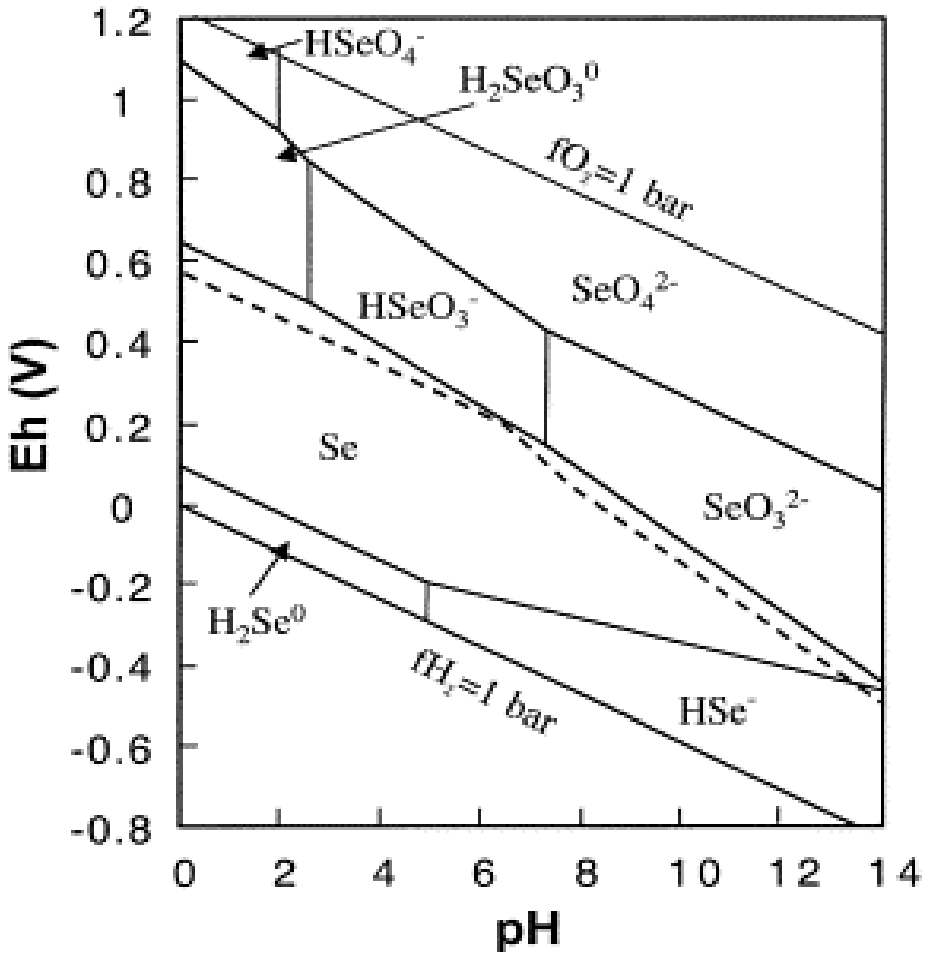

Figure D16 The pE–pH diagram for Se at 298 K, in an open system with total Se 1.0×10^{-6} M from Wagman et al. (1982).

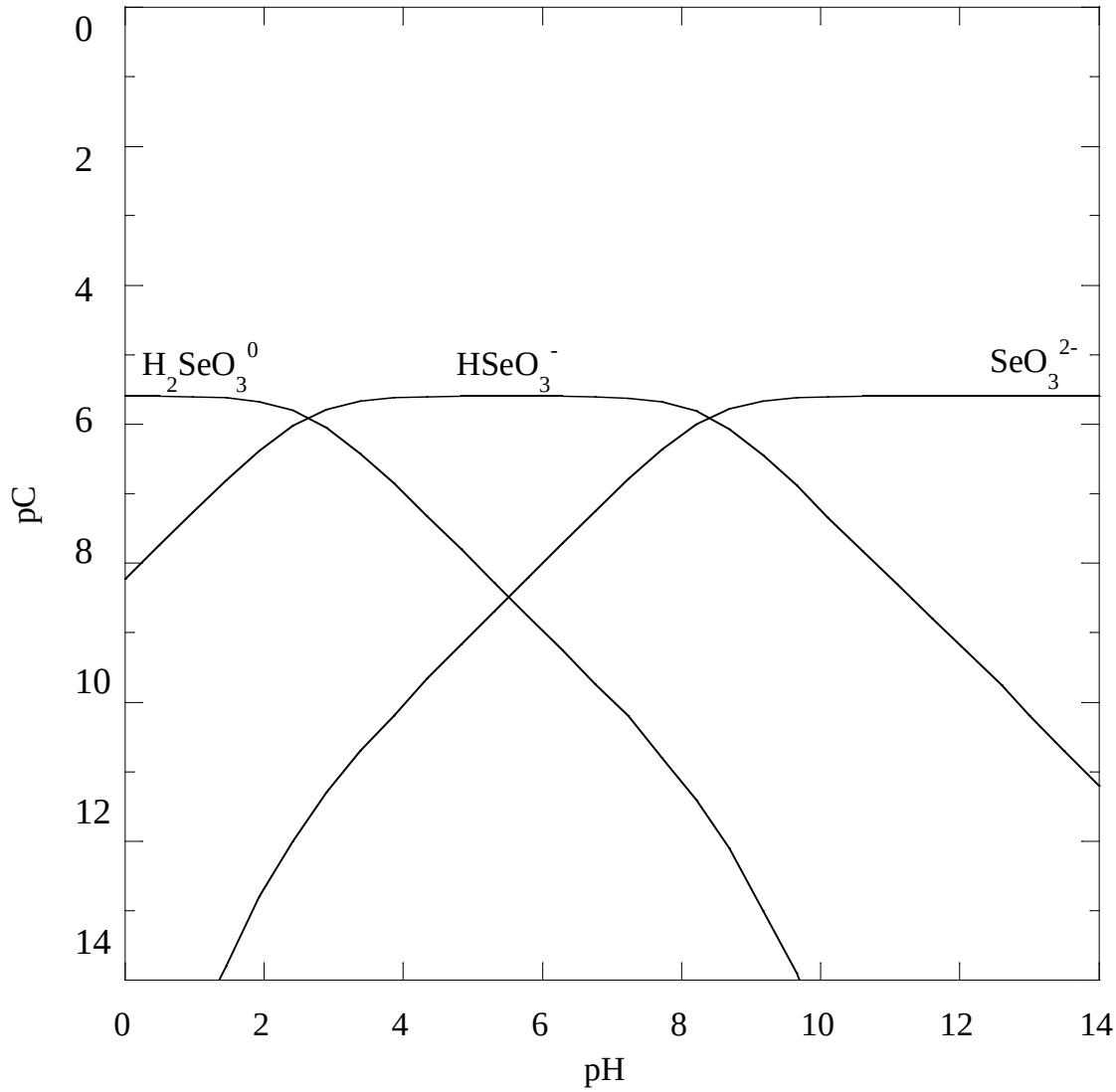

Figure D17 Se(IV) speciation in the leaching studies of paint waste, CH_3COOH at 0.1 M, 298 K and open to atmosphere. All the speciation was computed using MINEQL$^+$. The total concentration of Se leached was 2.5×10^{-6} M.

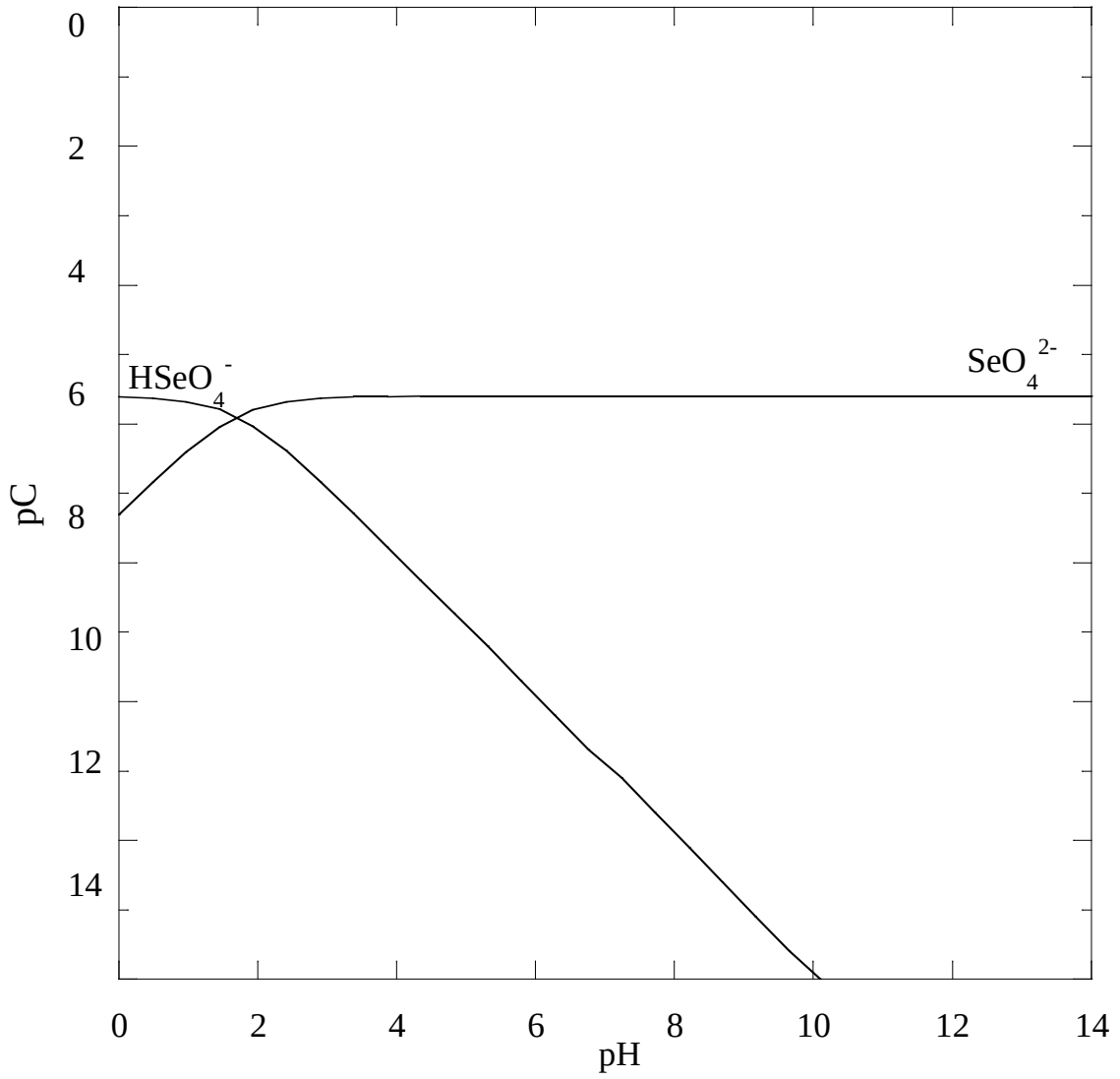

Figure D.18 Se(VI) speciation in the leaching studies of paint waste, CH_3COOH at 0.1 M, 298 K and open to atmosphere. All the speciation was computed using MINEQL$^+$. The total concentration of Se leached was 2.5×10^{-6} M.

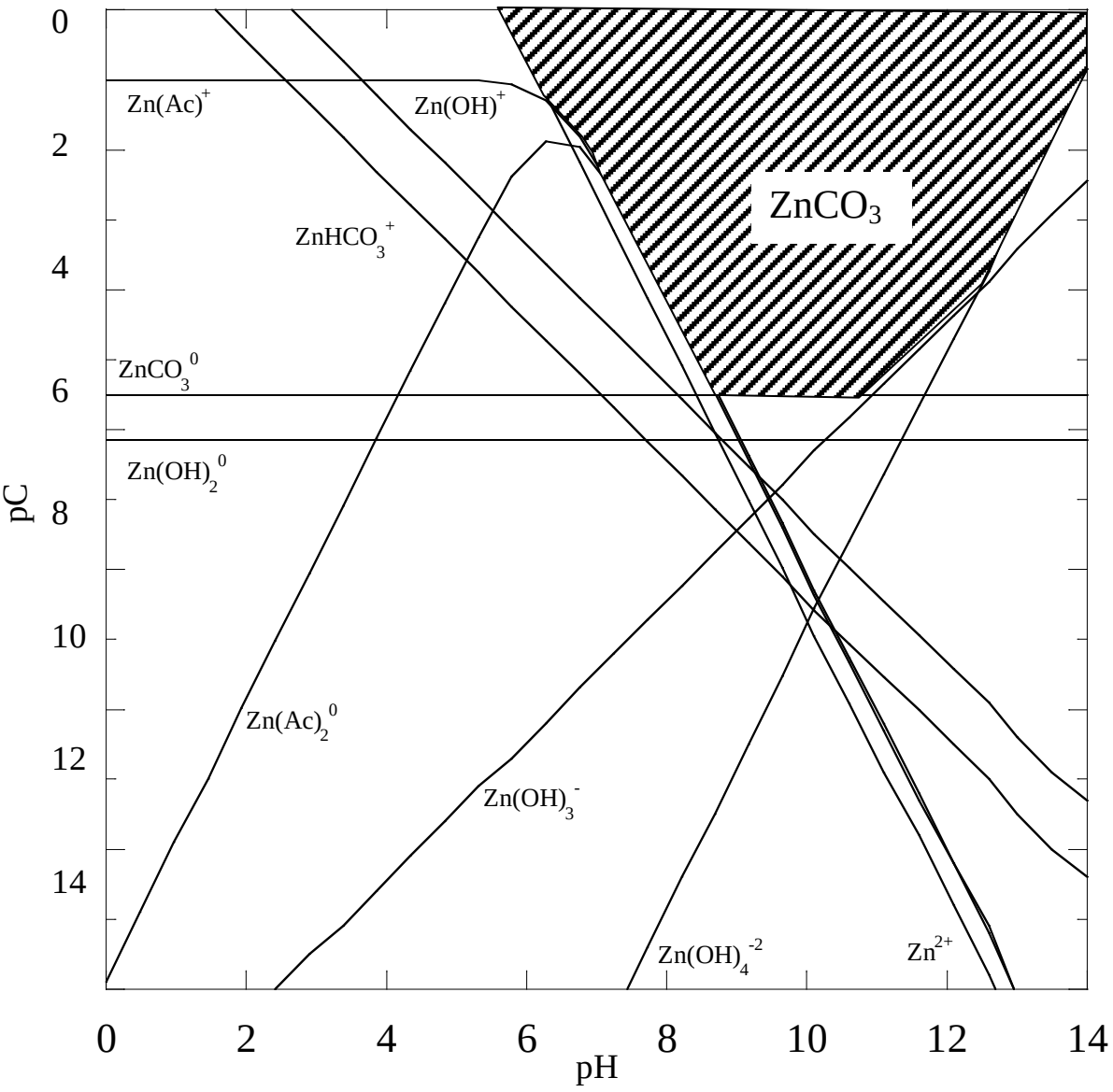

Figure D.19 Zn solubility in equilibrium with $ZnCO_3$, CH_3COOH at 0.1 M, 298 K and open to atmosphere. All the speciation was computed using MINEQL$^+$.

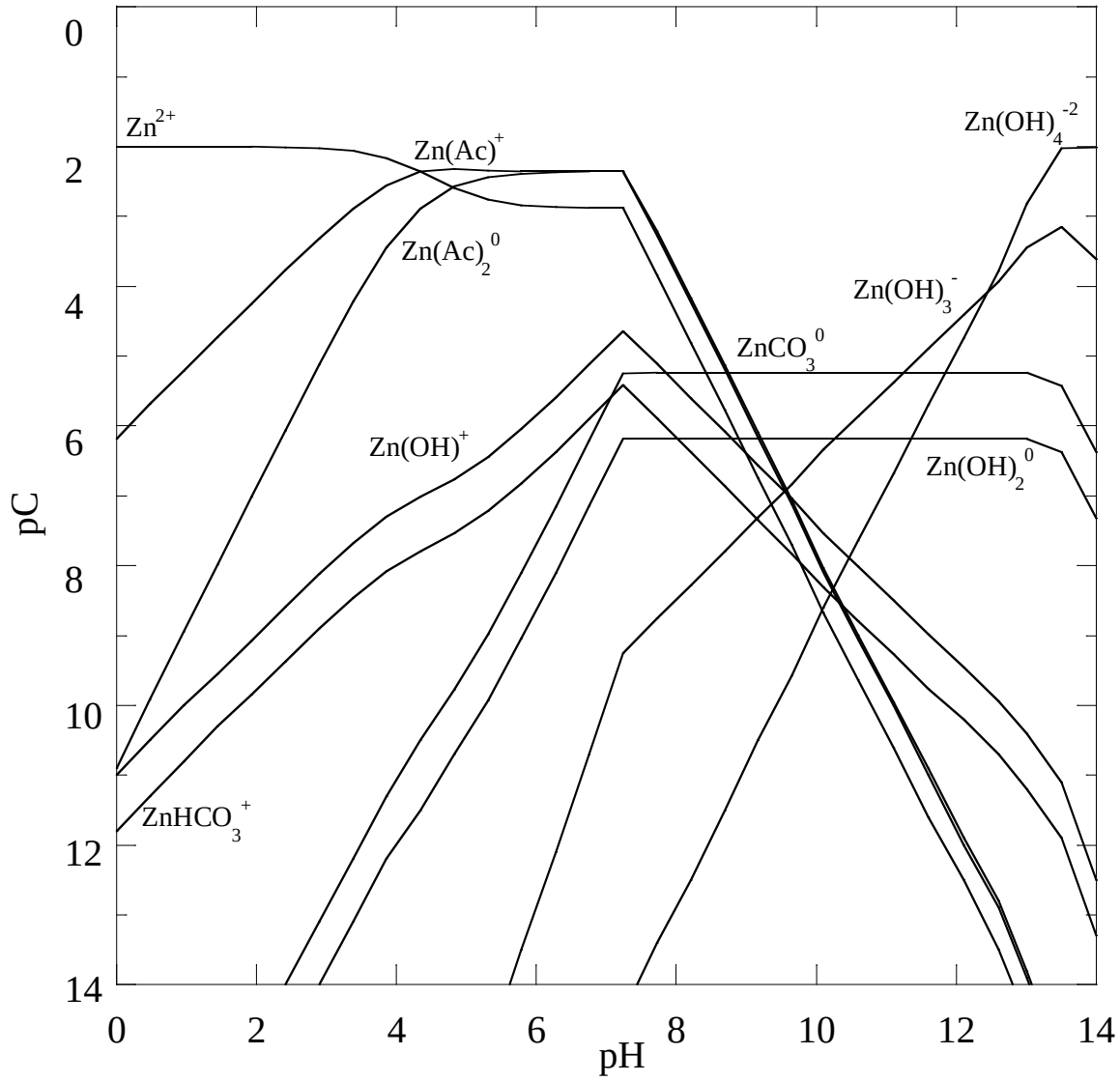

Figure D.20 Zn speciation in the leaching studies of paint waste, CH_3COOH at 0.1 M, 298 K and open to atmosphere. All the speciation was computed using MINEQL$^+$. The total concentration of Zn leached was 0.02 M.

APPENDIX E

XRD ANALYSIS DATA

Table E.1 Standard XRD Patterns for Minerals in the Paint Samples

XRF detected elements	Results measured in XRD	Relative Intensity 2θ (°)					
		100% ~ 91%	90% ~ 81%	80% ~ 61%	60% ~ 41%	40% ~ 21%	20% ~ 10%
Pb	lead tetroxide [Pb_3O_4]	26.4 (100%)			32.1 (45%)	52.0(26%) 34.0 (27%)	
	$Pb_2(CrO_4)O$	26.3 (99.9%)	29.9 (87.3%)			31.5 (34.5%) 31.0 (22.2%)	48.7 (19.7%) 44.0 (20.0%)
Cr	Cr_2O_3	33.6 (99.9%)	36.2 (82.3%)	54.9 (63.1%)	24.5 (56.2%)	65.2 (28.0%) 50.3 (33.7%)	
Zn	Zinc [Zn]	43.2 (99.9%)				39.0 (23.4%) 36.3 (38.9%)	70.1 (15.6%)
	Zinc oxide [ZnO]	36.6 (99.9%)			31.8 (57.7%) 34.4 (44.6%)	56.6 (30.9%) 62.9 (25.6%) 47.6 (22.6%) 68.0 (22.2%)	
Fe	Fe	44.7 (99.9%)					82.3 (17.9%) 65.0 (11.7%)
	Ferrihydrite	36.2 (99.9%)		34.3 (79%) 26.1 (77%) 36.0 (76%)	62.4 (57%) 62.3 (55%) 56.1 (42%)	19.5 (36%) 40.2 (36%)	
	Magnetite [Fe_3O_4)	35.4 (99.9%)	35.5 (81.8%)		62.6 (41.6%)	57.0 (21.7%) 43.1 (34.1%) 30.1 (35.7%)	
	geothite [FeO(OH)]	21.3 (99.9%)				36.6 (36.8%) 33.3 (26.7%)	53.3 (18.0%) 34.6 (14.5%)
	hematite [Fe_2O_3]	33.1 (100%)		35.6 (70%)		54.0 (36%) 49.4 (31%) 24.1 (33%)	
NA	Al	38.4 (99.9%)			44.6 (45.6%)	65.0 (23.8%) 78.1 (23.5%)	
NA	Silica [SiO_2]	26.6 (99.9%)				20.8 (21%)	50.1 (10.7%)
Ti	Rutile [TiO_2]	27.4 (99.9%)			36.0 (44.3%) 54.2 (47.2%)	41.2 (17.1%) 56.5 (13.9%) 68.8 (14.7%)	
Ca	$CaCO_3$	29.3 (99.9%)				48.4 (20.5%)	35.9 (13.9%) 39.3 (19.5%) 43.1 (14.5%) 47.4 (18.8%)

NA: not applicable

Table E.2 Possible Minerals in Paint Samples Measured by XRD

XRF elements	Results from XRD	2-1b	2-2 e	3-2 e	5-1 b	5-1 c	5-2 a	5-2 d	5-4 c	5-5 c	5-5 d	10-7b	10-9b	11-2 a	11-2 e
Pb	lead tetroxide [Pb_3O_4]			√											
	$Pb_2(CrO_4)O$											√	√	√	√
Cr	Cr_2O_3													√	√
Zn	Zinc [Zn]	√	√					√	√	√	√	√			
	Zinc oxide [ZnO]	√													
Fe	Fe	√	√	√	√	√	√	√	√	√	√				√
	Magnetite [Fe_3O_4)			√		√	√	√	√	√	√				
	geothite [FeO(OH)]										√				
	hematite [Fe_2O_3]				√			√							
NA	Al	√	√	√	√	√	√	√	√	√	√	√	√		√
NA	Silica [SiO_2]	√	√	√	√	√	√	√	√	√	√	√	√	√	√
Ti	Rutile [TiO_2]	√	√					√			√	√	√	√	
Ca	$CaCO_3$	√	√	√	√	√	√		√	√			√		√

Table E.3 XRD Analysis of Iron and Iron Oxides in Paint Waste Samples

Paint sample ID	Results measured in XRD															
	Fe				Magnetite [Fe_3O_4]				Geothite [FeO(OH)]				Hematite [Fe_2O_3]			
	2θ (°)	Relative Intensity	hkl planes	FWHM °2θ	2θ (°)	RI	hkl planes	FWHM °2θ	2θ (°)	RI	hkl planes	FWHM °2θ	2θ (°)	RI	hkl planes	FWHM °2θ
5-1 b	44.5 64.9 82.3	100.00 11.20 1.61	110 200 211	0.1535 0.1023 0.4093									24.1 33.1 35.6 54.0	4.39 13.88 8.50 5.11	012 104 110 116	0.1535 0.1535 0.2047 0.0936
5-2 d	44.6 65.0 82.2 99.1	100.00 23.67 4.29 4.60	110 200 211 220	0.1535 0.1023 0.6140 0.5117	35.6 43.2	11.90 55.26	103 004	0.1535 0.0624					33.1 41.0 54.3	18.69 3.63 16.16	104 113 116	0.1023 0.6140 0.0768
5-4 c	44.5 64.9 82.2 99.1	82.14 26.10 5.36 3.09	110 200 211 220	0.2047 0.1279 0.4093 0.6140	30.1 35.5 43.2	6.55 19.95 81.71	220 311 400	0.2558 0.2558 0.0512								
5-5 d	44.6 64.9 82.2 98.9	100.00 31.47 7.73 4.54	110 200 211 220	0.2047 0.1023 0.5117 0.8187	35.3 43.2	12.11 77.22	103 004	0.4093 0.0768	21.2 26.6 36.3 39.0 54.3	10.06 46.07 35.39 18.22 14.69	101 201 111 002 402	0.6140 0.1023 0.1023 0.1279 0.0768				

RI: Relative Intensity

Table E.4 XRD Analysis of Pb and Cr in Paint Waste Samples

Paint sample ID	Results measured in XRD											
	lead tetroxide [Pb_3O_4]				$Pb_2(CrO_4)O$				Cr_2O_3			
	2θ (°)	Relative Intensity	hkl planes	FWHM °2θ	2θ (°)	Relative Intensity	hkl planes	FWHM °2 θ	2θ (°)	Relative Intensity	hkl planes	FWHM °2θ
3-2 e	26.3480 30.8516 33.1330 47.4525	11.47 2.67 1.88 2.53	211 112 310 213	0.1279 0.3070 0.3070 0.4093								
10-7b					26.2 29.8 31.4	29.23 23.16 8.71	310 -112 020	0.1279 0.1535 0.1791				
10-9b					26.2 29.9 31.4	11.41 7.59 3.50	310 -112 020	0.1279 0.1535 0.1535				
11-2 a					26.3 29.9 31.5	36.01 23.21 9.91	310 -112 020	0.1279 0.1535 0.1791	33.7 36.3 50.2 54.9	4.42 10.99 11.18 7.50	104 110 024 116	0.1023 0.2047 0.0768 0.1023
11-2 e					26.2 27.4 29.9 31.4	26.67 20.05 18.18 6.21	310 002 -112 020	0.1279 0.1279 0.1791 0.1535	33.6 36.3 50.1 54.8 64.9	3.27 10.69 9.91 4.79 17.61	104 110 024 116 300	0.1535 0.1535 0.0768 0.1023 0.1279

APPENDIX F

MODELING RESULTS FOR METAL LEACHING

Fe=17% LogFe=5.23

Source	DF	Sum of Squares	Mean Square	F Value	Approx Pr > F
Model	15	25.6441	1.7096	4.04	0.0004
Error	32	13.5294	0.4228		
Corrected Total	47	39.1735			

Fe=19% LogFe=5.28

Source	DF	Sum of Squares	Mean Square	F Value	Approx Pr > F
Model	15	25.6441	1.7096	4.04	0.0004
Error	32	13.5294	0.4228		
Corrected Total	47	39.1735			

Same MSE are obtained for Fe = 20%, 21%, 22%, and 23%

Source	DF	Sum of Squares	Mean Square	F Value	Approx Pr > F
Model	15	25.8883	1.7259	4.16	0.0003
Error	32	13.2852	0.4152		
Corrected Total	47	39.1735			

Fe=24% LogFe=5.38

Source	DF	Sum of Squares	Mean Square	F Value	Approx Pr > F
Model	15	22.3640	1.4909	2.84	0.0065
Error	32	16.8095	0.5253		
Corrected Total	47	39.1735			

SSPC 6

Fe<=20% LogFe=5.30

Number of Observations Read	23
Number of Observations Used	20
Number of Observations with Missing Values	3

Analysis of Variance

Source	DF	Sum of Squares	Mean Square	F Value	Pr > F
Model	7	9.26512	1.32359	3.26	0.0351
Error	12	4.87631	0.40636		
Corrected Total	19	14.14142			

Root MSE	0.63746	**R-Square**	0.6552
Dependent Mean	-0.07695	**Adj R-Sq**	0.4540
Coeff Var	-828.39228		

Parameter Estimates

Variable	Label	DF	Parameter Estimate	Standard Error	t Value	Pr > |t|
Intercept	Intercept	**1**	-69.15753	29.21301	-2.37	0.0356
log_Fe_mg_Kg	log Fe mg/Kg	**1**	-5.93902	2.13020	-2.79	0.0164
log_Cr_XRF_mean	log Cr XRF mean	**1**	-5.17710	1.55181	-3.34	0.0059
log_mining_and_Soil_mode_Pb_mea	log mining and Soil mode Pb mea	**1**	15.38537	6.48355	2.37	0.0352
log_Ca_meban	log Ca mean	**1**	4.87680	2.56465	1.90	0.0815
log_Ti	log Ti	**1**	4.88315	1.57765	3.10	0.0093
log_Ag	log Ag	**1**	-20.11114	6.44002	-3.12	0.0088
log_Cd	log Cd	**1**	16.41169	5.87066	2.80	0.0162

The REG Procedure
Model: MODEL1
Dependent Variable: log_Pb_TCLP_mean log Pb TCLP mean

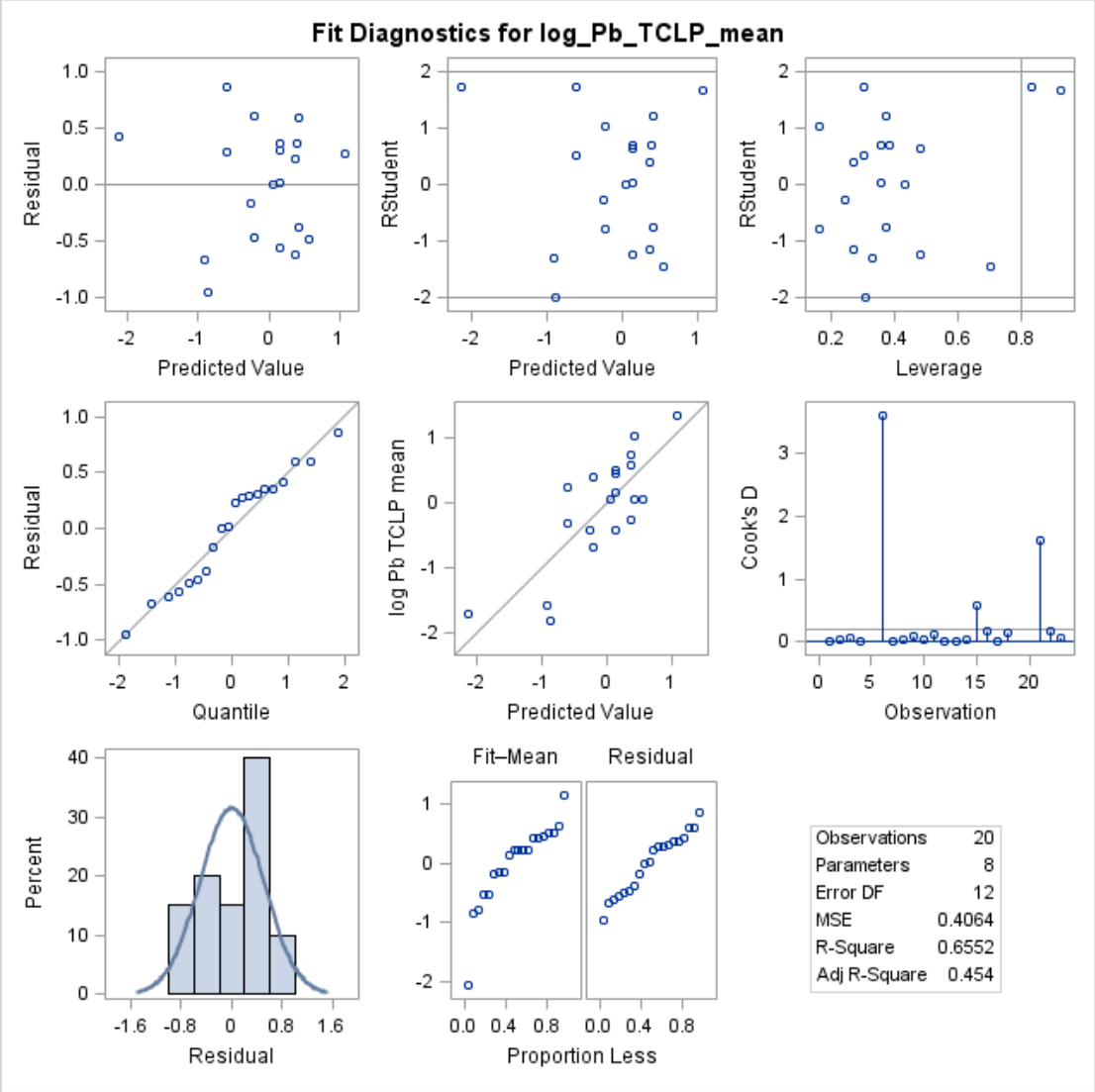

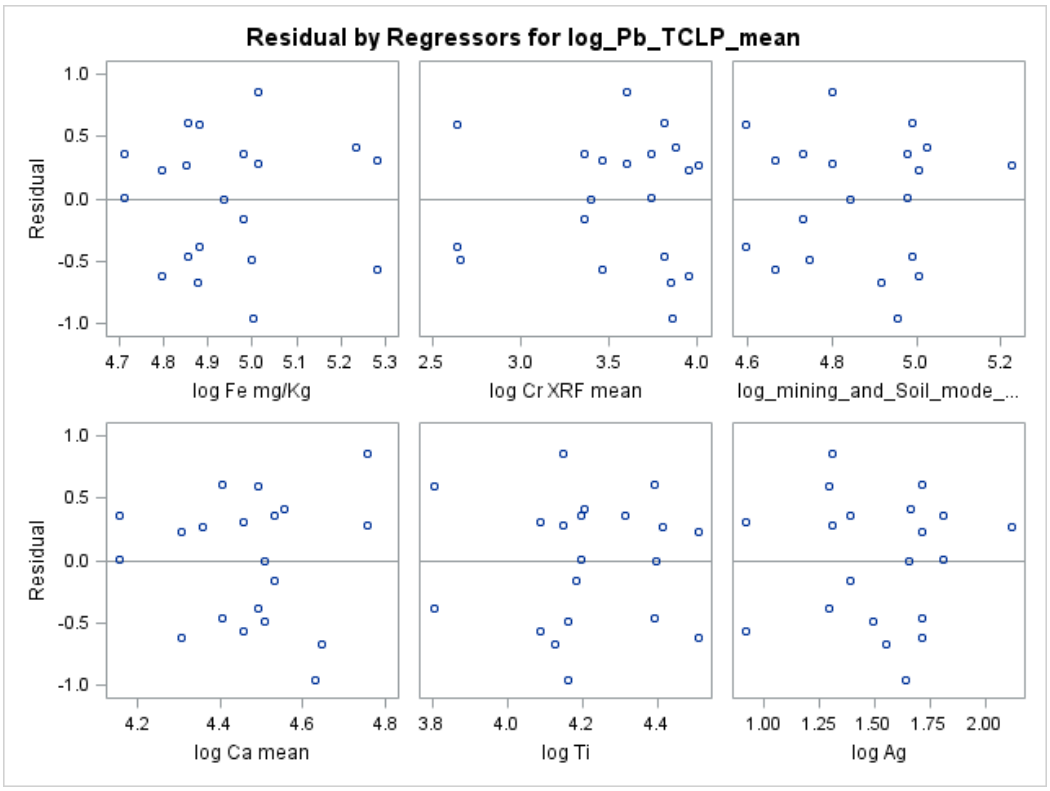
Residual by Regressors for log_Pb_TCLP_mean
Residual
1.0
0.5
0.0
-0.5
-1.0
4.7 4.8 4.9 5.0 5.1 5.2 5.3
log Fe mg/Kg
2.5 3.0 3.5 4.0
log Cr XRF mean
4.6 4.8 5.0 5.2
log_mining_and_Soil_mode_...
4.2 4.4 4.6 4.8
log Ca mean
3.8 4.0 4.2 4.4
log Ti
1.00 1.25 1.50 1.75 2.00
log Ag

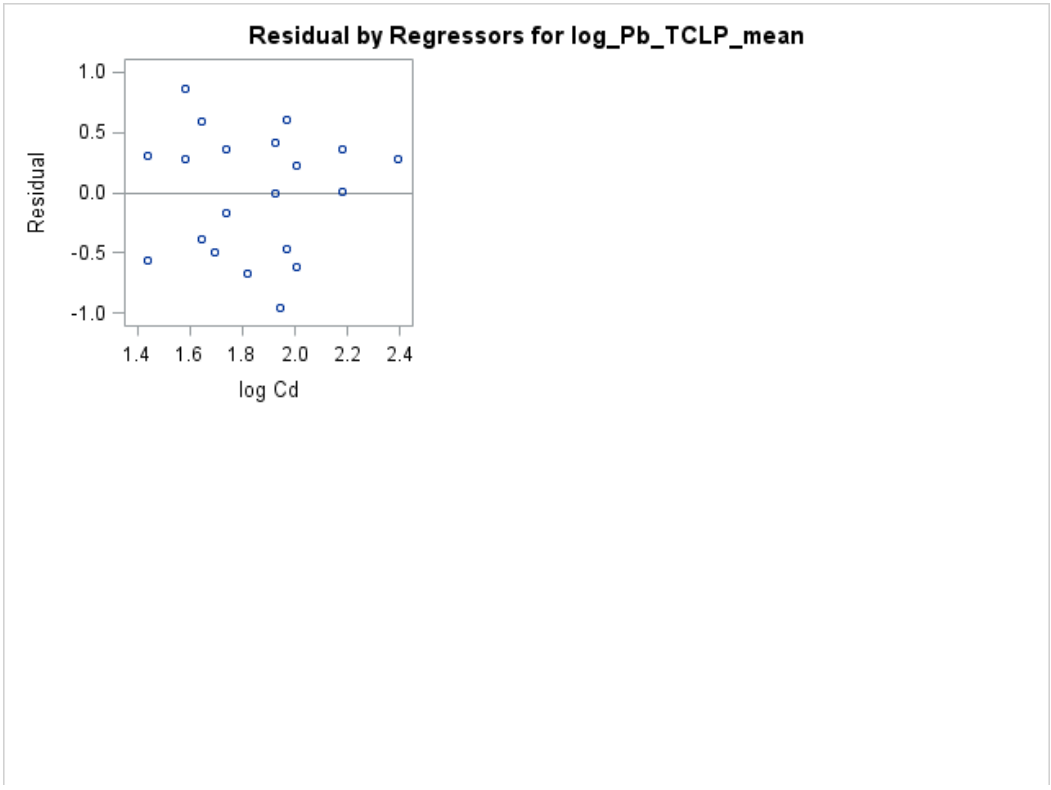
Residual by Regressors for log_Pb_TCLP_mean
Residual
1.0
0.5
0.0
-0.5
-1.0
1.4 1.6 1.8 2.0 2.2 2.4
log Cd

Fe>20% LogFe=5.30

Number of Observations Read	32
Number of Observations Used	28
Number of Observations with Missing Values	4

Analysis of Variance

Source	DF	Sum of Squares	Mean Square	F Value	Pr > F
Model	7	13.75489	1.96498	4.67	0.0031
Error	20	8.40891	0.42045		
Corrected Total	27	22.16381			

Root MSE	0.64842	**R-Square**	0.6206
Dependent Mean	-0.57279	**Adj R-Sq**	0.4878
Coeff Var	-113.20419		

Parameter Estimates

Variable	Label	DF	Parameter Estimate	Standard Error	t Value	Pr > |t|
Intercept	Intercept	**1**	-20.79269	11.49152	-1.81	0.0854
log_Fe_mg_Kg	log Fe mg/Kg	**1**	0.51414	1.36480	0.38	0.7104
log_Cr_XRF_mean	log Cr XRF mean	**1**	-0.90087	0.49284	-1.83	0.0825
log_mining_and_Soil_mode_Pb_mea	log mining and Soil mode Pb mea	**1**	4.14940	1.37129	3.03	0.0067
log_Ca_mean	log Ca mean	**1**	0.29854	0.71621	0.42	0.6812
log_Ti	log Ti	**1**	0.67605	0.55979	1.21	0.2413
log_Ag	log Ag	**1**	2.97630	1.56079	1.91	0.0710
log_Cd	log Cd	**1**	-4.28602	1.91712	-2.24	0.0369

The REG Procedure
Model: MODEL1
Dependent Variable: log_Pb_TCLP_mean log Pb TCLP mean

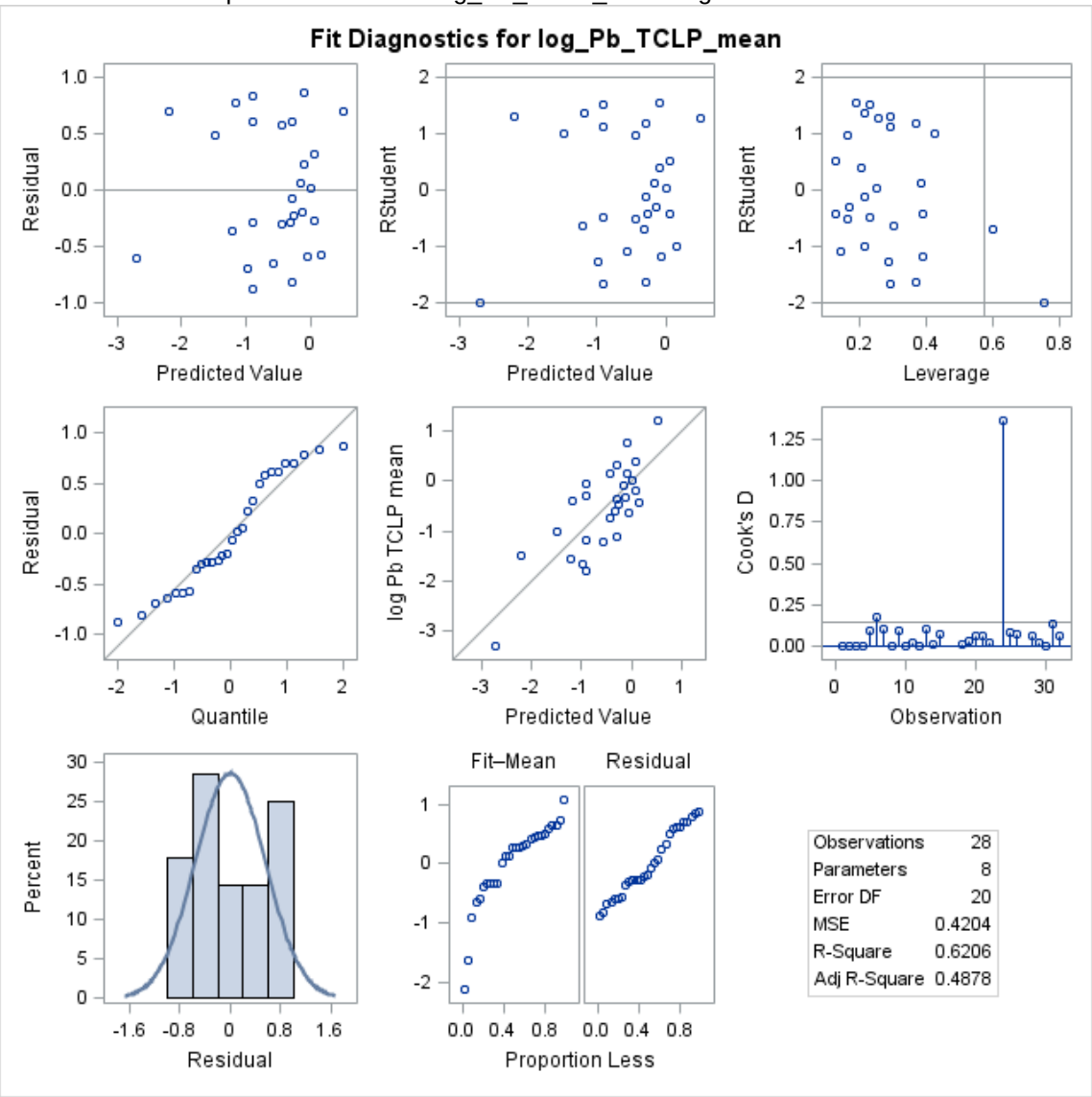

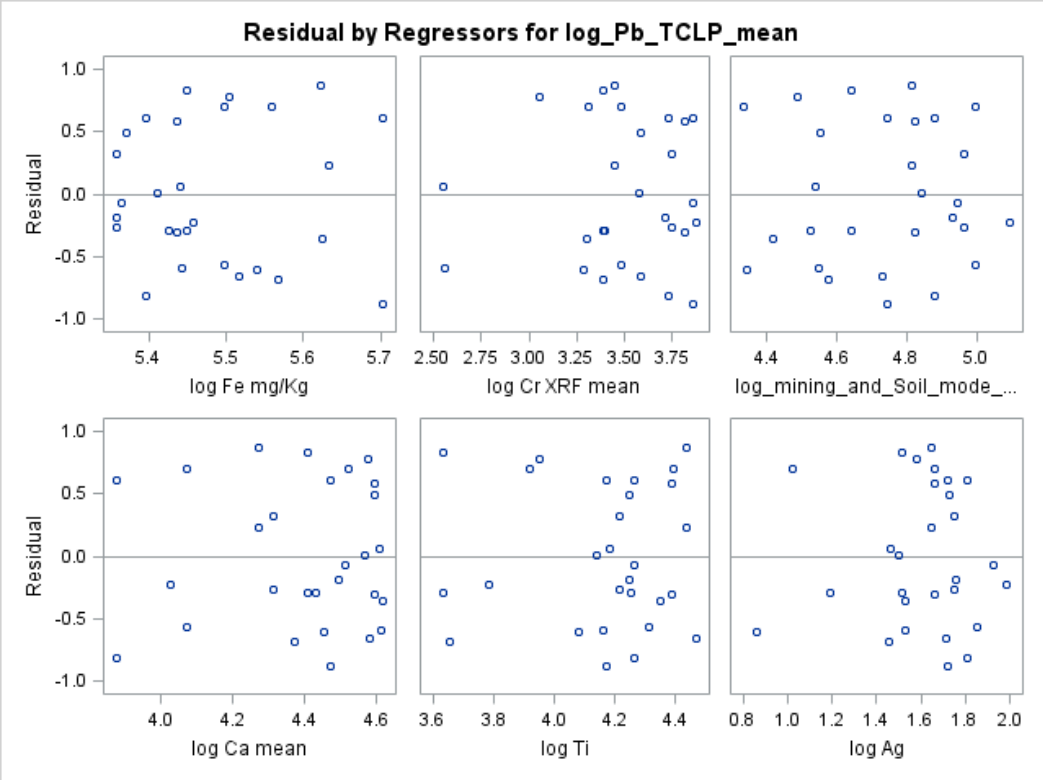
Residual by Regressors for log_Pb_TCLP_mean
Residual
1.0
0.5
0.0
-0.5
-1.0
5.4
5.5
5.6
5.7
log Fe mg/Kg
2.50
2.75
3.00
3.25
3.50
3.75
log Cr XRF mean
4.4
4.6
4.8
5.0
log_mining_and_Soil_mode_...
4.0
4.2
4.4
4.6
log Ca mean
3.6
3.8
4.0
4.2
4.4
log Ti
0.8
1.0
1.2
1.4
1.6
1.8
2.0
log Ag

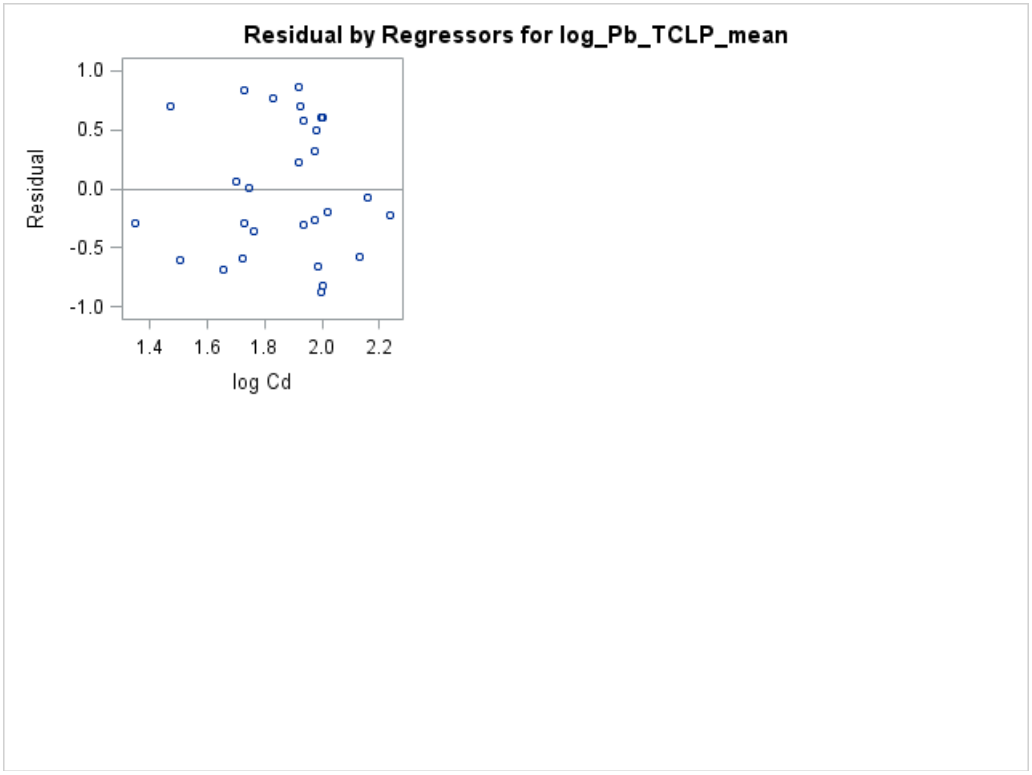
Residual by Regressors for log_Pb_TCLP_mean
Residual
1.0
0.5
0.0
-0.5
-1.0
1.4
1.6
1.8
2.0
2.2
log Cd

The SAS System

The NLIN Procedure
Dependent Variable log_Pb_TCLP_mean
Method: Marquardt

Source	DF	Sum of Squares	Mean Square	F Value	Approx Pr > F
Model	15	25.8883	1.7259	4.16	0.0003
Error	32	13.2852	0.4152		
Corrected Total	47	39.1735			

Parameter	Estimate	Approx Std Error	Approximate 95% Confidence Limits	
a1	-69.1575	29.5278	-129.3	-9.0114
a2	-18.0677	6.9834	-32.2924	-3.8430
b1	-5.9390	2.1532	-10.3249	-1.5532
b2	0.5141	1.3562	-2.2483	3.2766
c	5.3000	.	.	.
c1	-5.1771	1.5685	-8.3721	-1.9821
c2	-0.9009	0.4897	-1.8984	0.0967
d1	15.3854	6.5534	2.0365	28.7342
d2	4.1494	1.3626	1.3738	6.9250
e1	4.8768	2.5923	-0.4035	10.1571
e2	0.2985	0.7117	-1.1511	1.7482
f1	4.8831	1.5946	1.6350	8.1313
f2	0.6761	0.5563	-0.4570	1.8091
g1	-20.1111	6.5094	-33.3704	-6.8519
g2	2.9763	1.5510	-0.1829	6.1355
h1	16.4117	5.9339	4.3247	28.4987
h2	-4.2860	1.9050	-8.1665	-0.4056

Ba_TCLP Ba TCLP Fe<=20%

Number of Observations Read	23
Number of Observations Used	22
Number of Observations with Missing Values	1

Analysis of Variance

Source	DF	Sum of Squares	Mean Square	F Value	Pr > F
Model	7	50.54675	7.22096	2.01	0.1265
Error	14	50.34707	3.59622		
Corrected Total	21	100.89382			

Root MSE	1.89637	**R-Square**	0.5010
Dependent Mean	1.86727	**Adj R-Sq**	0.2515
Coeff Var	101.55857		

Parameter Estimates

Variable	Label	DF	Parameter Estimate	Standard Error	t Value	Pr > |t|
Intercept	Intercept	**1**	11.91855	6.34880	1.88	0.0815
Ba_XRF	Ba XRF	**1**	-0.00046243	0.00031811	-1.45	0.1681
Fe_mg_kg	Fe mg/kg	**1**	-0.00000912	0.00001297	-0.70	0.4933
Cr_XRF_mean	Cr XRF mean	**1**	0.00046681	0.00047298	0.99	0.3404
mining_and_Soil_mode_Pb_mean_pp	mining and Soil mode Pb mean pp	**1**	-0.00003793	0.00006857	-0.55	0.5889
Ca_mean	Ca mean	**1**	-0.00018381	0.00008683	-2.12	0.0527
Ti_mean	Ti mean	**1**	0.00012499	0.00008882	1.41	0.1812
Cd	Cd	**1**	-0.02083	0.02627	-0.79	0.4412

The REG Procedure
Model: MODEL1
Dependent Variable: Ba_TCLP Ba TCLP

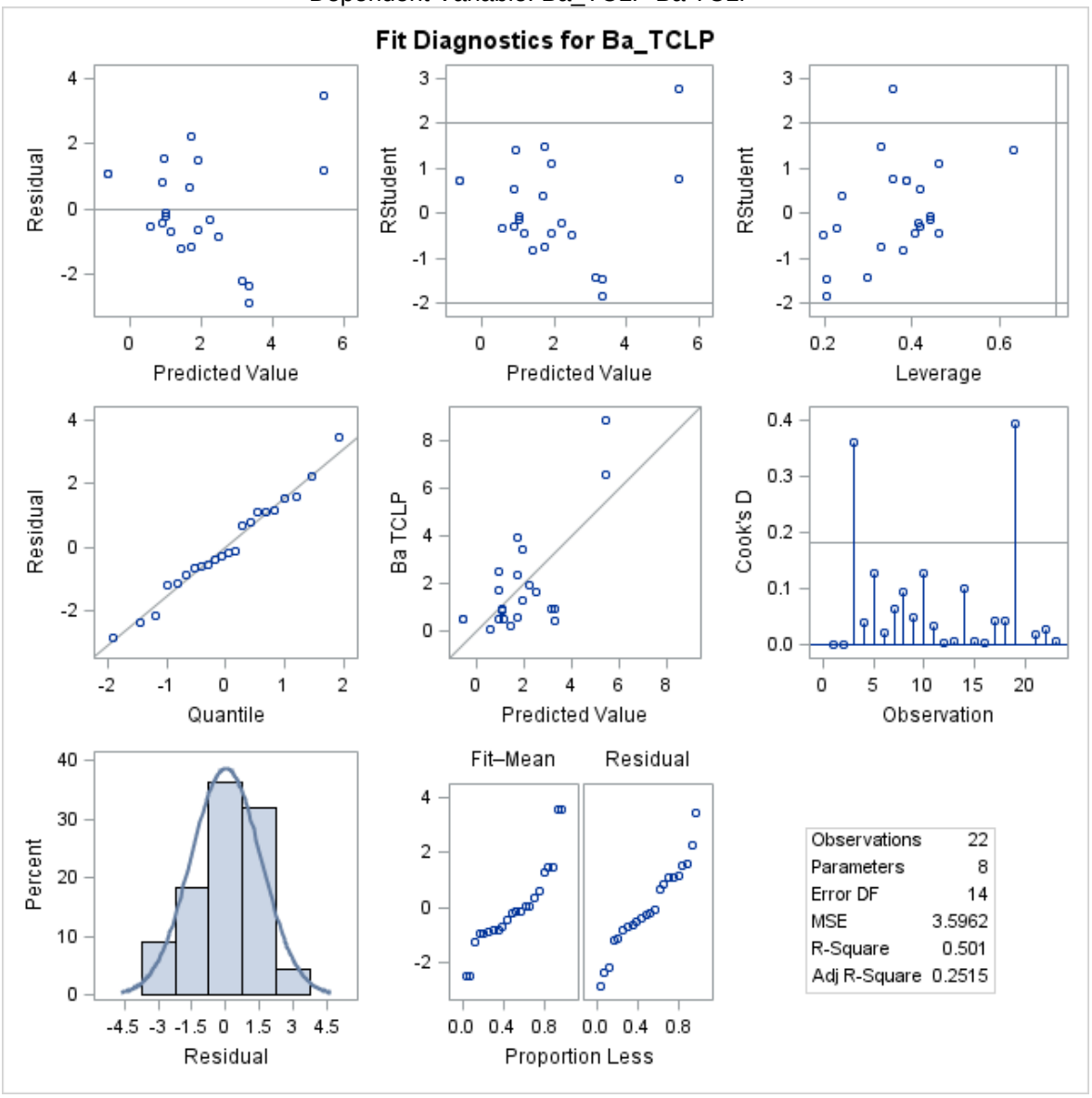

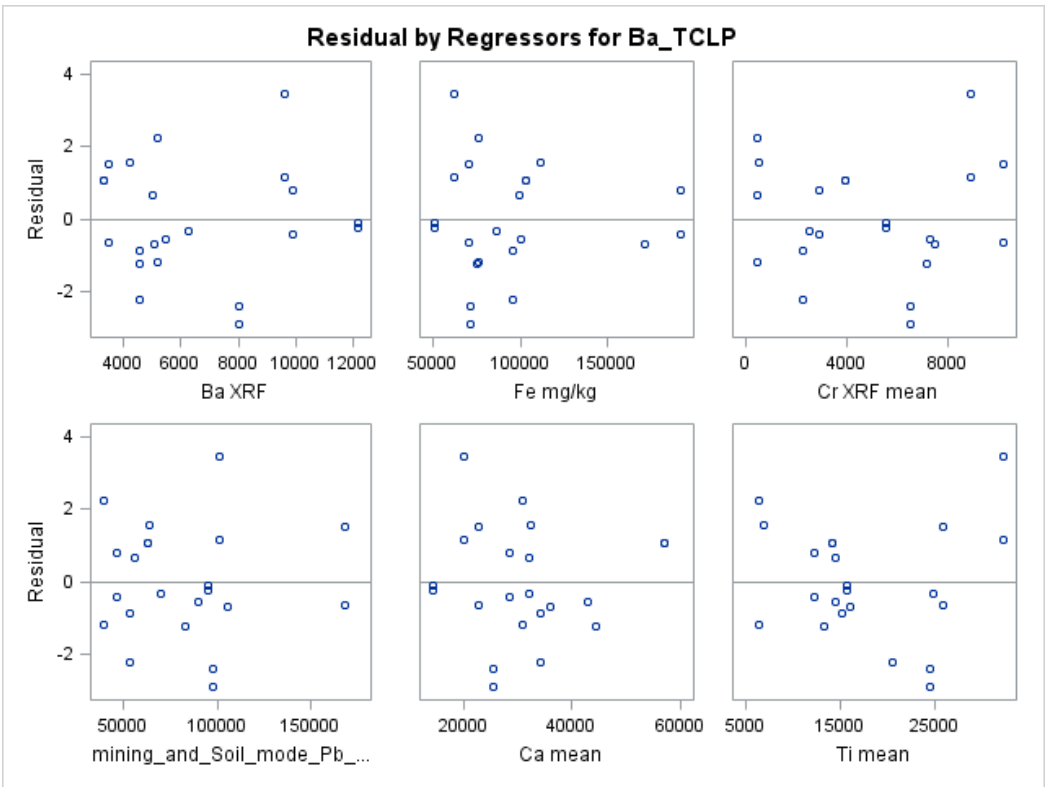
Residual by Regressors for Ba_TCLP
Residual
4
2
0
-2
4000 6000 8000 10000 12000
Ba XRF
50000 100000 150000
Fe mg/kg
0 4000 8000
Cr XRF mean
50000 100000 150000
mining_and_Soil_mode_Pb_...
20000 40000 60000
Ca mean
5000 15000 25000
Ti mean

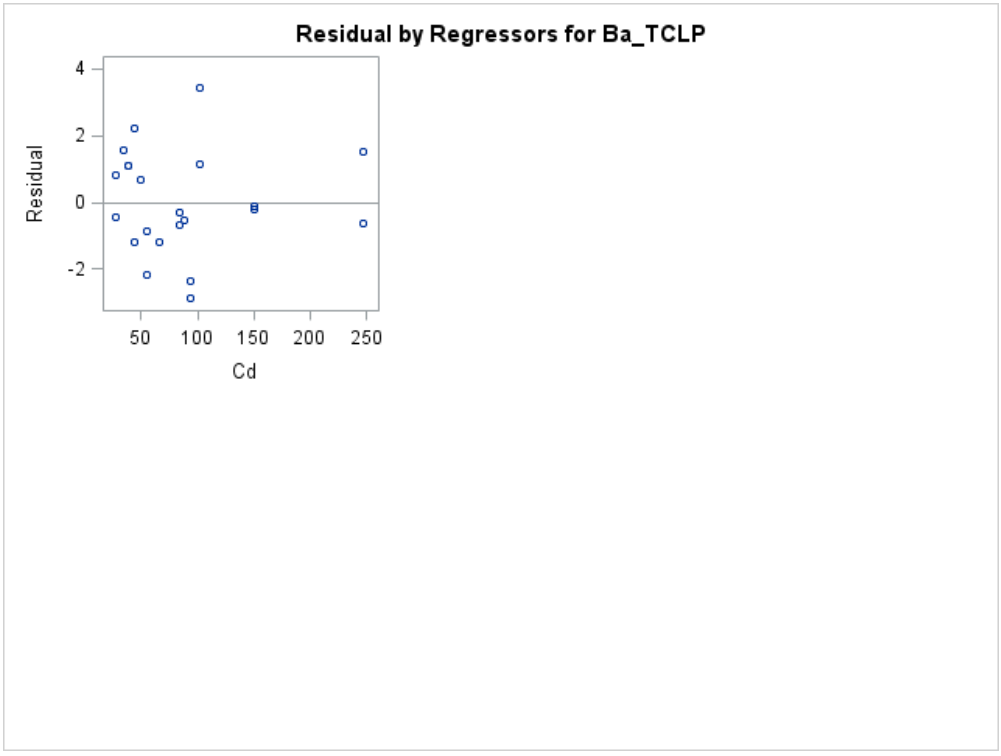
Residual by Regressors for Ba_TCLP
Residual
4
2
0
-2
50 100 150 200 250
Cd

Ba TCLP Fe>20%
The REG Procedure
Model: MODEL1
Dependent Variable: Ba_TCLP Ba TCLP

Number of Observations Read	32
Number of Observations Used	27
Number of Observations with Missing Values	5

Analysis of Variance

Source	DF	Sum of Squares	Mean Square	F Value	Pr > F
Model	6	5.79397	0.96566	3.10	0.0258
Error	20	6.22097	0.31105		
Corrected Total	26	12.01495			

Root MSE	0.55772	**R-Square**	0.4822
Dependent Mean	1.07568	**Adj R-Sq**	0.3269
Coeff Var	51.84768		

Parameter Estimates

Variable	Label	DF	Parameter Estimate	Standard Error	t Value	Pr > |t|
Intercept	Intercept	**1**	1.65037	0.77147	2.14	0.0449
Fe_mg_kg	Fe mg/kg	**1**	0.00000129	0.00000153	0.84	0.4093
Cr_XRF_mean	Cr XRF mean	**1**	-0.00012012	0.00007226	-1.66	0.1120
Ca_mean	Ca mean	**1**	-0.00002905	0.00001028	-2.83	0.0104
Ti_mean	Ti mean	**1**	-0.00002056	0.00001616	-1.27	0.2178
Cd	Cd	**1**	0.01854	0.01990	0.93	0.3626
Ag	Ag	**1**	-0.01817	0.03504	-0.52	0.6099

The REG Procedure
Model: MODEL1
Dependent Variable: Ba_TCLP Ba TCLP

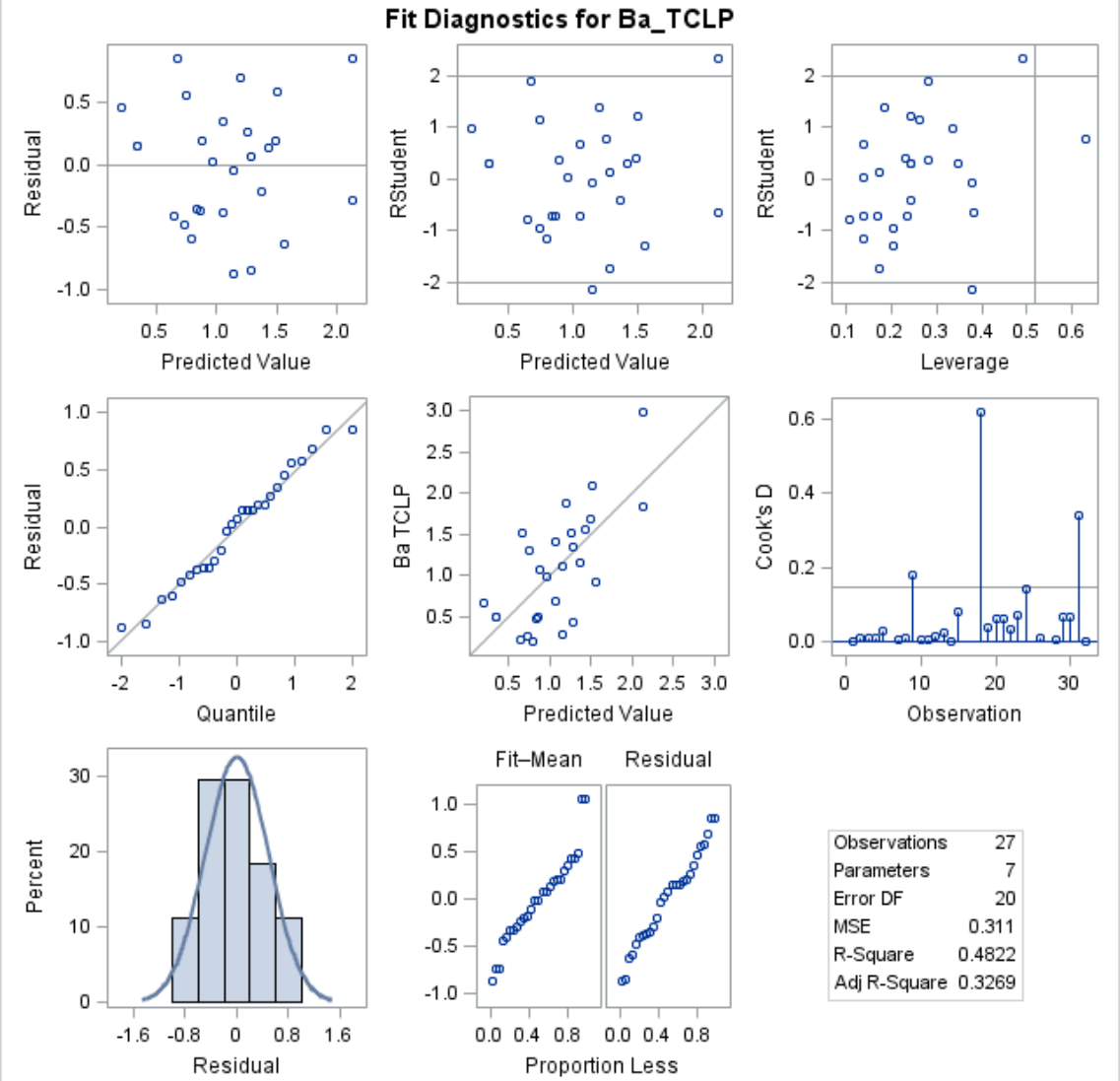

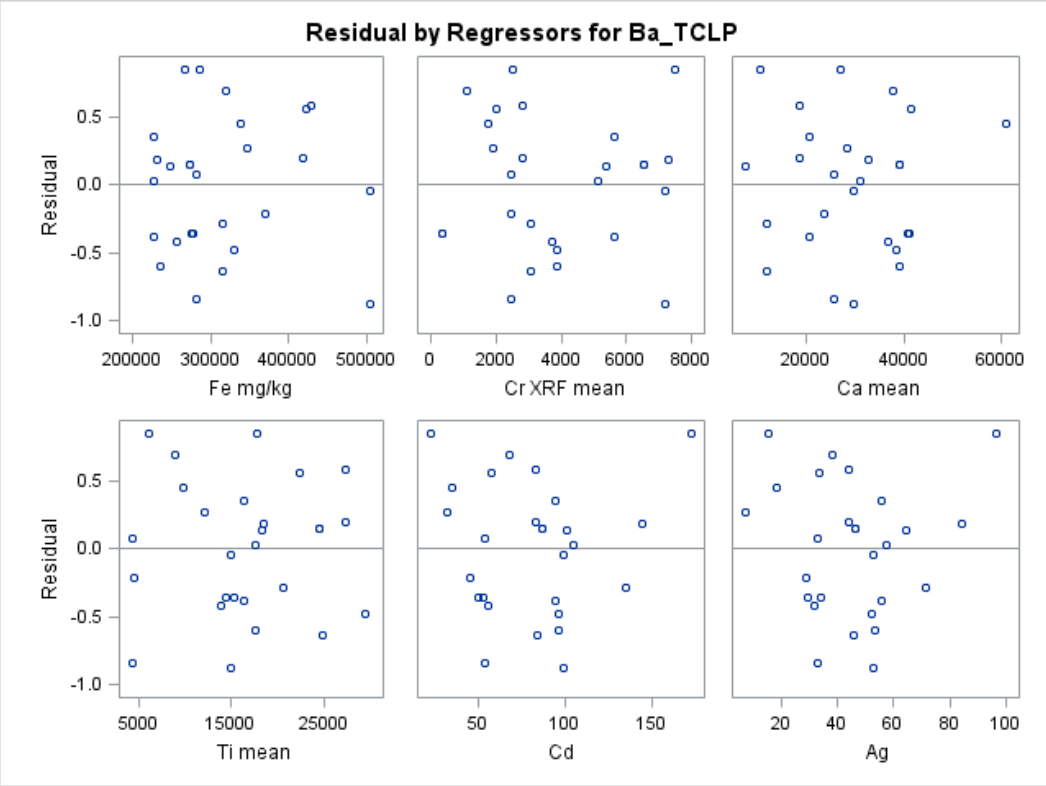
Residual by Regressors for Ba_TCLP
Residual
0.5
0.0
-0.5
-1.0
200000
300000
400000
500000
Fe mg/kg
0
2000
4000
6000
8000
Cr XRF mean
20000
40000
60000
Ca mean
5000
15000
25000
Ti mean
50
100
150
Cd
20
40
60
80
100
Ag

Zn SSPC 6<20%

Number of Observations Read	23
Number of Observations Used	22
Number of Observations with Missing Values	1

Analysis of Variance

Source	DF	Sum of Squares	Mean Square	F Value	Pr > F
Model	7	1450931	207276	5.55	0.0032
Error	14	522681	37334		
Corrected Total	21	1973612			

Root MSE	193.22100	**R-Square**	0.7352
Dependent Mean	341.17938	**Adj R-Sq**	0.6027
Coeff Var	56.63326		

Parameter Estimates

Variable	Label	DF	Parameter Estimate	Standard Error	t Value	Pr > |t|
Intercept	Intercept	**1**	415.90648	286.32989	1.45	0.1684
Soil___mining_Zn__ppm	Soil & mining Zn ppm	**1**	0.00195	0.00201	0.97	0.3494
mining_and_Soil_mode_Pb_mean_pp	mining and Soil mode Pb mean pp	**1**	-0.01676	0.00570	-2.94	0.0107
Cr_XRF_mean	Cr XRF mean	**1**	-0.06104	0.04923	-1.24	0.2354
Ca_mean	Ca mean	**1**	0.00676	0.00593	1.14	0.2735
Ti_mean	Ti mean	**1**	0.02477	0.01218	2.03	0.0614
Cd	Cd	**1**	4.98343	3.47707	1.43	0.1737
As	As	**1**	0.09522	0.09840	0.97	0.3496

The REG Procedure
Model: MODEL1
Dependent Variable: Zn_TCLP Zn TCLP

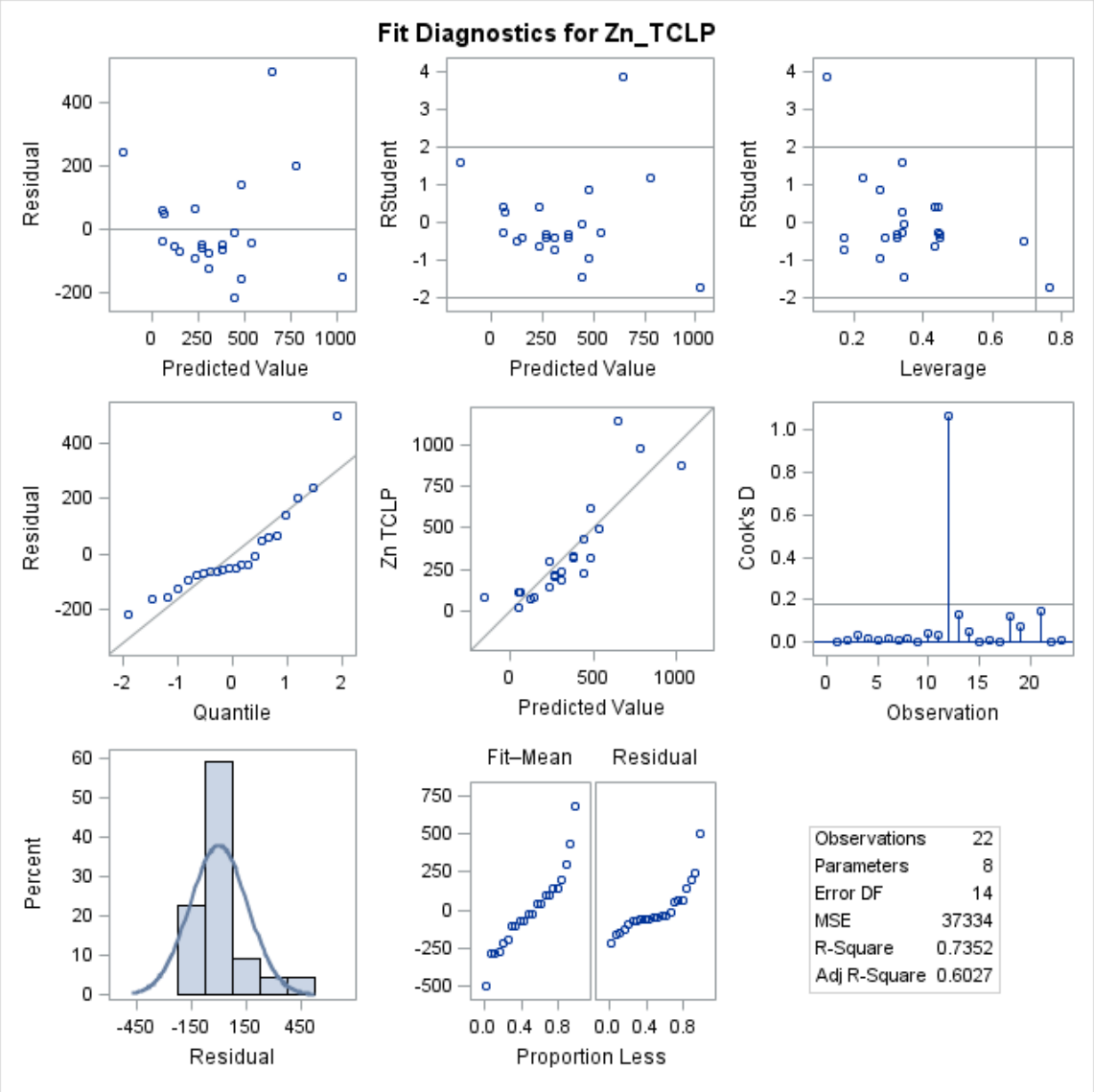

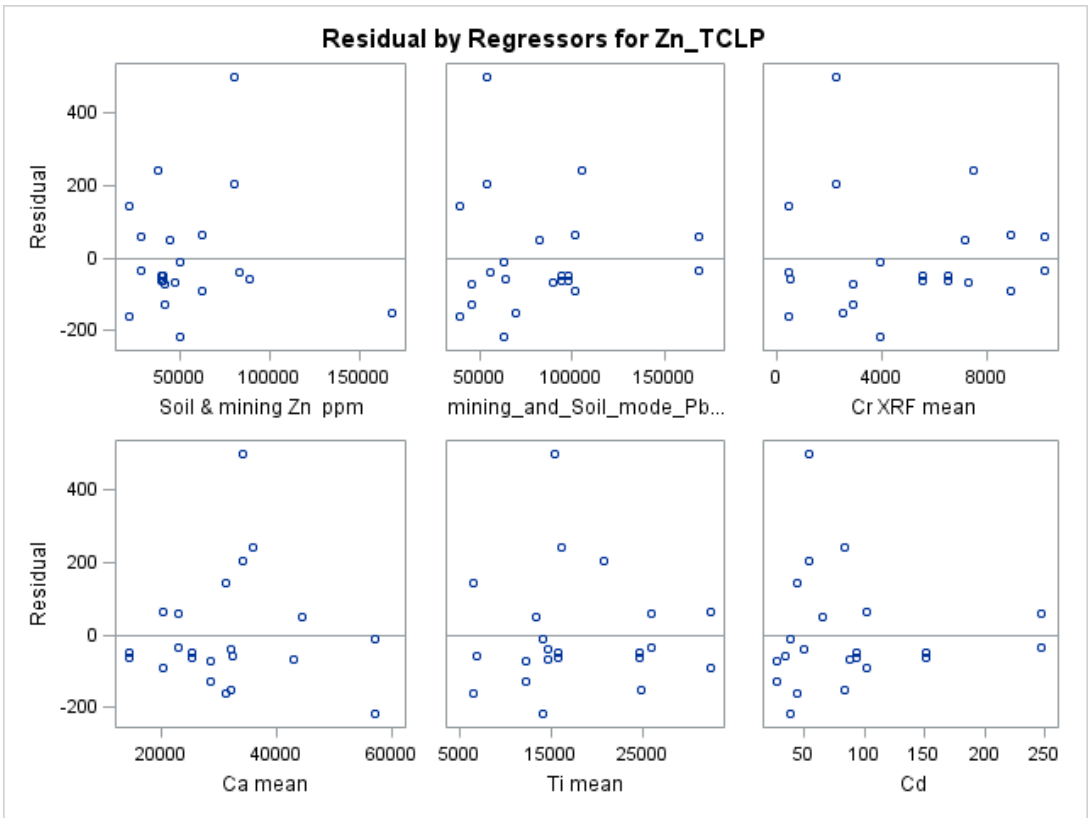
Residual by Regressors for Zn_TCLP
Residual
400
200
0
-200
50000
100000
150000
Soil & mining Zn ppm
mining_and_Soil_mode_Pb...
0
4000
8000
Cr XRF mean
20000
40000
60000
Ca mean
5000
15000
25000
Ti mean
50
100
150
200
250
Cd

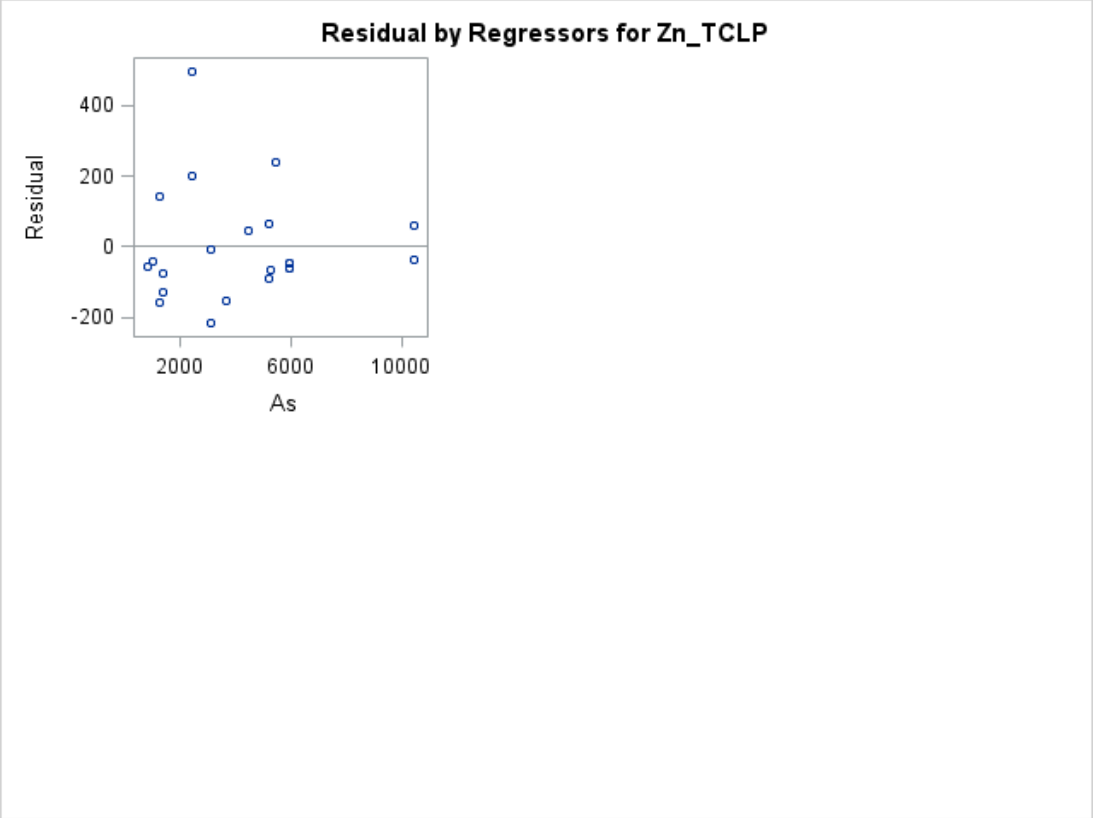
Residual by Regressors for Zn_TCLP
Residual
400
200
0
-200
2000
6000
10000
As

Zn SSPC 6 Fe>20%
The SAS System

Number of Observations Read	32
Number of Observations Used	29
Number of Observations with Missing Values	3

Analysis of Variance

Source	DF	Sum of Squares	Mean Square	F Value	Pr > F
Model	7	968313	138330	3.80	0.0081
Error	21	764268	36394		
Corrected Total	28	1732582			

Root MSE	190.77140	**R-Square**	0.5589
Dependent Mean	385.12725	**Adj R-Sq**	0.4118
Coeff Var	49.53464		

Parameter Estimates

Variable	Label	DF	Parameter Estimate	Standard Error	t Value	Pr > |t|
Intercept	Intercept	**1**	115.34611	252.96410	0.46	0.6531
Soil___mining_Zn__ppm	Soil & mining Zn ppm	**1**	0.00406	0.00132	3.07	0.0057
mining_and_Soil_mode_Pb_mean_pp	mining and Soil mode Pb mean pp	**1**	-0.00313	0.00291	-1.07	0.2950
Cr_XRF_mean	Cr XRF mean	**1**	-0.05728	0.02550	-2.25	0.0355
Ca_mean	Ca mean	**1**	-0.00418	0.00430	-0.97	0.3430
Ti_mean	Ti mean	**1**	0.00904	0.00545	1.66	0.1122
Cd	Cd	**1**	-5.55271	5.69407	-0.98	0.3406
Ag	Ag	**1**	19.68523	9.59007	2.05	0.0528

The REG Procedure
Model: MODEL1
Dependent Variable: Zn_TCLP Zn TCLP

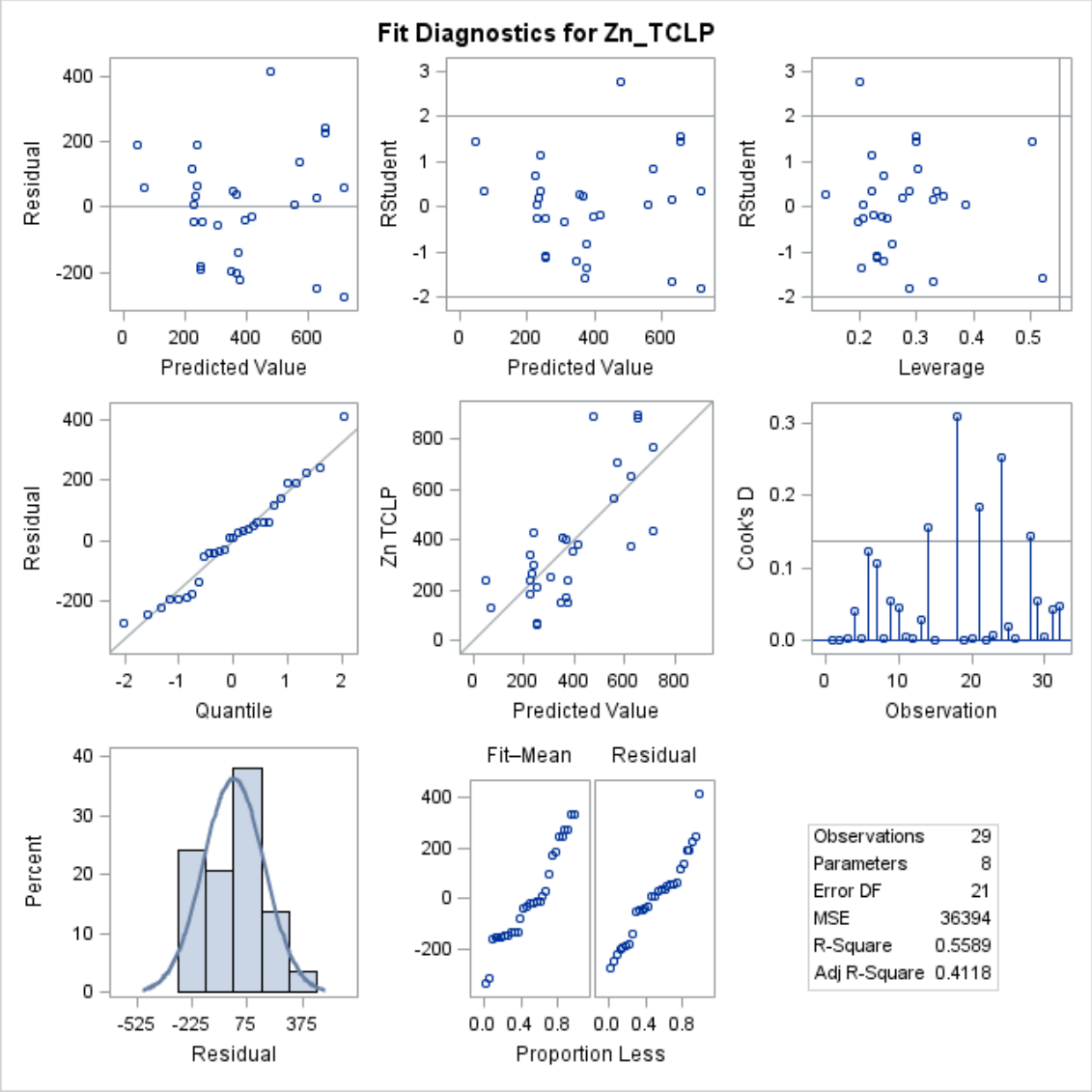

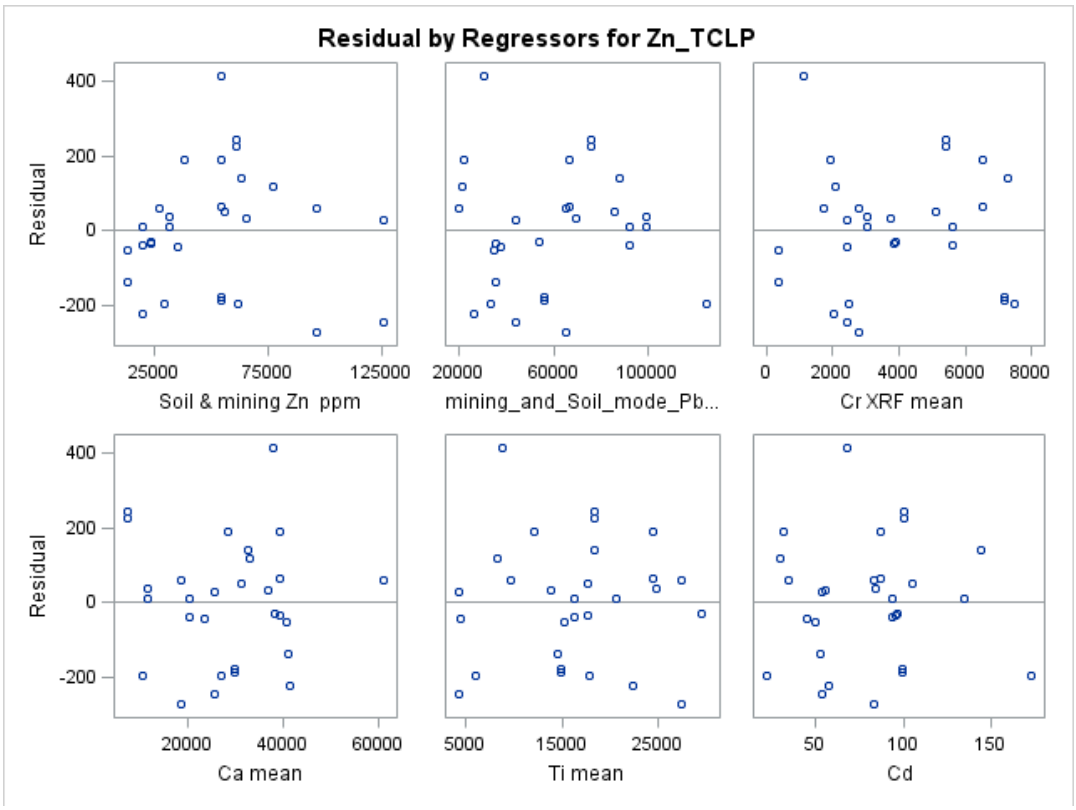
Residual by Regressors for Zn_TCLP
Residual
400
200
0
-200
25000
75000
125000
Soil & mining Zn ppm
20000
60000
100000
mining_and_Soil_mode_Pb...
0
2000
4000
6000
8000
Cr XRF mean
20000
40000
60000
Ca mean
5000
15000
25000
Ti mean
50
100
150
Cd

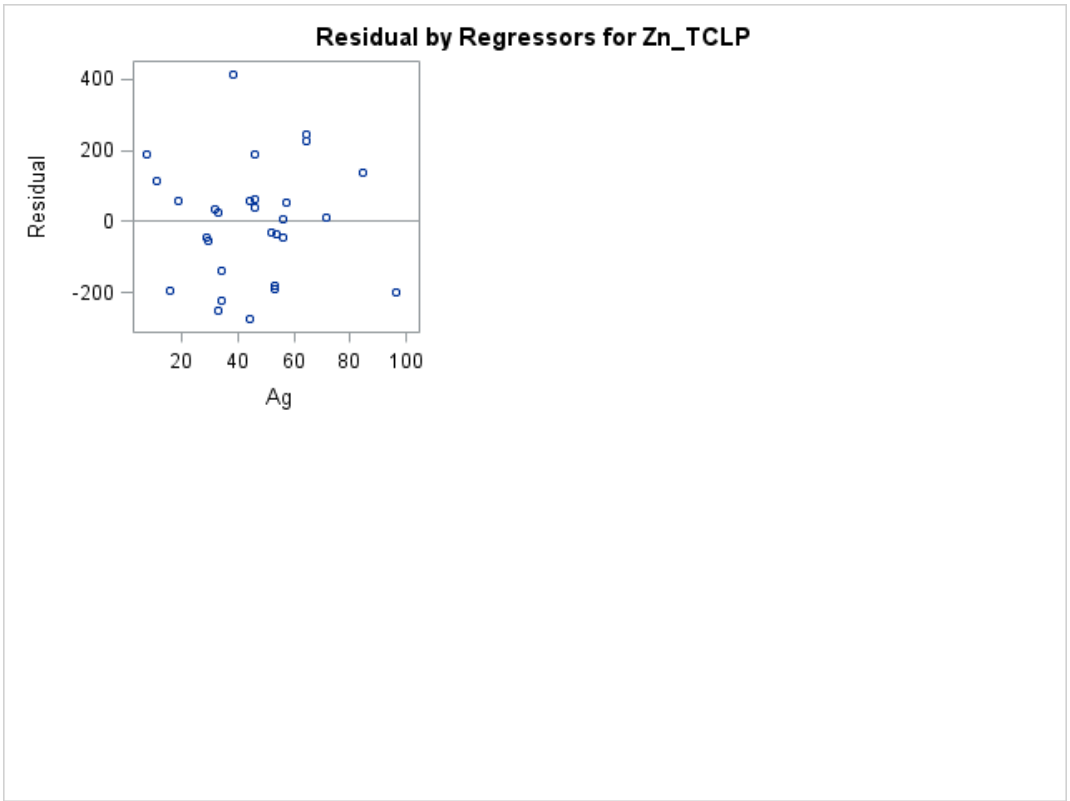
Residual by Regressors for Zn_TCLP
Residual
400
200
0
-200
20
40
60
80
100
Ag

log Cr TCLP Fe<=20%

Number of Observations Read	23
Number of Observations Used	21
Number of Observations with Missing Values	2

Analysis of Variance

Source	DF	Sum of Squares	Mean Square	F Value	Pr > F
Model	8	13.25249	1.65656	1.38	0.2960
Error	12	14.38824	1.19902		
Corrected Total	20	27.64073			

Root MSE	1.09500	**R-Square**	0.4795
Dependent Mean	-1.17620	**Adj R-Sq**	0.1324
Coeff Var	-93.09620		

Parameter Estimates

Variable	Label	DF	Parameter Estimate	Standard Error	t Value	Pr > |t|
Intercept	Intercept	**1**	-7.70322	22.34821	-0.34	0.7363
log_Fe_mg_Kg	log Fe mg/Kg	**1**	0.81362	2.76136	0.29	0.7733
log_Cr_XRF_mean	log Cr XRF mean	**1**	-3.92307	2.91001	-1.35	0.2025
log_mining_and_Soil_mode_Pb_mea	log mining and Soil mode Pb mea	**1**	1.05774	8.45756	0.13	0.9025
log_Soil___mining_Zn__ppm	log Soil & mining Zn ppm	**1**	1.68966	2.29364	0.74	0.4755
log_Ca_mean	log Ca mean	**1**	-4.14279	3.67663	-1.13	0.2819
log_Ti	log Ti	**1**	2.07326	3.78394	0.55	0.5938
log_Cd	log Cd	**1**	-8.83677	6.41314	-1.38	0.1934
log_As	log As	**1**	8.36765	6.21948	1.35	0.2034

Number of Observations Read	23
Number of Observations Used	21
Number of Observations with Missing Values	2

Analysis of Variance

Source	DF	Sum of Squares	Mean Square	F Value	Pr > F
Model	7	13.23374	1.89053	1.71	0.1925
Error	13	14.40699	1.10823		
Corrected Total	20	27.64073			

Root MSE	1.05273	**R-Square**	0.4788
Dependent Mean	-1.17620	**Adj R-Sq**	0.1981
Coeff Var	-89.50221		

Parameter Estimates

Variable	Label	DF	Parameter Estimate	Standard Error	t Value	Pr > |t|
Intercept	Intercept	**1**	-5.84227	16.03047	-0.36	0.7214
log_Fe_mg_Kg	log Fe mg/Kg	**1**	0.91473	2.53842	0.36	0.7244
log_Cr_XRF_mean	log Cr XRF mean	**1**	-3.76782	2.53035	-1.49	0.1603
log_Soil___mining_Zn__ppm	log Soil & mining Zn ppm	**1**	1.51911	1.77300	0.86	0.4071
log_Ca_mean	log Ca mean	**1**	-3.89170	2.96114	-1.31	0.2115
log_Ti	log Ti	**1**	2.37127	2.82590	0.84	0.4166
log_Cd	log Cd	**1**	-8.23881	4.10921	-2.00	0.0662
log_As	log As	**1**	8.24011	5.89845	1.40	0.1858

The REG Procedure
Model: MODEL1
Dependent Variable: log_Cr_TCLP log Cr TCLP

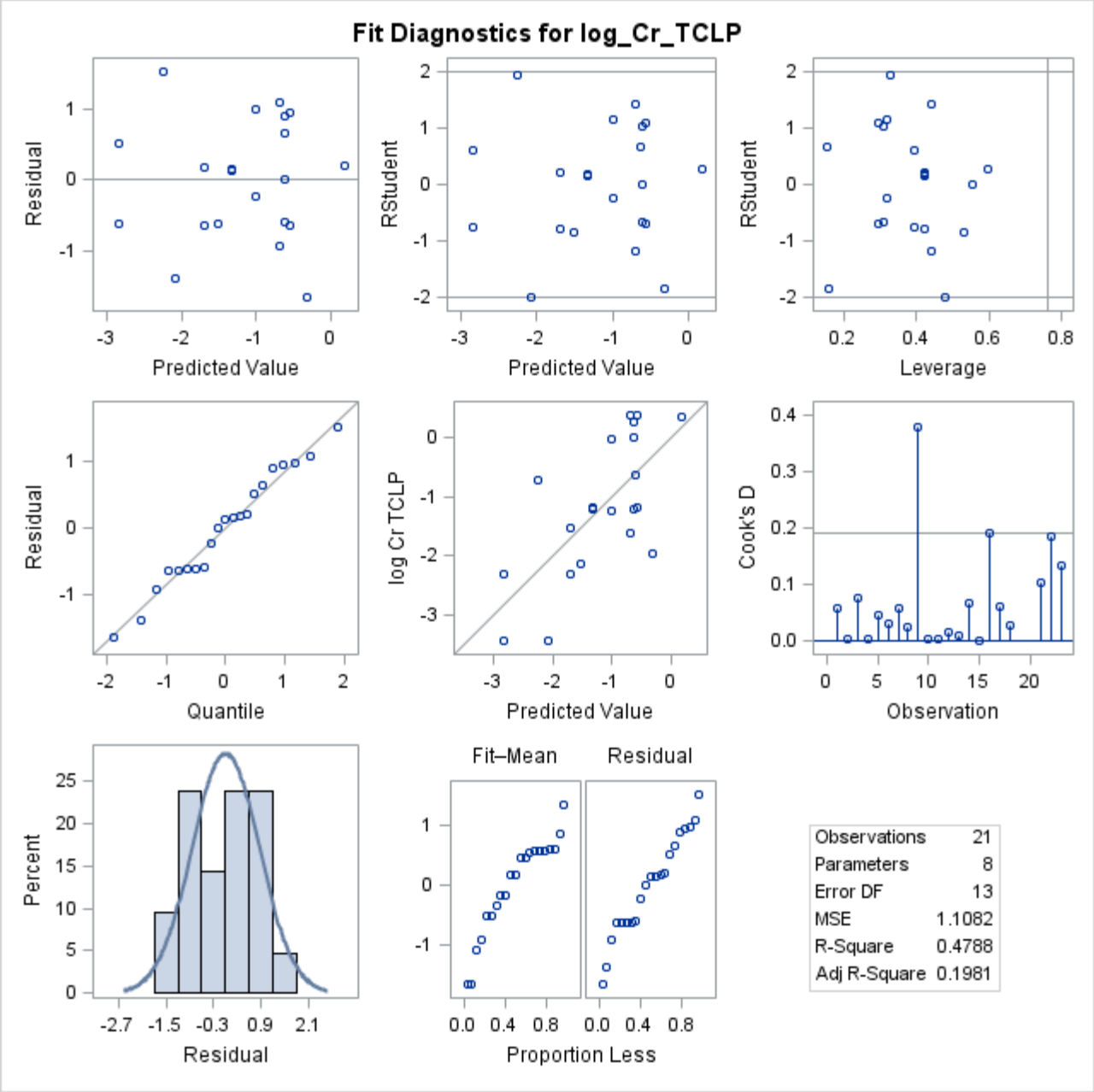

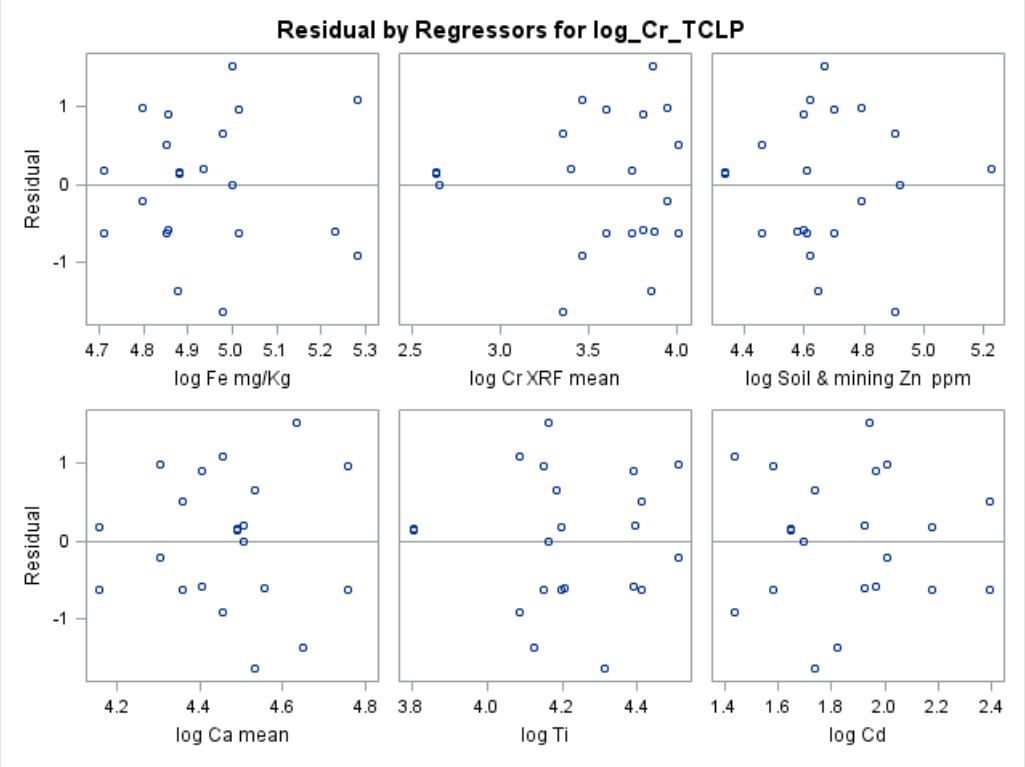
Residual by Regressors for log_Cr_TCLP
Residual
1
0
-1
4.7 4.8 4.9 5.0 5.1 5.2 5.3
log Fe mg/Kg
2.5 3.0 3.5 4.0
log Cr XRF mean
4.4 4.6 4.8 5.0 5.2
log Soil & mining Zn ppm
4.2 4.4 4.6 4.8
log Ca mean
3.8 4.0 4.2 4.4
log Ti
1.4 1.6 1.8 2.0 2.2 2.4
log Cd

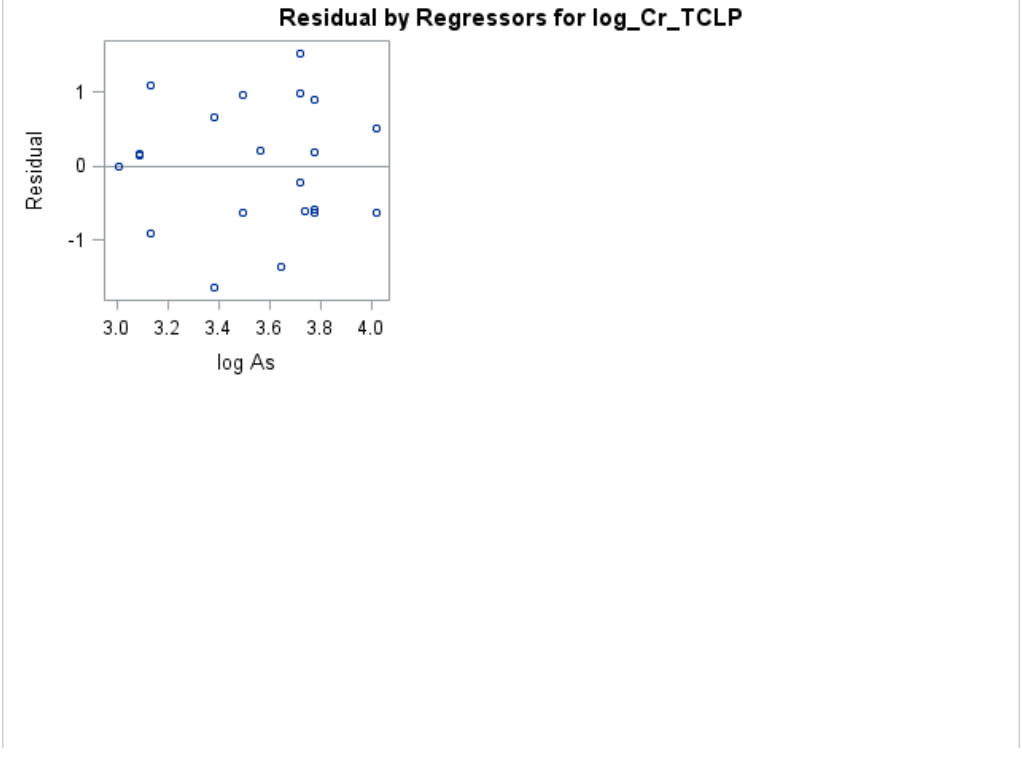
Residual by Regressors for log_Cr_TCLP
Residual
1
0
-1
3.0 3.2 3.4 3.6 3.8 4.0
log As

log Cr TCLP Fe<=20%

Number of Observations Read	32
Number of Observations Used	20
Number of Observations with Missing Values	12

Analysis of Variance

Source	DF	Sum of Squares	Mean Square	F Value	Pr > F
Model	8	6.84141	0.85518	0.47	0.8513
Error	11	19.88840	1.80804		
Corrected Total	19	26.72981			

Root MSE	1.34463	**R-Square**	0.2559
Dependent Mean	-0.76257	**Adj R-Sq**	-0.2852
Coeff Var	-176.32977		

Parameter Estimates

Variable	Label	DF	Parameter Estimate	Standard Error	t Value	Pr > |t|
Intercept	Intercept	**1**	27.27264	29.42342	0.93	0.3739
log_Fe_mg_Kg	log Fe mg/Kg	**1**	-4.71685	3.43898	-1.37	0.1975
log_Cr_XRF_mean	log Cr XRF mean	**1**	-1.42506	2.62016	-0.54	0.5974
log_mining_and_Soil_mode_Pb_mea	log mining and Soil mode Pb mea	**1**	1.80886	3.98198	0.45	0.6585
log_Soil___mining_Zn__ppm	log Soil & mining Zn ppm	**1**	-0.80484	1.40241	-0.57	0.5776
log_Ca_mean	log Ca mean	**1**	0.28277	2.11367	0.13	0.8960
log_Ti	log Ti	**1**	-0.22555	1.40102	-0.16	0.8750
log_Ag	log Ag	**1**	1.33259	3.28425	0.41	0.6927
log_As	log As	**1**	-1.29270	2.11217	-0.61	0.5530

The REG Procedure
Model: MODEL1
Dependent Variable: log_Cr_TCLP log Cr TCLP

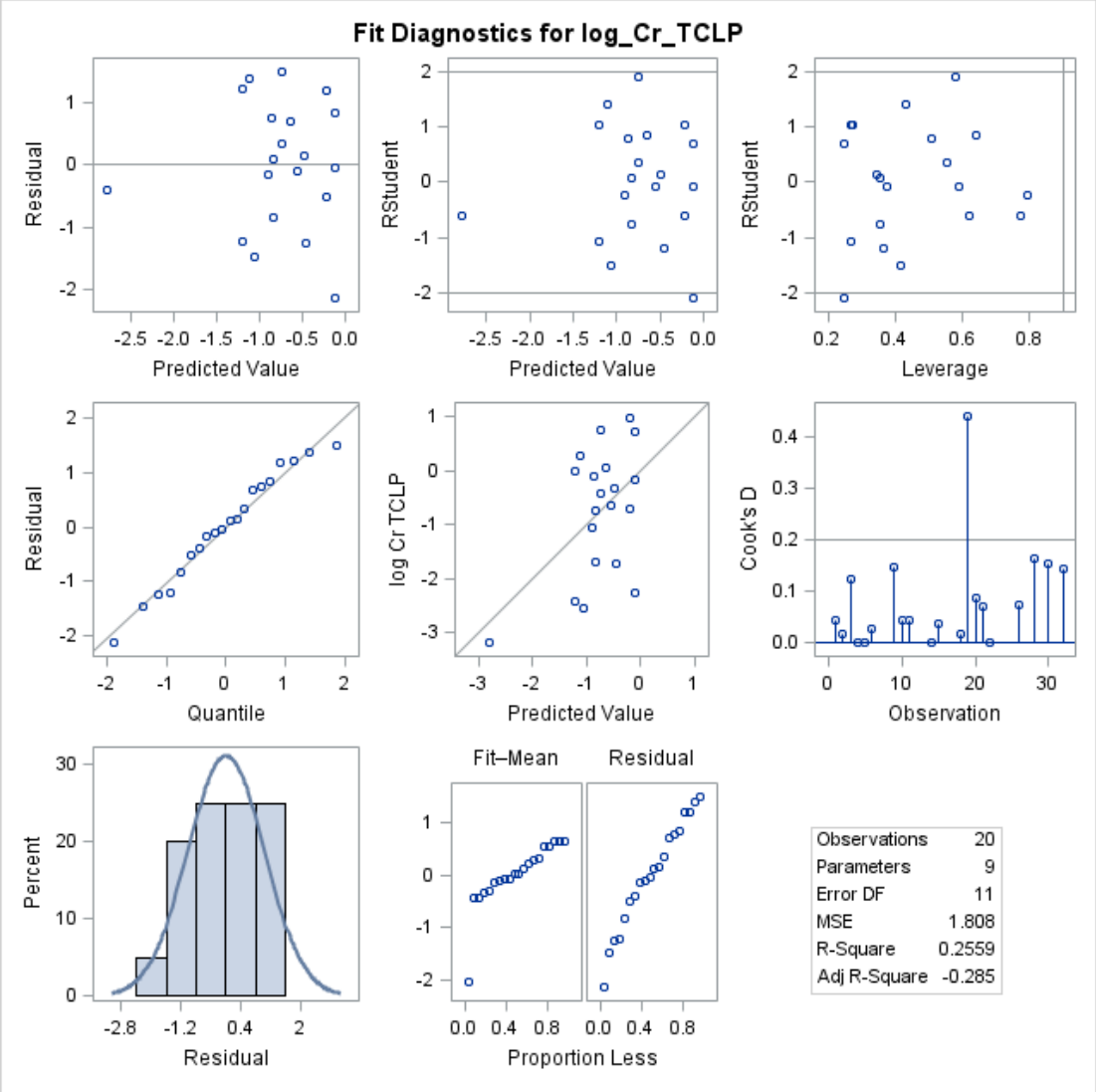

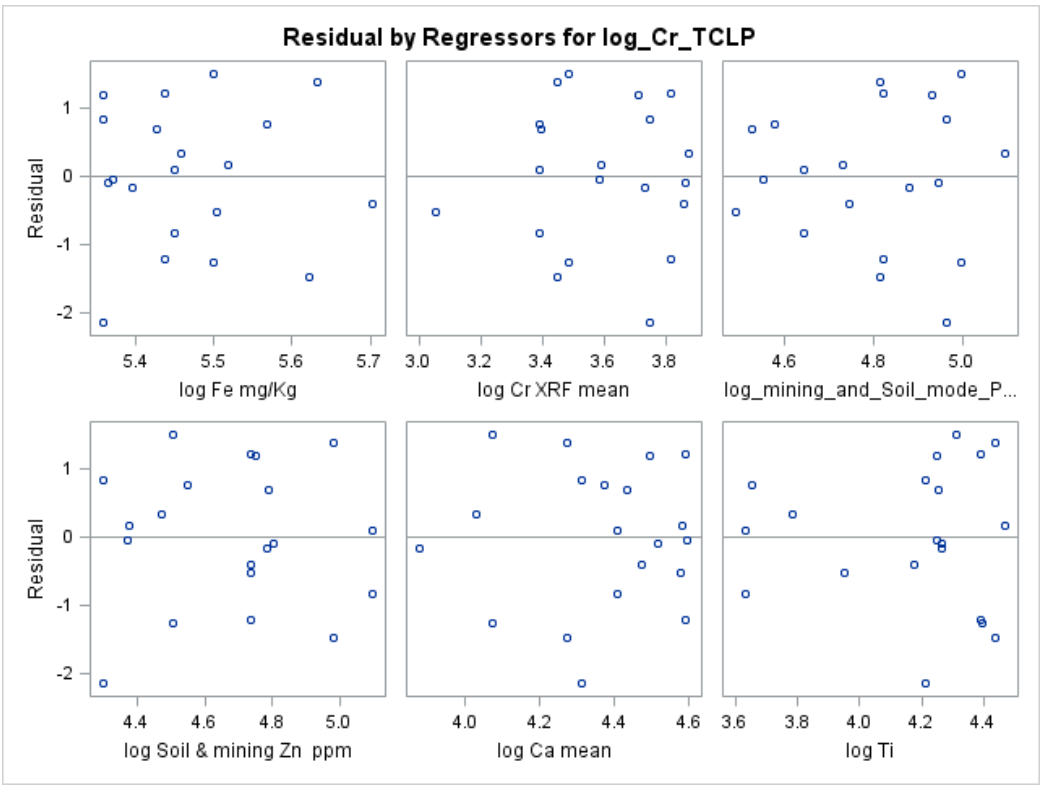
Residual by Regressors for log_Cr_TCLP
Residual
log Fe mg/Kg
log Cr XRF mean
log_mining_and_Soil_mode_P...
log Soil & mining Zn ppm
log Ca mean
log Ti

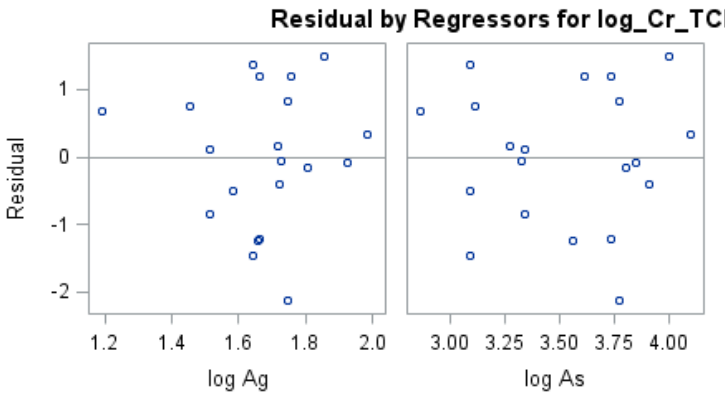
Residual by Regressors for log_Cr_TCLP
Residual
log Ag
log As

Chow test

The AUTOREG Procedure

Dependent Variable	log_Pb_TCLP_mean

The AUTOREG Procedure

Structural Change Test					
Test	**Break Point**	**Num DF**	**Den DF**	**F Value**	**Pr > F**
Chow	**23**	8	32	2.28	0.0467

The AUTOREG Procedure

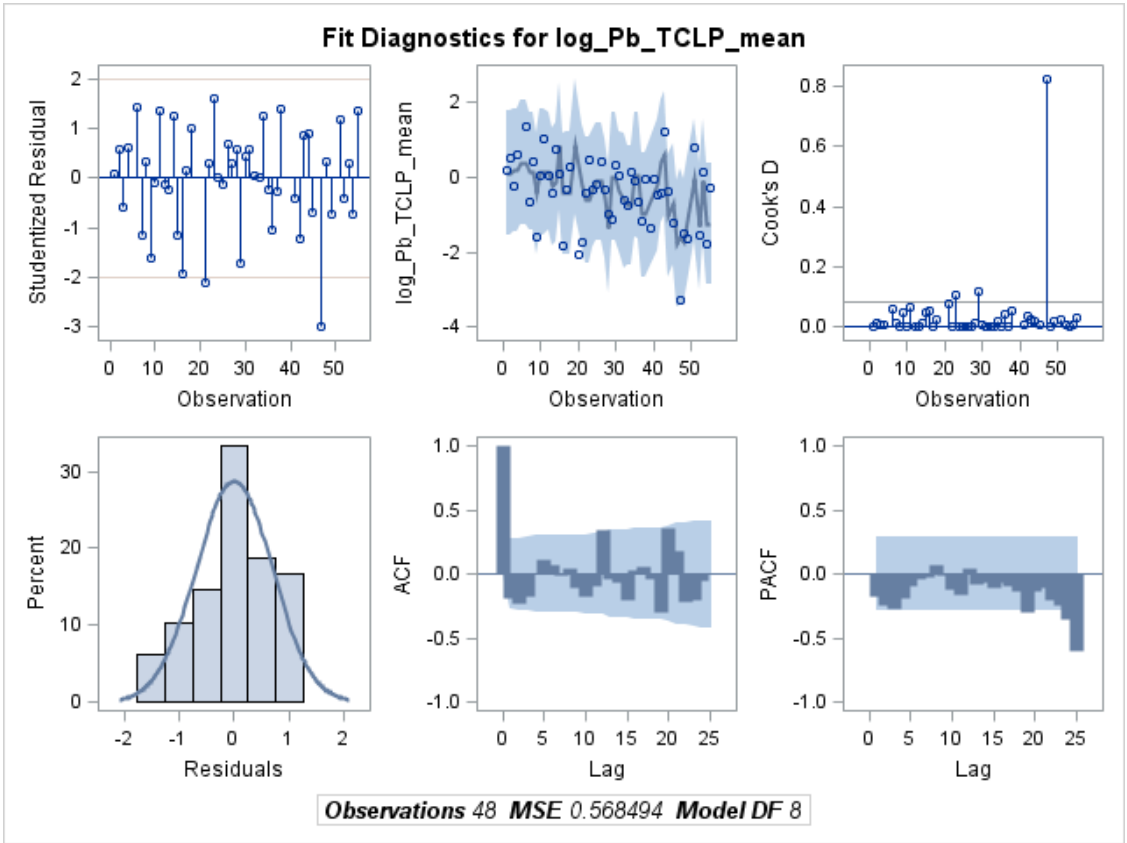

The AUTOREG Procedure

Dependent Variable Ba_TCLP

Structural Change Test					
Test	**Break Point**	**Num DF**	**Den DF**	**F Value**	**Pr > F**
Chow	**23**	10	29	1.33	0.2608

The AUTOREG Procedure

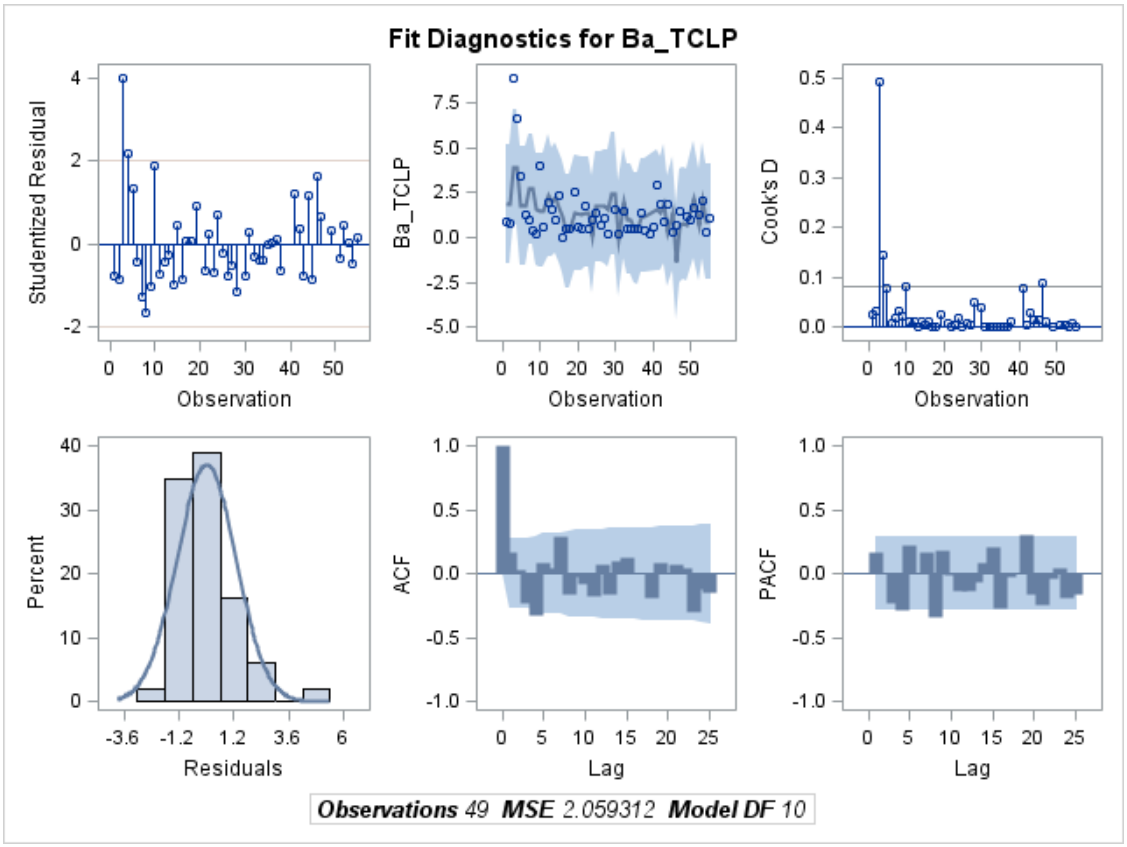

The AUTOREG Procedure

Dependent Variable Zn_TCLP

The AUTOREG Procedure

Structural Change Test

Test	Break Point	Num DF	Den DF	F Value	Pr > F
Chow	**23**	9	33	2.45	0.0294

The AUTOREG Procedure

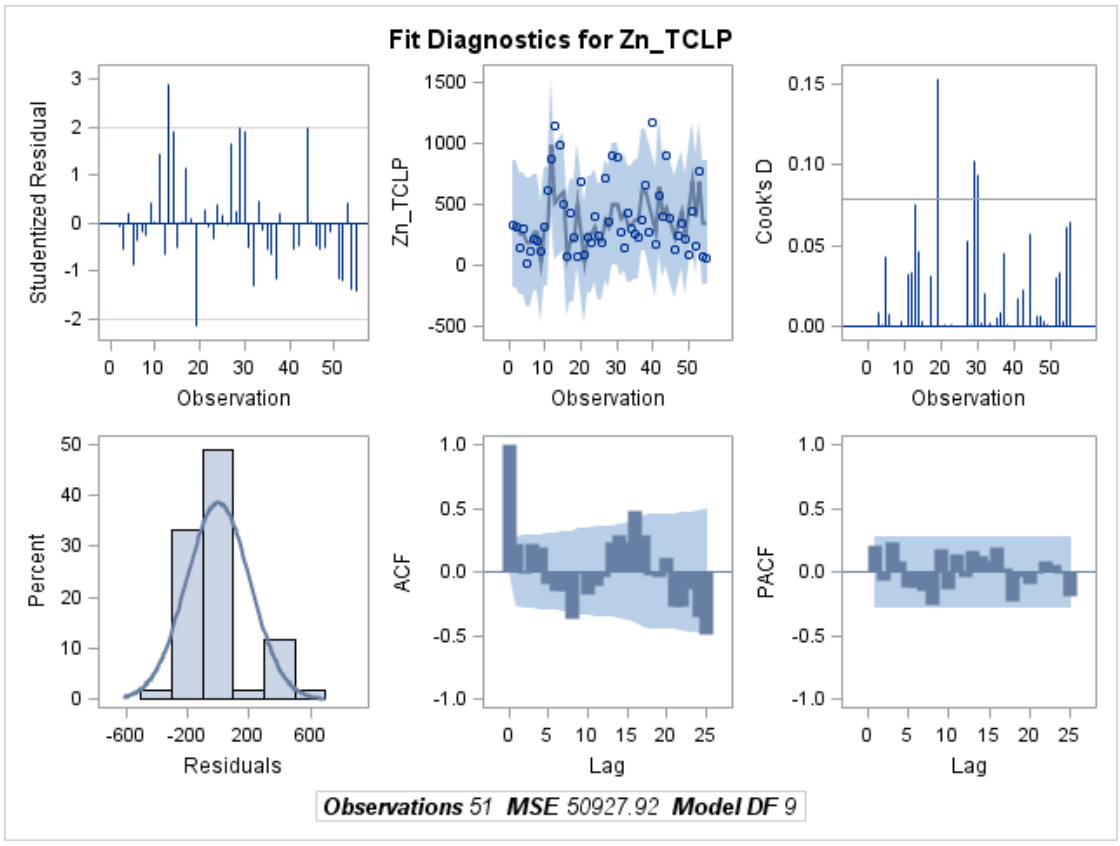

The AUTOREG Procedure

Dependent Variable Cr_TCLP

The AUTOREG Procedure

Structural Change Test

Test	Break Point	Num DF	Den DF	F Value	Pr > F
Chow	**23**	9	23	1.39	0.2479

The AUTOREG Procedure

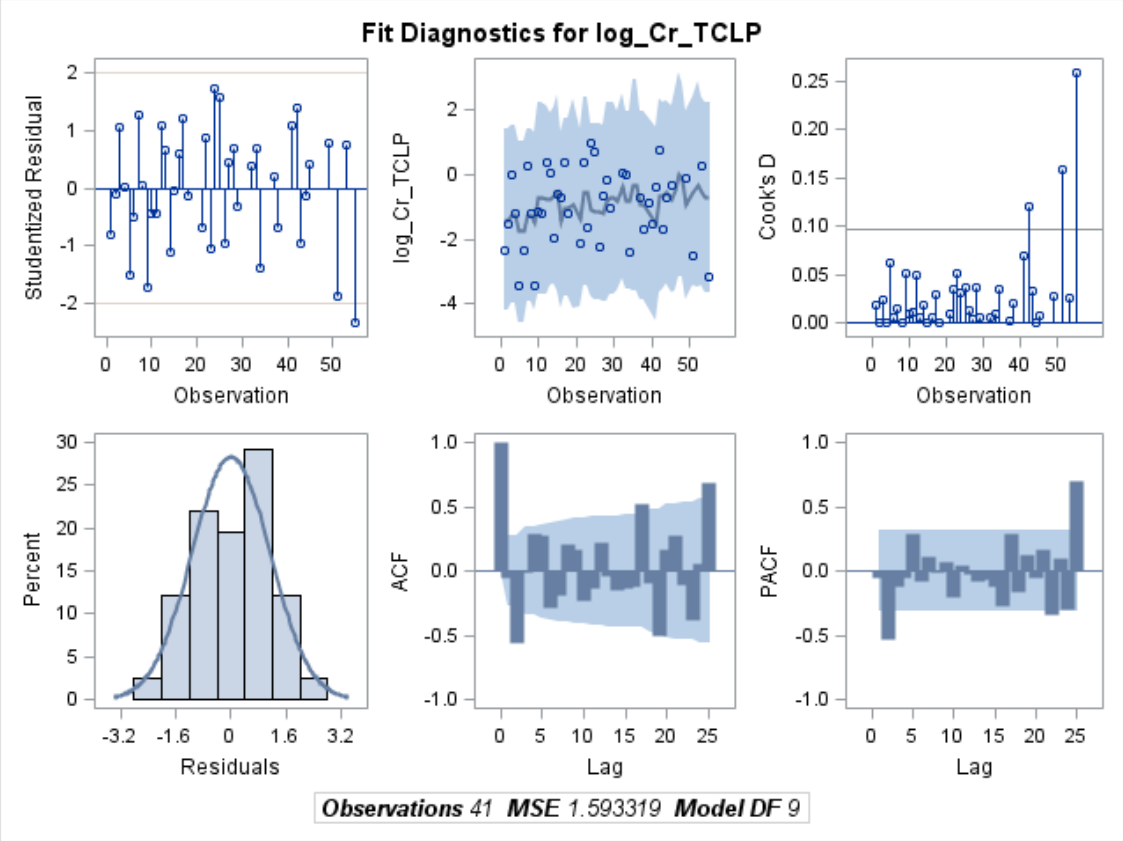

Pb, SSPC 10

```
Box-Cox transformation of the response with estimated lambda = -0.0992415
The 95% CI for lambda is (-0.413742, 0.359258)
Rounded lambda = 0 used in the regression analysis

Regression Equation

ln(Pb TCLP mean)  =  -5.09777 + 0.000384073 Pb mean pp + 5.5838e-005 Ca mean -
                     7.7842e-005 Ti mean


Coefficients

Term            Coef  SE Coef         T      P
Constant    -5.09777  1.01226  -5.03601  0.002
Pb mean pp   0.00038  0.00007   5.21958  0.001
Ca mean      0.00006  0.00003   2.17327  0.066
Ti mean     -0.00008  0.00002  -3.49596  0.010


Summary of Model

S = 0.776296     R-Sq = 85.39%        R-Sq(adj) = 79.13%
PRESS = 11.4196  R-Sq(pred) = 60.46%


Analysis of Variance

Source         DF   Seq SS   Adj SS   Adj MS        F         P
Regression      3  24.6596  24.6596   8.2199  13.6399  0.002611
  Pb mean pp    1  15.7580  16.4182  16.4182  27.2440  0.001226
  Ca mean       1   1.5364   2.8463   2.8463   4.7231  0.066297
  Ti mean       1   7.3652   7.3652   7.3652  12.2217  0.010048
Error           7   4.2185   4.2185   0.6026
  Lack-of-Fit   5   1.6446   1.6446   0.3289   0.2556  0.905100
  Pure Error    2   2.5739   2.5739   1.2869
Total          10  28.8781
```

Partial F test:

$$F\ (4\text{ variables}) = \frac{(3.27-2.65)/(5-4)/}{2.65/(11-5-1)} = 1.17$$

F(0.05,1,5) = 6.61>1.17. Hence, the coefficient removed from the model is not significant. Numbers of variables in the model were reduced from five to four.

$$F\ (3\text{ variables}) = \frac{(4.22-3.27)/(4-3)/}{3.27/(11-4-1)} = 1.74\,.$$

F(0.05,1,6) = 5.99>1.74. Hence, the coefficient removed from the model is not significant. Numbers of variables in the model were reduced from four to three.

$$F\ (2\text{ variables}) = \frac{(7.064-4.22)/(3-2)/}{4.22/(11-3-1)} = 4.72$$

F(0.05,176) = 5.59>4.72. However, since these two numbers are so close, we will not remove the third variables.

Cr, SSPC 10

The regression equation is
Cr TCLP = 12.4 - 0.000022 Soil & mining Zn ppm - 0.000032 Fe mg/kg + 0.0077 Cr XRF mean + 0.000053 mining and Soil mode Pb mean pp - 0.000198 Ca mean - 0.000038 Ti mean

8 cases used, 12 cases contain missing values

Predictor	Coef	SE Coef	T	P
Constant	12.38	19.46	0.64	0.639
Soil & mining Zn ppm	-0.00002232	0.00003736	-0.60	0.657
Fe mg/kg	-0.00003236	0.00005264	-0.61	0.649
Cr XRF mean	0.00771	0.01276	0.60	0.654
mining and Soil mode Pb mean pp	0.0000529	0.0001667	0.32	0.804
Ca mean	-0.0001983	0.0003084	-0.64	0.636
Ti mean	-0.00003833	0.00007606	-0.50	0.703

S = 0.694055   R-Sq = 44.9%   R-Sq(adj) = 0.0%

Analysis of Variance

Source	DF	SS	MS	F	P
Regression	6	0.3929	0.0655	0.14	0.75
Residual Error	1	0.4817	0.4817		
Total	7	0.8746			

Source	DF	Seq SS
Soil & mining Zn ppm	1	0.0900
Fe mg/kg	1	0.0003
Cr XRF mean	1	0.0387
mining and Soil mode Pb mean pp	1	0.0425
Ca mean	1	0.0991
Ti mean	1	0.1223

Ba, SSPC 10

```
Box-Cox transformation of the response with rounded lambda = 0.5
The 95% CI for lambda is (-0.075, 1.015)

Regression Equation

Ba TCLP^0.5  =  -0.662387 - 2.17667e-005 Ba XRF + 2.62614e-006 Soil & mining Zn
                ppm + 3.36626e-006 Fe mg/kg + 0.000111838 mining and Soil mode
                Pb mean pp - 1.14467e-005 Ca mean - 0.00140021 As

19 cases used, 1 cases contain missing values

Coefficients

Term                                  Coef   SE Coef         T      P
Constant                          -0.662387  0.510234  -1.29820  0.219
Ba XRF                            -0.000022  0.000010  -2.11097  0.056
Soil & mining Zn  ppm              0.000003  0.000001   1.84907  0.089
Fe mg/kg                           0.000003  0.000001   2.90043  0.013
mining and Soil mode Pb mean pp    0.000112  0.000028   4.02088  0.002
Ca mean                           -0.000011  0.000005  -2.15883  0.052
As                                -0.001400  0.000561  -2.49721  0.028

Summary of Model

S = 0.151198      R-Sq = 69.72%        R-Sq(adj) = 54.58%
PRESS = 0.737005  R-Sq(pred) = 18.65%

Analysis of Variance

Source                             DF    Seq SS    Adj SS    Adj MS        F
Regression                          6  0.631592  0.631592  0.105265   4.6046
  Ba XRF                            1  0.024745  0.101872  0.101872   4.4562
  Soil & mining Zn  ppm             1  0.009376  0.078163  0.078163   3.4191
  Fe mg/kg                          1  0.010538  0.192317  0.192317   8.4125
  mining and Soil mode Pb mean pp   1  0.419774  0.369603  0.369603  16.1675
  Ca mean                           1  0.024597  0.106544  0.106544   4.6606
  As                                1  0.142562  0.142562  0.142562   6.2360
Error                              12  0.274331  0.274331  0.022861
  Lack-of-Fit                       6  0.127487  0.127487  0.021248   0.8682
  Pure Error                        6  0.146844  0.146844  0.024474
Total                              18  0.905923

Source                                P
Regression                     0.011867
  Ba XRF                       0.056434
  Soil & mining Zn  ppm        0.089222
  Fe mg/kg                     0.013316
  mining and Soil mode Pb mean pp  0.001697
  Ca mean                      0.051819
  As                           0.028059
Error
  Lack-of-Fit                  0.565933
  Pure Error
Total
```

Zn, SSPC 10

Box-Cox transformation of the response with rounded lambda = 0.5
The 95% CI for lambda is (-0.125, 1.325)

Regression Equation

Zn TCLP^0.5 = 0.396622 - 0.00049622 Ba XRF + 5.25726e-005 Soil & mining Zn ppm + 4.79214 Ag - 0.0145836 As

19 cases used, 1 cases contain missing values

Coefficients

Term	Coef	SE Coef	T	P
Constant	0.39662	7.75561	0.05114	0.960
Ba XRF	-0.00050	0.00034	-1.46689	0.165
Soil & mining Zn ppm	0.00005	0.00001	4.16802	0.001
Ag	4.79214	1.82091	2.63173	0.020
As	-0.01458	0.00667	-2.18574	0.046

Summary of Model

S = 3.71799 R-Sq = 69.60% R-Sq(adj) = 60.91%
PRESS = 340.591 R-Sq(pred) = 46.50%

Analysis of Variance

Source	DF	Seq SS	Adj SS	Adj MS	F	P
Regression	4	443.077	443.077	110.769	8.0131	0.001409
Ba XRF	1	12.650	29.745	29.745	2.1518	0.164507
Soil & mining Zn ppm	1	331.923	240.147	240.147	17.3724	0.000948
Ag	1	32.463	95.741	95.741	6.9260	0.019720
As	1	66.041	66.041	66.041	4.7775	0.046321
Error	14	193.528	193.528	13.823		
Lack-of-Fit	8	138.422	138.422	17.303	1.8839	0.227975
Pure Error	6	55.107	55.107	9.184		
Total	18	636.606				

REFERENCES

Adebamowo, E.O., Scott Clark, C., Roda, S., Agbede, O.A., Sridhar, M.K., Adebamowo, C.A., 2007. Lead content of dried films of domestic paints currently sold in Nigeria. Science of the Total Environment 388, 116-120.

Alphen, M., 1998. Paint film components. National Environmental Health Forum Monographs, General Series No. 2.

American Society for Testing and Materials, A., 1990. Standard practice for decontamination of field equipment used at nonradioactive waste sites. Designation D5088-90, West Conshohocken, PA.

Anderson-Cook, C., Dorai-Raj, S., 2003. Making the concepts of power and sample size relevant and accessible to students in introductory statistics courses using applets. Journal of Statistics Education 11.

Andra, S.S., Datta, R., Reddy, R., Saminathan, S.K., Sarkar, D., 2011. Antioxidant enzymes response in vetiver grass: A greenhouse study for chelant-assisted phytoremediation of lead-contaminated residential soils. CLEAN–Soil, Air, Water 39, 428-436.

Appleman, B.R., 1992. Bridge paint: Removal, containment, and disposal. Transportation Research Board.

Appleman, B.R., 1997. Lead-based paint removal for steel highway bridges. Transportation Research Board.

Apul, D.S., Gardner, K.H., Eighmy, T.T., Fällman, A.M., Comans, R.N., 2005. Simultaneous application of dissolution/precipitation and surface complexation/surface precipitation modeling to contaminant leaching. Environmental Science and Technology 39, 5736-5741.

Arce, R., Galán, B., Coz, A., Andrés, A., Viguri, J., 2010. Stabilization/solidification of an alkyd paint waste by carbonation of waste-lime based formulations. Journal of Hazardous Materials 177, 428-436.

Axe, L., Anderson, P.R., 1995. Sr diffusion and reaction within Fe oxides: Evaluation of the rate-limiting mechanism for sorption. Journal of Colloid and Interface Science 175, 157-165.

Axe, L., Jahan, K., Dusseau, R.A., 2009. Field methods for determining lead content in bridge paint removal waste, New York State Department of Transportation, Project No. C-08-19.

Baes, C.F., Mesmer, J.R.E., 1976. The hydrolysis of cations Wiley: New York, NY.

Ball, J.W., Nordstrom, D.K., 1991. User's manual for WATEQ4F, with revised thermodynamic data base and test cases for calculating speciation of major, trace, and redox elements in natural waters.

Barnes, G.L., Davis, A.P., 1996. Dissolution of lead paint in aqueous solutions. Journal of Environmental Engineering 122, 663-666.

Beckley, R., Groenier, J.S., 2008. Using XRF hand-held devices to detect lead-based paint. in: United States Department of Agriculture Forest Service, T.D.P. (Ed.).

Benjamin, M.M., 2002. Water chemistry. McGraw-Hill: New York, NY.

Bentley, J., 1998. Introduction to paint chemistry: Principles of paint technology. Chapman & Hall: London, UK.

Bernecki, T.F., Nichols, G., Prine, D., Shubinsky, G., Zdunek, A., 1995. Issues impacting bridge painting: an overview. Final Report (No. FHWA-RD-94-098).

Bhuiyan, M.A.H., Suruvi, N.I., Dampare, S.B., Islam, M., Quraishi, S.B., Ganyaglo, S., Suzuki, S., 2011. Investigation of the possible sources of heavy metal contamination in lagoon and canal water in the tannery industrial area in Dhaka, Bangladesh. Environmental Monitoring and Assessment 175, 633-649.

Bidoglio, G., Gibson, P., O'Gorman, M., Roberts, K., 1993. X-ray absorption spectroscopy investigation of surface redox transformations of thallium and chromium on colloidal mineral oxides. Geochimica et Cosmochimica Acta 57, 2389-2394.

Binstock, D.A., Gutknecht, W.F., McWilliams, A.C., 2009. Lead in soil-an examination of paired XRF analysis performed in the field and laboratory ICP-AES results. International Journal of Soil, Sediment and Water 2, 1.

Borst, S., Laubender, T., Snyder, S., Greene, J., 2004. Adding value to industrial coatings by using epoxy functional silicone resins. Paint and Coatings Industry 20, 132-147.

Boxall, J., Von Fraunhofer, J.A., 1980. Paint Formulation: principles and practice. Godwin: London, UK

Boy, J.H., Race, T.D., Reinbold, K.A., Bukowski, J., Zhu, X., 1995. Chromium stabilization chemistry of paint removal wastes in Portland cement and blast furnace slag. Hazardous Waste and Hazardous Materials 12, 83-95.

Bradl, H.B., 2004. Adsorption of heavy metal ions on soils and soils constituents. Journal of Colloid and Interface Science 277, 1-18.

Brumis, S., Scholz, P., Materna, B., 2001. Lead exposure during hot cutting of stripped steel. Applied Occupational and Environmental Hygiene 16, 502-505.

Buchter, B., Davidoff, B., Amacher, M., Hinz, C., Iskandar, I., Selim, H., 1989. Correlation of Freundlich Kd and n retention parameters with soils and elements. Soil Science 148, 370-379.

Cao, X., Ma, L.Q., Chen, M., Hardison, D.W., Harris, W.G., 2003. Weathering of lead bullets and their environmental effects at outdoor shooting ranges. Journal of Environmental Quality 32, 526-534.

Caravanos, J., Weiss, A.L., Blaise, M.J., Jaeger, R.J., 2006. A survey of spatially distributed exterior dust lead loadings in New York City. Environmental Research 100, 165-172.

Catalano, J.G., Luo, Y., Otemuyiwa, B., 2011. Effect of aqueous Fe (II) on arsenate sorption on goethite and hematite. Environmental Science and Technology 45, 8826-8833.

Challener, C., 2011. The impact of additives on: 'Green' coatings. Journal of Coatings Technology 8, 36-40.

Charlatchka, R., Cambier, P., 2000. Influence of reducing conditions on solubility of trace metals in contaminated soils. Water, Air, and Soil Pollution 118, 143-167.

Choe, K.T., Trunov, M., Menrath, W., Succop, P., Grinshpun, S.A., 2002. Relationship between lead levels on painted surfaces and percent lead in the particles aerosolized during lead abatement. Applied Occupational and Environmental Hygiene 17, 573-579.

Chow, G.C., 1960. Tests of equality between sets of coefficients in two linear regressions. Econometrica 28, 591-605.

Chowdhury, S.R., Yanful, E.K., Pratt, A.R., 2012. Chemical states in XPS and Raman analysis during removal of Cr (VI) from contaminated water by mixed maghemite–magnetite nanoparticles. Journal of Hazardous Materials 235-236, 246-256.

Christophi, C.A., Axe, L., 2000. Competition of Cd, Cu, and Pb adsorption on goethite. Journal of Environmental Engineering 126, 66-74.

Clark, C., Rampal, K., Thuppil, V., Chen, C., Clark, R., Roda, S., 2006. The lead content of currently available new residential paint in several Asian countries. Environmental Research 102, 9-12.

Clark, C., Thuppil, V., Clark, R., Sinha, S., Menezes, G., D'Souza, H., Nayak, N., Kuruvilla, A., Law, T., Dave, P., 2005. Lead in paint and soil in Karnataka and Gujarat, India. Journal of Occupational and Environmental Hygiene 2, 38-44.

Clark, H.A., 1976. Paint compositions. Google Patents.

Clark, S., Menrath, W., Chen, M., Roda, S., Succop, P., 1999. Use of a field portable X-ray fluorescence analyzer to determine the concentration of lead and other metals in soil samples. Annals of Agricultural and Environmental Medicine 6, 27-32.

Clarkson, T.W., Friberg, L., Nordberg, G., Sager, P.R., 1988. Biological monitoring of toxic metals. Rochester Univ., NY (USA). School of Medicine and Dentistry; Karolinska Inst., Stockholm (Sweden); Umeaa Univ.(Sweden); Stauffer Chemical Co., Farmington, CT (USA).

Conroy, L.M., Menezes-Lindsay, R.M., Sullivan, P.M., Cali, S., Forst, L., 1996. Lead, chromium, and cadmium exposure during abrasive blasting. Archives of Environmental Health: An International Journal 51, 95-99.

Cornelis, G., Johnson, C.A., Gerven, T.V., Vandecasteele, C., 2008. Leaching mechanisms of oxyanionic metalloid and metal species in alkaline solid wastes: A review. Applied Geochemistry 23, 955-976.

Cornell, R.M., Schwertmann, U., 1996. The iron oxides. Structure, properties, reaction, occurrence and uses. Wiley: Weinheim,Germany.

CPSC, 1977. Notice reducing allowable levels of lead. Final Rule, Federal Register 42 (1): 44199.

Cravotta, C.A., 2008. Dissolved metals and associated constituents in abandoned coal-mine discharges, Pennsylvania, USA. Part 2: Geochemical controls on constituent concentrations. Applied Geochemistry 23, 203-226.

Crawford, R.J., Mainwaring, D.E., Harding, I.H., 1997. Adsorption and coprecipitation of heavy metals from ammoniacal solutions using hydrous metal oxides. Colloids and Surfaces A: Physicochemical and Engineering Aspects 126, 167-179.

Crown, D.A., 1968. The forensic examination of paints and pigments. Thomas: Springfield, Illinois, U.S.A

Daniels, A.E., Kominsky, J.R., Clark, P.J., 2001. Evaluation of two lead-based paint removal and waste stabilization technology combinations on typical exterior surfaces. Journal of Hazardous Materials 87, 117-126.

Das, S., Hendry, M.J., Essilfie-Dughan, J., 2011. Transformation of two-line ferrihydrite to goethite and hematite as a function of pH and temperature. Environmental Science and Technology 45, 268-275.

Davis, A.P., Burns, M., 1999. Evaluation of lead concentration in runoff from painted structures. Water Research 33, 2949-2958.

Davis, J.M., Elias, R.W., Grant, L., 1993. Current issues in human lead exposure and regulation of lead. Neurotoxicology 14, 15-27.

Davranche, M., Bollinger, J.-C., 2000. Heavy metals desorption from synthesized and natural iron and manganese oxyhydroxides: effect of reductive conditions. Journal of Colloid and Interface Science 227, 531-539.

De La Fuente, D., Díaz, I., Simancas, J., Chico, B., Morcillo, M., 2011. Long-term atmospheric corrosion of mild steel. Corrosion Science 53, 604-617.

Del Amo, B., Di Sarli, A.R., Lecot, J., Caprari, J.J., 2003. Protection of steel with only one coat. Surface Coatings International Part B: Coatings Transactions 86, 143-148.

Deng, Y., Stjernström, M., Banwart, S., 1996. Accumulation and remobilization of aqueous chromium (VI) at iron oxide surfaces: Application of a thin-film continuous flow-through reactor. Journal of Contaminant Hydrology 21, 141-151.

Dijkstra, J.J., Meeussen, J.C., Comans, R.N., 2009. Evaluation of a generic multisurface sorption model for inorganic soil contaminants. Environmental Science and Technology 43, 6196-6201.

Doroszkowski, A., Lambourne, R., Strivens, T., 1999. Paint and Surface Coatings: Theory and Practice. Elsevier: Cambridge, UK

Du, J., Lu, J., Wu, Q., Jing, C., 2012. Reduction and immobilization of chromate in chromite ore processing residue with nanoscale zero-valent iron. Journal of Hazardous Materials 215, 152-158.

Dunkerley, F.J., Gaudino, A.J., Vilyus, R.P., 1978. Steel abrasive materials. Google Patents.

Dupont, W.D., Plummer Jr, W.D., 1990. Power and sample size calculations. A review and computer program. Controlled Clinical Trials 11, 116-128.

Dyer, J.A., Trivedi, P., Scrivner, N.C., Sparks, D.L., 2003. Lead sorption onto ferrihydrite. 2. Surface complexation modeling. Environmental Science and Technology 37, 915-922.

Dzombak, D.A., Morel, F.M., 1986. Sorption of cadmium on hydrous ferric oxide at high sorbate/sorbent ratios: Equilibrium, kinetics, and modeling. Journal of Colloid and Interface Science 112, 588-598.

Dzombak, D.A., Morel, F.M., 1990. Surface complexation modeling: hydrous ferric oxide. Wiley: New York, NY.

Eaton, A.D., Clesceri, L.S., Rice, E.W., Greenberg, A.E., 2005. Standard methods for the examination of water and wastewater. American Public Health Association: Washington, DC.

Edavan, R.P., Kopinski, R., 2009. Corrosion resistance of painted zinc alloy coated steels. Corrosion Science 51, 2429-2442.

El Hajj, H., Abdelouas, A., El Mendili, Y., Karakurt, G., Grambow, B., Martin, C., 2013. Corrosion of carbon steel under sequential aerobic–anaerobic environmental conditions. Corrosion Science 76, 432-440.

Equeenuddin, S.M., Tripathy, S., Sahoo, P., Panigrahi, M., 2010. Geochemistry of ochreous precipitates from coal mine drainage in India. Environmental Earth Sciences 61, 723-731.

Erkens, L., Hamers, H., Hermans, R., Claeys, E., Bijnens, M., 2001. Lead chromates: A review of the state of the art in 2000. Surface Coatings International Part B: Coatings Transactions 84, 169-176.

Esakku, S., Karthikeyan, O.P., Joseph, K., Nagendran, R., 2008. Heavy metal fractionation and leachability studies on fresh and partially decomposed municipal solid waste. Practice Periodical of Hazardous, Toxic, and Radioactive Waste Management 12, 127-132.

Falk, R.H., Janowiak, J.J., Cosper, S.D., Drozdz, S.A., 2005. Remilling of salvaged wood siding coated with lead-based paint. Part 1. Lead exposure. Forest Products Journal 55, 76.

Fan, M., Boonfueng, T., Xu, Y., Axe, L., Tyson, T.A., 2005. Modeling Pb sorption to microporous amorphous oxides as discrete particles and coatings. Journal of Colloid and Interface Science 281, 39-48.

Ferlauto, E., 1994. Lead-based paint and the lead abatement issue in the United States, Journal of Coatings Technology 66, 69-74.

Fernández-Caliani, J.C., Barba-Brioso, C., Pérez-López, R., 2008. Long-term interaction of wollastonite with acid mine water and effects on arsenic and metal removal. Applied Geochemistry 23, 1288-1298.

Filgueiras, A.V., Lavilla, I., Bendicho, C., 2002. Chemical sequential extraction for metal partitioning in environmental solid samples. Journal of Environmental Monitoring 4, 823-857.

Fjelsted, L., Christensen, T.H., 2007. Household hazardous waste: composition of paint waste. Waste Management and Research 25, 502-509.

Flaherty, E., 2008. Safety first: the consumer product safety improvement act of 2008. Loy. Consumer L. Rev. 21, 372.

Florida Department of Environmental Protection (FDEP), 2009. Guidance for determining leachability by analysis of SPLP results, Tallahassee, FL. Bureau of Waste Cleanup.

Franquelo, M., Duran, A., Castaing, J., Arquillo, D., Perez-Rodriguez, J., 2012. XRF, μ-XRD and μ-spectroscopic techniques for revealing the composition and structure of paint layers on polychrome sculptures after multiple restorations. Talanta 89, 462-469.

Funatsuki, A., Takaoka, M., Oshita, K., Takeda, N., 2012. Methods of determining lead speciation in fly ash by X-ray absorption fine-structure spectroscopy and a sequential extraction procedure. Analytical Sciences 28, 481-490.

Ghosh, A., Mukiibi, M., Ela, W., 2004. TCLP underestimates leaching of arsenic from solid residuals under landfill conditions. Environmental Science and Technology 38, 4677-4682.

Gibbs, R.J., 1973. Mechanisms of trace metal transport in rivers. Science 180, 71-73.

Gidlow, D., 2004. Lead toxicity. Occupational Medicine 54, 76-81.

González, S.C., 2008. Lead-based residential paint in soils: A dissolution and a spatial analysis prevention approach. ProQuest.

Gooch, J.W., 1993. Lead-based paint handbook. Plenum Press: New York, NY.

Groenenberg, J., Römkens, P., Comans, R., Luster, J., Pampura, T., Shotbolt, L., Tipping, E., De Vries, W., 2010. Transfer functions for solid-solution partitioning of cadmium, copper, nickel, lead and zinc in soils: derivation of relationships for free metal ion activities and validation with independent data. European Journal of Soil Science 61, 58-73.

Halim, C.E., Amal, R., Beydoun, D., Scott, J.A., Low, G., 2003. Evaluating the applicability of a modified toxicity characteristic leaching procedure (TCLP) for

the classification of cementitious wastes containing lead and cadmium. Journal of Hazardous Materials 103, 125-140.

Halim, C.E., Scott, J.A., Natawardaya, H., Amal, R., Beydoun, D., Low, G., 2004. Comparison between acetic acid and landfill leachates for the leaching of Pb (II), Cd (II), As (V), and Cr (VI) from cementitious wastes. Environmental Science and Technology 38, 3977-3983.

Hall, S., 1972. Lead pollution and poisoning. Environmental Science and Technology 6, 30-35.

Hartley, W., Lepp, N.W., 2008. Remediation of arsenic contaminated soils by iron-oxide application, evaluated in terms of plant productivity, arsenic and phytotoxic metal uptake. Science of the Total Environment 390, 35-44.

Hass, A., Fine, P., 2010. Sequential selective extraction procedures for the study of heavy metals in soils, sediments, and waste materials—a critical review. Critical Reviews in Environmental Science and Technology 40, 365-399.

Haynes, R., 1982. Effects of liming on phosphate availability in acid soils. Plant and Soil 68, 289-308.

Heron, G., Crouzet, C., Bourg, A.C., Christensen, T.H., 1994. Speciation of Fe (II) and Fe (III) in contaminated aquifer sediments using chemical extraction techniques. Environmental Science and Technology 28, 1698-1705.

Hopwood, I., Palle, S., Younce, R., 2003. Environmental impacts of bridge cleaning operations. Kentucky Transportation Center Research Reports (KTC-03-03/SPR224-01-1F).

Howard, J.L., Dubay, B.R., McElmurry, S.P., Clemence, J., Daniels, W.L., 2013. Comparison of aequential extraction and bioaccessibility analyses of lead using urban soils and reference materials. Water, Air and Soil Pollution 224, 1-13.

Howard, J.L., Shu, J., 1996. Sequential extraction analysis of heavy metals using a chelating agent (NTA) to counteract resorption. Environmental Pollution 91, 89-96.

Huang, S.L., Yin, C.Y., Yap, S.Y., 2010. Particle size and metals concentrations of dust from a paint manufacturing plant. Journal of Hazardous Materials 174, 839-842.

HUD, 2003. Lead Safety for Remodeling, Repair, and Painting.

Ianni, C., Bignasca, A., Calace, N., Rivaro, P., Magi, E., 2014. Bioaccessibility of metals in soils: comparison between chemical extractions and in vitro tests. Chemistry and Ecology, 1-14.

Illés, E., Tombácz, E., 2003. The role of variable surface charge and surface complexation in the adsorption of humic acid on magnetite. Colloids and Surfaces A: Physicochemical and Engineering Aspects 230, 99-109.

Iowa Department of Transportation (IADOT), 2006. Chapter 10, Construction Manual, October, http://www.iowadot.gov/erl/archives/oct_2006/CM/content/10-50.htm.

Isaacs, L., 2007. Lead leaching from soils and in storm waters at twelve military shooting ranges. Journal for Hazardous Substance Research Volume Six 1, 1.

Jackson, R., Inch, K., 1989. The in-situ adsorption of ^{90}Sr in a sand aquifer at the Chalk River Nuclear Laboratories. Journal of Contaminant Hydrology 4, 27-50.

Jacobs, D.E., Clickner, R.P., Zhou, J.Y., Viet, S.M., Marker, D.A., Rogers, J.W., Zeldin, D.C., Broene, P., Friedman, W., 2002. The prevalence of lead-based paint hazards in US housing. Environmental Health Perspectives 110, A599.

Jambor, J.L., Dutrizac, J.E., 1998. Occurrence and constitution of natural and synthetic ferrihydrite, a widespread iron oxyhydroxide. Chemical Reviews 98, 2549-2586.

JCPDS, 1998. Handbook for diffraction data (PCPDFWIN ver. 2.00).

Jing, C., Liu, S., Korfiatis, G.P., Meng, X., 2006. Leaching behavior of Cr (III) in stabilized/solidified soil. Chemosphere 64, 379-385.

Kaiser, H.F., 1960. The application of electronic computers to factor analysis. Educational and psychological measurement.

Kalnicky, D.J., Singhvi, R., 2001. Field portable XRF analysis of environmental samples. Journal of Hazardous Materials 83, 93-122.

Kanungo, S.B., 1994. Adsorption of cations on hydrous oxides of iron: II. Adsorption of Mn, Co, Ni, and Zn onto amorphous FeOOH from simple electrolyte solutions as well as from a complex electrolyte solution resembling seawater in major ion content. Journal of Colloid and Interface Science 162, 93-102.

Karadaş, C., Kara, D., 2012. Chemometric evaluation for the relation of BCR sequential extraction method and in vitro gastro-intestinal method for the assessment of metal bioavailability in contaminated soils in Turkey. Environmental Science and Pollution Research 19, 1280-1295.

Karamalidis, A.K., Voudrias, E.A., 2008. Anion leaching from refinery oily sludge and ash from incineration of oily sludge stabilized/solidified with cement. Part II. Modeling. Environmental Science and Technology 42, 6124-6130.

Kartal, Ş., Aydın, Z., Tokalıoğlu, Ş., 2006. Fractionation of metals in street sediment samples by using the BCR sequential extraction procedure and multivariate statistical elucidation of the data. Journal of Hazardous Materials 132, 80-89.

Kelly, S.D., Lu, P., Bolin, T., Chattopadhyay, S., Newville, M.G., Shibata, T., Zhu, C., 2007. Molecular Structure of Lead (II) Coprecipitated with Iron (III) Oxyhydroxide. Developments in Earth and Environmental Sciences 7, 67-93.

Kendall, D.S., 2003. Toxicity characteristic leaching procedure and iron treatment of brass foundry waste. Environmental Science and Technology 37, 367-371.

Kilbride, C., Poole, J., Hutchings, T., 2006. A comparison of Cu, Pb, As, Cd, Zn, Fe, Ni and Mn determined by acid extraction/ICP–OES and ex situ field portable X-ray fluorescence analyses. Environmental Pollution 143, 16-23.

Komárek, M., Vaněk, A., Ettler, V., 2013. Chemical stabilization of metals and arsenic in contaminated soils using oxides - A review. Environmental Pollution 172, 9-22.

Kooner, Z., 1993. Comparative study of adsorption behavior of copper, lead, and zinc onto goethite in aqueous systems. Environmental Geology 21, 242-250.

Krishnamurti, G.S., Naidu, R., 2000. Speciation and phytoavailability of cadmium in selected surface soils of South Australia. Soil Research 38, 991-1004.

Krishnamurti, G.S., Naidu, R., 2002. Solid-solution speciation and phytoavailability of copper and zinc in soils. Environmental Science and Technology 36, 2645-2651.

Kutner, M.H., Nachtsheim, C.J., Neter, J., Li, W., 2005. Applied linear statistical models.

Kyger, J.R., Rinke, S.D., Biagioni, R.N., Sheets, R.W., 1999. Soil contamination from paint on highway bridge, Symposia Papers Presented Before the Division of Environmental Chemistry American Chemical Society, Anaheim, CA.

La Force, M.J., Fendorf, S., 2000. Solid-phase iron characterization during common selective sequential extractions. Soil Science Society of America Journal 64, 1608-1615.

Laforest, G., Duchesne, J., 2006. Characterization and leachability of electric arc furnace dust made from remelting of stainless steel. Journal of Hazardous Materials 135, 156-164.

Lanphear, B.P., Hornung, R., Ho, M., 2005. Screening housing to prevent lead toxicity in children. Public Health Reports 120, 305.

Lenth, R.V., 2001. Some practical guidelines for effective sample size determination. The American Statistician 55, 187-193.

Lofts, S., Spurgeon, D.J., Svendsen, C., Tipping, E., 2004. Deriving soil critical limits for Cu, Zn, Cd, and Pb: A method based on free ion concentrations. Environmental Science and Technology 38, 3623-3631.

Lu, P., Nuhfer, N.T., Kelly, S., Li, Q., Konishi, H., Elswick, E., Zhu, C., 2011. Lead coprecipitation with iron oxyhydroxide nano-particles. Geochimica et Cosmochimica Acta 75, 4547-4561.

Manceau, A., Charlet, L., Boisset, M., Didier, B., Spadini, L., 1992. Sorption and speciation of heavy metals on hydrous Fe and Mn oxides. From microscopic to macroscopic. Applied Clay Science 7, 201-223.

Marani, D., Macchi, G., Pagano, M., 1995. Lead precipitation in the presence of sulphate and carbonate: testing of thermodynamic predictions. Water Research 29, 1085-1092.

Marchebois, H., Savall, C., Bernard, J., Touzain, S., 2004. Electrochemical behavior of zinc-rich powder coatings in artificial sea water. Electrochimica Acta 49, 2945-2954.

Margrey, K.W., Riese., J.B., 2012. Email on February 24th 2012.

Markey, A.M., Clark, C.S., Succop, P.A., Roda, S., 2008. Determination of the feasibility of using a portable X-ray fluorescence (XRF) analyzer in the field for measurement of lead content of sieved soil. Journal of Environmental Health 70 (7), 24-29.

Martel, C.M., Atanassopoulos, C., Marinas, B.J., 1997. Mobility of Lead-based paint in a landfill. Solid Waste Association of North America 457-472

Martin, J., Sackett, D., 2005. X-ray fluorescence in the field. Advanced Materials and Processes 163, 51-53.

Mathews, P., 2010. Sample size calculations: practical methods for engineers and scientists. Mathews Malnar and Bailey: Fairport Harbor, OH

McBride, M., Sauve, S., Hendershot, W., 1997. Solubility control of Cu, Zn, Cd and Pb in contaminated soils. European Journal of Soil Science 48, 337-346.

Meima, J.A., Comans, R.N., 1997. Geochemical modeling of weathering reactions in municipal solid waste incinerator bottom ash. Environmental Science and Technology 31, 1269-1276.

Meima, J.A., Comans, R.N., 1998. Application of surface complexation/precipitation modeling to contaminant leaching from weathered municipal solid waste incinerator bottom ash. Environmental Science and Technology 32, 688-693.

Mielke, H.W., Gonzales, C., 2008. Mercury (Hg) and lead (Pb) in interior and exterior New Orleans house paint films. Chemosphere 72, 882-885.

Mielke, H.W., Powell, E.T., Shah, A., Gonzales, C.R., Mielke, P.W., 2001. Multiple metal contamination from house paints: consequences of power sanding and paint scraping in New Orleans. Environmental Health Perspectives 109, 973.

Miller, W., Martens, D., Zelazny, L., 1986. Effect of sequence in extraction of trace metals from soils. Soil Science Society of America Journal 50, 598-601.

Minnesota Department of Transportation (MnDOT), 2004. Air quality and waste management for the removal of paint (using dry abrasive blasting) on steel bridge structures.

Mishra, S.P., Tiwari, D., Dubey, R., 1997. The uptake behaviour of rice (Jaya) husk in the removal of Zn (II) ions-A radiotracer study. Applied Radiation and Isotopes 48, 877-882.

Mishra, S.P., Tiwary, D., 1999. Ion exchangers in radioactive waste management. Part XI. Removal of barium and strontium ions from aqueous solutions by hydrous ferric oxide. Applied Radiation and Isotopes 51, 359-366.

Monico, L., Van der Snickt, G., Janssens, K., De Nolf, W., Miliani, C., Verbeeck, J., Tian, H., Tan, H., Dik, J., Radepont, M., 2011. Degradation process of lead chromate in paintings by Vincent van Gogh studied by means of synchrotron X-ray spectromicroscopy and related methods. 1. Artificially aged model samples. Analytical Chemistry 83, 1214-1223.

Monnier, J., Neff, D., Réguer, S., Dillmann, P., Bellot-Gurlet, L., Leroy, E., Foy, E., Legrand, L., Guillot, I., 2010. A corrosion study of the ferrous medieval reinforcement of the Amiens cathedral. Phase characterisation and localisation by various microprobes techniques. Corrosion Science 52, 695-710.

Montgomery, D.C., Runger, G.C., Hubele, N.F., 2009. Engineering statistics. John Wiley & Sons.

Montgomery, M., Mathee, A., 2005. A preliminary study of residential paint lead concentrations in Johannesburg. Environmental Research 98, 279-283.

Morley, J.C., Clark, C.S., Deddens, J.A., Ashley, K., Roda, S., 1999. Evaluation of a portable X-ray fluorescence instrument for the determination of lead in workplace air samples. Applied Occupational and Environmental Hygiene 14, 306-316.

Mudd, G.M., Weaver, T.R., Kodikara, J., 2004. Environmental geochemistry of leachate from leached brown coal ash. Journal of Environmental Engineering 130, 1514-1526.

Müller, I., Pluquet, E., 1998. Immobilization of heavy metals in sediment dredged from a seaport by iron bearing materials. Water Science and Technology 37, 379-386.

National Institute for Occupational Safety and Health (1992), Health Hazard Evaluation Report: HUD Lead-Based Paint Abatement Demonstration Project, DHHS (NIOSH) Pub. No. 90-070-2181. NIOSH, Cincinnati, OH. .

National Paint and Coatings Association, 1992. National Paint and Coatings Association (1992) Preventing childhood lead exposure: putting the issues in perspective. .

Navidi, W.C., 2008. Statistics for engineers and scientists. McGraw-Hill Higher Education.

Nduka, J., Orisakwe, O., Maduawguna, C., 2008. Lead levels in paint flakes from buildings in Nigeria: a preliminary study. Toxicology and Industrial Health 24, 539-542.

Neumann, A., Olson, T.L., Scherer, M.M., 2013. Spectroscopic Evidence for Fe (II)–Fe (III) Electron Transfer at Clay Mineral Edge and Basal Sites. Environmental Science and Technology.

New Jersey Department of Environmental Protection (NJDEP), 2008. Guidance for the use of the Synthetic Precipitation Leaching Procedure to develop site-specific impact to ground water remediation standards.

New York State Department of Environmental Conservation (NYSDEC), 2006. New York State brownfield cleanup program development of soil cleanup objectives technical support document.

Nishimura, K., Shindo, H., Kato, K., 2000. Highly corrosion-resistant Zn-Mg alloy galvanized steel sheet for building construction materials. Nippon Steel Technical Report 81, no. 0, pp. 85-88.

NYSDOT, 1988. Specification for bridges − removal of lead based paints − new department paint system for structural steel. Engineering instruction, pp. 88-36

NYSDOT, 2008. Standard Specification.

Occupational Safety and Health Administration (OSHA), 1993. Lead exposure in construction: interim final rule (29 CFR 1926.62). Federal Register 58: 26590-26649. Washington, DC.

Padmanabham, M., 1983. Comparative study of the adsorption-desorption behaviour of copper (II), zinc (II), cobalt (II) and lead (II) at the goethite solution interface. Soil Research 21, 515-525.

Pagnanelli, F., Moscardini, E., Giuliano, V., Toro, L., 2004. Sequential extraction of heavy metals in river sediments of an abandoned pyrite mining area: pollution detection and affinity series. Environmental Pollution 132, 189-201.

Peterson, M.L., Brown, G.E., Parks, G.A., 1996. Direct XAFS evidence for heterogeneous redox reaction at the aqueous chromium/magnetite interface. Colloids and Surfaces A: Physicochemical and Engineering Aspects 107, 77-88.

Peterson, M.L., Brown, G.E., Parks, G.A., Stein, C.L., 1997. Differential redox and sorption of Cr (III/VI) on natural silicate and oxide minerals: EXAFS and XANES results. Geochimica et Cosmochimica Acta 61, 3399-3412.

Pierce, M.L., Moore, C.B., 1980. Adsorption of arsenite on amorphous iron hydroxide from dilute aqueous solution. Environmental Science and Technology 14, 214-216.

Pradhan, D., Mishra, D., Kim, D.J., Ahn, J.G., Chaudhury, G.R., Lee, S.W., 2010. Bioleaching kinetics and multivariate analysis of spent petroleum catalyst dissolution using two acidophiles. Journal of Hazardous Materials 175, 267-273.

Pueyo, M., Sastre, J., Hernandez, E., Vidal, M., López-Sánchez, J., Rauret, G., 2003. Prediction of trace element mobility in contaminated soils by sequential extraction. Journal of Environmental Quality 32, 2054-2066.

Quevauviller, P., 1998. Operationally defined extraction procedures for soil and sediment analysis I. Standardization. Trends in Analytical Chemistry 17, 289-298.

Quevauviller, P., Rauret, G., Muntau, H., Ure, A., Rubio, R., Lopez-Sanchez, J., Fiedler, H., Griepink, B., 1994. Evaluation of a sequential extraction procedure for the determination of extractable trace metal contents in sediments. Fresenius' Journal of Analytical Chemistry 349, 808-814.

Quinn, J., 2013. Email on May 6th, 2013.

Radu, T., Diamond, D., 2009. Comparison of soil pollution concentrations determined using AAS and portable XRF techniques. Journal of Hazardous Materials 171, 1168-1171.

Risher, J., DeWoskin, R., 1999. Toxicological profile for mercury. Agency for Toxic Substances and Disease Registry.

Roskovic, R., Stipanovic Oslakovic, I., Radic, J., Serdar, M., 2011. Effects of chromium (VI) reducing agents in cement on corrosion of reinforcing steel. Cement and Concrete Composites 33, 1020-1025.

Ryan, T.P., 2013. Sample size determination and power. John Wiley & Sons.

Sae Specification, 2006. J827 - High Carbon Steel Shot. http://www.blastmaster.net/select/datasheets/93710.pdf.

Sakia, R.M., 1992. The Box-Cox Transformation Technique: A Review. Journal of the Royal Statistical Society. Series D (The Statistician) 41, 169-178.

Sauve, S., Hendershot, W., Allen, H.E., 2000. Solid-solution partitioning of metals in contaminated soils: dependence on pH, total metal burden, and organic matter. Environmental Science and Technology 34, 1125-1131.

Sauvé, S., Norvell, W.A., McBride, M., Hendershot, W., 2000. Speciation and complexation of cadmium in extracted soil solutions. Environmental Science and Technology 34, 291-296.

Schecher, W.D., McAvoy, D.C., 1992. MINEQL+: a software environment for chemical equilibrium modeling. Computers, Environment and Urban Systems 16, 65-76.

Schwertmann, U., Murad, E., 1983. Effect of pH on the formation of goethite and hematite from ferrihydrite. Clays and Clay Minerals 31, 277-284.

Şerifaki, K., Böke, H., Yalçın, Ş., İpekoğlu, B., 2009. Characterization of materials used in the execution of historic oil paintings by XRD, SEM-EDS, TGA and LIBS analysis. Materials Characterization 60, 303-311.

Shanmuganathan, P., Lakshmipathiraj, P., Srikanth, S., Nachiappan, A., Sumathy, A., 2008. Toxicity characterization and long-term stability studies on copper slag from the ISASMELT process. Resources, Conservation and Recycling 52, 601-611.

Shaw, S., Benning, L., Terrill, N., Davidson, L., 2004. Nucleation and growth of iron oxyhydroxide nanoparticles from solution: An in situ time-resolved small angle X-ray scattering (SAXS) study. Geochem. Cosmochim. Acta 68, A158.

Shu, Z., Axe, L., 2010. Deliverable for Task 1: Identification of Sites for the Study. Report submitted to New York State Department of Transportation (NYSDOT).

Shu, Z., Axe, L., 2013a. Deliverable for Task 4: In-Situ Bridge Paint Analyses Using XRF. Report submitted to New York State Department of Transportation (NYSDOT).

Shu, Z., Axe, L., 2013b. Deliverable for Task 6: Collection of samples for laboratory analyses Report Submitted to New York State Department of Transportation (NYSDOT).

Shuman, L., 1979. Zinc, manganese, and copper in soil fractions. Soil Science 127, 10-17.

Singer, P.C., Stumm, W., 1970. Solublity of ferrous iron in carbonate-bearing waters. Journal / American Water Works Association 62, 198-202.

Sipos, P., Németh, T., Kis, V.K., Mohai, I., 2008. Sorption of copper, zinc and lead on soil mineral phases. Chemosphere 73, 461-469.

Smith, L., 1993. Oral presentation at the SSPC Sixth Annual Conference on Lead Paint removal and Abatement. Cincinnati, Ohio USA.

Somme-Dubru, M., Genet, M., Mathieux, A., Rouxhet, P., Rodrique, L., 1981. Evaluation by photoelectron spectroscopy and electron microscopy of the

stabilization of chrome-yellow pigments. Journal of Coatings Technology 53, 51-56.

Stipp, S., Hansen, M., Kristensen, R., Hochella, M., Bennedsen, L., Dideriksen, K., Balic-Zunic, T., Leonard, D., Mathieu, H.J., 2002. Behaviour of Fe-oxides relevant to contaminant uptake in the environment. Chemical Geology 190, 321-337.

Stover, R., Sommers, L., Silviera, D., 1976. Evaluation of metals in wastewater sludge. Journal (Water Pollution Control Federation), 2165-2175.

Strawn, D.G., Sparks, D.L., 1999. The use of XAFS to distinguish between inner-and outer-sphere lead adsorption complexes on montmorillonite. Journal of Colloid and Interface Science 216, 257-269.

Stumm, W., 1970. Aquatic Chemistry; An Introduction Emphasizing Chemical Equilibria in Natural Waters. Wiley-Interscience: New York, NY.

Stumm, W., Morgan, J., 1996. Aquatic chemistry, chemical equilibra and rates in natural waters. Vol. 126. John Wiley & Sons: New York, NY.

Sun, Y., Xie, Z., Li, J., Xu, J., Chen, Z., Naidu, R., 2006. Assessment of toxicity of heavy metal contaminated soils by the toxicity characteristic leaching procedure. Environmental Geochemistry and Health 28, 73-78.

Surface Coatings Association of Australia, 1993. Surface Coatings: Raw Materials and Their Usage. Chapman & Hall: London UK

Sutherland, R.A., Tack, F.M., 2002. Determination of Al, Cu, Fe, Mn, Pb and Zn in certified reference materials using the optimized BCR sequential extraction procedure. Analytica Chimica Acta 454, 249-257.

Swift, R., McLaren, R., Bolt, G., Boodt, M.d., Hayes, M., McBride, M., 1991. Micronutrient adsorption by soils and soil colloids. Interactions at the Soil Colloid-Soil Solution Interface., 257-292.

Takaoka, M., Yoshinaga, J., Tanaka, A., 2006. Influence of paint chips on lead concentration in the soil of public playgrounds in Tokyo. Journal of Environmental Monitoring 8, 393-398.

Tessier, A., Campbell, P.G., Bisson, M., 1979. Sequential extraction procedure for the speciation of particulate trace metals. Analytical Chemistry 51, 844-851.

The Consumer Product Safety Improvement Act, C., 2008. The Consumer Product Safety Improvement Act (CPSIA).

The Society for Protective Coatings (SSPC), 1993. Lead Paint Bulletin-special issue. .

Tiruta-Barna, L.R., Barna, R., Moszkowicz, P., 2001. Modeling of solid/liquid/gas mass transfer for environmental evaluation of cement-based solidified waste. Environmental Science and Technology 35, 149-156.

Todd, A.C., Wetmur, J.G., Moline, J.M., Godbold, J.H., Levin, S.M., Landrigan, P.J., 1996. Unraveling the chronic toxicity of lead: an essential priority for environmental health. Environmental Health Perspectives 104, 141.

Tomatis, L., 1976. The IARC program on the evaluation of the carcinogenic risk of chemicals to man. Annals of the New York Academy of Sciences 271, 396-409.

Tong, S., Schirnding, Y.E.v., Prapamontol, T., 2000. Environmental lead exposure: a public health problem of global dimensions. Bulletin of the World Health Organization 78, 1068-1077.

Torrecilla, J.S., García, J., Rojo, E., Rodríguez, F., 2009. Estimation of toxicity of ionic liquids in Leukemia Rat Cell Line and Acetylcholinesterase enzyme by principal component analysis, neural networks and multiple lineal regressions. Journal of Hazardous Materials 164, 182-194.

Townsend, T., Tolaymat, T., Leo, K., Jambeck, J., 2004a. Heavy metals in recovered fines from construction and demolition debris recycling facilities in Florida. Science of the Total Environment 332, 1-11.

Townsend, T., Tolaymat, T., Solo-Gabriele, H., Dubey, B., Stook, K., Wadanambi, L., 2004b. Leaching of CCA-treated wood: implications for waste disposal. Journal of Hazardous Materials 114, 75-91.

Trivedi, P., Axe, L., Tyson, T.A., 2001. An analysis of zinc sorption to amorphous versus crystalline iron oxides using XAS. Journal of Colloid and Interface Science 244, 230-238.

Turner, A., Singh, N., Richards, J.P., 2009. Bioaccessibility of metals in soils and dusts contaminated by marine antifouling paint particles. Environmental Pollution 157, 1526-1532.

Turner, A., Sogo, Y., 2012. Concentrations and bioaccessibilities of metals in exterior urban paints. Chemosphere 86, 614-618.

U. S. EPA, 1992. Toxicity Characteristic Leaching Procedure (TCLP), SW-846 Method 1311. Federal Register, 55 (March 29), Washington, DC. .

U. S. EPA, 1995. A field test of Lead-Based Paint testing technologies: Summary Report, EPA-747-R-95-002a, Washington, DC.

U. S. EPA, 1996a. Approved/Accepted Hach Methods, Cincinnati, OH. .

U. S. EPA, 1996b. Lead exposure associated with renovation and remodeling activities: Summary Report, EPA-747-R-96e005, Washington, DC.

U. S. EPA, 1998. Method 6200, Field portable x-ray fluorescence spectrometry for the determination of elemental concentrations in soil and sediment (EPA/600/R-97/150, Revision 0), Retrieved November 1, 2007.

U. S. EPA, 2000a. Lead exposure associated with renovation and remodeling activities: Phase III, Wisconsin Childhood Blood-Lead Study, EPA-747-R-99e002, Washington, DC.

U. S. EPA, 2001a. Federal Register, FR 66(4) Rules and Regulations, Residential Lead Hazard Standards - TSCA Section 403, Washington, DC. http://www.epa.gov/lead/pubs/leadhaz.htm.

U. S. EPA, 2001b. Hazard Standards for lead in paint, dust and soil (TSCA Section 403). http://www.epa.gov/fedrgstr/EPA-TOX/2001/January/Day-05/t84.pdf.

U. S. EPA, 2003. Test Methods for Evaluating Solid Waste, SW-846, third ed., Office of Solid Waste and Emergency Response, EPA, Washington, DC.

http://www.epa.gov/epawaste/hazard/testmethods/sw846/pdfs/3050b.pdf.

U. S. EPA, 2004. Method 1310B Extraction Procedure (EP) Toxicity Test Method and Structural Integrity Test, Revision 2. Washington, DC.

U. S. EPA, 2007. Method 6020A Inductively coupled plasma-mass spectrometry. SW-846 Chapter 3.

U. S. EPA, 2009. List of contaminants & their MCLs http://www.epa.gov/safewater/contaminants/index.html.

U. S. EPA, 1990. News release Appendix D: use of mercury compounds in indoor latex paint eliminated. Press release: http://www.paint.org/protocol/app-d.cfm [Accessed on 5 September 2007].

U. S. EPA, 2000b. Phenyl mercuric acetate listing background document for the inorganic chemical listing determination.. www.epa.gov/epaoswer/hazwaste/id/inorchem/docs/phenyl.pdf[Accessed 14 September 2007].

U. S. EPA, 1996. Method 3052 Microwave-Assisted Acid Digestion of Siliceous and Organically Based Matrices, Revision 0. Washington, DC.

U.S. EPA, 1986. Method 1320 multiple extraction procedure, Revision 0. Washington, DC.

U.S. EPA, 1997. Emissions factors & AP 42, compilation of air pollutant emission factors, Chapter 13: Miscellaneous Sources.

U.S. EPA, 1998. Groundwater pathway analysis for lead-based paint (LBP) architectural debris. Office of Solid Waste, Washington, DC.

Vaishya, R.C., Gupta, S.K., 2004. Batch kinetic modeling of arsenic removal from water by mixed oxide coated sand (mocs). Journal of Environmental Science and Engineering 46, 123-136.

Van Belle, G., 2011. Statistical rules of thumb. John Wiley & Sons.

Vann, K., Musson, S., Townsend, T., 2006b. Evaluation of a modified TCLP methodology for RCRA toxicity characterization of computer CPUs. Journal of Hazardous Materials 129, 101-109.

Vann, K.N., Musson, S.E., Townsend, T.G., 2006a. Factors affecting TCLP lead leachability from computer CPUs. Waste Management 26, 293-298.

Vithanage, M., Rajapaksha, A.U., Dou, X., Bolan, N.S., Yang, J.E., Ok, Y.S., 2013. Surface complexation modeling and spectroscopic evidence of antimony adsorption on iron-oxide-rich red earth soils. Journal of Colloid and Interface Science 406, 217-224.

Wadanambi, L., Dubey, B., Townsend, T., 2008. The leaching of lead from lead-based paint in landfill environments. Journal of Hazardous Materials 157, 194-200.

Weng, C.H., Huang, C., Allen, H., Sanders, P.F., 2001. Cr (VI) adsorption onto hydrous concrete particles from groundwater. Journal of Environmental Engineering 127, 1124-1131.

Weng, C., Huang, C., Allen, H.E., Leavens, P.B., Sanders, P.F., 1996. Chemical interactions between Cr (VI) and hydrous concrete particles. Environmental Science and Technology 30, 371-376.

Winchester, C.M., 1988. Nitrocellulose-urethane traffic paint. Google Patents.

Xu, Y., Boonfueng, T., Axe, L., Maeng, S., Tyson, T., 2006. Surface complexation of Pb (II) on amorphous iron oxide and manganese oxide: Spectroscopic and time studies. Journal of Colloid and Interface Science 299, 28-40.

Zamurs, J., Bass, J., Williams, B., Fritsch, R., Sackett, D., Heman, R., 1998. Real-time measurement of lead in ambient air during bridge paint removal. Transportation Research Record: Journal of the Transportation Research Board 1641, 29-38.

Zar, J., 2000. Biostatistical analysis (2nd Eds) Prentice-Hall International. Inc.: Englewood Cliffs, New Jersery.

Zhou, Y. F., Haynes, R.J., 2010. Sorption of heavy metals by inorganic and organic components of solid wastes: Significance to use of wastes as low-cost adsorbents and immobilizing agents. Critical Reviews in Environmental Science and Technology 40, 909-977.